Analysis and control of a spark ignition free-piston engine generator

Thesis by

Boru Jia

In Partial Fulfilment of the Requirements

for the Degree of

Doctor of Philosophy

Sir Joseph Swan Centre for Energy Research

Newcastle University

Newcastle upon Tyne

United Kingdom

July 2016

Abstract

In this research, the performance analysis and control strategy of a spark-ignited free-piston engine generator were presented. A literature review of the free-piston engine fundamental information and the recent research development on the free-piston engine generator (FPEG) was provided, mainly focussing on previous work on numerical modelling, prototype design as well as the control strategy. The design and simulation of a dual-piston spark-ignited FPEG suitable for operation using either a two-stroke or four-stroke thermodynamic cycle were presented. Model validation and the general engine performance of the system were discussed. For the first time, this research demonstrated the potential advantages and disadvantages of the FPEG on using different thermodynamic gas-exchange cycles. A fast response real time model of the FPEG was designed and validated. The simplicity and flexibility of the proposed model make it feasible to be implemented and coupled with real-time hardware in the loop control system development. In addition, since it revealed how an FPEG operates according to a resonant principle, the model is useful for parameter selection in the design process. For the first time, cascade control was proposed and investigated for the piston stable operation control, using both the measured piston top dead centre of the previous stroke and the measured piston velocity at the current stroke as feedbacks, with the injected fuel mass as the control variable. The system performance was improved by implementing the cascade control compared with single loop control in terms of the controller response time, peak error and settling time.

Acknowledgements

I would like to express my sincere gratitude to my supervisor, Professor Tony Roskilly, for his encouragement, guidance and support throughout my PhD journey. I would also like to thank my co-supervisors, Dr Andrew Smallbone, Dr Rikard Mikalsen for their contributions to my research. I also thank Dr Guohong Tian and Dr Mohd Razali Hanipah for their help on my project, and their work on the prototype development. Without your consistent and illuminating instruction, this thesis would not have reached its present form.

Special thanks to the staff of Sir Joseph Swan Centre for Energy Research include Dr Yaodong Wang, Mr Leigh Ingle, Mrs Jan Fairless, Mrs Janie Ling Chin, Mr Stephen Crosby, Mr Ian Douglass, and Mr John Richardson. Thanks to all who have been involved in project management, technical and administration work.

I would like to express my special appreciation and thanks to my supervisors in China, Professor Zhengxing Zuo and Dr Huihua Feng for their support throughout my PhD study. I would also like to thank my colleagues in Beijing Institute of Technology for their contributions to my research.

To my family and friends who have supported and encouraged me during the work with this project.

List of Publications

I. Boru Jia, Zhengxing Zuo, Huihua Feng, Guohong Tian, Anthony Paul Roskilly, "Development approach of a spark-ignited free-piston engine generator", SAE Technical Paper, 2014-01-2894.

II. Boru Jia, Zhengxing Zuo, Huihua Feng, Guohong Tian, Anthony Paul Roskilly, "Investigation of the Starting Process of Free-piston Engine Generator by Mechanical Resonance", Energy Procedia, 61, 572-577, 2014.

III. Boru Jia, Guohong Tian, Huihua Feng, Zhengxing Zuo, Anthony Paul Roskilly, "An experimental investigation into the starting process of free-piston engine generator", Applied Energy, 157, 798–804, 2015.

IV. Boru Jia, Zhengxing Zuo, Guohong Tian, Huihua Feng, Anthony Paul Roskilly, "Development and validation of a free-piston engine generator numerical model", Energy Conversion and Management, 91, 333-341, 2015.

V. Huihua Feng, Chendong Guo, Chenheng Yuan, Yuyao Guo, Zhengxing Zuo, Anthony Paul Roskilly, Boru Jia, "Research on combustion process of a free piston diesel linear generator", Applied Energy, 161, 395-403, 2016.

VI. Boru Jia, Andrew Smallbone, Huihua Feng, Guohong Tian, Zhengxing Zuo, Anthony Paul Roskilly, "A fast response free-piston engine generator numerical model for control applications", Applied Energy, 162, 321-329 , 2016.

VII. Boru Jia, Zhengxing Zuo, Huihua Feng, Guohong Tian, Andrew Smallbone, Anthony Paul Roskilly, "Effect of closed-loop controlled resonance based mechanism to start free piston engine generator: simulation and test results", Applied Energy, 164, 532-539. 2016.

VIII. Boru Jia, Andrew Smallbone, Zhengxing Zuo, Huihua Feng, Anthony Paul Roskilly, "Design and simulation of a two- or four-stroke free-piston engine

generator for range extender applications", Energy Conversion and Management, 111, 289-298, 2016.

IX. Boru Jia, Rikard Mikalsen, Andrew Smallbone, Huihua Feng, Zhengxing Zuo, Anthony Paul Roskilly, "Stable operation control of a spark ignition free-piston engine generator: a new approach", Applied Energy, 2016.

X. Boru Jia, Andrew Smallbone, Rikard Mikalsen, Huihua Feng, Zhengxing Zuo, Anthony Paul Roskilly, "Disturbance analysis of a free-piston engine using a fast-response model", Manuscript submitted to Control Engineering Practice.

XI. Boru Jia, Zhengxing Zuo, Andrew Smallbone, Huihua Feng, Anthony Paul Roskilly, "Design parameters decoupled analysis of a free-piston engine generator using a validated fast-response numerical model", Manuscript submitted to Applied Energy.

Contents

List of Figures

List of Tables

Nomenclature

A	piston surface area
A_{cyl}	area of the in-cylinder surface in contact with the gas
A_d	reference area of the flow
A_f	friction parameter
AFR	air-fuel ratio
a	shape factor for Wiebe function
B	magnetic flux density
B_f	friction parameter
b	shape factor for Wiebe function
C	capacitance
C_d	discharge coefficient
C_e	load constant of the generator
C_p	heat capacity at constant pressure
C_v	specific heat capacity at constant volume
c	damping coefficient
c_c	critical damping coefficient
CD	combustion duration
CR	set compression ratio
D_v	diameter of the valve

d	cylinder diameter
d_0	reference cylinder diameter
E	average temperature of lubrication oil at liner
F_e	load force of the linear electric generator
F_f	mechanical friction force
F_{fm}	friction force from the linear electrical machine
F_{fl}	friction force from left cylinder
F_{fr}	friction force from right cylinder
F_l	gas forces from the left cylinder
F_r	gas forces from the right cylinder
f	overall scaling factor for friction equation
H	magnetic field strength
H_n	engine speed
h	coefficient of heat transfer
h_i	enthalpy per unit mass of the mass flow
i	current in the coil
g_0	air gap
K_d	derivative gain
K_p	proportional gain
K_i	integral gain
K_t	throttle opening coefficient
k	spring constant or stiffness
L	inductance of the circuit

L_v	valve lift
L_s	half stroke length (m)
L_c	clearance length (m)
M_{PM}	air-gap magneto motive force
m_{air0}	initial gas mass in the cylinder
m_f	injected fuel amount
$\dot{m}_{flow}$	mass flow rate through a poppet valve
m_i	air mass flows into or out of the cylinder
m_{in}	inlet air-fuel mass through the intake valve
m_{out}	burnt gas mass through the exhaust valve
m_l	gas leakage mass through the piston rings
p	simultaneous in-cylinder pressure
p_0	ambient pressure
p_{cm}	pressure due to heat release
p_{cp}	cylinder pressure due to volume change
p_d	downstream air pressure
p_u	upstream air pressure
Q_c	heat released during the combustion process
Q_{ht}	heat transferred to the cylinder wall
Q_{in}	overall heat input for each cylinder in one running cycle
R	resistance of the circuit
R_L	resistance of the external load
R_S	internal resistance

T_u	temperature of the inlet gas
T_w	average surfaces temperature of the cylinder wall
t	operation time
t_s	time when combustion process starts
U	internal energy of the in-cylinder gas
V	cylinder volume
V_o	cylinder volume at the middle stroke
V_c	clearance volume
V_l	volume for the left chamber
V_r	right chamber's volume
v	piston axial velocity
v_p	average piston speed
W	output work
W_m	stored magnetic energy
x	piston displacement
x_{TDC}	target piston TDC
Δp_cm	pressure increase heat release process
ω_n	angular natural frequency
σ	unit step function
η_c	combustion efficiency
γ	heat capacity ratio
θ_0	reference temperature
ψ	fuel mass fraction burned

ε	voltage
λ	flux linkage in a coil
μ_0	vacuum permeability
τ	pole pitch
τ_p	width of permanent magnet
$\emptyset$	magnetic flux
0/1D	zero/one-dimensional
aBDC	after bottom dead centre
aTDC	after top dead centre
bBDC	before bottom dead centre
BDC	bottom dead centre
BIT	Beijing Institute of Technology
bTDC	before top dead centre
CTU	Czech Technical University
ECU	engine control unit
EM	electromagnetic force
EVC	exhaust valve close
EVO	exhaust valve open
FPE	free-piston engine
FPEC	free-piston engine converter
FPEG	free-piston engine generator
HCCI	homogeneous charge compression ignition
HIL	hardware-in-the-loop
IVC	intake valve close

IVO	intake valve open
NIT	Nanjing Institute of Technology
NU	Newcastle University
PM	permanent magnetic
pV	pressure-volume/indicator diagram
PID	proportional–integral–derivative
SISO	single input single output
SNL	Sandia National Laboratory
TDC	top dead centre
TTL	transistor-transistor logic
WVU	West Virginia University

Chapter 1. Introduction

1.1 Background

The free-piston engine (FPE) is a linear engine in which the requirement for a crankshaft system is eliminated and the piston assembly has a free and linear motion [1]. First proposed around 1930, FPEs were in use in the period 1930–1960 as air compressors and gas generators and provided some advantages over present-time conventional combustion engines and gas turbine systems [2]. They are known to have a greater thermal efficiency (40-50%) than an equivalent and more conventional reciprocating engine (30-40%) [3].

After initial investigations and development of free-piston related products during the early to mid-20th century, recent advances in control and real time actuation systems have enabled the technology to become a viable alternative to reciprocating technologies, and as such, research is now being carried out by a number of groups worldwide [3-9]. Modern applications of the FPE concept have been proposed for the generation of electric and hydraulic power, typically in hybrid electric vehicles [10-16]. Successful operation of FPE coupled with hydraulic pump has been reported [17-23] .

For FPEs, the elimination of the crank mechanism significantly reduces the number of moving parts and therefore the complexity of the engine [24]. This gives a number of advantages: reduced frictional losses due to the mechanical simplicity and the elimination of the piston side force in crankshaft engines; reduced heat transfer losses and NOx generation due to faster power stroke expansion; potentially lower maintenance cost and higher reliability due to a compact and simple design; and multi-

fuel/combustion mode possibility due to combustion optimization flexibility that resulted from the variable compression ratio [25].

1.2 Free-piston engine generator

Known FPE applications include electric generators, hydraulic pumps and air compressors [2]. In this research, the FPE connected with linear electric generator (free-piston engine generator, FPEG) is investigated with the objective to utilisation within a hybrid-electric automotive vehicle power system.

The FPEG considered here consists of a FPE coupled to a linear electric generator. Combustion in the chambers of the engine makes the translator reciprocate in a resonant-like way and the linear electrical machine converts some of the mover's kinetic energy to electrical energy, which will be stored and/or used to power an external load. The effective efficiency is estimated to be at least 46% (including friction and compressor losses) at a power level of 23 kW and shows promising results with respect to engine performance and emissions [3].

FPEG technology is currently being explored by a number of research groups worldwide. The high efficiencies of electrical machinery, along with flexibility and controllability, make this an interesting concept. A driving force behind the interest in free-piston engine generators is the automotive industry's increasing interest in hybrid-electric vehicle technology. Much work has been undertaken by a number of research groups worldwide, including the authors' group, to explore the operation characteristics of FPEGs [25-29].

1.3 Aims and objectives

This research will focus on a spark-ignited dual piston type FPEG, and aims to analyse the basic performance of the spark-ignited dual piston type FPEG prototype developed in Newcastle University and identify an optimal control strategy. The main objectives of the study are as follows:

- To develop a detailed numerical model for the engine and the linear electric machine.

- To calibrate and validate the model against test results from the prototype;
- To investigate the technical feasibility of operating Newcastle University's FPE in both a two- and a four-stroke thermodynamic cycle;
- To predict the basic performance of the prototype and to identify factors and variables that will influence the engine operating characteristics;
- To develop a fast-response numerical model for the application of the future real time Hardware-in-the-Loop control system;
- To analyze the possible disturbances to the FPEG prototype and develop a feasible control strategy.

1.4 Methodology

In order to accomplish this research, the following methodologies were adopted:

(1) A detailed FPEG model was developed in Matlab/Simulink. The model was able to describe the working performance of the FPEG in operation of both two- and four-stroke thermodynamic cycles. The model took the following variables into consideration:

- Heat transfer from the cylinder gas to the chamber walls;
- Air leakage through piston rings;
- Mass flow through poppet valves;
- Friction in the linear electrical machine and friction between the piston rings and cylinder wall;
- Compression, expansion and heat release processes;
- Design parameters of the linear electric machine.

The model was used to investigate:

- Piston dynamics, including piston displacement, velocity, acceleration;
- Engine performance, including in-cylinder pressures and temperatures;
- Power output, including indicated power, brake power, and electric power;
- Fuel efficiency, electrical efficiency;
- Optimal working conditions, *i.e*. ignition timing, injected fuel mass, valve timing, electric load force, etc. which will produce best performance.

(2) Experimental work was undertaken to validate the simulation model. Experiments will be done for both of the starting process and the combustion process. Test data was collected for analysis and validation, including:

- Piston displacement;
- Cylinder pressure;
- Ignition timing;
- Injected fuel mass;

Engine compression ratio, output power, fuel consumption, and efficiency were calculated for further analyses based on the experimental results.

(3) By linearizing the system model, a forced vibration equation with viscous damping was achieved to describe the piston dynamics of the FPEG. Both the compression pressure force and the pressure increase by the heat release were taken into consideration in this fast-response numerical model. The solution for the displacement was derived, which could be used for the future real time Hardware-in-the-Loop control system.

(4) The possible disturbances to the FPEG system and their influence were simulated using the fast-response model. By identifying different types of system disturbance with specific occurring timings, their respective influence on the FPEG system could be obtained. The possible disturbances include:

- Electric load change during the expansion/gas exchange/compression/ heat release processes.
- Cycle-to-cycle variations during the heat release process.
- Unsuccessful ignition.
- Electric load change and cycle-to-cycle variations during the heat release process.
- Electric load change and unsuccessful ignition during the heat release process.

(5) A global control structure of the FPEG was designed. The control structure comprised a multi-layer control system. Each level is summarised as follows:

- The top level is the engine start/restart control level to decide the working mode of the linear electric machine.
- The supervisory control level decides the TDC set point, the throttle opening.
- The piston motion control level updates the control variables to the system.
- The timing control level outputs the suitable values for the ignition timing, injection timing, and valve timing.
- The actuator control level generates transistor-transistor logic (TTL) command signals to the actuators.
- The basic level on the structure is the FPEG prototype with control actuators and sensors.

As the piston stable motion control level is the only level with significant difference from the control of a conventional engine, this was further investigated and simulated. A cascade control system was implemented, and the controller performance was simulated in Matlab/Simulink.

1.5 Structure of the Text

The main body of this dissertation is organised as follows:

- Chapter 2 gives a detailed literature review of the development of the FPEG on numerical modelling, prototype design and testing, as well as the control strategy;
- Chapter 3 discusses the design and modelling of a two- or four- stroke FPEG for range extender applications to investigate the technical feasibility of operating Newcastle University's FPE in both a two- and a four-stroke thermodynamic cycle;
- Chapter 4 provides the model validation and simulation results;
- Chapter 5 derives a fast-response numerical model for the further real-time Hardware-in-the-Loop control systems, and provides a disturbance analysis using the proposed fast response model.
- Chapter 6 presents a global control structure of the FPEG, and discusses the implementation and performance of a cascade control strategy to maintain piston stable motion.
- Chapter 7 gives discussions and conclusions of the whole thesis.

Chapter 2. Literature review

This chapter presents a literature review of the free-piston engine fundamental information and recent research development on the free-piston engine generator (FPEG). From the recent patents and publications, the previous work on numerical modelling, prototype design and test, as well as the control strategy of the FPEG are summarised and presented in this chapter. This review aims to provide an overview of previous research in this area, and identify the challenges to be acknowledged to the prototype development in Newcastle University.

2.1 Free-piston engine basis

The free-piston engine is a linear energy conversion system, and the term 'free-piston' is widely used to distinguish its linear characteristics from a conventional reciprocating engine [2]. Without the limitation of the crankshaft mechanism, as known for the conventional engines, the piston is free to oscillation between its dead centres. The piston assembly is the only significant moving component for the FPEs, and its movement is determined by the gas and load forces acting upon it [1]. In this section, the fundamental information on the FPEs are introduced, giving a general idea of the possible FPE loads and different FPE configurations, as well as the recent development of the FPEG by various groups internationally.

2.1.1 Free-piston engine loads

During the operation of FPEs, combustion takes place in the internal combustion chamber, and the high pressure exhaust gas pushes the piston assembly backwards. The chemical energy from the air fuel mixture is then converted to the mechanical energy of

the moving piston assembly. Due to the linear characteristic, a FPE requires a linear load to convert this mechanical energy for the usage of the target application [30]. As the load is coupled directly to the piston assembly, the technical requirements for the free-piston engine loads are high, which are summarised as:

- The load must provide satisfactory energy conversion efficiency to make the overall system efficient;
- The load may be subjected to high velocity;
- The load may be subjected to high force from the cylinder gas;
- The load device may be subjected to heat transfer from the engine cylinders.
- The size, moving mass and load force profile are feasible to be coupled with the designed FPEs.

Reported load devices for the FPEs include air compressor, electric generator and hydraulic pump. The typical characteristics for these load devices are listed in Table 2.1, and typical resisting force profiles are illustrated in Figure 2.1.

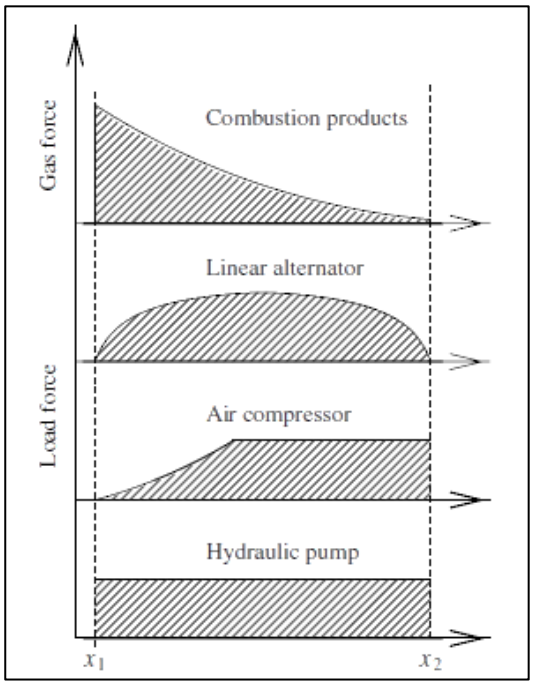

Figure 2.1 Force profile of free-piston engine loads [2]

Load type	Resisting force profile	Characteristics
Air compressor	○ Similar with that of a bounce chamber filled with gas during compression phase; ○ Approximate to constant force when discharge valves open.	○ Original FPE load devices; ○ Stepped compressor pistons can be applied, giving a compact multi-stage compressor; ○ Without supercharge, a large compressor cylinder is required, resulting in oversized configuration; ○ Variable stroke may lead to poor volumetric efficiency of the air compressor.
Electric generator	○ Proportional to the translator speed	○ Relatively compact in size; ○ Generally high efficiency; ○ Magnets or back iron in the mover may lead to high moving mass.
Hydraulic pump	○ Approximate to constant due to the constant discharge pressure.	○ Typically works against a high discharge pressure; ○ Combined with the incompressible working fluid, this allows a small unit with very low moving mass; ○ Generally high efficiency and high operational flexibility.

Table 2.1 Characteristics of free-piston engine loads

2.1.2 Free-piston engine configurations

FPEs can be divided into three categories according to piston/cylinder configuration: single piston, dual piston and opposed piston [2]. Their schematic representation and general advantages and drawbacks are illustrated in Table 2.2. The basic operation principles are equal for each concept; differences between the concepts are the number of combustion chambers and compression stroke realization [30]. Details about each configuration is introduced below.

Type	Representation	Comments
Single piston	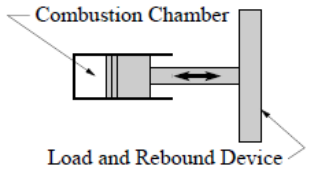	○ Simple and easy to control; ○ Unbalanced; ○ Counterweights may be used.
Opposed piston	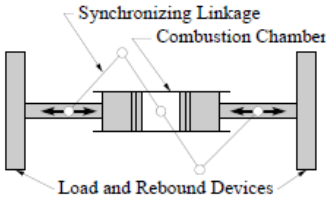	○ Intrinsically balanced; ○ Vibration free with equal piston masses; ○ Piston synchronization required.
Dual pistons	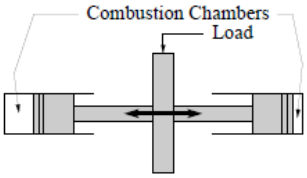	○ Higher power density ○ potentially higher efficiency; Unbalanced; ○ Relatively difficult to control.

Table 2.2 Free-piston engine configurations [2]

An example of single piston FPE is shown in Figure 2.2, which consists of a combustion chamber, and a load and rebound device. A hydraulic pump is used to serve as both load and rebound device in the below illustration. In the other single piston FPE configurations, the load and rebound devices could be two individual devices, *e.g.* an electric generator as load and gas spring chamber as rebound device [31, 32]. The rebound device could make it easy to control the amount of energy put into the compression process and thus regulating the compression ratio and stroke length [33]. There has been successful implementation of the single piston type, coupled with a gas spring rebound chamber [5, 34].

Figure 2.2 Single piston hydraulic free-piston engine from Innas BV [5]

The opposed piston FPE was used almost exclusively in the early stage of the FPE development (1930-1960). It served successfully as air compressors and later as gas generators in large-scale plants [35]. This kind of FPE configuration essentially consists of two opposed pistons with a sharing combustion chamber. Each piston requires a rebound device, and a load device may be coupled to one or both of the pistons. Figure 2.3 demonstrates an opposed piston FPE with mechanical synchronisation system to ensure symmetric piston motion.

The main advantage of the opposed piston FPE design is the balanced and vibration free characteristics. Due to the elimination of the cylinder head, the heat transfer loss would be reduced, and also the application of uniflow scavenging process improves the scavenging efficiency. However, the piston synchronisation system is absolutely required, which is the most significant disadvantage for this configuration. The synchronisation mechanism, together with the dual set of rebound devices make this engine type complicated and bulky [2, 30].

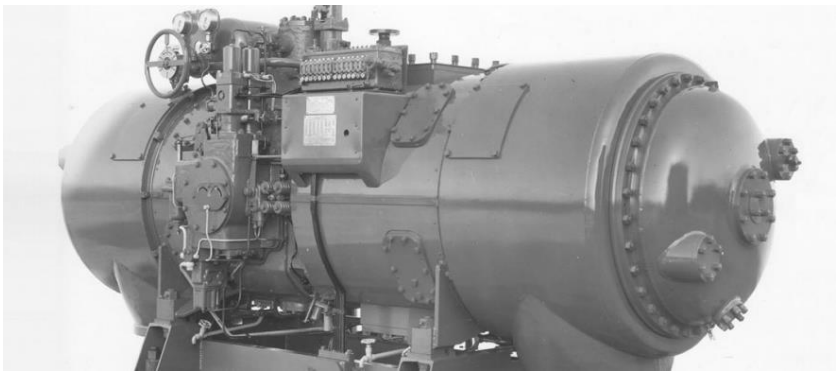

Figure 2.3 Opposed piston FPE with synchronisation mechanism [36]

The dual piston (or dual combustion chamber) configuration, shown in Figure 2.4, has been topic for much of the recent research in free-piston engine technology. A number of dual piston designs have been proposed and a few prototypes have emerged, both with hydraulic and electric power output [12, 37-39]. The dual piston engine configuration eliminates the need for a rebound device, as the (at any time) working piston provides the work to drive the compression process in the other cylinder. This allows a simple and more compact device with higher power to weight ratio.

Some problems with the dual piston design have, however, been reported. The control of piston motion, in particular stroke length and compression ratio, has proved to be difficult [38]. This is due to the fact that the combustion process in one cylinder drives the compression in the other, and small variations in the combustion will have high influence on the next compression. This is a control challenge if the combustion process is to be controlled accurately in order to optimise emissions and/or efficiency [40]. Experimental work with dual piston engines has reported high sensitivity to load nuances and high cycle-to-cycle variations [41].

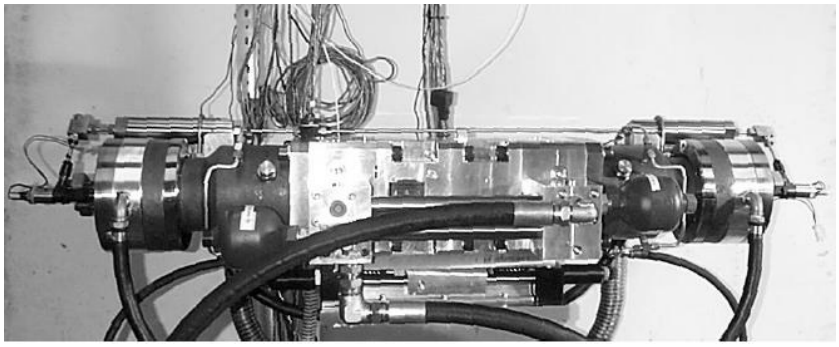

Figure 2.4 Hydraulic dual piston free-piston engine [17]

2.1.3 Free-piston engine generator development

In this research, the FPE connected with linear electric generator (free-piston engine generator, FPEG) is investigated with the objective to utilisation within a hybrid-electric automotive vehicle power system. Since the FPEG was first proposed, it has attracted interests from all over the world. Different research methods and prototype designs have been reported using the FPEG concept [7, 42-45]. However, to date, none of these have been commercially successful. This section gives an overview of known FPEG

development, with an emphasis on engines where simulation results or prototype performance data have been reported. Main research groups and the reported progress are summarised in Table 2.3.

From the results shown in Table 2.3, the reported FPEG prototypes are classified into four concepts based on the number of combustion chambers and the engine operating cycle these are:

- Single-piston two-stroke FPEG;
- Dual-piston two-stroke FPEG;
- Opposed-piston two-stroke FPEG;
- four-stroke engine FPEG;

There are successful implementations of a single piston FPEG concept, coupled with a gas spring rebound chamber. The German Aerospace Centre (DLR) developed a prototype which operated at 21 Hz, realising a power (electric) output of approximately 10 kW [46]. Increasing the frequency up to 50 Hz should lead to a power output of 25 kW of a single piston FPEG system [47, 48]. A prototype was also developed by Toyota Central R&D Labs Inc., this researchers reported stable operation for extended periods of time albeit with abnormal combustion (pre-ignition) [49, 50] .

The dual-piston configuration is the most common layout due to the elimination of the rebound device [51-53]. The only significant moving part is the mover of the generator coupled with piston at each end, and located in the middle of two opposing combustion chambers. Combustion occurs alternatively, the expanding exhaust gases drive the piston thus overcoming the compression pressure force imposed by second cylinder. The effective efficiency of dual piston FPEG was estimated to be up to 46% (including friction and compressor losses) at a power level of 23 kW [3] . The process of successful engine starting and ignition processes by the linear electric machine with mechanical resonance have also been reported [25, 28, 41, 54, 55] .

Research group	FPEG design		Time
West Virginia University	1#	Spark-ignited, two stroke dual piston	1998
	2#	Diesel, two stroke, dual piston engine	2000
	3#	Four-stroke, four-piston conceptual engine	2001
Sandia National Laboratory	1#	Dual piston, homogeneous charge compression ignition (HCCI) combustion	1998
	2#	Opposed Free-Piston, HCCI	2008
European funded project	Dual piston, HCCI combustion		2002
Czech Technical University	Dual piston, spark-ignited engine		2007
Australian Pempek Systems Pty. Ltd.	Dual piston, four free-piston modules		2005
Newcastle University	1#	Single piston engine, gas respond device	2007
	2#	Dual piston, spark-ignited engine	2012
Beijing Institute of Technology	1#	34 cc Dual piston, spark-ignited engine	2008
	2#	100 cc Dual piston, spark-ignited engine	2011
	3#	Dual piston, diesel engine	2012
German Aerospace Centre	Single piston engine, gas spring rebound		2007
Universities in Malaysia	Dual piston, spark-ignited engine		2003
Toyota	Single piston engine, gas spring rebound device		2012
South Korea	Dual piston engine		2012
Nanjing Institute of Technology	Single piston, four stroke engine, mechanical spring respond device		2008
Shanghai Jiaotong University	Dual piston engine, spark-ignited engine		2009

Table 2.3 Main research groups FPEG development

The opposed-piston FPEG concept consists of two pistons with a common combustion chamber. Each piston is connected to a rebound device and a linear electric generator is coupled to both pistons. The main advantage of this configuration lies in the balanced and vibration-free characteristics [2, 56]. However, synchronizing the opposed free pistons is a significant technical challenge. Johnson *et al.* proposed a piston synchronization method through a) passive coupling of linear alternators and b) using a common load for both stators, thus providing a stabilizing force [57].

A single-piston four-stroke FPEG prototype was developed by Xu and Chang [58]. The engine was designed and manufactured based around an existing reciprocating four-stroke engine and modified to operate as four-stroke FPE connected to a linear electric machine. In this prototype, a mechanical spring was connected to the piston assembly, operating as a "kickback" device to return the piston during the non-power stroke. A reversible energy storage device was integrated to accumulate the energy from the electric power output. Stable running of the prototype was reported, and a 2.2 kW average output (electric) power with a generating efficiency of 32% reported [58].

The basic working principles are similar for each concept: combustion occurs in the closed chamber, the exhaust gas expands causing the piston to move backwards, the linear generator utilises this energy to convert the mechanical work on the piston into electricity. However, despite the problems being reported, the dual piston configuration remains the most popular layout due to the following advantages over single piston and opposed piston configurations:

- The only moving part is a linear magnet mover coupled with pistons at each end and placed between two opposing combustion chambers. This allows a simple and more compact device with higher power to weight ratio.
- It eliminates the need for a rebound device, as the combustion force drives the piston assembly to overcome the compression pressure in the other cylinder.

2.2 Numerical modelling and simulation

As the piston motion of the FPEG is not restricted by the crankshaft mechanism, the piston is only influenced by the gas and load forces acting upon it [1]. As a result, the

FPEG have specific operation characteristics compared to conventional reciprocating engines. Free-piston engine is commonly modelled using simplified zero-dimensional models. In this section, the modelling and simulation of the FPEG based on available literature are summarised, providing a useful guidance on the numerical modelling, simulation methods as well as model linearization for extender applications.

2.2.1 Numerical modelling

Christopher M. Atkinson along with other researchers in West Virginia University (WVU) developed the engine computational model with the combination of dynamic and thermodynamic analyses [10, 59-63]. The dynamic analysis performed consisted of an evaluation of the frictional forces and the load across the full operating cycle of the engine. The only forces considered to act on the moving assembly were the resultant pressure forces given by the difference between the pressures in the two cylinders, a frictional force, the inertial force, and the load. The piston motion was derived from Newton's second law, which was

$$F_e + F_l - F_r - F_f = m\frac{d^2x}{dt^2} \tag{2.1}$$

Where x is the mover and piston displacement, m is the moving mass of the piston assembly, F_e is the thrust supplied by the electric linear motor, F_l is the gas force from the left cylinder, F_r is the gas force from the right cylinder, F_f is the friction force.

In their experimental testing of the engine, in order to obtain an approximate simulation of the load that a linear alternator would provide, a friction brake provided a retarding force on the shaft. According to the measurements made, the frictional drag was roughly constant across the full range of motion of the piston assembly with an average value of about 130 N [63].

The thermodynamic analysis consisted of an evaluation of each process that characterized the engine cycle based on the thermodynamic theories. A time-based Wiebe function was used to express the mass fraction burned for the combustion process shown as Equation (2.2 and 2.3). Engine parameters used in this numerical simulation were summarised in Table 2.4.

$$\chi(t) = 1 - \exp\left(-a\left(\frac{t-t_0}{t_c}\right)^{1+b}\right) \quad (2.2)$$

$$\frac{dQ_c}{dt} = Q_{in}\frac{d\chi(t)}{dt} \quad (2.3)$$

Where a is the shape factor of Wiebe function; t represents time (s); t_0 represents the time when combustion begins (s); t_c is the combustion duration (s); Q_{in} is the total input energy from the fuel in one running cycle (J).

Parameters [Unit]	Value
Bore [mm]	36.4
Maximum possible stroke [mm]	50.0
Intake pressure [bar]	1.35
Intake temperature [K]	341.0
Exhaust port height [mm]	10.0
Intake port height [mm]	10.0

Table 2.4 Engine parameters used in this numerical simulation [10]

To ensure the numerical model usefulness, the parameters used were based on test data obtained from the working prototype, illustrated in Figure 2.5, including piston position, piston velocity and cylinder pressure. A parametric study was undertaken to predict the engine performance over a wide operating range, and parts of the results were shown in Figure 2.6.

It was observed that, when the engine was operated at the same load, by decreasing the combustion duration, the peak cylinder pressure increased. However, the influence to the overall shape of the Pressure-Volume diagram was not that significant. The engine speed, or the operation frequency would be higher with higher peak cylinder pressure. Also, longer stroke length or higher compression ratio was found with higher peak cylinder pressure [63].

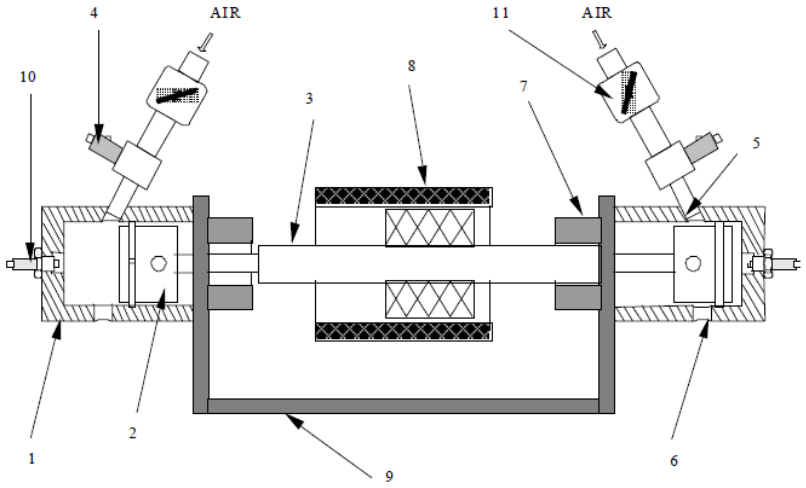

(1.Cylinder, 2. Piston, 3. Connecting rod, 4. Pulsed Solenoid Fuel Injector, 5. Intake Port, 6. Exhaust Port, 7. Motoring Coil, 8.Linear Alternator, 9.Frame, 10.Spark Plug, 11. Throttle)

Figure 2.5 FPEG configuration from WVU [63]

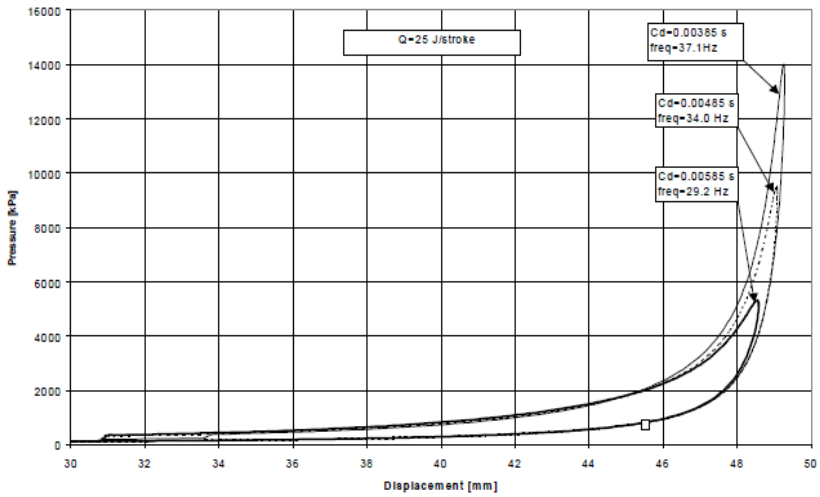

Figure 2.6 P-V diagram from WVU [63]

Mikalsen and Roskilly from Newcastle University (NU) proposed a FPEG design shown in Figure 2.7 [64]. The configuration consisted of a combustion chamber, a gas spring rebound device and a linear electric generator [1, 31] . The only moving part was the piston assembly, *i.e.* the two pistons connected with the mover of the generator, and it would move freely between its dead centres. The piston movement was found to be determined by the instantaneous balance of the cylinder gas forces, resistance fore from the electric generator, and the frictional forces [1].

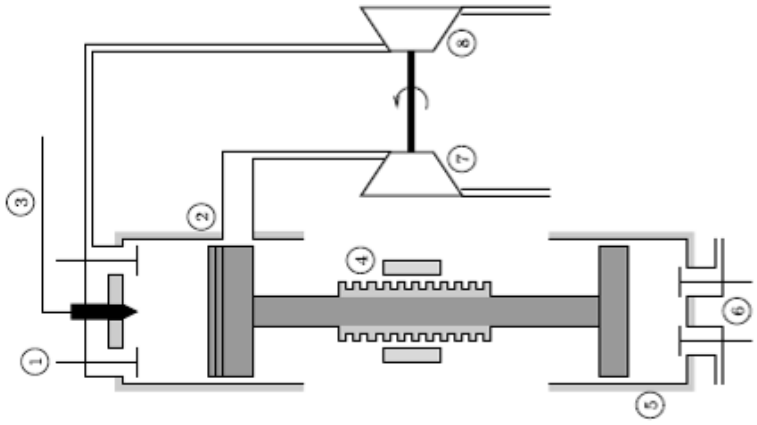

(1. Exhaust poppet valves, 2. Scavenging ports, 3. Common rail fuel injection, 4. Linear alternator, 5.Bounce chamber, 6. Bounce chamber pressure control valves, 7. Turbocharger compressor, 8. Turbocharger turbine.)

Figure 2.7 FPEG design from NU [65]

The sub models for their modelling of the in-cylinder thermodynamics were based on the widely used single-zone models in the simulation of conventional reciprocating diesel engines. The engine specifications and useful boundary parameters are summarised in Table 2.5. The simulation model was validated using the test data from a six-cylinder, turbocharged Volvo TAD 1240 diesel engine located at Newcastle University [1]. The comparison was undertaken aiming to verify the realistic of the simulation model. Results showed that the model was able to predict the real trends of the engine with various operation conditions [1].

Design stroke [mm]	150
Bore [mm]	131
Scavenging ports height [mm]	22
Nominal compression ratio	15:1
Piston mass [kg]	22
Bounce chamber bore [mm]	150
Bounce chamber compression ratio	15:1
Exhaust back pressure [Pa]	150000

Table 2.5 Free-piston engine specifications from NU [1]

Parts of the simulation results are shown in Figure 2.8. Figure 2.8a demonstrated the simulated piston profile within one operation cycle, compared with that of a conventional engine operating at the same engine speed. It was obvious that the piston spent less time around the top dead centre (TDC) for the FPEG, where the cylinder gas pressure and temperature were the highest. Figure 2.8b illustrates an enlarged figure of piston profile around TDC. The comparison of piston velocity profile between FPEG and conventional engine is shown in Figure 2.8c, and lower peak piston velocity was found for the FPEG. Figure 2.8d shows a comparison of piston acceleration in one engine cycle, and significant difference was observed. Very high acceleration was found after ignition for the FPEG, when the cylinder pressure was high and the piston was not restricted by the crankshaft mechanism in conventional engines. Simulated peak acceleration of the FPEG was reported to be around 60% higher than that of the conventional engine [1].

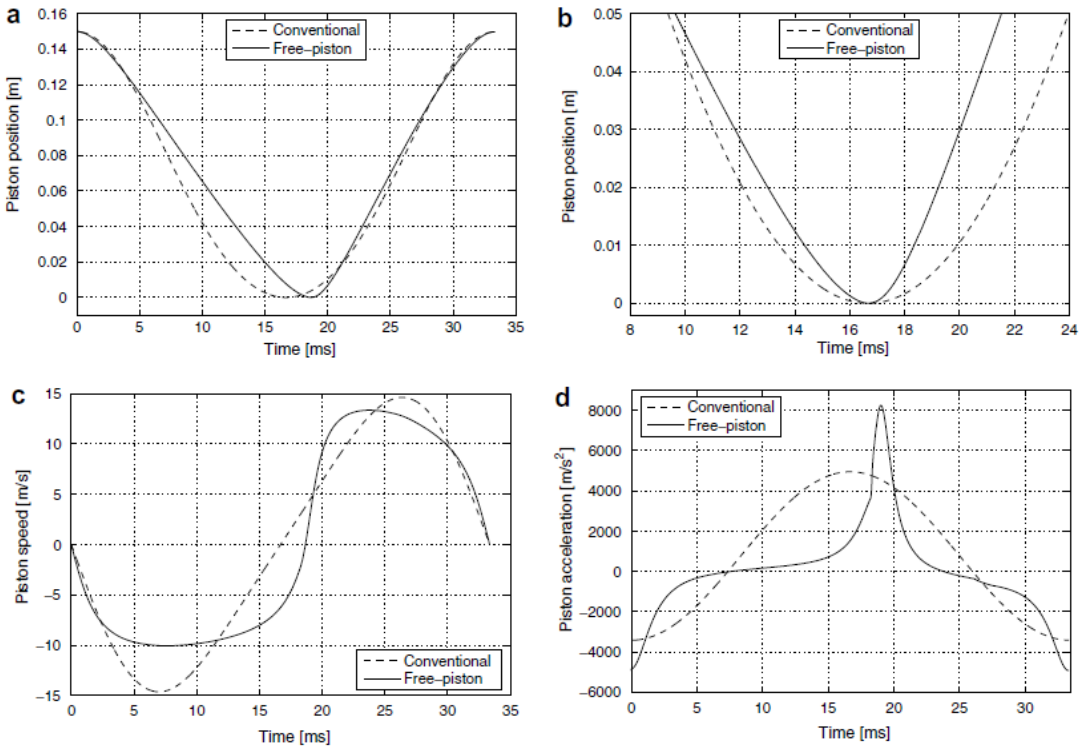

Figure 2.8 Predicted piston dynamics of the FPEG from NU [1]

S. Goldsborough along with other researchers at Sandia National Laboratories (SNL) analysed the steady-state operating characteristics of the FPEG configuration shown in

Figure 2.9 [9, 11, 66, 67]. A zero-dimensional thermodynamic numerical model was developed with detailed chemical kinetics, empirical scavenging, heat transfer and friction sub models. Hydrogen was used as the fuel, and the simulation results indicated the critical factors affecting the engine performance, and suggested the limits of improvement compared to conventional engine technologies [66].

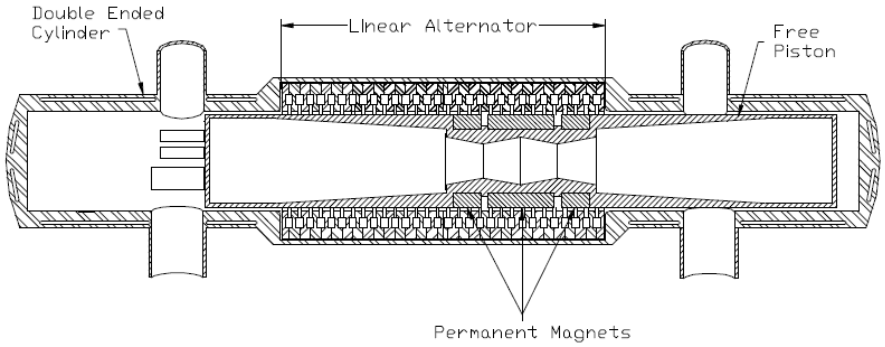

Figure 2.9 Proposed FPEG configuration from SNL [66]

Their analysis of the in-cylinder gas thermodynamics was based on a zero-dimensional approach, and the fluid dynamic and spatial effects were not taken into consideration. The state of the in-cylinder gas was determined by applying the energy conversion equation, and it was expressed as [66]:

$$\frac{dU}{dt} = -p\frac{dV}{dt} + \left(\frac{dQ_c}{dt} - \frac{dQ_{ht}}{dt}\right) + \sum_i \dot{H}_i - \sum_e \dot{H}_e - \sum_l \dot{H}_l \qquad (2.4)$$

Where U is the internal energy of the in-cylinder gas (J); V is displaced volume of the cylinder from the in-cylinder gas (m3); Q_c is the heat released from the combustion process (J); Q_{ht} is the heat transferred to the cylinder (J); H_i is the enthalpy of the intake air (J); H_e is the enthalpy of the exhaust air (J); H_l is the enthalpy of the air leaked from the piston rings (J).

A graphical representation of the in-cylinder gas thermodynamic analysis was presented and shown in Figure 2.10. The in-cylinder charge was assumed to exit as a homogeneous medium throughout the simulation model with uniform temperature and composition. During the simulation of gas exchange process, the in-cylinder gas was assumed to perform as two zones: one filled with burned gas after combustion, the other

one of fresh charge. The two zones mentioned above were considered to remain immiscible, while homogeneous within each other. The gas from these two zones was assumed to mix instantaneously at the end of scavenging process.

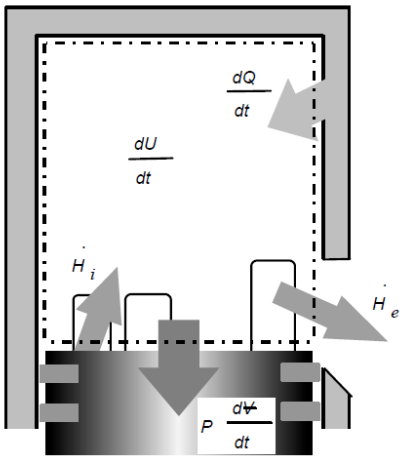

Figure 2.10 A graphical representation of thermodynamic system from SNL [66]

However, the validation of the FPEG numerical model proved difficult due to the limited amount of experimental data available for the prototype. As a result, the simulation results were compared to data that currently available. The specifications of the simulated FPEG from SNL were summarised in Table 2.4.

Cylinder length [mm]	65.0
Cylinder bore [mm]	70.0
Piston mass [kg]	2.7
Intake temperature [K]	300.0
Intake pressure [bar]	1.5
Exhaust pressure [bar]	1.0

Table 2.6 Simulated free-piston engine specifications from SNL [66]

Figure 2.11 demonstrated the simulated piston dynamics from SNL, compared with that of the conventional crankshaft-driven engine of the same stroke length and engine speed. It was evident that the free piston spent less time at TDC, and accelerated/decelerated faster at the end of the stroke. The corresponding characteristic

of shorter time at TDC for the FPEG could be attractive in terms of heat transfer losses and NOx formation, since shorter time at higher temperature was desirable [66].

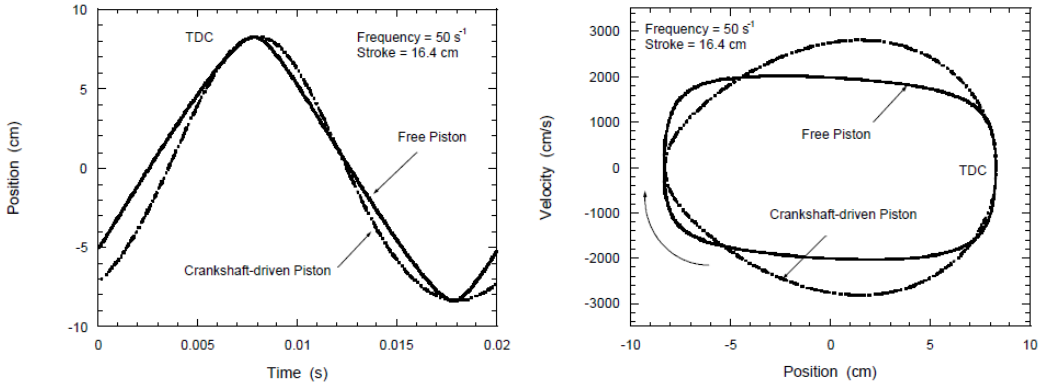

Figure 2.11 Simulated piston dynamics from SNL [66]

A European Commission-funded Free Piston Energy Converter (FPEC) project was started in 2002 [3, 44, 68-72]. The layout of the design prototype was shown in Figure 2.12. A numerical model was developed by Erland Max, for investigations of engine control, dynamics and parameters [3]. The model was constructed by a combination of thermodynamic laws to describe pressure and temperature variations, ignition and heat release models for combustion and Newton's second law for translator dynamics. The main input parameter for the simulation were summarised in Table 2.7.

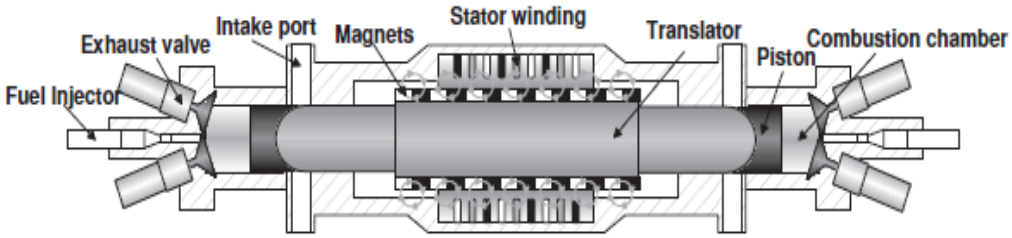

Figure 2.12 Layout of the FPEG from FPEC project [72]

Peak power [kW]	45
Peak generator force [kN]	4
Bore [mm]	102
Translator mass [kg]	9

Table 2.7 Specifications of the FPEG from FPEC project [3]

The movement of the piston assembly simulated by the FPEC team is shown in Figure 2.13. The piston position over time was not sinusoidal as in conventional crankshaft engines. For a crankshaft engine, the piston profile is determined by a crankshaft mechanism, which would resulted in sinusoidal piston motion and fixed compression ratio determined by the set piston TDC during the design process [3].

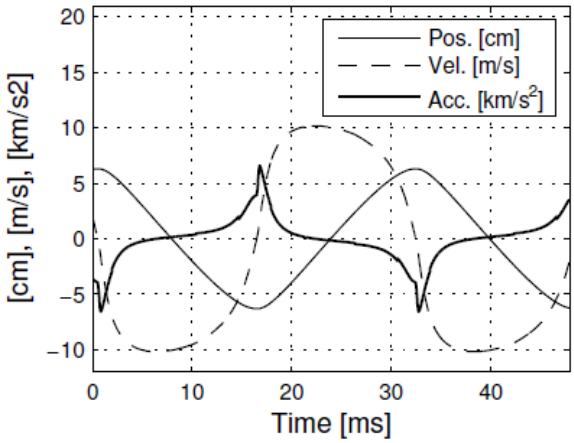

Figure 2.13 Piston dynamics from FPEC project [3]

The linear electric machine was operated as a generator during power stroke. Electrical current was drawn from the alternator coils through the continuous back and forth movement of the mover. According to previous publications, the load force F_e (N) from the electric generator was proportional to the current of the circuit, and its direction was always opposite to the piston velocity, v [1, 66, 73]. It was described by:

$$F_e = -cv \tag{2.5}$$

Where c is the load constant of the generator, which is determined by the physical design parameters of the generator as well as the external load.

Reserchers at Beijing Institute of Technology (BIT) presented numerical simulation on piston motion, using a time-based numerical simulation program built in Matlab to define the piston's motion profiles [29, 51, 74-82]. The simulated prototype configuration is shown in Figure 2.14.

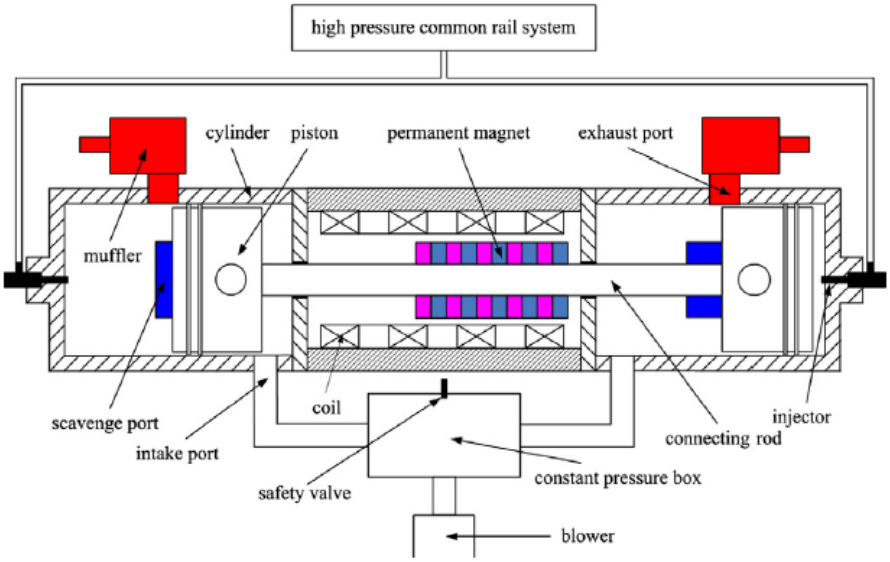

Figure 2.14 FPEG configuration from BIT [51]

They developed a detailed model for a three-phase, U shaped linear generator with permanent magnets. The model for the linear alternator was shown in Figure 2.15.

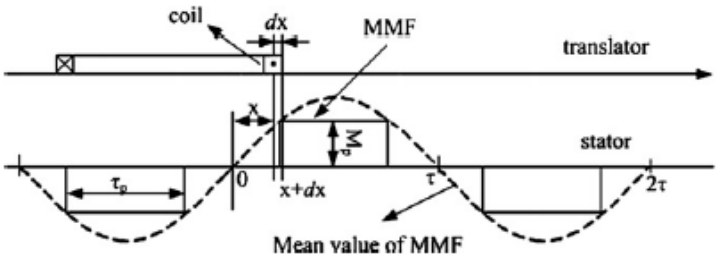

Figure 2.15 Model of the linear electric generator from BIT [51]

The total electromagnetic force produced by a three-phase linear alternator was derived [78]. Moreover, a multi-dimensional investigation on gas flows during the scavenging process of the FPEG was undertaken, based on the numerical simulation results. A wide range of design parameters and operating conditions were investigated to find out their influence on the scavenging performance, which including the effective stroke length, valve overlapping, engine speed and the charging pressure. The cylinder pressure and pressure in the scavenging pump were collected from a running prototype and used to define the boundary conditions [51].

2.2.2 Model simulation

In this section, the model simulation methods used to solve the 1-dimentional numerical models for the FPEG are summarised, aiming to give a general idea of the possible simulation methods for the future FPEG researchers. Software used in reported FPEG 1 dimensional simulation is listed in Table 2.8. Matlab/Simulink is found to be the most widely used software for the FPEG simulation, and a detailed example of a FPEG model in Matlab/Simulink is shown below.

Research group	Simulation software
Newcastle University	Matlab, Matlab/Simulink
Beijing Institute of Technology	Matlab, Matlab/Simulink
South Korea	Fortran
Sandia National Laboratories	chemical kinetics software HCT
Czech Technical University	Matlab/Simulink
Nanjing Institute of Technology	Matlab/Simulink
Toyota	Dymola

Table 2.8 Software used for FPEG simulation

Researchers at Czech Technical University (CTU) described the modelling and control of a FPEG. The model was based on a simplified description of the thermodynamic process, with the assumption that the gas was ideal and all actions performed by the gas were reversible [83-86]. The model developed was composed several parts, *i.e.* mechanical system model, linear motor-generator model, thermodynamic processes model, the gas state equation and the thermal energy production model. The simulation model build in Matlab/Simulink is shown in Figure 2.16. The model was composed of seven particular sub-blocks, which were consistent with individual parts of prototype. The first block was the intake block, to simulate the pressure and temperature of the intake manifold. The exhaust block simulated the gas pressure and temperature of the exhaust manifold. The cylinder block for both sides were used to simulate the development of mixture, pressure and temperature in the cylinder throughout the engine operation. The mechanic features of the model were described by the block Mechanics,

and the function of the linear electric machine was simulated by the block e-motor. The function of the linear lambda sensor was also described using block AFR [83]. Despite the simplifications in this model, the simulation results showed good correspondence with the real prototype. However, the development of a more accurate numerical model for the thermodynamic process of the FPEG was suggested by them for the future work [83, 84].

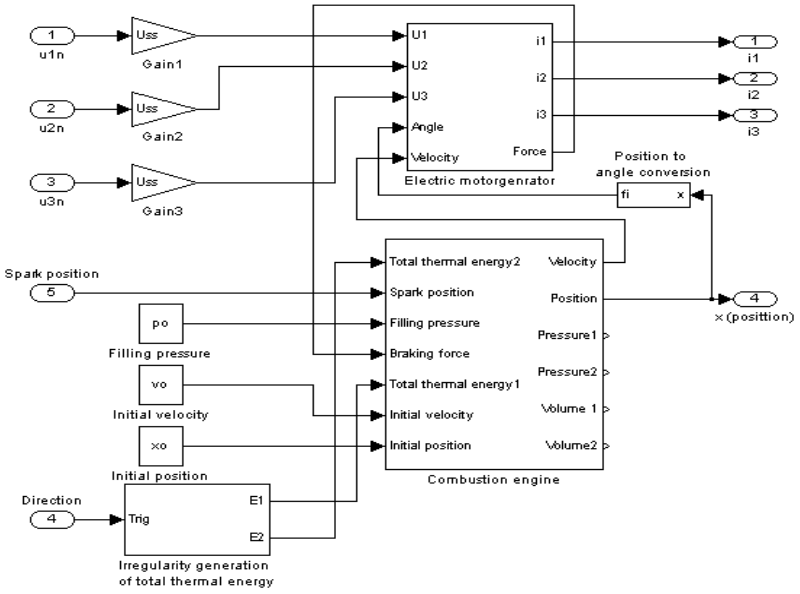

Figure 2.16 Simulation model from CTU [83]

2.2.3 Model linearization method

Modelling and simulation are key elements of machine design, and the FPEG is commonly modelled using zero-dimensional models to obtain the piston dynamics and predict engine performance. There have been detailed numerical models validated and reported, in which the effects of the heat transfer, gas leakage were considered [66, 69, 73] . Many of the numerical models were developed in Matlab/Simulink, and multiple sub-systems were required to represent each equation [24]. However, the differential equations are solved iteratively and require a considerable computational cost, which makes it challenging to be implemented to real-time Hardware-in-the-Loop systems. Therefore, when more complicated control strategy needs to be developed and

implemented, a simplified model is necessary for the further real-time control system development.

A free-piston Stirling engine was considered as a heat driven mechanical oscillator by Redlich *et al.* from which power can be extracted. Linear dynamics was applied to obtain a stability criterion, a means for calculating the frequency, characteristics of the oscillation system, and effects of friction force on starting process and the locus of the roots of the system determinant. Three common configurations of these engines were investigated [87].

G. Nakhaie Jazar, *et al.* presented a nonlinear modelling for a hydraulic engine mount. They introduced a simple nonlinear mathematical model, which showed agreement with the test results available in the literature [88]. Applying the multiple scale perturbation method, they examined the behaviour of the mount at resonance. The nonlinear resonance results in a large amplitude response for a wide range of frequencies, or unstable behaviour at high frequencies, which is not predicted by the linear model [88].

Xiao, *et al.* established a numerical model of a FPEG [12, 15, 89]. The natural frequency of the oscillation system was obtained from their model. A simulation program was developed in Matlab/Simulink to solve these mathematical equations, and the simulation results showed that the motion of FPEG was a forced vibration system with variable damping coefficient and stiffness [89].

Hansson, *et al.* investigated the resonant behaviour of FPEG. They linearized the system after expanding the equation around an equilibrium point [90]. Finally, the approximations of the free-piston oscillation characteristics were achieved. However, only compression pressure forces were calculated in their model, and the pressure increase by the heat release of the gas fuel mixture was not considered. They also investigated how the losses in a free piston engine during starting, stop and idling energy consumption and required power from the supply system [90].

As the gas in the combustion chambers acted like nonlinear spring, the FPEG would behave almost like a mass-spring system. A mass spring system reciprocated with a natural frequency and was preferably operated near, or at, this frequency as this required

the least additional energy. If only pressure forces were considered, the reciprocating frequency of the translator was approximated by Hansson *et al.* as:

$$f \approx \frac{1}{2\pi}\sqrt{\frac{2p_0 A_p \gamma}{m_p L}} \tag{2.6}$$

The pressure p_0 is the cylinder pressure when the translator is in the middle, γ is the gas constant, A_p is the bore, L is the maximal stroke length and m_p is the translator mass.

The engine was operated in a two-stroke gas exchange process, thus every stroke was considered power stroke. Consequently, increasing the engine speed or the operation frequency resulted in an increased power output. From Equation (2.6), it was concluded that if a high operation frequency was expected for high power output, then a low translator mass, short stroke length and large cylinder bore were required [90].

2.2.4 Summary

The FPEG was commonly modelled using simplified zero-dimensional models for conventional engines. Most of the reported models hold for an adiabatic and isentropic processes, in which no heat or mass is gained or lost. However, the actual system cannot be taken as isentropic system because of the low operating speed. The gas leakage through the piston rings from the upstream restriction to the downstream restriction cannot be completely isolated from one another by the piston rings.

At low speed, the in-cylinder gas characteristic is heavily affected by piston speed due to the gas leakage around the piston. Meanwhile, when the charge temperature rises above the wall temperature, gas in the cylinder will release energy, which affects the piston's dynamics as well according to the model validation above. Thus, the ideal gas relationship is not sufficient for the present modelling of FPEG. Moreover, the reported models for friction force were commonly taken as a constant value [1, 10, 66], which is not that accurate. Furthermore, there hasn't been any model validation reported due to the limited amount of test data from the running prototype.

2.3 Prototype design and testing approach

In recent years, different prototype designs have been reported using the FPEG concept. In Chapter 2.1.3, the FPEG configurations were categorised in four different types, *i.e.* single-piston two-stroke engines, dual-piston two-stroke engines, opposed-piston two-stroke engines, four-stroke engines. This section gives an overview of known FPEG development on each categories, with an emphasis on reports where prototype performance data have been reported.

2.3.1 Single-piston two-stroke FPEG

Researchers at German Aerospace Centre analysed several power packs for hybrid powertrains and concluded that both super capacitors and FPEG could be used as future candidates to fuel cells in terms of efficiency and cost [46-48, 91, 92]. As shown in Figure 2.17, the FPEG prototype developed by them consisted of three main subsystems: an internal combustion engine, a linear generator and a gas spring system [93]. The internal combustion engine was operated on a two-stroke gas exchange process, with two inlet and two outlet valves equipped on the cylinder head. Direct fuel injection was applied to reduce emissions. The cylinder dead volume at TDC had been minimized to achieve sufficient compression ratio at short stroke. The size of the generator was reported to be sufficient to extract the energy input to the system [92, 94].

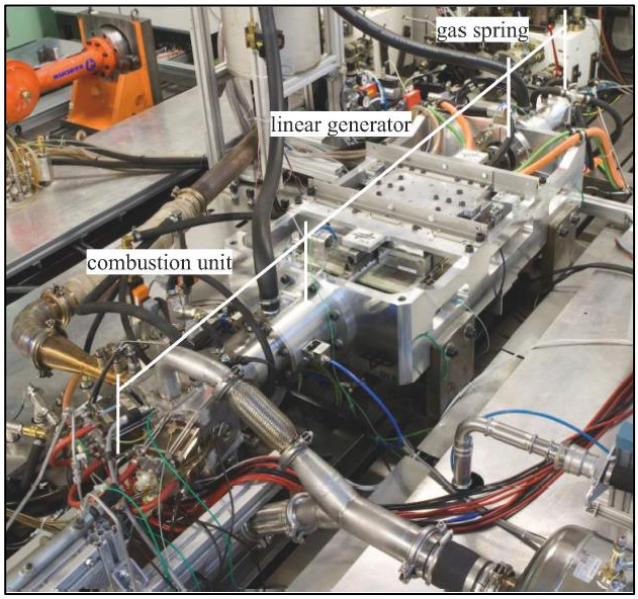

Figure 2.17 FPEG test bench from German Aerospace Centre [94]

The specifications of the prototype are summarised and shown in Table 2.9. From the test results, the external forces of the three subsystems at one particular operating point was shown in Figure 2.18. The TDC achieve was found to be at 57.5% of the periodic time, and the engine speed was reported to be 21 Hz at this particular operating point [92]. The frequency of the system can only be partly altered by changing setup parameters. The mass of the piston used in this experiment was 25 kg, which could be reduced sharply to 4 kg. A power output of approximately of 10 kW was measure at this stage, and increasing the frequency up to 50 Hz should lead to a power output of 25 kW of a single FPLG system [93].

Bore [mm]	82.5
Stroke[mm]	40-95
Piston mass [kg]	25
Inlet Pressure (bar)	0-3
Fuel Pressure (bar)	100

Table 2.9 Specifications of prototype from German Aerospace Centre [94]

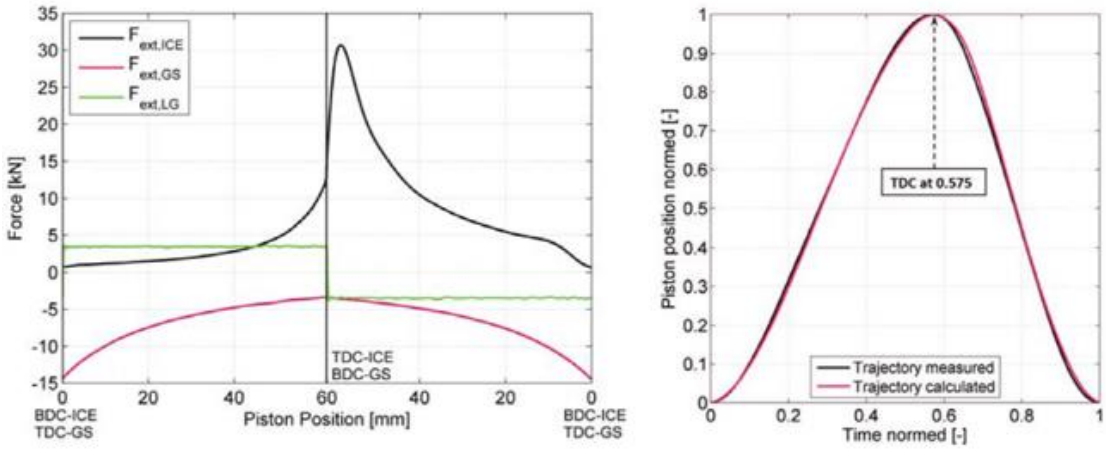

Figure 2.18 Test results from German Aerospace Centre [94]

As demonstrated in Figure 2.19, the FPEG prototype developed by Toyota Central R&D Labs Inc. consisted of a two-stroke combustion chamber, a linear generator and a gas spring chamber, which was similar with that described by German Aerospace Centre. The main feature of this design was a hollow circular step-shaped piston [49].

The smaller side of the piston constituted the combustion chamber, and the larger side constituted the gas spring chamber. An oil cooling passage was built to improve the cooling performance of the piston [49, 50]. The characteristics of the FPEG design are listed in Table 2.10.

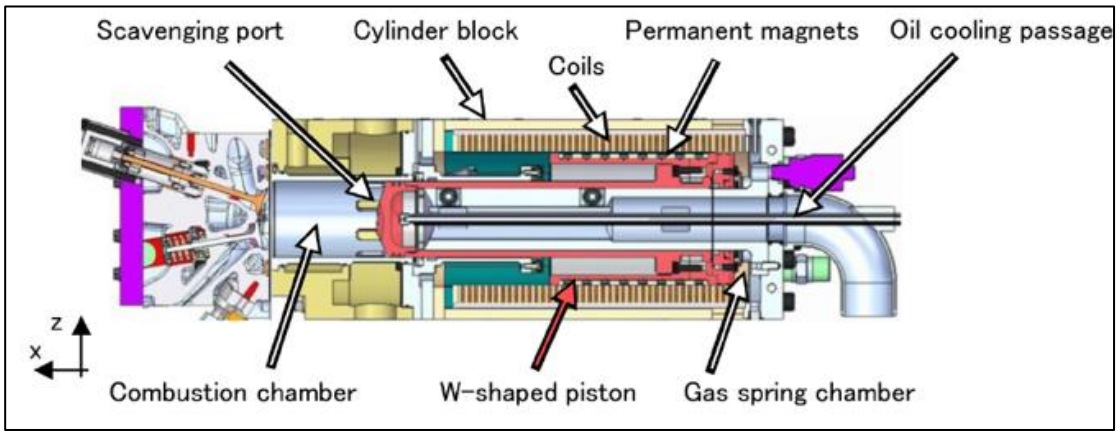

Figure 2.19 Schematic figure of the prototype from Toyota [50]

Outer dimensions of the cylinder block [mm]	200 × 180
Maximum TDC/BDC [mm]	50 /-50
Bore [mm]	68
Maximum stroke [mm]	100
Distance between the poles of the magnets [mm]	33.6

Table 2.10 Characteristics of the FPEG design from Toyota [49]

A power generation experiment was carried out, and the results demonstrated that the prototype operated stably for a long period of time, despite of the abnormal combustion during the test [50]. The unique piston motion and its effect on combustion and power generation in the FPEG prototype were experimentally analysed. Parts of the experimental results were presented in Figure 2.20. Periodic and stable operation was reported to be achieved successfully. A TDC of 45 mm, with a corresponding compression ratio of 6, was achieved without consuming electricity in the compression stroke. The frequency and phase were also well controlled [50].

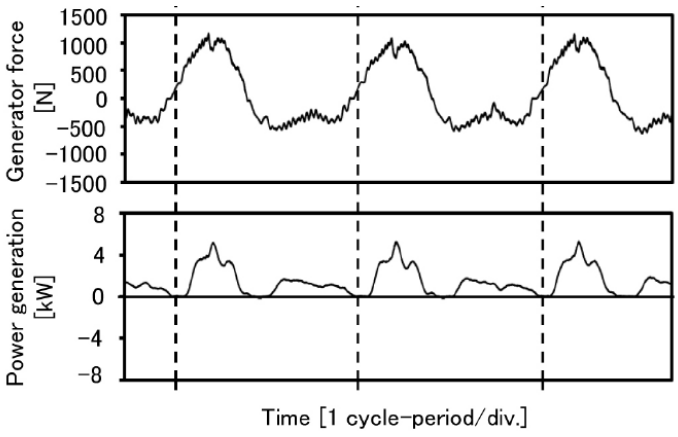

Figure 2.20 Experimental results from Toyota [50]

2.3.2 Dual-piston two-stroke FPEG

Researchers at West Virginia University (WVU) described the development of a spark ignited dual piston engine generator [63]. They have thoroughly documented their work and findings in a number of publications, which concern linear alternator design, design and operation of the combustion engine and analysis of the combined system. A spark-ignited FPEG prototype shown in Figure 2.21 was reported to have achieved 316W power output at 23.1 Hz, with 36.5 mm bore and 50 mm maximum stroke. High cycle-to-cycle variations on the in-cylinder pressure and engine compression ratio were reported, particularly at low loads [63]. The potential reasons for the variations were due to changes in mixture strength, variations in mixture motion within the cylinder, and variations in mixing of fresh mixture, and residual gases within the cylinder during each cycle [63]. The coefficient of variation on the calculated mean effective pressure was reported to be up to 19.9% with the application of the external load [63].

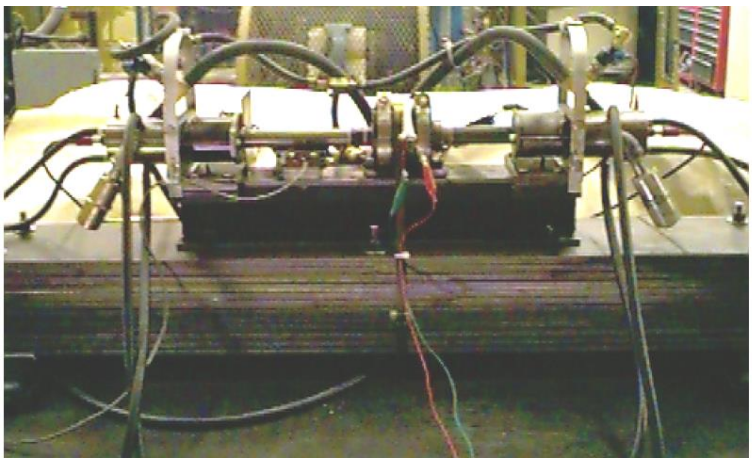

Figure 2.21 Spark-ignited dual piston FPEG from WVU [63]

The fuel was supplied to each cylinder by two pulse width modulated gasoline fuel injectors. Cooling water was forced through the cylinder heads in order to keep the engine temperature within a reasonable operating range. An electronic control device allowed the adjustment of the ignition timing and fuel injection timing and quantity. The engine stroke was controlled by the ignition timing and the amount of fuel injected. The engine was equipped with two motoring coils used as a starting device, which would be automatically disabled after the engine reached a certain frequency. Descriptions of the components are summarised in Table 2.11.

Component	Description
Cylinder/head	Length 102mm
Pistons	36.5mm Homelite Classic 180 Chainsaw
Connecting rod assembly	Piston-to-main:102mm length, 13mm diameter Main shaft: 508mm length, 29mm diameter
Fuel injector	GM Part 17109448F
Fuel pump	Holley Automotive

Table 2.11 Components descriptions for the spark-ignited FPEG from WVU [63]

Figure 2.22 shows the tested P-V diagram for the right cylinder under no load conditions, with the engine operating at 2914 strokes/min [63]. It was evident from the diagram that there were three distinct regions of work, *i.e.* a small area associated with

gas exchange, a region of positive work at low compression, and a region of adverse work at high compression. It was this adverse work that was primarily responsible for opposing the stroke energy and it can be attributed to the high heat loss (high surface area to volume ratio) and high mass loss (single ring, high ring length to volume ratio) found near the outermost point.

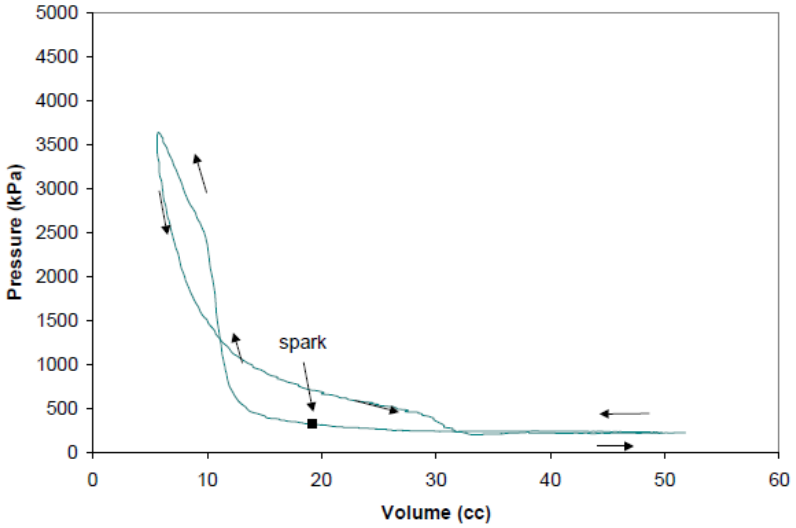

Figure 2.22 Tested P-V diagram under no load condition from WVU [63]

A compression ignition FPEG prototype was also developed at WVU. The engine shown similar mechanical arrangement to the spark ignition prototype and this prototype is presented in Figure 2.23. The fuel delivery system for the engine was performed by a common rail direct injection system, and a high-pressure fuel pump supplied the two injectors. The engine lubrication was provided in a spray through the intake air in sufficient amount to ensure the integrity of the piston rings. The engine was water-cooled, water was forced in to the bottom of the cylinder jackets and out through the cylinder heads. The linear generator was also operated as a starting device, and each cylinder was equipped with glow plugs in order to aid the cold start of the engine [95].

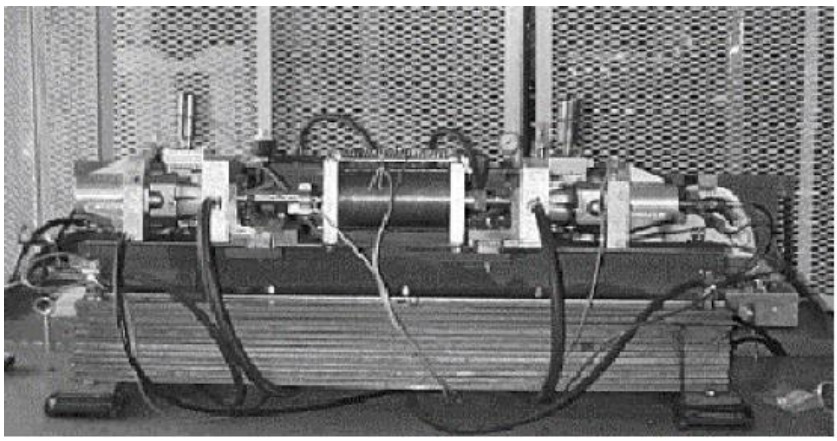

Figure 2.23 Compression ignition FPEG prototype from WVU [95]

The operation of these auxiliaries namely, injectors, fuel pump and the use of the linear alternator as starting device, were controlled by an electronic control unit (ECU). The prototype component description is summarised in Table 2.12.

Component	Description
Cylinders	Kawasaki Jetski 300sx 75 mm bore, 71 mm stroke
Pistons	75 mm Kawasaki Jetski 300sx
Fuel Injectors	Bosch part B 445110130
Fuel Pump	High pressure Bosch part B445010035-01
Rail pressure transducer	Omega part PX 605
Position sensor	Micro-Epsilon part VIP 50-ZA-2-SR-I

Table 2.12 Component description of the compression ignition FPEG from WVU [95]

The research team at Sandia National Laboratory (SNL) presented the design of a dual piston FPEG, shown in Figure 2.24.The engine employed a homogeneous charge compression ignition (HCCI) and aiming to operate on a variety of hydrogen-containing fuels [9, 66]. Test results from a compression–expansion machine showed nearly constant volume combustion with hydrogen, bio-gas, and ammonia at equivalence ratios of approximately 0.3. The target efficiency was 50% overall considering 56% engine thermal efficiency and 96% generator efficiency [9]. They stated that operation on lean mixtures with low mean effective pressures was possible without efficiency penalties because of the low frictional losses in the free piston engine.

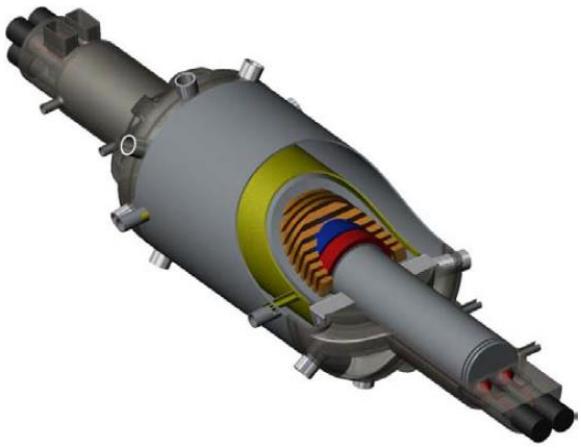

Figure 2.24 Dual piton FPEG prototype from SNL [66]

A European Commission-funded Free Piston Energy Converter (FPEC) project researched the subject of FPEG aimed at developing an efficient new technology suitable for vehicle propulsion, auxiliary power units and distributed power generation since 2002 [3, 44, 68]. Shown in Figure 2.25, the prototype ran on diesel fuel in HCCI mode, and was used primarily for validation of the specific FPEG issues. The engine was equipped with fuel injectors, pneumatic operated valves, cylinder pressure sensors, and translator displacement sensors. The scavenging process was completed by a two-stroke gas exchange process with scavenging ports [3]. However, few test results have been presented in the literature.

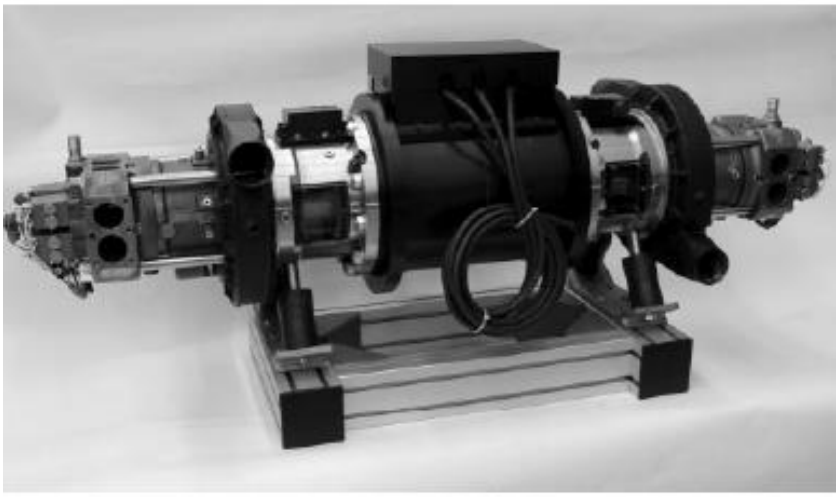

Figure 2.25 FPEG prototype from European FPEC project [3]

Researchers at Beijing Institute of Technology (BIT) developed a spark-ignited dual piston FPEG as shown in Figure 2.26. Experiments had already been done to this prototype and results show that the engines could work for a few cycles but continuously operation had not been reported. According to the cylinder pressure data collected, the engine misfired every one or two strokes and the whole device would power off without the aid of the linear alternator [75]. They also investigated the multidimensional scavenging performance of this engine type with different design and operating conditions to find out the best parameters combination with good scavenging performance [51, 75, 76].

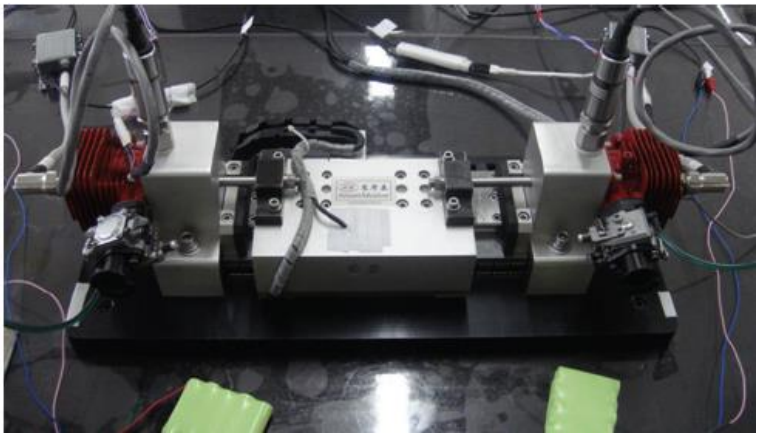

Figure 2.26 FPEG prototype from BIT [75]

Pempek Systems Pty. Ltd., an Australian company, undertook research on this field [96]. The conceptual target of their free piston engine generator was a series type hybrid vehicle which runs as fast as 160 km/h, requires only 5.4 sec for zero to 100 km/h in acceleration, and was equipped with a brake recovery system. For their target, they designed a 25 kW FPEG which shows 50% engine thermal efficiency and higher than 93% of the generator efficiency [97]. FP3, their third prototype, is demonstrated in Figure 2.27. The intake valve operated in a completely passive manner, there were no external controls. The motion of the intake valve was governed by the difference in pressures of the cylinder and compressor acting across the valve, the force of a gas return spring and the dynamics of the mover [97].

The general specifications were summarised as:

- 100 kW peak power
- Displacement 2.82 litres
- 8 cylinders (consisting of 4 free-piston modules, each with 2 cylinders)
- 30 Hz operation – equivalent to 1800 cycles per minute

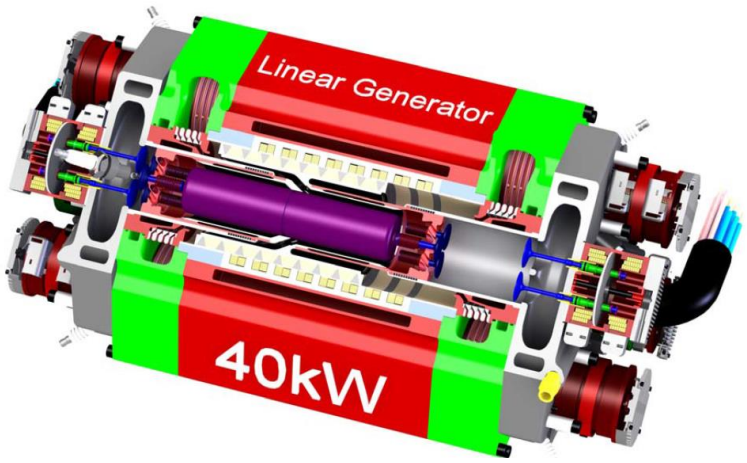

Figure 2.27 Australian FP3 configuration [97]

Shown in Figure 2.28, the FPEG prototype developed by researchers at Czech Technical University (CTU) was a two-stroke, two cylinder combustion engine [83, 84, 98]. The prototype employed two 50ccm cylinders with the direct fuel injectors. These cylinders were from scooter Aprillia SR 50 Ditech. The linear motor generator was a product of VUES Company and was driven through the 3-phase power bridge with IGBT transistors. The ignition unit was capacitor type with one ignition coil, spark was simultaneous on both spark plugs whist combustion took place in the cylinder with gas-fuel mixture. The injectors with the air assisted fuel injection method (product of Aprilia Company) were used in the FPEG. All the described hardware was coupled with the dSpace via an interface board. When the prototype was operated at 27 Hz with a compression ratio of 9:1, the tested average power output was approximately 350 W [84].

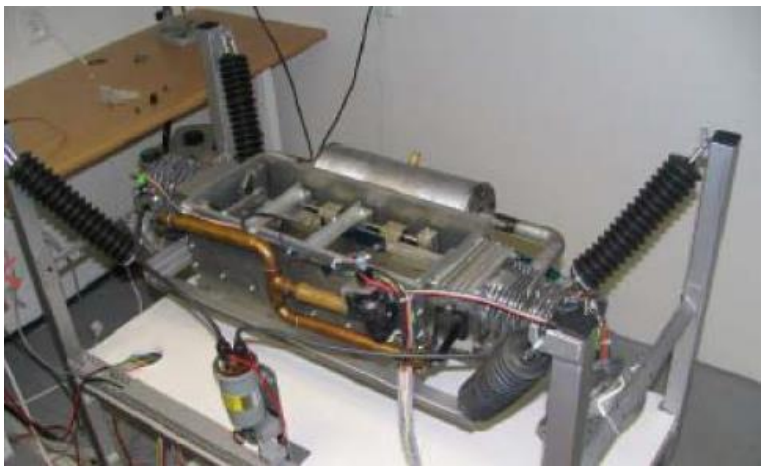

Figure 2.28 FPEG prototype from CTU [84]

Researcher at University of Ulsan, South Korea, presented a FPEG power pack as illustrated in Figure 2.29. It consisted of a two-stroke engine, linear generators and compressors [99-103]. Propane was used as fuel, and wide open throttle was applied. The air and fuel mass flow rate were varied by a mass flow controller and premixed by a pre-mixing device, and then supplied to each combustion chamber directly. The test results indicated that the power generation varied with different operating conditions. With the operating conditions set as in Table 2.13, the piston oscillation frequency was 57.2 Hz, and the maximum generating power was 111.3 W [99].

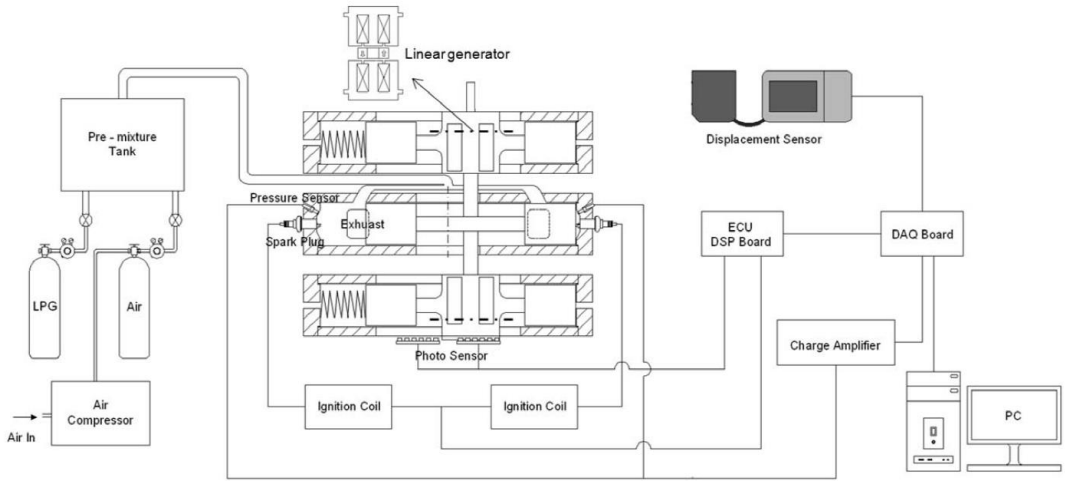

Figure 2.29 A schematic diagram of the experimental system from South Korea [99]

Parameters [Unit]	Value
Equivalence ratio [-]	1.0
Electric resistance [Ω]	30.0
Air gap length [mm]	1.0
Bore [mm]	30.0
Maximum stroke [mm]	31.0
Translator mass [kg]	0.8

Table 2.13 Operating conditions of the prototype from South Korea [99]

2.3.3 Opposed-piston two-stroke engines

In 2008, researchers at SNL changed the dual piston configuration into the opposed piston type shown in Figure 2.30. The opposed piston type was adopted to utilize the self-balance effect, which occurred when the two pistons act together while the combustion took place in between them [104, 105]. Piston synchronization was achieved through passive coupling of linear alternators. Loads also acted to synchronize pistons, reducing complexity and cost. Stators on either side of centre were tied to a common load, proving a stabilizing force. Currently, the research team in the SNL is looking into the prototype to assess piston synchronization, thermal response and compression ratio control. They have plans to measure the indicated thermal efficiency and emissions at various compression ratios and equivalence ratios with hydrogen and other resources [105].

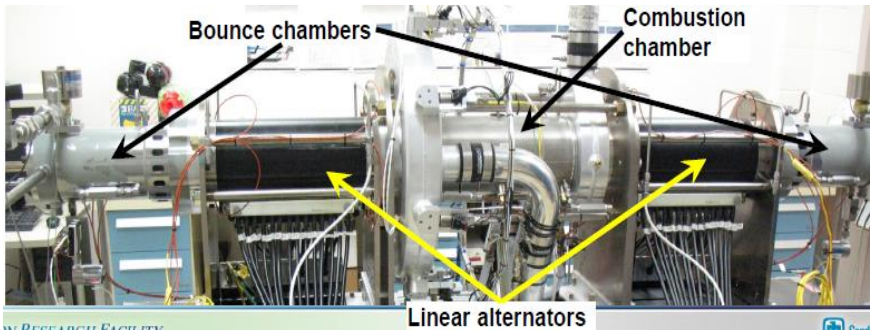

Figure 2.30 Opposed piston FPEG prototype from SNL [105]

2.3.4 Four-stroke FPEG

Researcher at Nanjing Institute of Technology (NIT) proposed a novel new FPEG design, which consisted of a single cylinder operating on four-stroke cycle, a linear electric generator, and a mechanical spring system. Shown as Figure 2.31, the spring system was used as a kickback device, because of the low efficiency of the linear generator at low speed. Scavenging was completed through electromagnetic valves at the cylinder head [58, 106-109]. A reversible energy storage device was used to store the electric power output, and a bi-directional power converter was applied to match the linear generator and energy storage device [58, 110].

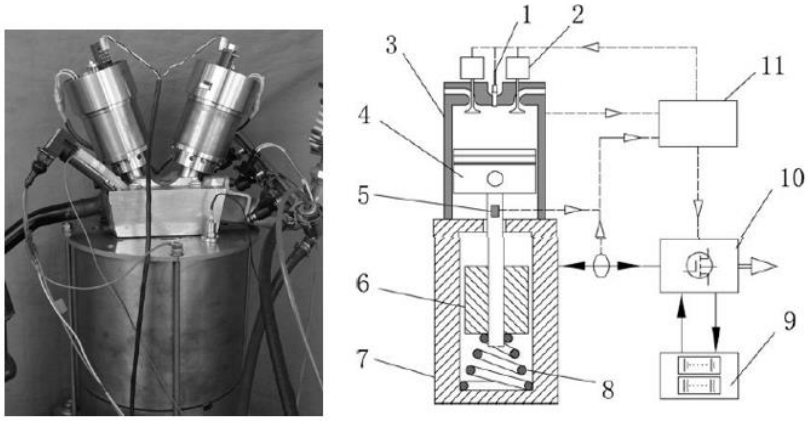

Figure 2.31 Four-stroke FPEG developed by NIT [58]

One complete working cycle of the proposed FPEG system included four strokes. During the intake stroke, the piston was driven by the linear motor, and the fresh charge was drawn to the cylinder through the valve, then the gas fuel mixture was compressed by the spring kickback device to the TDC. The ignition of the mixture initialised the power stroke, and finally the piston was pushed back by the kickback device to expel the exhaust gas. Stable running of the prototype was reported, and some of the test results were presented in Figure 2.32. A 2.2 kW average power output was obtained with an efficiency of 32% [58]. The feasibility and performance of the proposed design were verified and detailed test results were analysed, giving insight into the performance and dynamic behaviours of the novel power system.

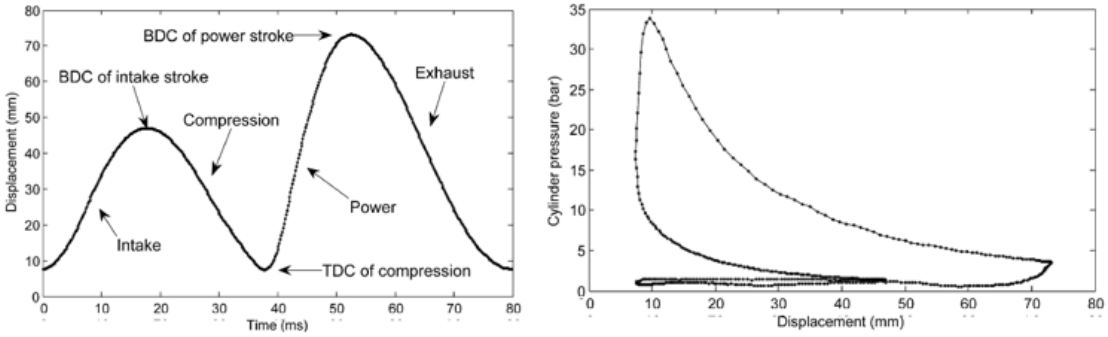

Figure 2.32 Test results of the four-stroke FPEG from NIT [58]

Shown in Figure 2.33, a four-stroke four-piston conceptual FPEG was presented by researcher at West Virginia University. The engine consisted of four pistons linked by a connecting rod to a linear generator. A series of numerical simulations of this type of PFEG were undertaken to predict the engine performance over a wide operating range. Two combustion modes, direct injection compression ignition mode and Homogeneous Charge Compression Ignition (HCCI) mode were simulated and analysed [111].

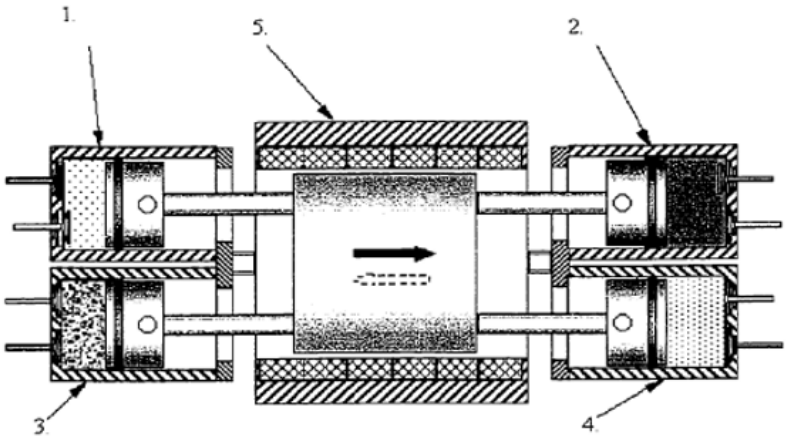

1. Cylinder 1 (Intake); 2. Cylinder 2 (Exhaust); 3. Cylinder 3 (Expansion);
4. Cylinder 4 (Compression); 5. Linear Alternator.

Figure 2.33 Four-stroke FPEG from WVU [111]

Based on the parametric study, a conceptual design for a 15kW FPEG was developed, while engine analysis indicated that this engine had a limited range of operation. When operated in direct injection mode, the efficiency achieved was between 46% and 49%, with the corresponding compression ratio from 17 to 35. If operated as HCCI mode, it was found that this particular mode depended critically on the start of combustion.

Although the HCCI operation allowed to reach an efficiency of up to 60%, the power output was much narrower than operated in direct injection mode, and control strategy was more difficult [111].

2.3.5 Summary

The dual piston FPEG was the topic of most reported prototype research, for which the only moving part is a linear magnet mover coupled with pistons at each end and placed between two opposing combustion chambers. It eliminates the need for a rebound device, as the moving piston provides the force to overcome the compression pressure in the other cylinder. No synchronization system is needed, as combustion occurs alternatively, the expanding exhaust gases drive the piston thus overcoming the compression pressure force imposed by second cylinder. The only significant moving part is the mover of the generator coupled with piston at each end, and located in the middle of two opposing combustion chambers. Due to the advantages mentioned above, the dual piston type FPEG was selected in this research.

2.4 Control strategy

In conventional engines the crankshaft mechanism provides piston motion control, defining both the outer positions of the piston motion (the dead centres) and the piston motion profile. Due to the high inertia of the crankshaft system, the piston motion cannot be influenced in the timeframe of one cycle [112]. In the free-piston engine the piston motion is determined by the instantaneous sum of the forces acting on the mover, and the piston motion is therefore influenced by the progress of the combustion process [73]. Moreover, the piston motion profile may be different for different operating conditions. Variations between consecutive cycles due to cycle-to-cycle variations in the in-cylinder processes are also possible. Controlling of the FPEG engine is a challenging task. In this section, a literature review on the control strategy of the FPEG is presented, giving a general view on the potential unstable running, and control strategies.

2.4.1 Reported unstable running

Mikalson and Roskilly from Newcastle University investigated the FPEG control variables and disturbances using a full-cycle simulation model [40, 113, 114]. The load force from the electric machine was identified as a disturbance to the FPE, and a high influence on both engine speed and dead centre positions was seen [40]. Variations in the injected fuel mass was found to affect the indicated mean effective pressure and peak in-cylinder pressure, and the variations were higher for the FPE than for the conventional engine. This was due to the variations in the combustion energy from one cycle would influence the compression ratio for the next. The combination of variations in both compression ratio and injected fuel mass might give significantly higher peak cylinder pressure variations in the FPEG [40].

A high-speed free-piston diesel engine was developed by Johansen *et al*. aimed at marine applications as an alternative to both gas turbines and traditional diesel engines [115-117]. Timing inaccuracies were reported to lead to disturbance on the piston force balance, and the piston motion would vary from cycle to cycle. A slightly late opening of the exhaust valve would induce to a higher pressure in the combustion chamber and undesired increase in the stroke length [117]. Cycle-to-cycle variations would also induce to pressure disturbance in the intake and exhaust manifold. The variability in the stroke was suggested to be controlled within 2 mm out of a stroke of about 200 mm [115].

The free-piston engine generator (FPEG) prototype developed by Beijing Institute of Technology was reported to misfire frequently, with severe cycle-to-cycle variations [41, 54, 118]. The possible reasons of the variations and unstable operation were analysed. The air/fuel mixture formation might vary from cycle to cycle in cold engine conditions, and the spark and initial flame propagation could have cyclic variations as normal SI engines. Meanwhile, the unstable combustion could lead to an undesired piston profile and then influence the heat release process in the next cycle [41].

The FPEG prototype developed by Toyota Central R&D Labs Inc. was a single piston type with a gas rebound device. A power generation experiment was carried out, and results demonstrated that the prototype operated stably for a long period of time. Pre-

ignition was found to occur during the test, and the cylinder pressure in the combustion chamber increased earlier than the spark timing [49, 50]. As a result, the oscillation frequency was disturbed, and temporary unstable operation was observed. With the help of the designed feedback control system, the system was reported to recover from the unstable state in less than 1 s [50].

2.4.2 Control strategy

A model-based controller was developed for the European Commission-funded Free Piston Energy Converter (FPEC) project, and the general control structure is shown in Figure 2.34. The controller was implemented in a real-time control prototype system and tested on a FPEG simulation model [119]. The controller was consisted of an observer, and output power controller, an ignition time controller, and a servo controller that controlled the velocity of the moving mass. The outer control loop was used to meet the output power requirement, and the inner loop was applied to set the optimal ignition timing for ignition. The electromagnetic force and the input fuel mass were selected as control inputs, and output power and ignition timing were the control outputs [119].

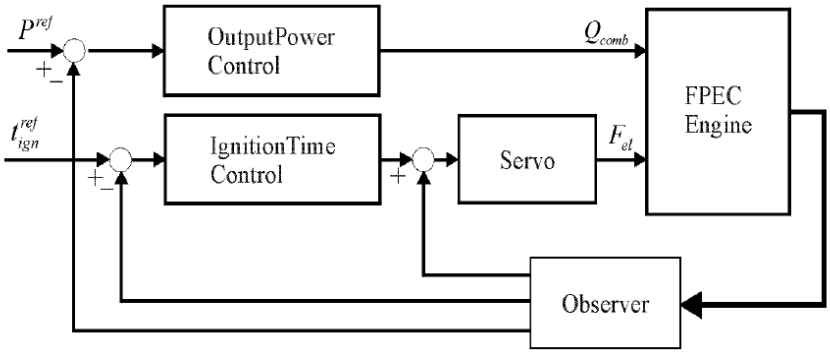

Figure 2.34 General control structure from the FPEC project [119]

Figure 2.35 illustrates the proposed control structure for the FPE presented by Johansen *et al.* [115-117], which was a multi-level control system. The upper level was the supervisory control and optimization, aimed to perform logic control and adapt the operating characteristic. The next level was the piston motion control, where commands were given to the timing subsystems to control the piston motion. At the most bottom

level there was timing control, *i.e.* fuel injection timing and valve timing for each cycle. A hierarchical multi-rate electronic control system was developed for an experimental engine, focusing on piston motion parameter estimation, valve and injector timing, and a piston motion control system. The present results showed that today's electronic control technology provided the required processing capacity and resolution to implement the required control system functionality of modern high-speed free-piston diesel engines. A major challenge was to optimise the engine and control system to get sufficiently high reliability, fault tolerance and robustness [115, 116].

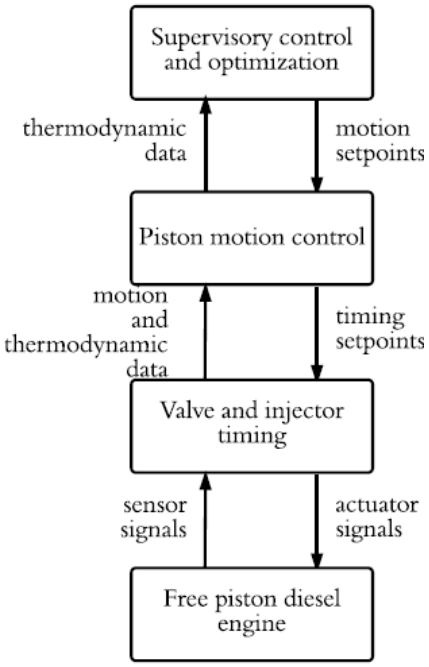

Figure 2.35 Control structure from Johansen [115]

Mikalsen and Roskilly discussed the basic features of a single piston FPEG under development at Newcastle University and investigated engine control issues using a full-cycle simulation model [40, 113, 114]. The control structure was similar to that presented by Johansen. The response of the engine to rapid load changes was investigated using decentralised PID, PDF and disturbance feed forward. It was found that PDF feedback control was more suitable for the FPEG than conventional PID controller, and the control structure for PDF control system is demonstrated in Figure 2.36. The engine was found to be sensitive to immediate electric load changes, whilst the effect of cycle-to-cycle combustion variations was reported not critical. It was

concluded that the control of the FPEG was a challenge, but the proposed control strategy was feasible [113].

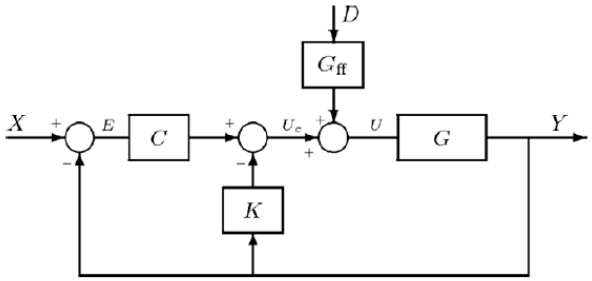

Figure 2.36 PDF control system with disturbance feedforward [113]

To reduce the time delay in the control loop, a predictive control system was further proposed by Mikalsen and Roskilly, which is shown in Figure 2.37. The piston TDC was predicted from the piston velocity in the compression stroke, rather than measured from the previous operation cycle to improve the dynamic performance of the controller. Significant improvement was observed using the proposed control method compared with the conventional PI feedback controller, including a faster response and lower error [114]. The TDC prediction process and the controller performance are demonstrated in Figure 2.38. The proposed control scheme was suggested to make use of a more advanced fuzzy control system to take the nonlinear and multi-variable characteristic of the control problem into consideration [114].

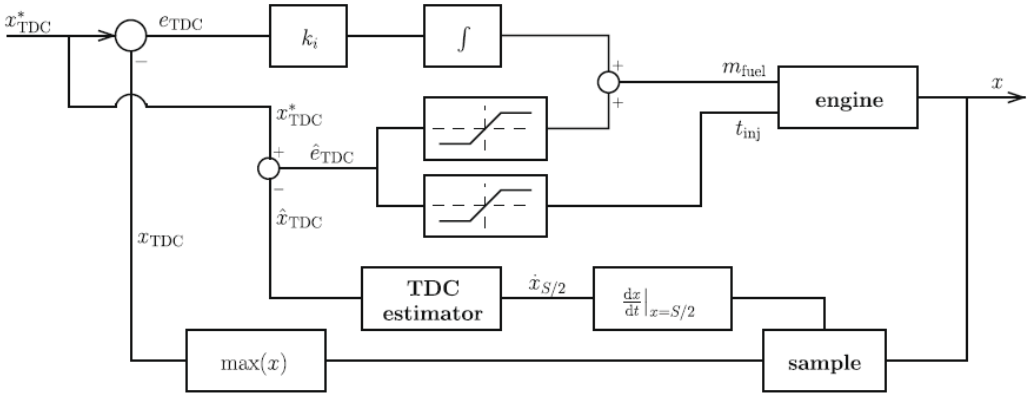

Figure 2.37 Predictive control system [114]

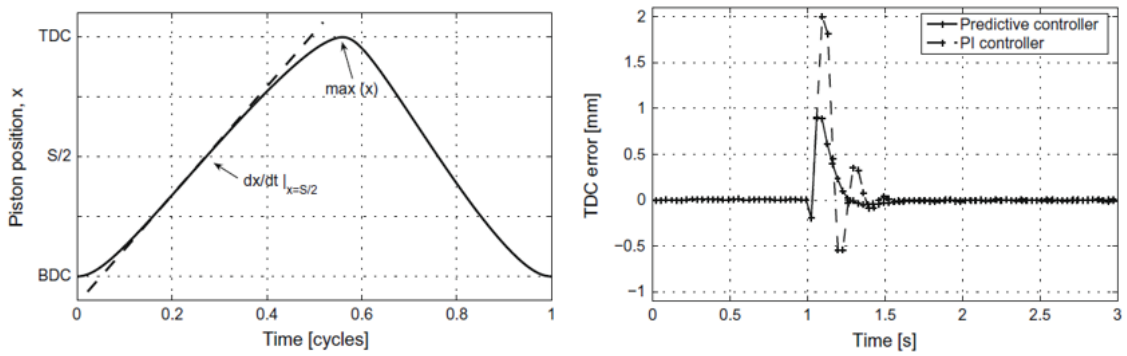

Figure 2.38 TDC prediction illustration and controller performance [114]

2.4.3 Summary

As the piston motion of FPEG is not restricted by a crankshaft - connection rod mechanism, the piston is free to move between its TDC and BDC, and the movement is only controlled by the gas and load forces acting upon it. This induces to problems such as difficulties in starting process, misfire, unstable operation and complex control strategy [1, 25, 28]. For different configurations, the control objectives varies and they are summarised in Table 2.14.

FPEG configuration	Control objectives	
	Similarity	Difference
Single piston	○ System's demands for energy ○ Reach target TDC • Ensure compression ratio • Avoid mechanical contact ○ Timing control • Valve timing • Ignition timing • Injection timing	○ Control of rebound device ○ Engine frequency
Opposed piston		○ Synchronization control ○ Rebound device control ○ Engine frequency
Dual piston		○ Accurate BDC control (TDC for the other side)

Table 2.14 Control objectives for different configurations

To meet these challenges, a robust control system is required for the FPEG. Control of piston TDC position is crucial for stable operation. It should be controlled within tight limits to ensure sufficient compression ratio for ignition and efficient combustion, and also to avoid mechanical contact between the piston and cylinder head. However, the

implementation of an effective control strategy to a prototype still needs to be investigated.

2.5 Summary

This chapter has presented recent research reported on the FPEG development, including numerical modelling, prototype design, and control strategy. Previous publications and patents on the FPEG were reviewed and summarised in the chapter, providing a useful reference for the future research on this subject. Despite the progress made to this technology, the FPEG is not commercially successful, and challenges still exist in this promising energy conversion device.

The FPEG has commonly been modelled using simplified zero-dimensional models for conventional engines. Most of the reported models hold for an adiabatic and isentropic process, in which no heat or mass is gained or lost. However, the actual system cannot be taken as an isentropic system because of the low operating speed. Moreover, there hasn't been any extensive model validation reported due to the limited amount of test data from running prototypes. There have been various FPEG prototypes reported, however, very few of them are successful. The lack of crankshaft mechanism makes it difficult to start, and prone to unstable operation, and a robust control strategy is necessary for the FPEG. In summary, a validated numerical model and an effective control strategy are still needed to fully understand the operating characteristics of FPEGs.

Chapter 3. Design and modelling of a two- or four- stroke FPEG for range extender applications

FPEGs are known to have a greater thermal efficiency (40-50%) than an equivalent and more conventional reciprocating engine (30-40%) [3, 24]. Attempts to improve the thermal efficiency have resulted in numerous FPEG configurations which are almost exclusively operated using a two-stroke thermodynamic cycle. Whilst common, it is well known that the application of two-stoke cycles in conventional reciprocating engines are limited by noise and exhaust gas emissions. In this chapter, a numerical model was developed to investigate the technical feasibility of operating Newcastle University's FPE prototype design in both a two- and a four-stroke thermodynamic cycle.

3.1 Working principle description

3.1.1 Prototype schematic configuration

The conceptual design of a dual-piston FPEG is based on the patent by Mikalsen and Roskilly [120], and is illustrated in Figure 3.1. The prototype comprises two opposing internal combustion cylinders, each with its corresponding combustion chamber, set of poppet valves (5&6), spark electrode (1) and piston (2). A linear electric machine (8) is located between the opposed cylinders/pistons. The two pistons are connected using the mover (7) of the linear electric machine, this component is the only significant moving part of the system.

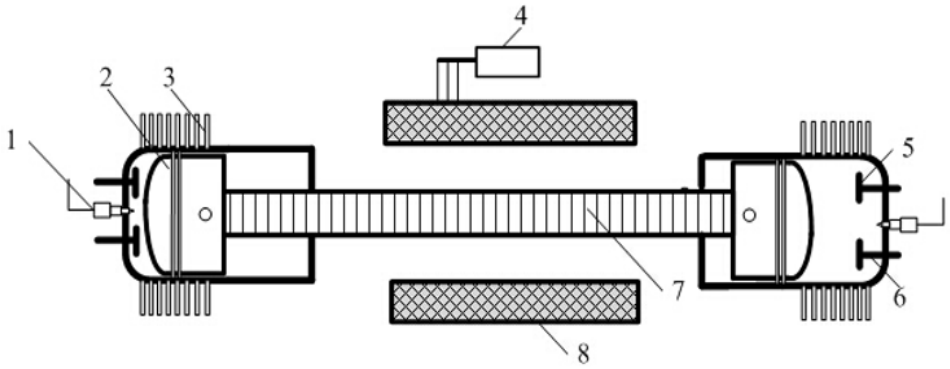

1 Spark plug; 2 Piston; 3 Cooling fin; 4 Load; 5 Intake valve; 6 Exhaust valve; 7 Mover; 8 Stator

Figure 3.1 Prototype schematic configuration

In general terms, the starting process is initiated by operating the linear electric machine as a motor, however once the system is operating at steady-state the machine will be switched to "generator" mode. Switching between motor/generator is managed using an active controller supports the current vector control system, which will drive or brake the piston assembly in real time to ensure a stable operation and meet the target of compression ratio and power output. Without rotational motion and corresponding camshaft timing system, the engine employs an alternative independent intake and exhaust linear actuated valves control system [120].

The majority of reported dual-piston FPEG configurations such as the one employed here use a conventional two-stroke thermodynamic cycle, *i.e.* the power stroke is controlled to take place alternately in each cylinder and to drive the compression stroke of the other cylinder. However, the hardware employed in this configuration can be extended also operate on four-stroke thermodynamic cycle by simple modification of its control parameters, *i.e.* fuel flow rates, spark timing, intake/exhaust valve timing and working mode of the linear electric machine. Hence, by performing the intake and compression strokes separately from the expansion and exhaust strokes, the FPEG can operate on a four-stroke cycle [120].

3.1.2 Two-stroke cycle control mode

The two-stroke thermodynamic cycle operation in each cylinder results in a steady but reciprocating motion of the piston assembly. The power stroke takes place alternately

by each cylinder and the linear electric machine is operated as a generator throughout the generating process. The two strokes are:

(1) Compression stroke: Initiated when both the intake valve and exhaust valve are closed by the control system. The air-fuel mixture in the cylinder is compressed until the system achieves its required equivalent TDC or Compression Ratio (CR).
(2) Power stroke: The timing of the start of the power stroke is controlled using the spark timing and corresponding ignition and expansion of the mixture, the piston assembly is driven backwards by the expanding exhaust gas. Next the exhaust and intake valves are opened by the control system and the burnt gas exits the cylinder and the fresh charge is drawn into the cylinder.

3.1.3 Four-stroke cycle control mode

Similar with the working principle of traditional four-stroke engine, each cylinder in the FPEG requires four strokes of its piston assembly or two oscillation cycles to complete the sequence of events which complete a single power stroke. The four-stroke cycle of the FPEG comprises four processes [120]:

(1) Intake stroke: The stroke is initiated when the piston approaches its equivalent TDC and the intake valve is opened by the control system; and is terminated by the closing of the intake valve when the piston is at its required BDC.
(2) Compression stroke: Initiated when both the intake and exhaust valves are closed by the control system, and the air-fuel mixture is compressed by the piston. The end of the compression stroke is controlled by controlling the spark timing and initiation of flame propagation (heat release).
(3) Power stroke: The expanding exhaust gases drives the piston assembly toward its BDC, and the linear electric generator converts part of the kinetic energy of the moving mass to electricity.
(4) Exhaust stroke: Initiated by control of the exhaust valve opening time and terminated as the exhaust valve is closed at its required TDC. The exhaust gases exit the cylinder, and the cycle is restarted after the exhaust valve closes.

3.1.4 Comparison

The sequence of process steps for each cylinder and the corresponding control modes associated with the linear machine for the two simultaneous cycles are summarised in Table 3.1. When operated in two-stroke cycle control mode, the sequence of process steps for the two simultaneous cycles are complementary. However in four-stroke cycle control mode, the simultaneous process steps are not complementary throughout the cycle and the non-power stroke must be driven by the linear electric machine.

3.2 Numerical model description

What follows is a description of the numerical model for a FPE generator. This model is built on many of the same principles and assumptions of 0/1D thermo –fluid dynamics sub-models employed routinely across the engine research and development community [121-123]. The main differences relate to how the piston /in-cylinder gas interacts with a linear generator/motor.

3.2.1 System dynamic sub-model

As the same hardware will be employed to operate on both two- and four-stroke cycle control modes, the basic geometrical relationships and the equations used to characterise the engine operation are identical. The forces acting on the pistons are from the in-cylinder gas (from both cylinders), linear electric machine, mechanical friction and the inertia of the moving mass. The corresponding dynamic equation is derived as:

$$\overrightarrow{F_l} + \overrightarrow{F_r} + \overrightarrow{F_e} + \overrightarrow{F_f} = m\frac{d^2x}{dt^2} \tag{3.1}$$

Where F_l (unit: N) and F_r (N) are the gas forces from the left and right cylinders respectively; F_e (N) is the force output from the linear electric machine – a parameter which is varied depending if the machine is operated in motoring or generation modes; F_f (N) is the mechanical friction force; m (kg) is the moving mass of the piston assembly with the mover of the electric machine, x (m) is the mover displacement.

	Two-stroke			Four-stroke		
	Left cylinder	Right cylinder	Linear machine	Left cylinder	Right cylinder	Linear machine
Stroke →	Power + Gas exchange	Gas exchange + Compression	Generator	Air intake	Air exhaust	Motor
Stroke ←	Gas exchange + Compression	Power + Gas exchange	Generator	Compression	Air intake	Motor
Stroke →	Power + Gas exchange	Gas exchange + Compression	Generator	Power	Compression	Generator
Stroke ←	Gas exchange + Compression	Power + Gas exchange	Generator	Air exhaust	Power	Generator

Table 3.1 Comparison of two-stroke and four-stroke FPEG engine cycles

The gas force can be calculated using the gas pressure, p (Pa) and piston surface area, A (m^2) which can be approximated from the cylinder bore, B(m), as:

$$A = \frac{\pi B^2}{4} \tag{3.2}$$

3.2.2 Friction model

An analysis of engine friction mechanisms in four stroke spark ignition and diesel engines is presented by Heywood [123]. An approximate breakdown of rubbing and accessory friction is: piston assembly 50 percent; valve train 25 percent; crankshaft bearings 10 percent; accessories 15 percent [123]. Friction work in the FPEG is expected to be lower than conventional internal combustion engines due to the elimination of the crank mechanism. Thus the friction in the wrist pin, big end, crankshaft, camshaft bearings, the valve mechanism, gears, or pulleys and belts which drive the camshaft and engine accessories is removed. Frictional losses of FPEG are mainly from the piston assembly, along with the linear electrical machine.

As there is no side forces which act on the piston of FPEG and the movement of the piston is linear, piston assembly friction is dominated by the ring friction, and the friction from the piston skirt is negligible. Thus the friction force of the FPEG is divided to three components, i.e. friction force from the linear electrical machine (F_{fm}) and friction forces between the piston rings and cylinder wall from both left (F_{fl}) and right (F_{fr}) cylinders of the engine. The total friction force is written as follows

$$F_f = F_{fm} + F_{fl} + F_{fr} \tag{3.3}$$

The friction of linear electrical machine comes from the contact of the mover and the stator. It is assumed to be constant as the velocity of the piston is low.

In the model (and prototype) each piston contains two compression rings and no oil ring. The initial tensions in both piston rings hold them out against the cylinder wall and hence generate friction. The in-cylinder gas pressure normally acts on the top and back

of the rings and the pressure acting on the back of the rings increases this radial force and consequently the friction force. Correlations for piston ring friction have been developed in the following categories: boundary condition friction (primarily between the rings and the cylinder wall due to ring tension, and gas pressure behind the compression rings) and viscous ring and piston friction [123]. The component due to ring tension is essentially constant, and the component due to in-cylinder gas pressure behind the rings will vary depending on operation conditions.

Based on the discussion above, an empirical relationship is used to calculate the parameterized friction for the contact between the rings and the cylinder wall [73].

$$F_{fring/liner} = f\left[-sign(v)\cdot A_f\cdot\sqrt{|v|}\right]\left[1-B_f\cdot\frac{E-\theta_0}{\theta_0}\right]\left[1+K_v\cdot\frac{p(t)}{p_0}\right]\left(\frac{d}{d_0}\right) \qquad (3.4)$$

Where f is the overall scaling factor (-); v is axial velocity of piston (m/s) and *sign* (v) means the direction of piston velocity; A_f, B_f and K_v are all friction parameter (-); E is the average temperature of lubrication oil at liner (℃); d is cylinder diameter (mm); p is simultaneous in-cylinder pressure (bar); θ_0 is reference temperature (℃); p_0 is reference pressure (1 bar); d_0 is reference cylinder diameter (165mm).

3.2.3 Engine thermodynamic sub-model

The in-cylinder gas was considered as ideal gas in closed system with corrections such as gas leakage and heat transfer. The analysis of the in-cylinder gas property during the compression and expansion phases of the cycle is based on a zero-dimensional, thermodynamic approach. When the intake or exhaust port is open during the gas exchange process, the in-cylinder pressure is assumed to be ambient pressure. Other important assumptions are: the in-cylinder gas exists as a homogeneous medium, uniform in temperature and composition; the in-cylinder gas kinetic and potential energy are neglected. The thermodynamic model is derived based on the energy conservation equations and the ideal gas equations.

Cylinder pressure description

The in-cylinder thermodynamic processes include the compression/expansion process due to the cylinder volume change, heat transfer from the in-cylinder gas to the wall, heat release due to combustion, gas leakage past the piston rings, as well as the inlet and exhaust gas exchange processes. The important assumptions and simplifications for this sub-model are: the in-cylinder gas exists as a homogeneous medium, uniform in temperature and composition; in-cylinder gas kinetic and potential energy are neglected. Applying the first law of thermodynamics on the cylinder charge gives:

$$\frac{dU}{dt} = -p\frac{dV}{dt} + \left(\frac{dQ_c}{dt} - \frac{dQ_{ht}}{dt}\right) + \sum_i \dot{m}_i h_i \tag{3.5}$$

Where U is the internal energy of the in-cylinder gas (J); V is the volume of the cylinder (m^3); Q_c is the heat released from the combustion process (J); Q_{ht} is the heat transferred to the cylinder wall (J); m_i is the mass flows into or out of the cylinder (kg); h_i is the enthalpy per unit mass of the mass flow (kJ/kg).

As the in-cylinder charge is assumed to be ideal gas, its internal energy is a function of temperature only, giving

$$U = m_{air} C_v T \tag{3.6}$$

The differential form of the equation above is derived as

$$dU = m_{air} C_v dT + C_v T dm_{air} \tag{3.7}$$

Where m_{air} is the mass of the in-cylinder gas (kg); C_v is the specific heat capacity at constant volume (J/kg·K) that is considered constant through the temperature range; T is the temperature of the in-cylinder gas (K).

As the in-cylinder gas follows the ideal gas equation,

$$pV = m_{air} RT, \tag{3.8}$$

the ideal gas state equation is formulated in its differential form for further deriving the model:

$$pdV + Vdp = m_{air} RT + RT dm_{air} \tag{3.9}$$

Using the Mayer's relation for the ideal gas,

$$C_p = C_v + R \tag{3.10}$$

Where C_p is the heat capacity at constant pressure, which is again considered constant through the temperature range.

The ratio of heat capacities γ is expressed as:

$$\gamma = \frac{C_p}{C_v} \tag{3.11}$$

A thermodynamic model is then derived based on the energy conservation equation and ideal gas equations:

$$\frac{dp}{dt} = \frac{\gamma-1}{V}\left(\frac{dQ_c}{dt} - \frac{dQ_{ht}}{dt}\right) - \frac{p\gamma}{V}\frac{dV}{dt} - \frac{p\gamma}{m_{air}}\frac{dm_{air}}{dt} + \frac{\gamma-1}{V}\sum_i \dot{m}_i\, h_i \tag{3.12}$$

Where γ is the ratio of the heat capacities; m_{air} is the mass of the gas in the cylinder (kg),

$$m_{air} = m_{air0} + \int_0^t \dot{m}_{air} dt \tag{3.13}$$

The mass flow rate of the in-cylinder gas can be calculated by:

$$\dot{m}_{air} = \dot{m}_{in} - \dot{m}_{out} - \dot{m}_l \tag{3.14}$$

Where m_{in} is the inlet air-fuel mass through the intake valve (kg), m_{out} is the burnt gas through the exhaust valve (kg), m_l is the mass leakage through the piston rings (kg); and m_{air0} is the initial gas mass in the cylinder (kg).

Mass flow rate calculation

The mass flow rate through the valves and the piston rings are assumed to be represented by compressible flow through a flow restriction. It is determined by temperature, composition, the in-cylinder gas pressure, gas pressure in the scavenging pump and a reference air leakage area [123]. The same equation is used to describe the

mass flow rate of inlet gas through intake valve and the burnt gas through the exhaust valve, as well as the mass flow rate of gas through piston rings, which is [26]:

$$\dot{m}_{flow} = \begin{cases} \frac{C_d A_d p_u}{(RT_u)^{\frac{1}{2}}} \left(\frac{p_d}{p_u}\right)^{\frac{1}{\gamma}} \sqrt{\frac{2\gamma}{\gamma-1}\left[1-\left(\frac{p_d}{p_u}\right)^{\frac{(\gamma-1)}{\gamma}}\right]}, & p_d/p_u > [2/(\gamma+1)]^{\gamma/(\gamma-1)} \\ \frac{C_d A_d p_u}{(RT_u)^{1/2}} \gamma^{1/2} \left(\frac{2}{\gamma+1}\right)^{(\gamma+1)/2(\gamma-1)}, & p_d/p_u \leq [2/(\gamma+1)]^{\gamma/(\gamma-1)} \end{cases} \quad (3.15)$$

Where $\dot{m}_{flow}$ is the mass flow rate through a poppet valve (kg/s); C_d is the discharge coefficient; A_d is the reference area of the flow; T_u is the temperature of the inlet gas (K); p_u is the pressure of the upstream of the flow restriction (Pa); p_d represents the downstream air pressure of the flow restriction (Pa).

The valve curtain area is used to calculate the reference area of the valve [123]:

$$A_d = \pi D_v L_v \quad (3.16)$$

Where D_v is the diameter of the valve (m); L_v is the lift of the valve (m).

Heat transfer

The in-cylinder charge temperature and the flow pattern vary significantly through the cycle. Both of these variables have a major influence on heat transfer. During the intake process, the intake charge is usually cooler than the walls and the flow velocity is high. During compression the charge temperature rises above the wall temperature, and gas velocity decreases, therefore heat is then transferred from the cylinder gas to the chamber walls [123]. The heat transfer between the cylinder walls and the in-cylinder gas is modelled according to Hohenber [124]:

$$\dot{Q}_{ht} = hA_{cyl}(T - T_w) \quad (3.17)$$

Where $\dot{Q}_{ht}$ is heat flow rate (J/s); h is the coefficient of heat transfer (W/m^2·K); A_{cyl} is area of the in-cylinder surface in contact with the gas (m^2); T_w is the average surfaces temperature of the cylinder wall (K).

The heat transfer coefficient is given by [124]:

$$h = 130V^{-0.06}\left(\frac{p(t)}{10^5}\right)^{0.8} T^{-0.4}\left(v_p + 1.4\right)^{0.8} \quad (3.18)$$

Where V is the instantaneous cylinder volume (m^3); v_p is the average piston speed (m/s).

Heat release function

The simulation of the free-piston engine heat release in combustion process is one of the factors with the highest degree of uncertainty in this model. The piston motion of the FPEs differs significantly from that of conventional engines, and very little research result has been reported on how this influences the combustion process for spark ignition FPE engines.[1]. According to previous research, the energy released in the combustion is modelled using a modified Wiebe function [123]. Generally, the Wiebe function is related to the crankshaft angle, however this is not suitable for a linear engine. Therefore, a time based Wiebe function is used to express the mass fraction burned in the combustion process as [10, 51]:

$$\psi = 1 - \exp\left(-a\left(\frac{t-t_s}{C_d}\right)^{b+1}\right) \quad (3.19)$$

$$\frac{dQ_c}{dt} = Q_{in}\frac{d\psi(t)}{dt} \quad (3.20)$$

Where ψ is the fuel mass fraction burned; a and b are shape factors, with the fitting value of 5 and 2 respectively [123]; C_d is the combustion duration with a constant value of 5ms; t_s is the time at which the combustion process starts. Q_{in} is the overall heat input for each cylinder in one running cycle. Combining Equation (3.19) and (3.20), we have:

$$\frac{dQ_c}{dt} = a\frac{b+1}{C_d}\left(\frac{t-t_s{}^b}{C_d}\right)\exp\left(-a\left(\frac{t-t_s}{C_d}\right)^{b+1}\right)Q_{in} \quad (3.21)$$

Equation (3.21) is used to predict the thermal energy delivered to the gas and the resulting pressure in the cylinder.

3.2.4 Linear electric machine sub-model

Energy conversion equation

Linear electric machines are electromagnetic, electrostatic, piezoelectric force devices capable of producing directly progressive or oscillatory translational (linear) motion. They transform electric energy to linear motion mechanical energy via magnetic, electrostatic, etc., energy storage [125-127]. As the electromechanical energy conversion process is reversible, similar with rotary electric machines, they could be operated as motors (from electric to mechanical energy) or generators (from mechanical to electric energy) [127, 128]. The energy transformation processes are generally illustrated in Figure 3.2 for both motor mode and generator mode.

From this standpoint, the linear electric machine used in the FPEG prototype can be operated as:

- a motor to drive the piston to the required compression ratio for ignition during starting process;
- a generator to produce electricity in stable generating operation, and the electrical current is generated from the alternator coils;
- a motor for the four-stroke engine during the non-power stroke.

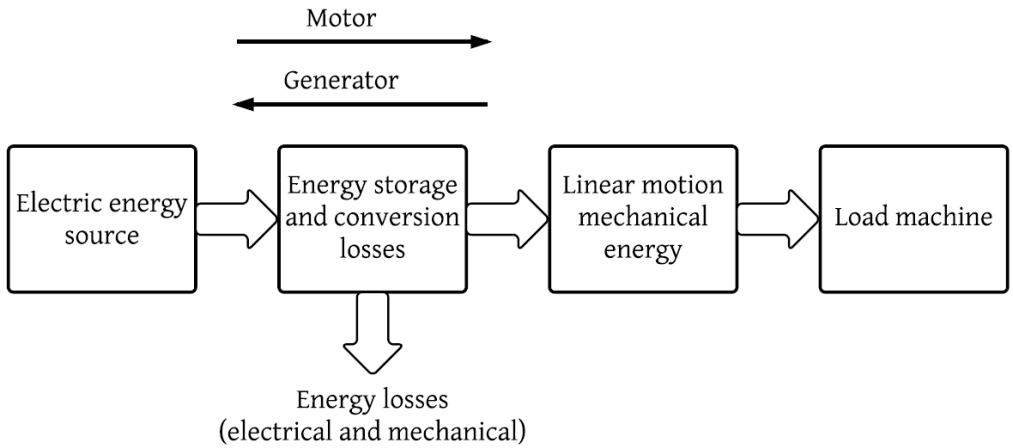

Figure 3.2 Energy transformation process for the linear electric machine

Because the electromechanical energy conversion process is reversible, motors may be operated as linear electric generators, in which case mechanical energy is transformed into electric energy. Energy conservation principles make it possible to determine the magnitudes of mechanical forces arising from magnetic field effects [126]. The fundamental energy conversion equation in the linear electric machine of the FPEG is:

Input mechanical work=Output electric energy + Increase in stored energy + Energy converted to heat

Energy converted to heat can be described by:

Energy converted to heat = Resistance losses + Friction and windage losses + Field losses

If the losses in the system are assumed to be zero, then the energy conservation equation above can be written as:

Input mechanical work = Output electric energy + Increase in stored energy

Or symbolically:

$$F_e dx = \varepsilon i dt + dW_m \tag{3.22}$$

According to Faraday's law, $\varepsilon = d\lambda/dt$ and thus

$$F_e dx = i d\lambda + dW_m \tag{3.23}$$

Where F_e is the mechanical force acted on the mover, i is the current, ε is voltage, and dW_m is the increase in stored magnetic energy, λ is the flux linkage in a coil.

In an electomechanical system, either (i, x) or (λ, x) may be chosen as independent variable. If (λ, x) is taken as the independent variable, the increase in stored energy is given by$W_m = W_m(\lambda, x)$, which can be expressed in terms of small changes as

$$dW_m = \frac{\partial W_m}{\partial \lambda} d\lambda + \frac{\partial W_m}{\partial x} dx \tag{3.24}$$

Substituted it into the energy conversion equation given above, this yields

$$F_e dx = i d\lambda + \frac{\partial W_m}{\partial \lambda} d\lambda + \frac{\partial W_m}{\partial x} dx \tag{3.25}$$

Because the increase changes $d\lambda$ and dx are arbitrary, F_e must be independent of these increase changes. Thus, the coefficient of di must be zero, which means:

$$\frac{\partial W_m}{\partial \lambda} = -i \tag{3.26}$$

Consequently, the energy equation above becomes:

$$F_e = \frac{\partial W_m}{\partial x}(\lambda, x) \tag{3.27}$$

The increase in energy stored during the transition is;

$$W_{m=} \int_{\lambda_2}^{\lambda_1} i d\lambda \tag{3.28}$$

When the flux linkage is increased from zero to λ, the total energy stored in the field is:

$$W_{m=} \int_{0}^{\lambda} i d\lambda \tag{3.29}$$

The term dW_mincludes core losses due to the changing magnetic field. Since these losses are usually small for permanent magnet motor, the model will neglect them. Then the required mechanical force, or electromagnetic force becomes

$$F_e = i\frac{d\lambda}{dx} \tag{3.30}$$

Flux calculation

In previously reported work, different types of linear electric machines for the FPEG device have been investigated. It was found that one appropriate machine for this device that could meet the requirement was the Permanent Magnetic (PM) machine [125]. Moreover, due to the high forces during the combustion process, the pressure on the piston assembly is high. Thus a tubular cross section of the translator was suggested since the forces that act on the translator will be more equally distributed and will have minimum mechanical impact on the translator. Furthermore, there is no net radial force between the armature and stator and no end-windings [127]. As a result, the electric

linear machine used in this prototype applies the tubular configuration with permanent magnetic translator.

The tubular linear permanent magnet synchronous motors, are three-phase distributed or tooth-wound winding primary and PM-secondary tubular configurations with sinusoidal or trapezoidal electromagnetic forces (EMFs), supplied by sinusoidal or trapezoidal bipolar currents, to produce a low ripple electromagnetic thrust [128]. The three-phase (or coil) PM actuator, with short-mover-primary and long-PM-secondary stator, will be investigated. The flux paths in the magnetic system are illustrated in Figure 3.3.

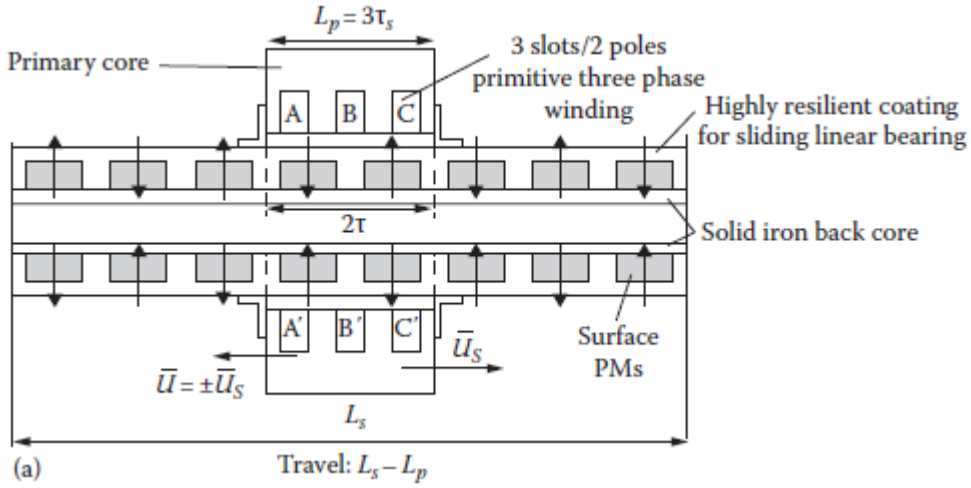

Figure 3.3 Flux paths in the magnetic system [128]

Then the air-gap magneto motive force $M_{PM}(x)$ is a rectangular wave, which may be described by a Fourier series of space harmonics:

$$M_{PM}(x) = \frac{a_0}{2} + \sum_{n=1}^{N}(a_n \cos\theta_e + b_n \sin\theta_e) \tag{3.31}$$

$$\theta_e = \frac{\pi x}{\tau} \tag{3.32}$$

$$a_n = \frac{1}{\tau}\int_{x_0}^{x_{0+2\tau}} M_{PM}(x)\cos\left(\frac{\pi n x}{\tau}\right)dx \tag{3.33}$$

$$b_n = \frac{1}{\tau}\int_{x_0}^{x_{0+2\tau}} M_{PM}(x)\sin\left(\frac{\pi n x}{\tau}\right)dx \tag{3.34}$$

The fundamental component of the rectangular magneto motive force wave was used as an approximation to represent the rectangular wave:

$$M_{PM}(x) \approx \frac{a_0}{2} + a_1 \cos\theta_e + b_1 \sin\theta_e \tag{3.35}$$

$$a_0 = \frac{1}{\tau}\int_0^{2\tau} M_{PM}(x)\, dx = 0 \tag{3.36}$$

$$a_1 = \frac{1}{\tau}\int_0^{2\tau} M_{PM}(x) \cos\left(\frac{\pi x}{\tau}\right) dx = 0 \tag{3.37}$$

$$b_1 = \frac{1}{\tau}\int_0^{2\tau} M_{PM}(x) \sin\left(\frac{\pi x}{\tau}\right) dx = \frac{4}{\pi} M_{PM} \sin\left(\frac{\pi\tau_P}{2\tau}\right) \tag{3.38}$$

Where M_{PM} is the amplitude of the rectangular wave, μ_0 is the vacuum permeability (H/m), τ is pole pitch (m), τ_p is the width of permanent magnet (m).

Then

$$M_{PM}(x) \approx M_{PM1} \sin\theta_e \tag{3.39}$$

Its amplitude of the fundamental component $M_{PM1}$is:

$$M_{PM1} = \frac{4}{\pi} M_{PM} \sin\left(\frac{\pi\tau_P}{2\tau}\right) \tag{3.40}$$

The magneto motive force wave can finally be expressed by:

$$M_{PM}(x) \approx \frac{4}{\pi} M_{PM} \sin\left(\frac{\pi\tau_P}{2\tau}\right) \sin\left(\frac{\pi x}{\tau}\right) \tag{3.41}$$

From the basic magnetic equations, the Magnetic field strength H in the air gap g_0 can be expressed by:

$$H(x) = M_{PM}(x)/g_0 \tag{3.42}$$

Then the magnetic flux density B can be given by:

$$B(x) = \mu_0 H(x) \tag{3.43}$$

Substituting for $H(x)$ and $M_{PM}(x)$ from the equations above yields:

$$B(x) = \frac{4}{\pi}\frac{\mu_0}{g_0} M_{PM} \sin\left(\frac{\pi\tau_P}{2\tau}\right) \sin\left(\frac{\pi x}{\tau}\right) \tag{3.44}$$

The flux $\phi(x)$ in a coil is:

$$\phi(x) = B(x)S(x) \tag{3.45}$$

$$S(x) = \int_{x_1}^{x_2} l_m dx \tag{3.46}$$

The corresponding total flux linkage λ in a coil made of N turns is:

$$\lambda(x) = N\phi(x) \tag{3.47}$$

Substitute for $\phi(x)$ from the equations above yields:

$$\lambda(x) = \int_{x_1}^{x_2} \frac{4}{\pi}\frac{\mu_0}{g_0} N l_m M_{PM} \sin\left(\frac{\pi\tau_P}{2\tau}\right) \sin\left(\frac{\pi x}{\tau}\right) dx \tag{3.48}$$

$$\lambda(x) = \int_{x-\tau}^{x} \frac{4}{\pi}\frac{\mu_0}{g_0} N l_m M_{PM} \sin\left(\frac{\pi\tau_P}{2\tau}\right) \sin\left(\frac{\pi x}{\tau}\right) dx \tag{3.49}$$

Hence:

$$\lambda(x) = -\frac{\mu_0}{g_0}\frac{8}{\pi^2} \tau N l_m M_{PM} \sin\left(\frac{\pi\tau_p}{2\tau}\right) \cos\left(\frac{\pi}{\tau}x\right) \tag{3.50}$$

Then the electromagnetic force can be calculated by:

$$F_e = i\frac{d\lambda(x)}{dx} \tag{3.51}$$

Simplified model for commercial linear electric motor

As the linear electric motor is selected from available commercial linear motors at this early stage, some of the design parameters are protected and remain unknown. It would be difficult to calculate the electromagnetic force using Equation (3.50) and (3.51). As a result, it is necessary to simplify the numerical model to make it feasible with limited amount of motor design parameters known to the users. Figure 3.4 illustrates an equivalent circuit of the linear electric machine.

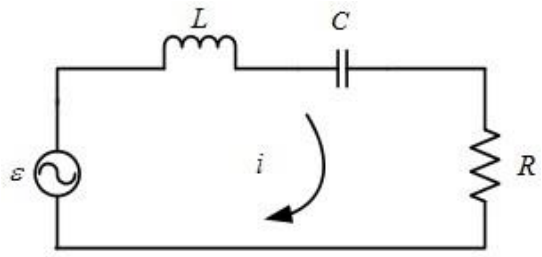

Figure 3.4 Equivalent circuit of the linear electric machine

The voltage across the generator ε can be written as:

$$\varepsilon(t) = -\frac{d\lambda(t)}{dt} \tag{3.52}$$

Then the Faraday's electromagnetic induction laws give the electromotive voltage ε as

$$\varepsilon(t) = -N\frac{d\emptyset}{dt} = -K_v\frac{dx}{dt} = -K_v \cdot v \tag{3.53}$$

Where $\emptyset$ is the magnetic flux; K_v is a motor property and determined by the design parameters of the motor and can be found in the manual.

The induced current is determined by the voltage and the load circuit, which can be derived by:

$$\varepsilon(t) = (R_S + R_L)i(t) + L\frac{di(t)}{dt} + C\int idt \tag{3.54}$$

Where R is the resistance of the circuit, R_S is the internal resistance and $R_L$is the resistance of the external load; i is the current; L is the inductance of the circuit and C is the capacitance.

Assuming the load circuit is purely resistive ($C = 0, L = 0$), the current in the coil is then expressed by:

$$i(t) = -\frac{K_v}{R_S+R_L} \cdot v \tag{3.55}$$

As the load force of the electric machine is assumed to be proportional to the current of the circuit according to electromagnetic theory, the resistance force from the generator is then written as:

$$F_e = -C_e v \tag{3.56}$$

Where C_e is the load constant of the generator, which can be calculated from the physical parameters of the generator design specifications.

3.3 Model simulation implementation

3.3.1 Holistic model structure

The numerical model primarily aims to precisely describe the piston motion which is governed by the Newton's second law. Therefore an engine dynamic model was developed on the top level. The specific forces acting upon the pistons are determined by the in-cylinder gas thermodynamic processes, mechanical friction force and linear electric machine force. Thus three sub-models that describe the abovementioned three groups of forces were developed on a lower level and the calculated forces are fed into the top level dynamic model to determine the piston motion.

The in-cylinder thermodynamic processes include compression or expansion process of the piston, heat transfer from the in-cylinder gas to the wall, gas leakage through the piston rings, and heat release of the combustion process. The scavenging process was also included since a two stroke engine was considered in this work. The friction sub-model describes the friction force acting on the piston rings which is determined by a number of operating factors and is always a resistance force. The linear electric machine force however, can be either a driving force or a resisting force depending on its working mode. A schematic diagram of the model architecture is illustrated in Figure 3.5.

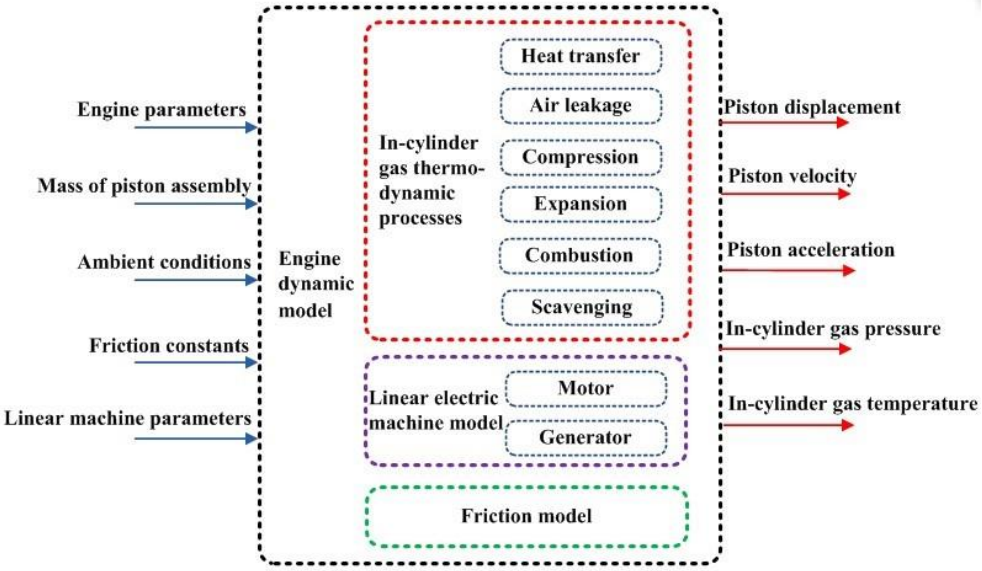

Figure 3.5 Schematic diagram of model architecture

3.3.2 Simulation implementation

The model was developed in Matlab/Simulink. It was calibrated by the parameters from the prototype developed at Newcastle University. As the 2/4-stroke operating modes are employed on the same prototype, the design parameters for the prototype and initial boundary conditions are fixed. The significant differences are the valve timing strategy and the working mode of the electric machine. Both the piston displacement and velocity are selected as feedbacks to determine the valve timing and the mode of the electric machine respectively. The engine dynamic model in Simulink is demonstrated in Figure 3.6. The equations were solved using Runge-Kutta solver with a fixed step size of 10^{-6}. The blocks "PressureLeft" and "PressureRight" in Figure 3.6 represent the cylinder pressure in the left side and the right side respectively, which is calculated using the Equation (3.12). The "Friction" block describes the friction force of the system using Equation (3.4). The block "Electric load force" in Figure 3.6 calculates the output force from the linear electric machine with Equation (3.56).

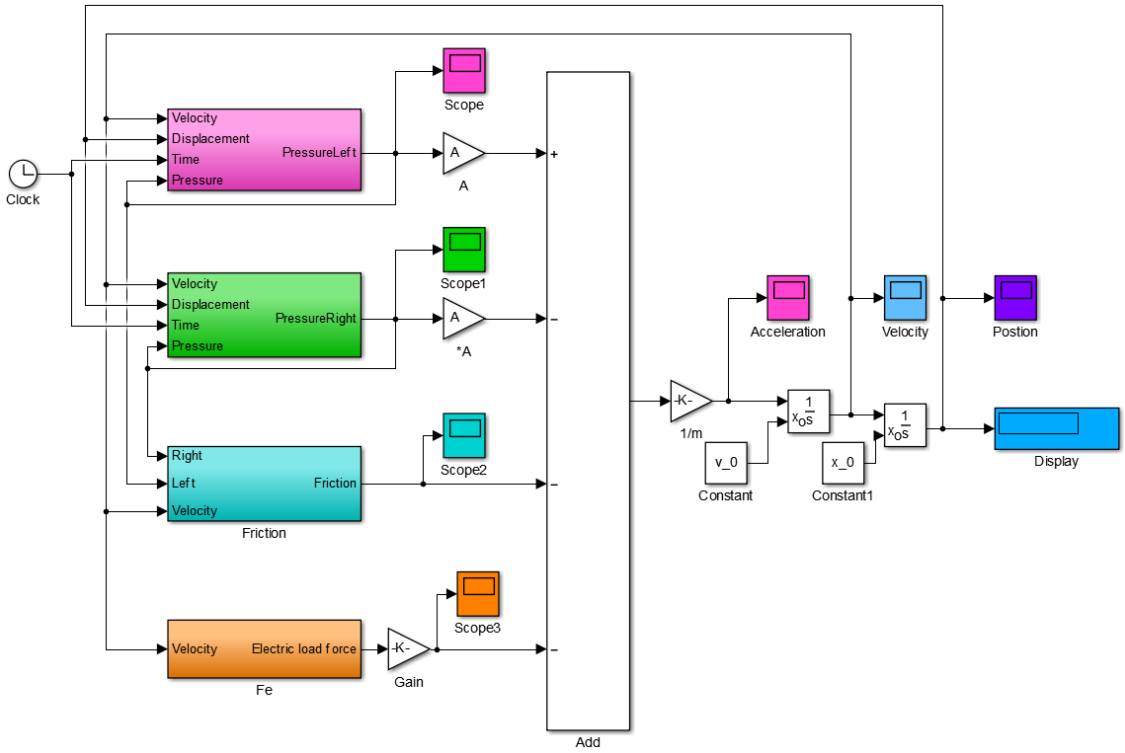

Figure 3.6 Engine dynamic model in Simulink

This model was used for the investigations into both the motoring process and the generating mode. In motoring mode, the combustion sub-model was disabled and the linear electric machine was controlled to work as a motor, i.e. providing a driving force. In generating mode, the combustion sub-model was enabled and the linear electric machine works as a generator, *i.e.* providing a resistance force. An illustration of the in-cylinder gas thermodynamic model in Simulink is shown in Figure 3.7. Six sub-model were built on this level, and they are enabled or disabled based on the piston displacement using State flow Chart function in Simulink.

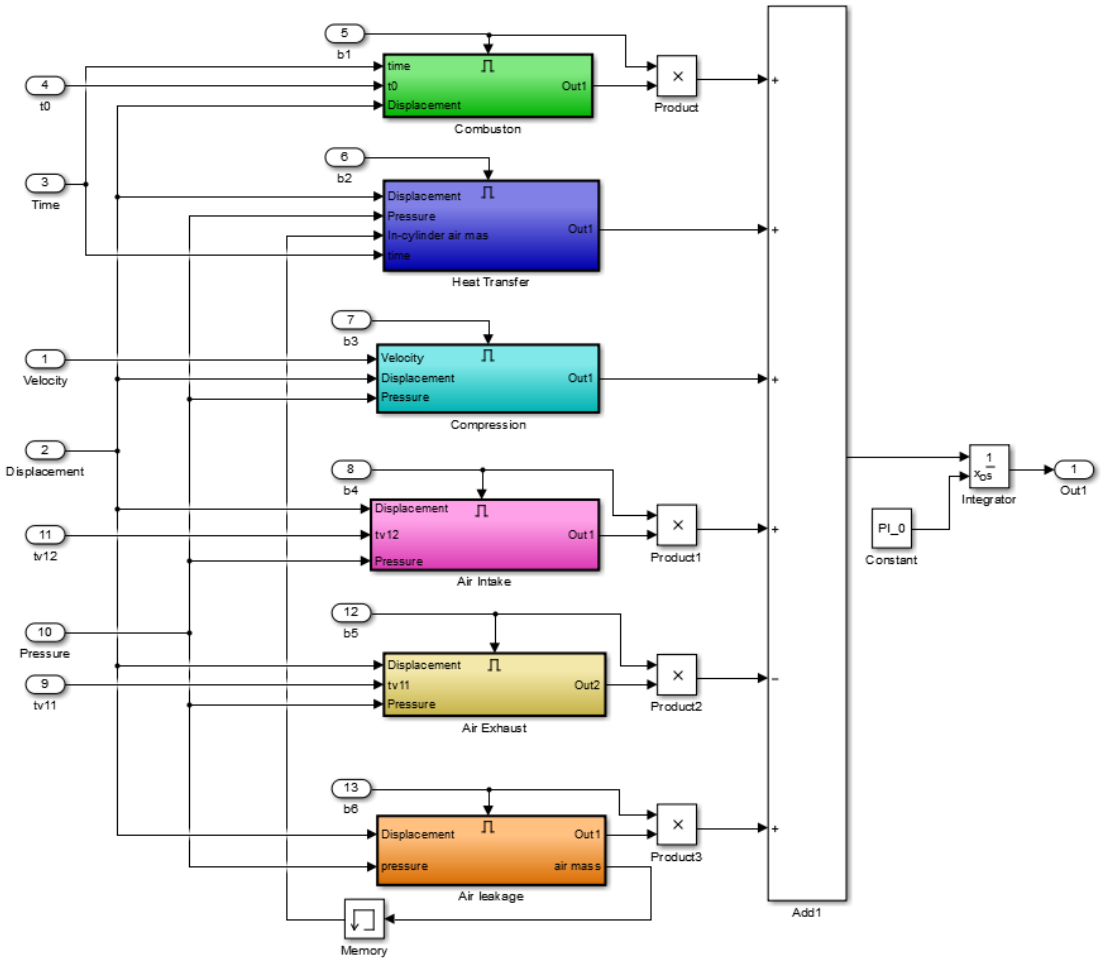

Figure 3.7 In-cylinder gas thermodynamic model in Simulink

3.3.3 Specifications for both cycles

The prototype specifications and the values of the input parameters for both engine operation cycles are listed in Table 3.2. Step functions are used to describe the valve-lift profiles as these proved most consistent with response of the installed air actuated valve system, the opening and closing valve timings were adjusted to optimise the scavenging process. In this paper, the primary goal is to describe the operational domain for this configuration operation based on two-stroke and four-stroke cycles, as such the engine design parameters and the input boundary parameters are not optimised.

Design parameter [unit]	Value
Moving mass [kg]	7.0
Cylinder bore [mm]	50.0
Maximum stroke length [mm]	40.0
Max. intake/exhaust valve lift [mm]	4.0
Intake valve diameter [mm]	20.0
Exhaust valve diameter [mm]	18.0
Intake manifold pressure [bar]	1.3
Exhaust manifold pressure [bar]	1.0
Ignition position from cylinder head [mm]	5.0
Load constant of the generator [$N/(m \cdot s^{-1})$]	810

Table 3.2 Prototype specifications and input parameters

For the designed FPEG configuration operating on a two-stroke engine cycle, a compressor is used to increase the manifold pressure and each outward stroke corresponds to a power stroke. The valve actuation position specifications for the two-stroke FPEG are presented in Table 3.3. As the compression process is initiated after the exhaust valve closes, the maximum compression stroke of the two-stroke FPEG is reduced to 31mm. The scavenging process for two-stroke operation cycle is a combined intake and exhaust gas exchange process, *i.e.* EVO (Exhaust Valve Opening) is actuated before IVO (Intake Valve Opening) and EVC (Exhaust Valve Closing) is actuated after IVC (Intake Valve Closing).

Valve actuation position [unit]	Value
IVO aTDC [mm]	28
IVC bTDC [mm]	34
EVO aTDC [mm]	23
EVC bTDC [mm]	31

Table 3.3 Specifications for two-stroke FPEG

The four-stroke mode FPEG is assumed to be operated at the same condition. However in this mode, the IVO is actuated at the end of the exhaust process when the piston reserves its motion and IVC is at the end of the compression process, thus the maximum compression stroke is 40 mm, thus the compression volume of the four-stroke mode (78.5 cc) is larger than that when operated in the two-stroke mode (60.8 cc). The EVO is actuated at the end of the power stroke when the direction of the piston velocity changes and the valve remains open during the whole exhaust process. As the valves are actuated based on the piston position, the scavenging durations for both operating modes will be significantly affected by the engine speed and piston profile. The corresponding un-optimised valve-lift profiles as a function of piston displacement are illustrated in Figure 3.8.

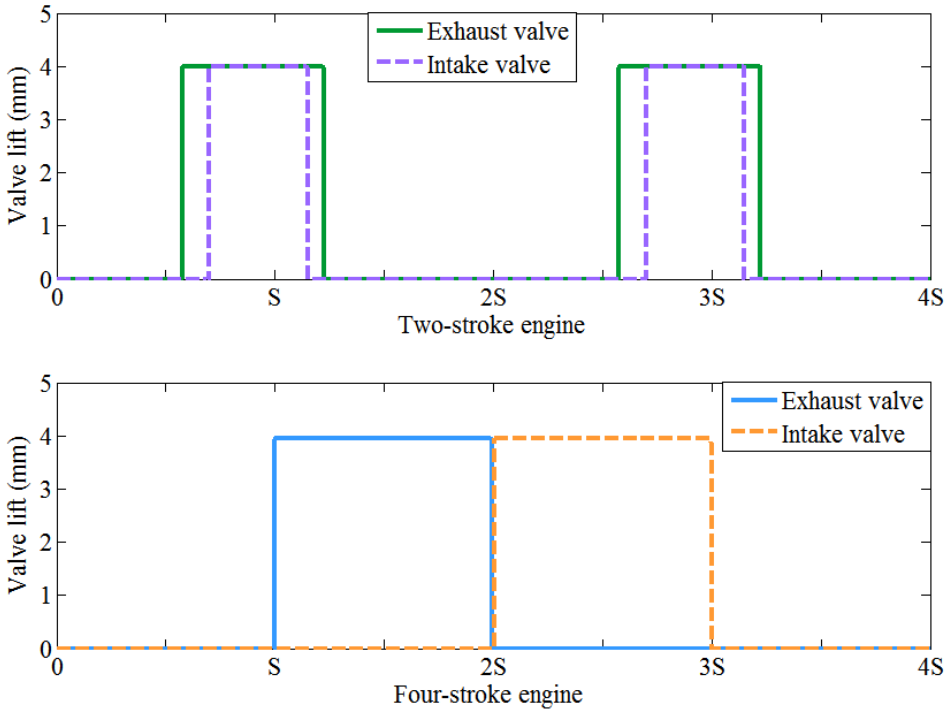

Figure 3.8 Valve-lift profiles for the two-stroke and four-stroke modes

3.4 Summary

This chapter presents the design and simulation of a free-piston engine generator which can be operated using either a two-stroke or four-stroke cycle gas exchange process. The working principles for both gas exchange processes are described and compared.

For the two-stroke cycle, the linear electric machine is operated as a generator throughout, and the system is balanced without external force. For the four-stroke cycle, the system is not balanced and the generator has to be switched to motor mode to drive the piston during the gas exchange process.

Detailed system dynamic sub-model, friction model, engine in-cylinder thermodynamic model, and linear electric machine model were derived and presented. The compression and expansion processes were not regarded as ideal gas isentropic processes; both heat transfer and air leakage were taken into consideration. The model was implemented in Matlab/Simulink. Specifications for both cycles on valve timings were described, and Sequence events for four-stroke operating mode were presented.

Chapter 4. Numerical model validation and simulation results

In this chapter, the model validation and the simulation results for the designed FPEG configuration operating in both two- and four-stroke thermodynamic cycles are described. The piston velocity, displacement, and in-cylinder gas pressure are collected from the prototype and compared with the simulation results. The operation parameters *i.e.* valve timing, ignition timing, etc. are manually tuned and optimised, the simulation is run until the system operation is stable, and the engine performance for two consecutive cycles are identical. In order to avoid misfire and mechanical contact between the piston and cylinder head, for different throttle settings the electric load is reduced correspondingly. The simulation results of the piston dynamics, engine performance, and indicated power distribution are presented, along with a detailed parametric sensitivity analysis. The piston dynamics and the power output with different throttle opening, different ignition timing, and different motor force for the four-stroke engine will be discussed. The main advantages and disadvantages for both operating cycles are summarised, which provides a guidance for the selection of engine operating cycle, as well as for future engine optimisation.

4.1 Model validation

4.1.1 Prototype information

The FPEG developed at Newcastle University is illustrated in Figure 4.1, which was developed by Dr. Mohd Razali Hanipah. It is comprised of two internal combustion cylinders, and a linear electric machine placed between the two cylinders. The two pistons are connected using the mover of the linear electric machine, and this component is the only significant moving part of the system. Spark ignition combustion

mode is used, as it is easier to initialize combustion using a spark plug than traditional compression ignition or homogenous charge compression ignition. More details on the FPEG developed at Newcastle University can be found in [129].

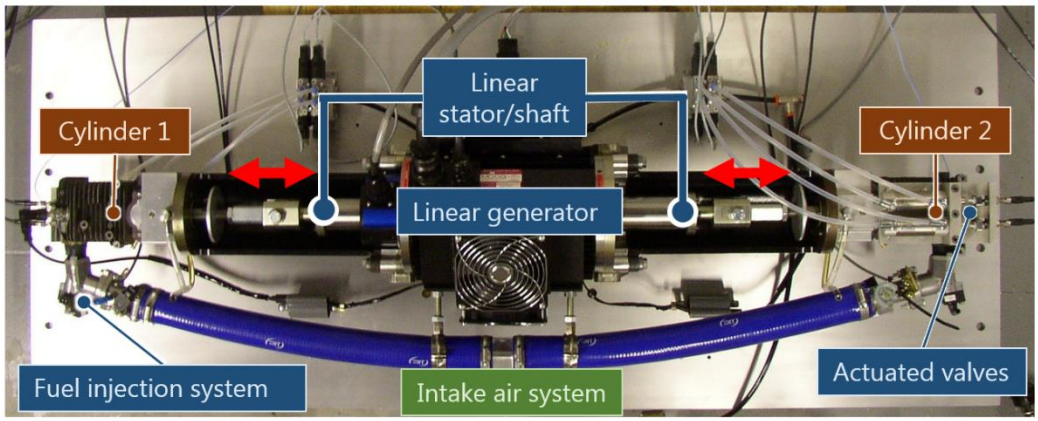

Figure 4.1 FPEG prototype at Newcastle University [129]

Poppet valves are used for both intake and exhaust processes instead of scavenging ports design. The main issue in using scavenging ports for a FPEG is that the port opening and closing timing is controlled by the piston movement, which is fixed during the design process. By applying intake and exhaust valves with independent timing control, the gas exchange process is then decoupled from the piston motion. The prototype specifications and the values of the input parameters are listed in Table 3.2. The main components of the FPEG prototype and the test setup will be described separately.

Free-piston engine

For a conventional internal combustion engine, the engine conversion process usually comprises three stages:

- The chemical energy of the fuel is converted into thermal energy of the in-cylinder gas during the heat release process;
- The high pressure gas pushes the piston backwards, thus producing the mechanical motion of the piston;
- The mechanical energy of the piston is then transformed into rotational kinetic energy of the shaft and flywheel.

For a FPE, this linear motion of the piston can be directly converted into electrical energy by linear electric generator. The engine subsystem for the FPEG prototype comprises all the systems essential to the operation of an internal combustion engine. The cylinder units for the FPEG prototype are modified from a commercial Stihl 4-MIX engine. As illustrated in Figure 4.2, the crankshaft mechanism and flywheel of the original engine are absent, and a cylinder base was added to seal the bottom part of the cylinder.

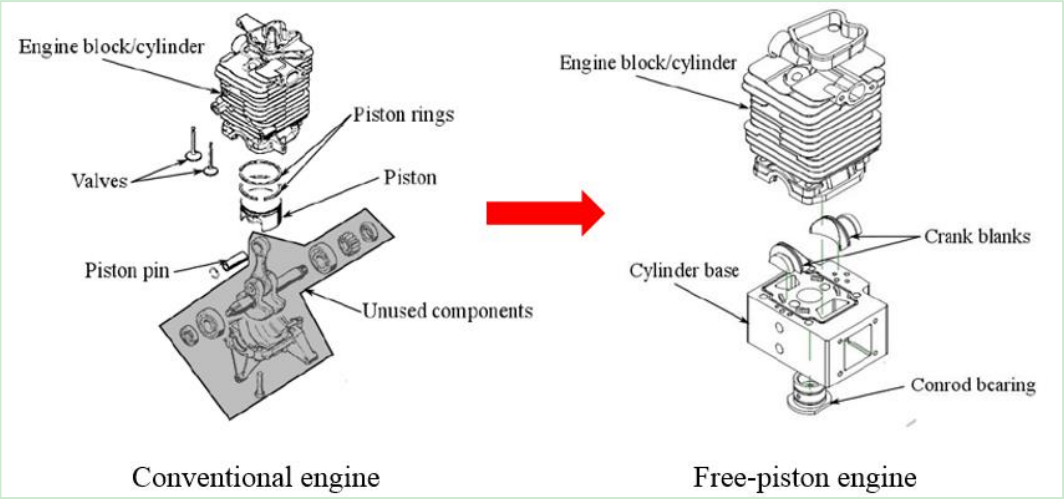

Figure 4.2 Comparison of the free-piston engine with original commercial engine [129]

A Festo pneumatic system was used to activate the valves since it is capable of providing sufficient force. The valve lift was 4 mm, and it is adjustable, which allows for further improvement and optimization of the valve operation. The main pneumatic supply is provided through a manifold at 6 bar before connected via a 6mm inner diameter tubing to the pneumatic cylinder. This valve actuation system has been tested successfully, and it is capable to meet the requirements at 10 Hz engine operation speed.

An electronic port fuel injection system is employed in this prototype, consisting of an intake manifold with throttle, injector, and fuel pump. Petrol is selected as the input fuel, and it is pre-mixed with engine lubrication oil at an oil to petrol ratio of 1:25. The injection timing and injected fuel amount are controlled by the CompactRIO system with a tailored injection control program developed in LabVIEW.

The ignition system used in this prototype is a capacitor discharge ignition system, which consists of a 12 V battery, oscillator-transformer-rectifier circuit, capacitor, coil, and spark plug. The 12 V battery will be stepped to a very high voltage of up to 20 kV by this ignition system, and a spark will be generated to ignite the air-fuel mixture. A Bosch spark plug is selected for this prototype with an integrated AVL pressure sensor model ZI21.

Linear electric machine

The linear electric machine used in the FPEG prototype is intended to be operated as: a motor to drive the piston to the required compression ratio for ignition during starting process; a generator to produce electricity in stable generating operation, and the electrical current is generated from the alternator coils; and a motor for the four-stroke engine during the non-power stroke. However, the available commercial linear motors are limited, and most of them are designed for manufacturing applications rather than electricity generation. A Moog linear motor (model 50204D) was finally selected, shown in Figure 4.3, mainly based on its capability to provide sufficiently thrust force during the starting process.

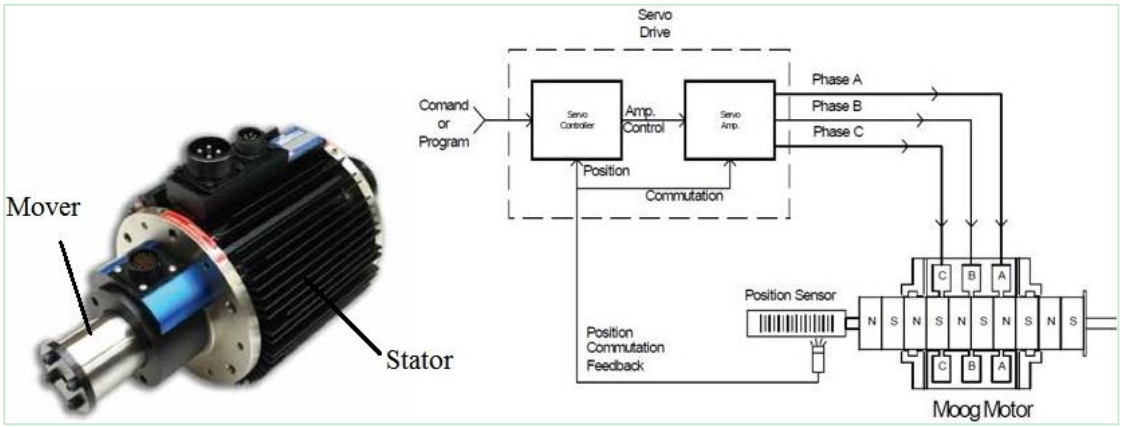

Figure 4.3 Linear generator selected for the prototype at Newcastle University

The Parker model Compax3H was used as the motor drive, which needed to be configured using C3 Manager Software via RS232 connection on a personal computer. The motor is driven via sinusoidal electrical commutation of three-phase coils. The mover's position, velocity, and acceleration information are provided by the linear encoder, and were used as feedbacks to the mover control system. The control

parameters that required to be manually entered in the motion control software include mover starting and stopping positions, speed, acceleration, et al, which set the motion profile.

Control and data acquisition system

The control of the FPEG prototype and the data acquisition are implemented using the National Instrument CompactRIO system, with the program in the LabVIEW software. All sensors and actuators are connected to I/O modules on the CompactRIO system, and the collected data can be stored in the CompactRIO memory temporarily and then streamed to the host PC. A standardised colour coding method was employed for the wirings to avoid incorrect connections. The front panel of the developed program in LabVIEW is shown in Figure 4.4.

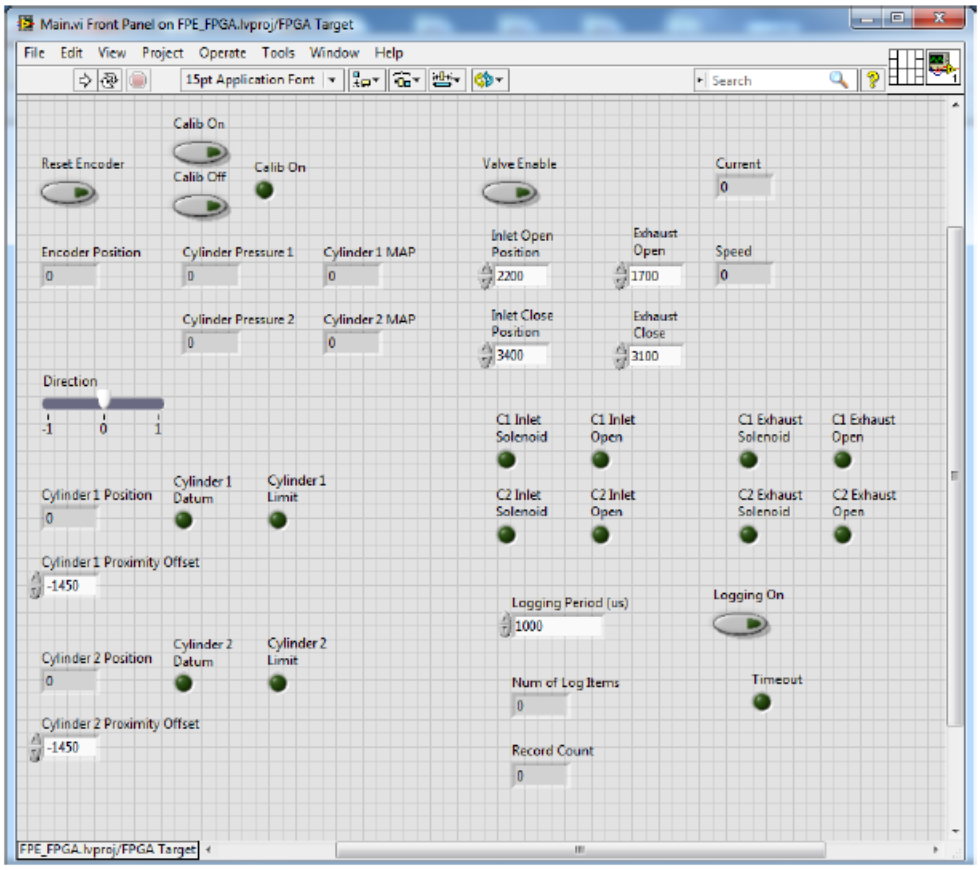

Figure 4.4 Front panel of the developed program in LabVIEW [129]

4.1.2 Control method implementation

The prototype was operated without combustion, and the test data during the starting process was collected for model validation. Validation results for the combustion process can be found in Appendix I. During the starting process, the linear electric machine was operated as a motor to drive the piston to reach the required compression ratio for ignition, and the control method is identical for both the two-stroke mode and the four-stroke mode. The ignition and injection systems were disabled during the motoring process. The motoring experiments have been conducted with the following objectives:

- To evaluate the valve performance;
- To collect the cylinder pressure during the starting process;
- To validate the simulation model developed in Chapter 3.

The linear electric motor was controlled by four parameters during the motoring process as shown in Table 4.1, which are also the inputs to the control software. The piston starts at the home position, and then moves with very high acceleration (1000000 mm/s^2) until it reaches the set speed (200 mm/s). The motion continues with the constant set speed until it reaches the target position 1 (18 mm from the middle stroke). Then the piston reverses and accelerates in the other direction, and employs a constant speed to reach the target position 2 (-18 mm from the middle stroke). The mover with pistons is controlled to follow that pre-set profile. As the acceleration period is minimal compared with the operation period (approx. 0.2% of the operation period from the test results), the piston can be assumed to move between its two target positions with constant speed.

Parameter [unit]	Value
Target position 1 [mm]	18
Target position 2 [mm]	-18
Speed [mm/s]	200
Acceleration [mm/s^2]	1000000
Deceleration [mm/s^2]	1000000

Table 4.1 Control parameters during the motoring process

The control method for the starting process was successfully implemented in the simulation program in Matlab/Simulink as shown in Figure 4.5. And the motor control system for the real FPEG prototype is shown in Figure 4.6. In the simulation, an Embedded Matlab Function was used to take the target position and the speed as input, and then to generate the desired velocity profile. An integrator is used to calculate the piston displacement from the velocity profile. The sub-models introduced in Chapter 3 are employed to calculate the cylinder pressure and friction force. In the cylinder pressure calculation sub-model, the heat release function is disabled during the motoring process, but all the other sub-models mentioned in Chapter 3 remain unchanged.

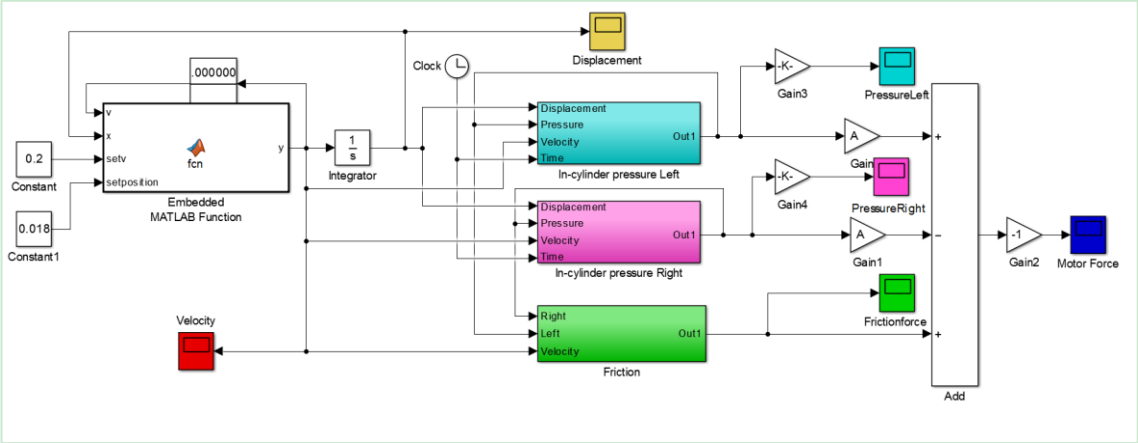

Figure 4.5 Simulink model for starting process

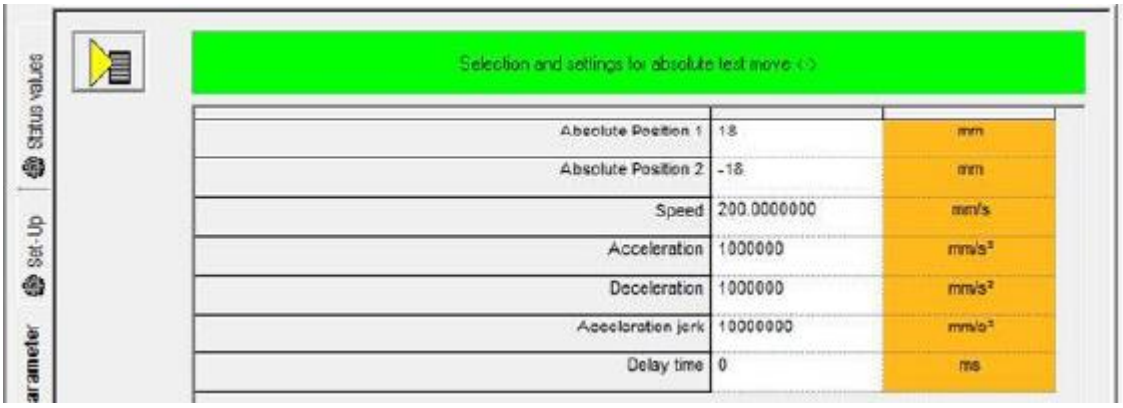

Figure 4.6 Control software settings for starting process [129]

4.1.3 Validation results

The validation results for the piston velocity with time are shown in Figure 4.7. The two curves show good agreement with each other. For the simulation, the piston is assumed to move with constant speed, and the direction will change instantaneously when the piston reaches the expected dead centres. However, for the real prototype operation, it takes time for the piston to accelerate/decelerate to the set speed, and there are variations for the speed. Despite the differences, model can predict the changing trends of the piston velocity.

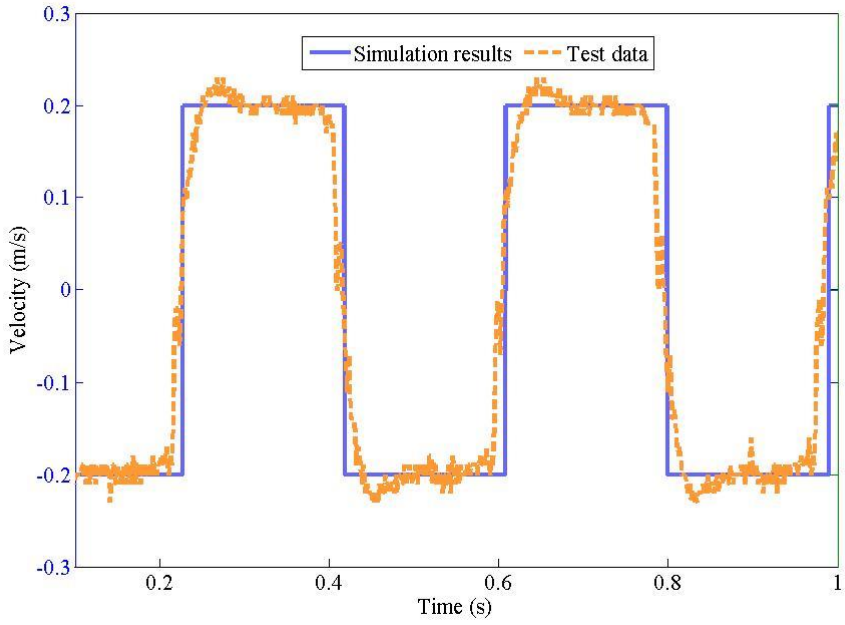

Figure 4.7 Velocity profile validation results for starting process

The tested piston displacement is demonstrated in Figure 4.8, with the simulation results as comparison. By implementing the above mentioned control strategy, despite the variations in piston velocity, the output displacements show good agreement. The errors in piston velocity are not significant from the piston displacement results. The model assumptions are considered acceptable. The actual piston TDC achieved at the end of the compression stroke is nearly 2.0 mm from the cylinder head. As the exhaust valve closes at 31.0 mm from the cylinder head, the compression ratio reached during the starting process is 15.5:1, which is definitely enough for a successful ignition.

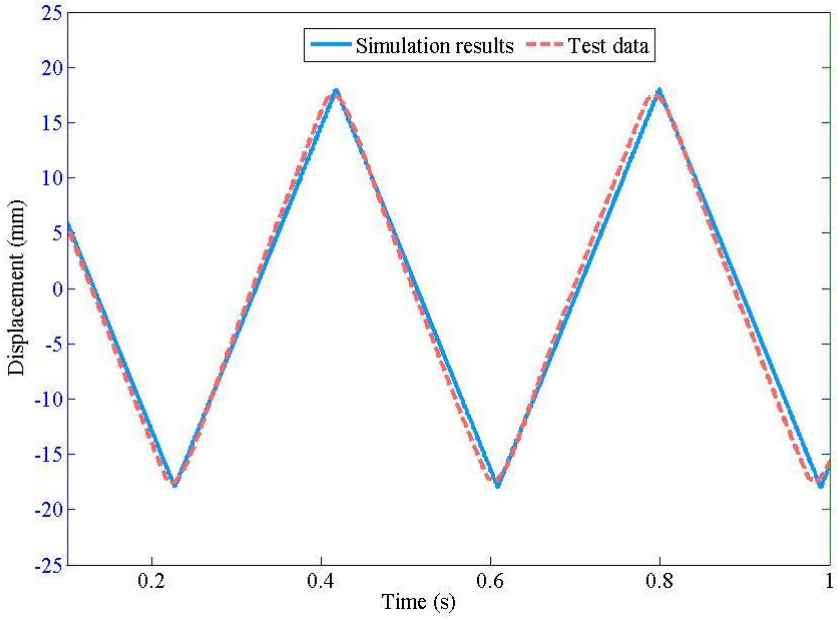

Figure 4.8 Piston displacement validation results for starting process

By importing the piston displacement and velocity profiles to the cylinder pressure sub-model introduced in Chapter 3, the cylinder pressure is calculated. The comparison of test pressure with simulated results during stable operation is shown in Figure 4.9. The changing trends of the two profiles are similar, and the peak cylinder pressures are tuned to be identical by varying the coefficients of the gas leakage and heat transfer functions, which means that the tuned model is of considerable accuracy to predict cylinder pressure. Meanwhile, the setting of valve timings is the same for both of the simulation and the prototype, indicating that the valve performance is acceptable. Furthermore, the cylinder pressure achieved at the end of compression stroke is approximately 11 bar from the test data, which is considered sufficient for successful ignition. The proposed control method for the engine code start is then proved to be feasible.

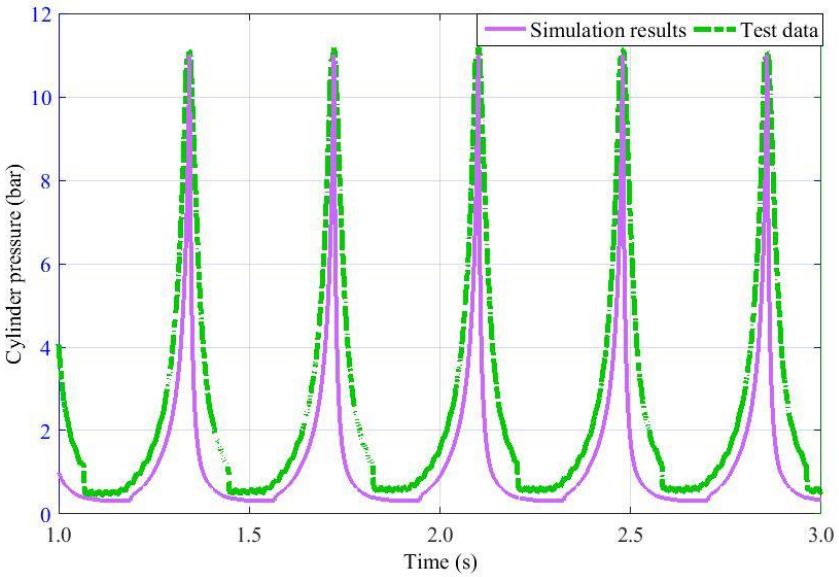

Figure 4.9 Tested cylinder pressure compared with simulation results

4.2 Simulation results and comparison for both cycles

4.2.1 Dynamic comparison

The engine is simulated to be operated at stoichiometric air-fuel ratio with a wide open throttle setting, and the injected fuel mass is calculated based on the engine compression volume (60.8 cc for the two-stroke mode, and 78.5 cc for the four-stroke mode). As a result, the injected fuel amount of the four-stroke engine is higher than the two-stroke engine. The simulated piston profiles for both two-stroke and four-stroke cycles are illustrated in Figure 4.10. It is apparent that during the stable operation process, the piston profile of the two-stroke cycle is similar to that of a constant amplitude and frequency oscillatory system. Conversely, it is noticeable how the four-stroke cycle operates with a variable duration of each stroke depending on its function. Another observation was that with the same ignition timing and same amount of injected fuel, the TDC position and therefore corresponding compression ratio proved higher for the four-stroke engine.

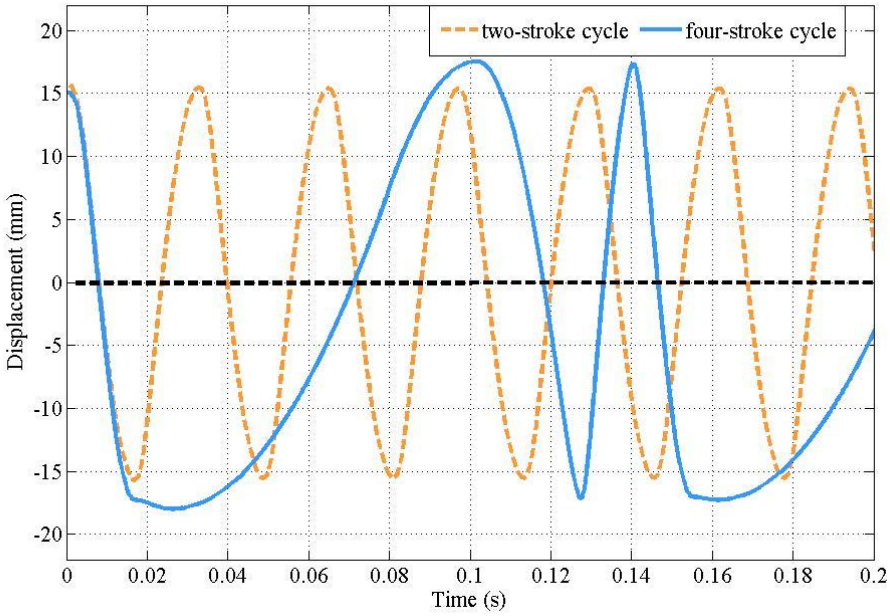

Figure 4.10 Piston dynamics at steady generating operation for both cycles

One complete cycle of the four-stroke cycle is shown in Figure 4.11 in terms of piston position and the simultaneous forces of the linear electric machine. It is apparent that the duration of Stroke 1 and Stroke 2 for the four-stroke FPEG are significantly longer than the other two strokes. This is because the piston is not limited by the crankshaft mechanical connections, and its movement is only affected by the forces acting on it. Thus the piston dynamics varies as the sequence event is different for each stroke and the piston velocity is higher during the power stroke, when the significantly higher combustion pressure acts on the piston assembly, compared to the forces from the electric machine in motoring mode. The peak combustion pressure produces a force of approximately 15300 N on the piston, whereas the peak motoring force from the electric machine is 4000 N, as can be seen from Figure 4.11. It was observed that these characteristics could be controlled and reduced by optimising the motor forces.

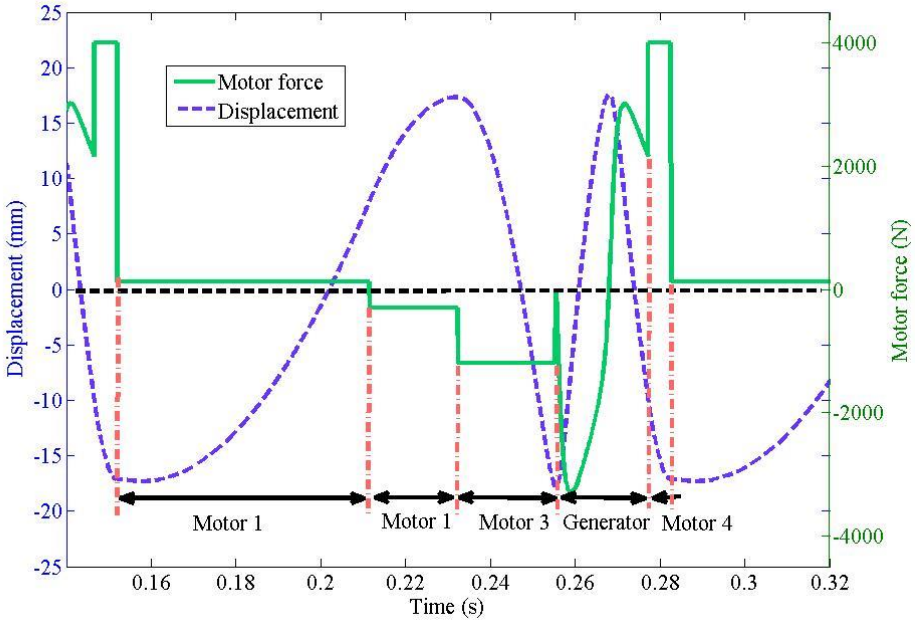

Figure 4.11 Piston dynamics and motor force for four-stroke engine cycle

As demonstrated in Figure 4.12, during the power stroke, the changing profile of the piston velocity for the four-stroke is similar with that of the two-stroke. The piston velocity changes greatly after ignition at BDC and TDC, while remains relatively constant at the middle of the stroke. For the four-stroke cycle, the piston speed is higher during the expansion process. However, for the non-power strokes of the four-stroke cycle, the piston speed is much lower, and there are sharp turning points for the velocity profile during stroke 1 (at around 8 mm) and stroke 4 (at -10 mm). This is due to the immediate mode switch of the motor, *i.e.* a constant motor force is applied on the piston assembly in the opposite direction of piston velocity, which acts as brake force to stop the piston from contacting the cylinder head.

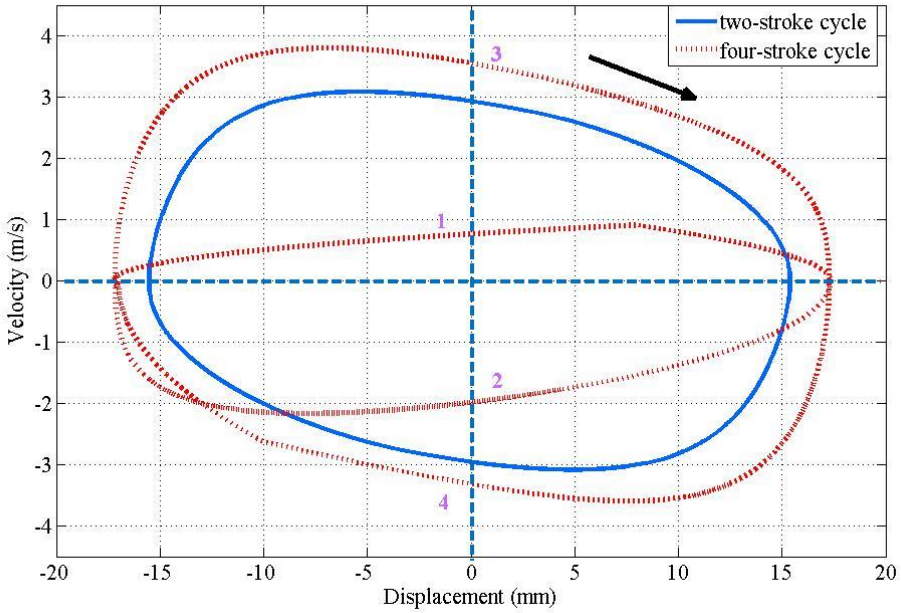

Figure 4.12 Piston velocity vs displacement for both cycles

4.2.2 Engine performance

Figure 4.13 shows the simulated pressure-volume diagram during steady operation state. The heat release process is more aligned with a constant volume process when operated on two-stroke mode, and the peak cylinder pressure is lower than that of the four-stroke cycle. As the piston in the FPEG is not restricted by mechanical components, its movement is only influenced by cylinder gas forces, electrometric force, and friction force acting on it. When cycle-to-cycle variation occurs, the resulting TDC also changes, and therefore the overall engine performance is affected. As a result, the piston TDC is suggested to be controlled within a small range to ensure stable and smooth engine operation [40]. For the four-stroke cycle, the motor force during motoring event can make these corresponding changes when TDC varies. Thus, a more complex and robust control system will be required to operate using a four-stroke cycle.

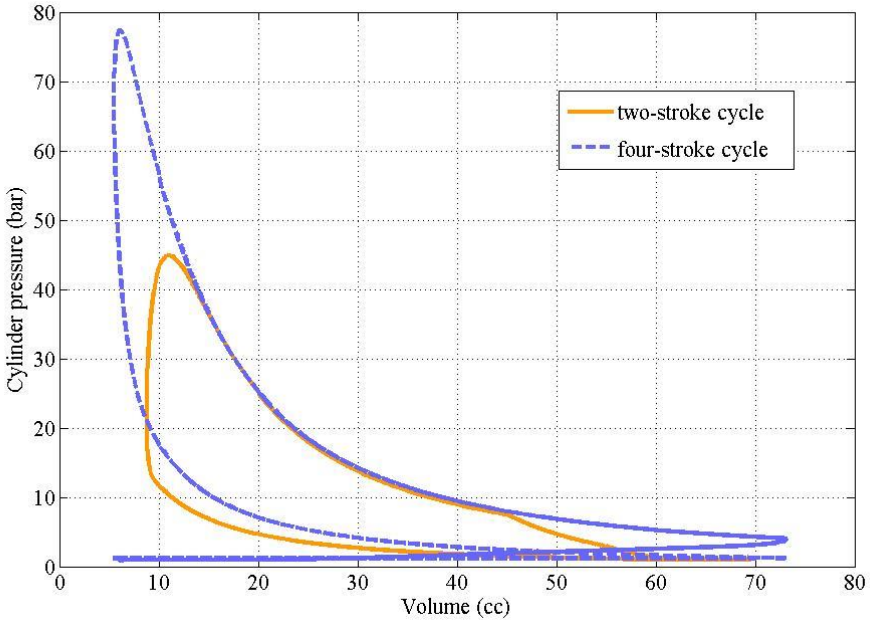

Figure 4.13 Pressure-volume diagram for both cycles

During simulations of the four-stroke cycle, it was observed that if the working mode of the linear electric machine follows the sequence presented in Table 3.1 in Chapter 3, it will result in mechanical contact between the piston and the cylinder head during Stroke 1 and Stroke 4. This is because during the exhaust gas exchange process, the exhaust valve is open and the cylinder pressure force is too low to overcome the expansion force from the other side (similar with a free-piston expander without bounce chamber). In order to avoid mechanical contact, the working mode of the linear electric machine was switched at a specific point during Stroke 1 and Stroke 4. When the linear electric machine is operated as a motor, a constant motor force is applied on the piston assembly in the opposite direction of piston velocity, which acts as brake force to stop the piston from contacting the cylinder head. The updated sequence of events for the four-stroke FPEG are summarised in Table 4.2, where the forces of Motor 1, Motor 2 and Motor 4 are all adjustable corresponding to the switching point of the working mode.

	Left cylinder	Right cylinder	Linear machine	
			Mode	Force [N]
Stroke 1 →	Air intake	Air exhaust	Motor 1	$120 \cdot sign(v)$
			Motor 2	$-300 \cdot sign(v)$
Stroke 2 ←	Compression	Air intake	Motor 3	$1000 \cdot sign(v)$
Stroke 3 →	Power	Compression	Generator	$-cv$
Stroke 4 ←	Air exhaust	Power	Generator	$-cv$
			Motor 4	$-4000 \cdot sign(v)$

Table 4.2 Sequence events for four-stroke FPEG

The predicted engine performance of both operating cycles (at wide opened throttle) is shown in Table 4.3. It was noted that even with observed higher engine thermal efficiencies, the indicated power is much lower if the prototype is operated on four-stroke engine cycle. This is because the engine speed for the four-stroke cycle is lower, and the power stroke takes place only every two oscillation cycles. Meanwhile, higher maximum piston speed and the peak cylinder pressure may induce heavier system vibration. In addition, the cylinder pressure changing rate of the four-stroke engine is more rapid with a peak value of 76 bar, and the compression ratio achieved is 16.2.

The maximum electric power output P_e is calculated by:

$$P_e = P_i - P_f - P_c \tag{4.1}$$

Where P_i is the engine indicated power (kW); P_f is the frictional loss (kW); P_c is the electric power used to compensate the overall power consumptions during motoring process.

For the two-stroke cycle, $P_c = 0$; and for the four-stroke cycle,

$$P_c = \sum P_{\text{motor}} \tag{4.2}$$

Where P_{motor} is the electric power consumed by the linear machine during each motoring event.

	Two-stroke engine	Four-stroke engine	
		2 cylinders	4 cylinders
Mean equivalent crankshaft rotational speed [rpm]	2000	900	
Maximum piston velocity [m/s]	3.1	3.8	
Peak cylinder pressure [bar]	47	76	
Fuel consumption [kg/kW·h]	0.22	0.20	
Thermodynamic efficiency [%]	34.5	44.9	
Indicated power [W]	3900	1230	2460
Electric power output [W]	3760	640	1280
Maximum effective compression ratio	7.36	16.20	
Engine power/weight ratio [W/kg]	0.070	0.022	0.022

Table 4.3 Performance comparison for both cycles

4.2.3 Indicated power distribution

The relative proportions of indicated power losses for the two-/four-stroke cycles are illustrated in Figure 4.14. It is found that due to reduced components and minimal piston side forces, the frictional loss of the FPEG operated on either engine cycle is low, which is reported to be around 10% of the indicated power for the conventional reciprocating engine [123]. For the four-stroke cycle, approximately half of the indicated power will be consumed in supplying additional electric power injected during the motoring process (marked as compensation in Figure 4.14).

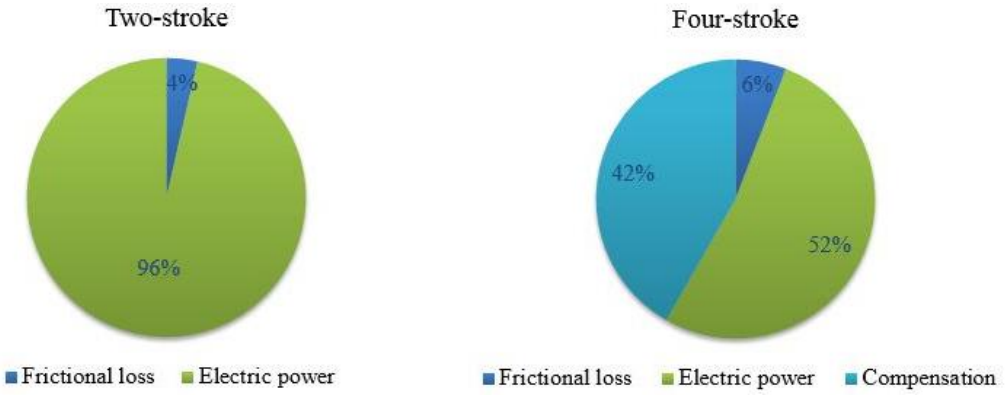

Figure 4.14 Relative proportions of indicated power losses for both cycles

4.3 Parametric sensitivity analysis

4.3.1 Engine throttle setting

The influence of varying engine throttle setting on generated indicated power and electric power are demonstrated in Figure 4.15. In order to avoid misfire and mechanical contact between the piston and cylinder head for different throttle settings the electric load is reduced. While the other input parameters such as ignition position, valve timing *et al.* remain unchanged. It is apparent that there is significant drop, from nearly 5 kW to 1.8 kW for the indicated power of the two-stroke cycle when the throttle opening changes from 100% to 50%. Meanwhile, the generated electric power is slightly lower than the indicated power, and global trend is similar. For the four-stroke cycle, both of the indicated power and electric power are much lower than that of the two-stroke cycle with the same throttle opening. This indicates that if the FPEG prototype is operated on a four-stroke cycle, a narrower operating range of powers can be achieved.

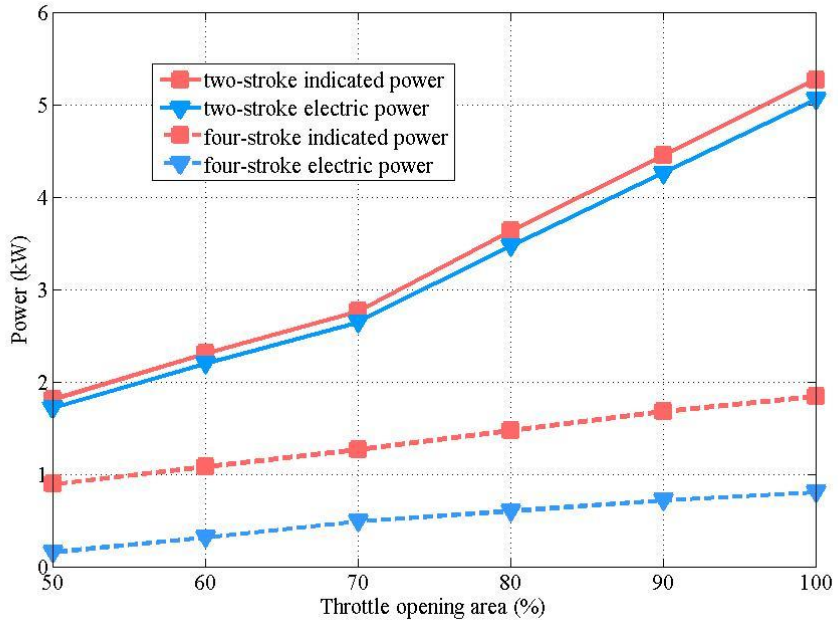

Figure 4.15 Power generated with various throttle settings for both cycles

As the gap for between the indicated power and the electric power of the four-stroke engine is significant, the distributions of the generated indicated power with various engine loads are illustrated in Figure 4.16. It is found that when the throttle opening changes from 100% to 50% of its full area, the indicated power drops linearly from 1.8 kW to nearly 0.8 kW. While the change of the amount of energy consumed by frictional loss and compensation to the injected electric power during the motoring process (marked as compensation in Figure 4.16) is not that obvious. This is because the motor forces during the motoring processes are fixed throughout the simulation. However, the generated electric power is getting lower significantly, and the energy conversion efficiency of the system is minimal when the engine load is operated below 50% of full load. As a result, for the four-stroke FPEG, the engine is suggested to be operated at high load in order to get better engine efficiency.

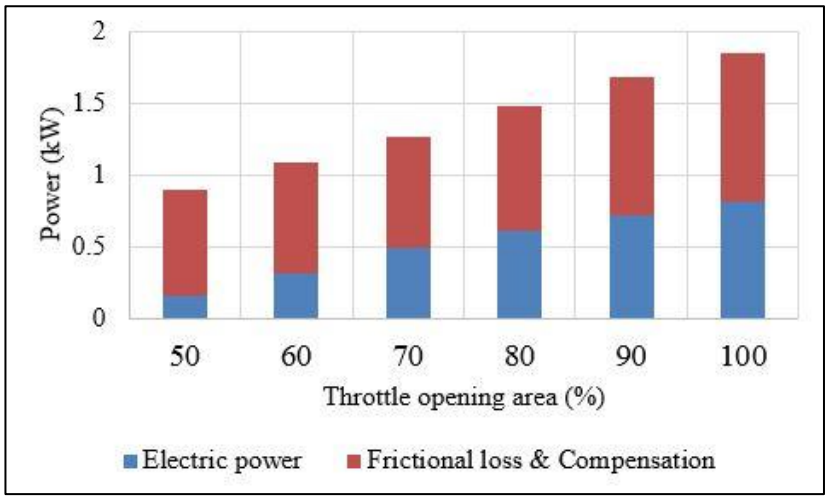

Figure 4.16 Distribution of indicated power for four-stroke engine with various loads

4.3.2 Ignition timing

Ignition timing advance is usually expressed as mechanical degrees before TDC for conventional engines. However, for the FPEG, as there is no crankshaft to define the piston movement in crank angle, the piston displacement signal is used as a feedback to set the ignition timing advance, which is given by:

$$\frac{\Delta x_{ign}}{N \cdot S} = \frac{\Delta \theta_{ign}}{N \cdot 180^{\circ}} \tag{4.3}$$

Where Δx_{ign} (unit: mm) is the length before TDC when ignition takes place for the FPEG; N is the stroke number, and for two-stroke engine, $N = 2$, for four-stroke engine, $N = 4$; S (mm) is the stroke of FPEG, $\Delta \theta_{ign}$ (degree) is equivalent ignition timing advance. As a result, the ignition will be triggered when the piston arrives Δx_{ign} before TDC during the compression stroke, and combustion is assumed to take place afterwards.

A series of equivalent ignition timing advances of 18°, 20°, 22° and 24° are selected as references for the FPEG, and the engine is running at wide open throttle. The influence of different ignition timing on the pressure-volume diagram is shown in Figure 4.17. With earlier ignition timing, the compression ratio achieved drops while the peak cylinder pressure increases for both engine cycles, and the difference of the cylinder pressure is not significant during the non-power stroke. Compared with the two-stroke

cycle, the area enclosed by the pressure-volume diagram of the four-stroke cycle is higher. This is because the compression volume of the four-stroke engine is higher, thus more gas is trapped and more fuel is injected. While for the two-stroke cycle, the combustion process is closer to a constant-volume heat release process, which could be further optimised for the implementation of Otto cycle on the FPEG prototype. As a result, the ignition timing can be used as a potential variable for the control system.

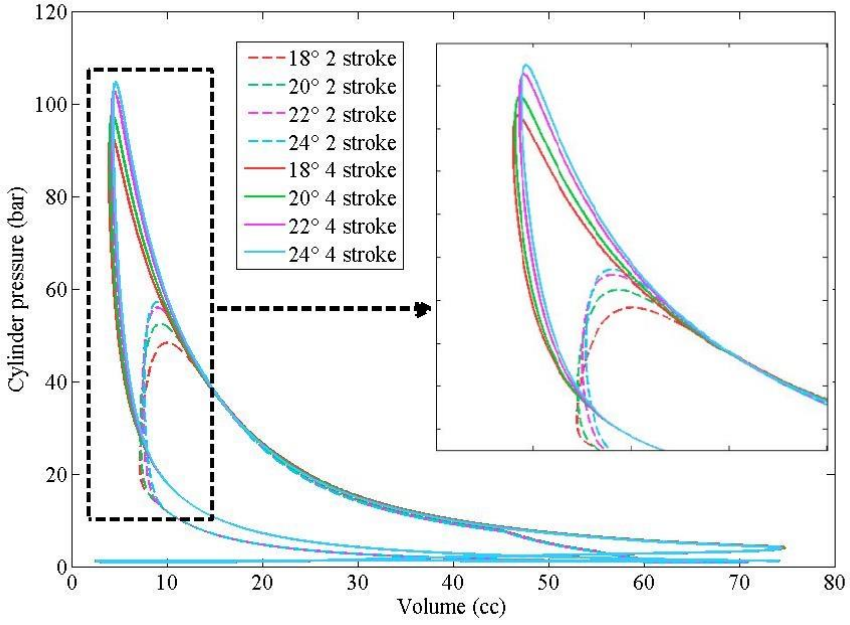

Figure 4.17 Pressure-volume diagram with various ignition positions for both cycles

The energy distributions of the indicated power with various ignition timing advances are illustrated in Figure 4.18. For the two-stroke cycle, both of the indicated power and the generated electric power grow with ignition timing advance. When the ignition timing advance changes from 18° to 24°, the increase of the generated electric power is around 0.3 kW (around 7% of the electric power generated with an ignition timing advance of 18°). However, for the four-stroke cycle, when the ignition timing changes, no significant change was observed for neither indicated nor electric power. Meanwhile, the percentage of the power used to compensate the electric power during the motoring process (marked as compensation in Figure 4.18) remains unchanged, which is approximately 50% of the indicated power.

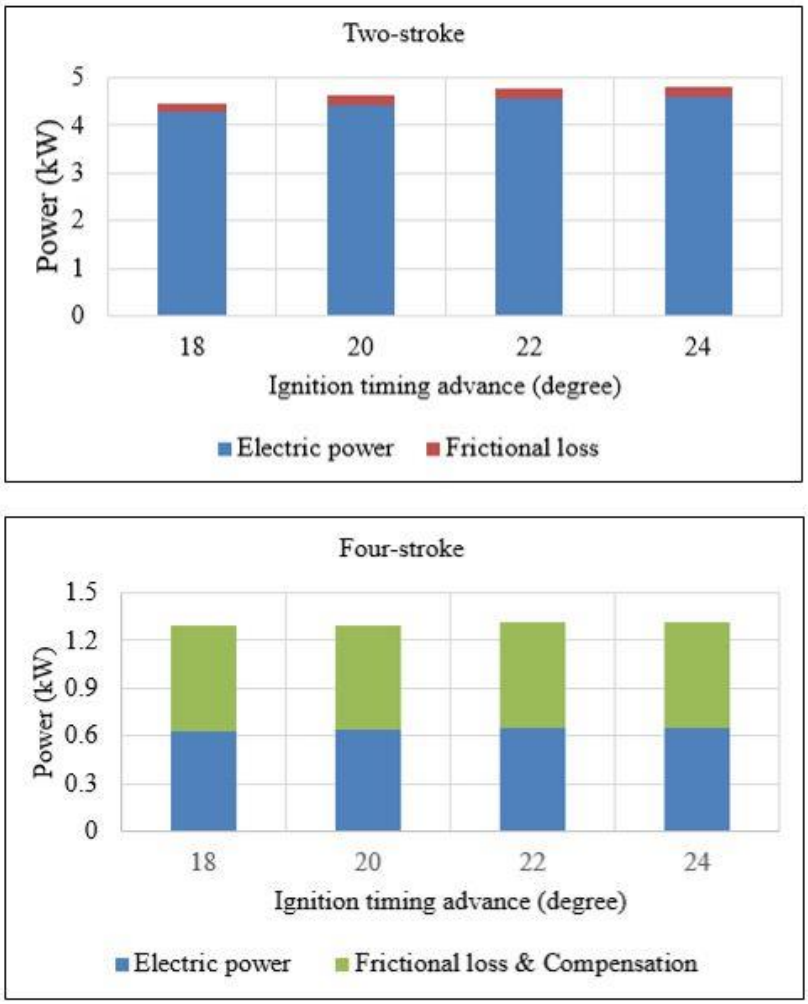

Figure 4.18 Distribution of indicated power with various ignition positions

4.3.3 Motoring force for four-stroke engine

As motor force is an important input variable for the four-stroke cycle, the fixed force value of the Motor 1 in Table 3.4 was varied to investigate its influence on piston dynamics. In addition, the motor force values of both Motor 2 and Motor 3 are increased correspondingly to balance the piston profile. The simulation results are shown in Figure 4.19. It can be observed that during the first cycle, the piston profiles are the same during the power stroke and begin to differ from each other at BDC when the motor force is induced. With higher motor force, the duration difference between the power stroke and gas pumping stroke is reduced, the engine speed is accelerated, and the engine compression ratio is increased.

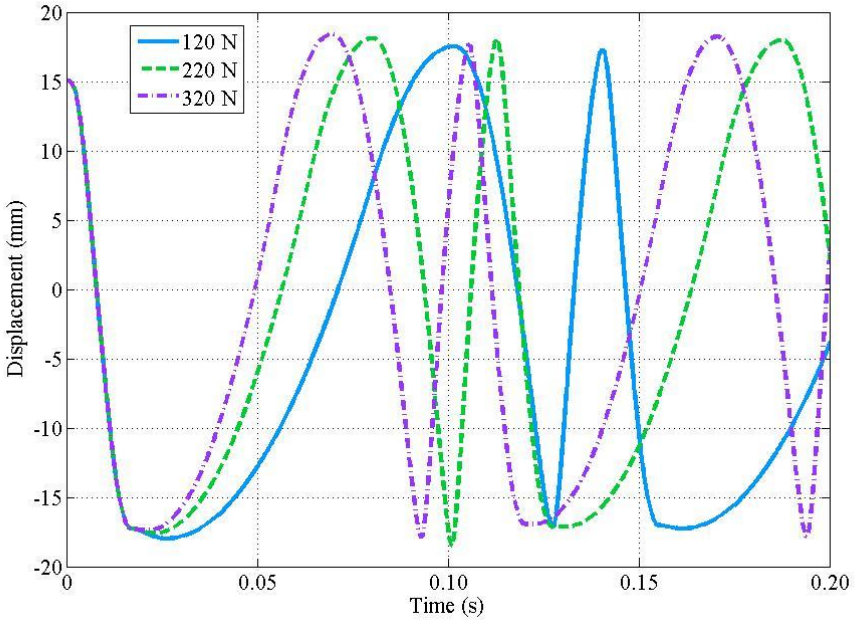

Figure 4.19 Piston dynamics with different motor forces for four-stroke cycle

The distributions of the indicated power with different motor forces are demonstrated in Figure 4.20. The engine indicated power increases with higher motor force due to the accelerated engine speed. However, more power will be consumed to compensate the electric power injected during the motoring process. Meanwhile, the general percentage of compensation power remains unchanged, which is approximately 50% of the indicated power. Further optimisation of the motor forces are under investigation in order to achieve maximum power output.

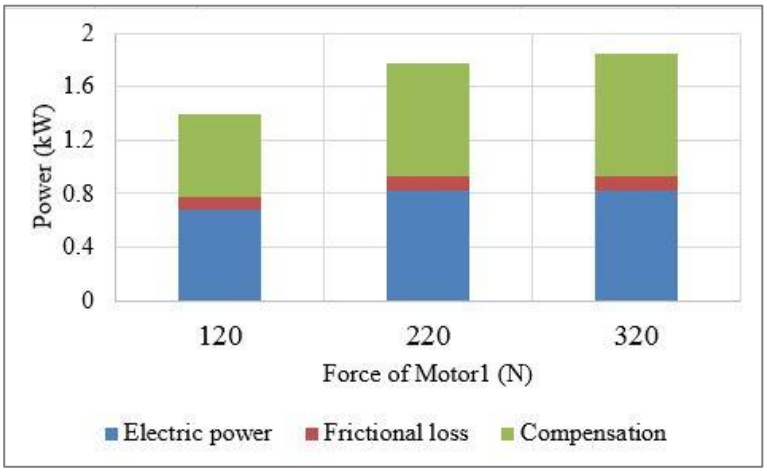

Figure 4.20 Power distribution with different motor forces for four-stroke cycle

4.4 Summary

In this chapter, the model validation and the simulation results were described. The prototype developed at Newcastle University was introduced. During the starting process, the piston is controlled to move with constant speed, and change its direction when the piston reaches the expected dead centres. The piston velocity, displacement, and in-cylinder gas pressure were collected from the prototype. The simulation results showed good agreement with the test data, indicating that the numerical model is valid.

The simulation results of the piston dynamics, engine performance, and indicated power distribution during the stable generating process were presented for both the two-stroke and the four-stroke thermodynamic cycle, along with a detailed parametric sensitivity analysis. The main advantages and disadvantages for both operation cycles are summarised in Table 4.3. Due to the higher power output and easier control system, the two-stroke cycle is applied to the FPEG prototype in Newcastle University. The following chapters will focus on characteristics of the FPEG operated in a two-stroke cycle.

	Advantages	Disadvantages
Two-stroke	• High power output • High engine speed • Low vibration • Self-sustained operation without external force • Wide range of power output	• Low scavenging efficiency • Sensitive to working condition
Four-stroke	• Better scavenging performance • High engine efficiency • Low fuel consumption • High compression ratio	• Complicated control system • Heavy vibration • Low power output • Requires driving of the gas exchange stroke

Table 4.4 Advantages and disadvantages for both cycles

Chapter 5. A fast response numerical model for control applications

Modelling and simulation are key elements of machine design, and the FPEG has conventionally been modelled using zero-dimensional models to obtain the piston dynamics and predict engine performance. However, the differential equations in such models are solved iteratively and require a considerable computational cost, which makes it challenging to be implemented in real-time Hardware-in-the-Loop (HIL) systems. Therefore, when more advanced control strategies need to be developed and implemented, simplified models are employed for the further real-time control system development. In this chapter, a derivation of a fast response numerical model is described for the future control applications, along with an application of the proposed model to analyse the potential analysis to the FPEG system.

5.1 Linear dynamics model

5.1.1 Dynamic equation

The main parts of the FPEG consist of two opposing combustion chambers and a linear electric machine. A linear magnet mover with pistons at each end is located between the two combustion chambers, which is the only moving part of the FPEG. Frictional loss in the FPEG is expected to be lower than in a reciprocating engine due to the elimination of the crank mechanism. As a result, the friction force is insignificant compared with the in-cylinder gas forces [10]. Because of this, the friction force is neglected through this investigation.

As there is compressible gas in both cylinders, the cylinders will act like nonlinear springs, and the FPEG system is analogous to a mass-spring system. For the dual piston FPEG, the engine is operated in a two-stroke cycle, and combustion occurs alternately in each chamber during stable operation. This means that the system is running under an external excitation, which is determined by the heat released during the combustion process. As a result, the dual piston FPE will show similar characteristics with the vibration system under external excitations after proper simplification [119].

If friction force is neglected, a dynamic equation of the mover can be derived from Newton's second law and illustrated in Figure 5.1.

$$m\ddot{x} = \overrightarrow{F_l} + \overrightarrow{F_r} + \overrightarrow{F_e} \tag{5.1}$$

Where m is the moving mass of the mover with the pistons (unit: kg); x is the mover displacement (m); F_l is the gas force from the left cylinder (N); F_r is the gas force from the right cylinder (N): F_e is the resistant force from the linear electric generator (N). The gas force can be calculated using the gas pressure, p (Pa) and piston surface area, A (m^2) which can be approximated from the cylinder bore, B (m), as:

$$A = \frac{\pi B^2}{4} \tag{5.2}$$

The in-cylinder pressure and the gas force are functions of the mover displacement, x.

$$F_l = p_l \cdot A \tag{5.3}$$

$$F_r = p_r \cdot A \tag{5.4}$$

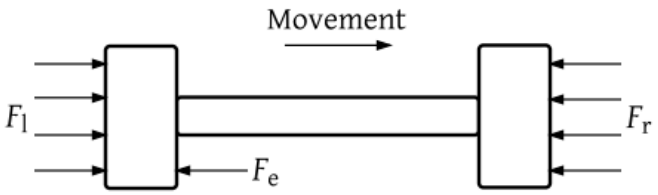

Figure 5.1 Schematic figure of the dynamic equation

The load force of the electric generator is known to have a high influence on the performance of the FPEG. According the equations in Chapter 3, the load force is a function of the design parameters of the machine, the mover's velocity as well as the load resistance. It is assumed to be proportional to the mover's speed, and the direction of the load force is always opposite to the direction of piston velocity:

$$F_e = -C_e\dot{x} \tag{5.5}$$

Where C_e is the coefficient of the load force, and it varies with the load resistance [19].

By rewriting Equation (5.1),

$$m\ddot{x} = \overrightarrow{F_l}(x) + \overrightarrow{F_r}(x) + \overrightarrow{F_e}(\dot{x}) \tag{5.6}$$

it can be seen that if the non-linear in-cylinder pressure force is simplified properly, the dynamic equation of FPEG can be linearized to a forced vibration system with viscous damping, which is illustrated in Figure 5.2. The analogy between a mass-spring damper and a FPEG system is expressed in Table 5.1. The objective form of the dynamic equation after the linearization is expressed as:

$$m\ddot{x} + c\dot{x} + kx = F(t) \tag{5.7}$$

where the constant c is the damping coefficient; the constant of proportionality k is the spring constant; and $F(t)$ is the continuing excitation force.

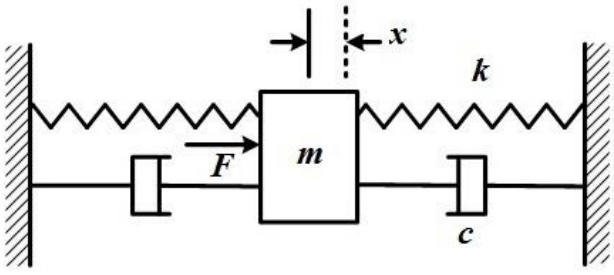

Figure 5.2 Illustration of the analogous forced vibration system

Then the angular natural frequency, ω_n of FPEG can be defined as:

$$\omega_n = \sqrt{\frac{k}{m}} \tag{5.8}$$

Mass-spring damper	FPEG system
Moving mass, m	Mass of the piston assembly and mover
Damping coefficient, c	Linear generator load force
Spring constant, k	In-cylinder pressure
Excitation force, F	Heat release force

Table 5.1 Analogy between a mass-spring damper and a FPEG system

5.1.2 Thermodynamic cycle

The typical thermodynamic cycle of FPEG can be described by a compression process, a heat release process (combustion) followed by an expansion process. As a result, the in-cylinder pressure is influenced by two factors, *i.e.* the cylinder volume change caused by the piston motion and the heat release from the chemical energy of the burnt fuel. The in-cylinder pressure can be written as:

$$p_l = p_{lcp} + p_{lcm} \cdot \sigma_l \tag{5.9}$$

$$p_r = p_{rcp} + p_{rcm} \cdot \sigma_r \tag{5.10}$$

Where p is the in-cylinder pressure (Pa); p_{cp} is the pressure due to the cylinder volume change (Pa); p_{cm} is the pressure due to heat release during the combustion process (Pa); the subscripts r and l represent the values of the right and left cylinder respectively.

Usually a spark defines and establishes the start of combustion, initially the pressure rise is very small and compression will still continue until it is large enough to reverse the piston direction into an expansion stroke. A unit step function σ is induced to enable/disable the influence from the heat release for both cylinders, which is shown in Equation (5.11) and (5.12) respectively.

$$\sigma_l = \begin{cases} 1, \dot{x} \geq 0 \\ 0, \dot{x} < 0 \end{cases} \tag{5.11}$$

$$\sigma_r = \begin{cases} 0, \dot{x} \geq 0 \\ 1, \dot{x} < 0 \end{cases} \tag{5.12}$$

According to the reported simulation and experimental results, the combustion process of FPEG can be simplified to be represented by a constant volume heating process [1, 54]. If no heat transfer to the cylinder walls and no gas leakage through the piston rings are considered in the thermodynamic model, the ideal running cycle of FPEG can be described by two adiabatic processes connected by a constant volume heat release process, illustrated in Figure 5.3.

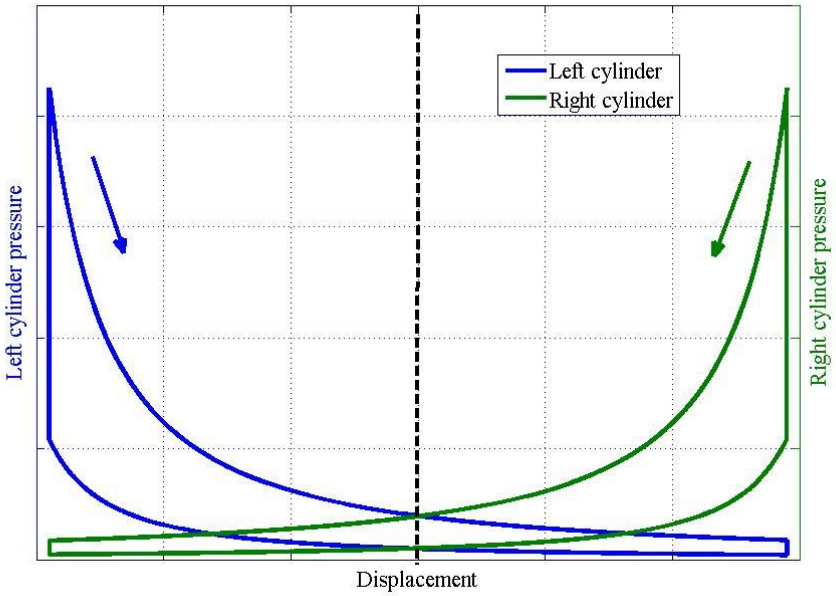

Figure 5.3 Ideal operating cycle of the FPEG

The cylinder pressures due to the adiabatic volume change for both sides are expressed by the following equations:

$$p_{lcp} = p_0 \left(\frac{V_0}{V_l}\right)^{\gamma} \tag{5.13}$$

$$p_{rcp} = p_0 \left(\frac{V_0}{V_r}\right)^{\gamma} \tag{5.14}$$

$$V_0 = L_s \cdot A \tag{5.15}$$

Where the in-cylinder pressure is assumed to be equal to the ambient pressure, p_0 (Pa) at the middle stroke; V_o is the cylinder volume at the middle stroke (m^3); V is the cylinder volume (m^3), L_s is the length of half stroke (m).

The volume for the left chamber, V_l is:

$$V_l = (L_s + x) \cdot A \tag{5.16}$$

The right chamber's volume, V_r can be calculated by:

$$V_r = (L_s - x) \cdot A \tag{5.17}$$

The in-cylinder pressures due to heat release can be expressed as:

$$p_{lcm} = \Delta p_{cm} \left(\frac{V_c}{V_l}\right) \tag{5.18}$$

$$p_{rcm} = \Delta p_{cm} \left(\frac{V_c}{V_r}\right) \tag{5.19}$$

$$V_{\mathrm{c}} = L_c \cdot A \tag{5.20}$$

Where Δp_{cm} is the pressure increase during the constant volume heat release process (Pa) and the value is the same for both sides; L_c is the length of the clearance (m); V_{c} is the clearance volume (m^3).

From Equation (5.9) to (5.20), the cylinder force can be written as:

$$F_l = A \cdot \left(p_0 \left(\frac{L_s}{L_s + x}\right)^{\gamma} + \Delta p_{cm} \left(\frac{L_c}{L_s + x}\right)^{\gamma} \cdot \sigma_l\right) \tag{5.21}$$

$$F_r = A \cdot \left(p_0 \left(\frac{L_s}{L_s - x}\right)^{\gamma} + \Delta p_{cm} \left(\frac{L_c}{L_s - x}\right)^{\gamma} \cdot \sigma_r\right) \tag{5.22}$$

5.1.3 Constant volume heat release process

A constant-volume combustion assumption is used to obtain the pressure difference, Δp_{cm} after heat release process. Applying the first law of thermodynamics on the cylinder charge, it can be obtained that:

$$\Delta U = Q_{in} - W \tag{5.23}$$

Where ΔU is the difference of the internal energy of the in-cylinder charge (J); $Q_{in}$is the total amount of heat released from the combustion process (J); W is the output work done by the cylinder charge (J).

Since the heat release process is assumed to be constant-volume process, the output work done by the cylinder charge is zero. Then all of the heat released from the combustion process is transferred to increase the internal energy of the in-cylinder gas, that is:

$$\Delta U = Q_{in} \tag{5.24}$$

If m_{air0} (kg) is trapped mass of air at wide open throttle, thus at maximum load, applying the ideal gas equation, m_{air0} can be calculated from

$$p_0 V_0 = m_{\mathrm{air0}} R T_0 \tag{5.25}$$

When the engine is operated at part load, the amount of trapped intake air is:

$$m_{\mathrm{air}} = K_t \cdot m_{\mathrm{air0}} \tag{5.26}$$

Where K_{t} is a proportional factor $[0 - 1]$ which would be considered to be function of the throttle opening, volumetric efficiency, *etc*. [123].

The engine is assumed to be operated at stoichiometric air-fuel ratio (AFR). The mass of fuel in the mixture m_{fuel} is:

$$m_{\mathrm{fuel}} = m_{\mathrm{air}}/\mathrm{AFR} \tag{5.27}$$

Substitution for m_{air} from Equation (5.25) - (5.27), gives

$$m_{\text{fuel}} = K_t \cdot \frac{p_0 V_0}{R T_0 \text{AFR}} \tag{5.28}$$

Then Q_{in} is calculated from m_{fuel} and the low heating value of the fuel Q_{LHV} (J/kg) with the combustion efficiency of η_c

$$Q_{in} = m_{\text{fuel}} \cdot Q_{\text{LHV}} \cdot \eta_c \tag{5.29}$$

By using Equation (5.28), and assume $H_u = Q_{\text{LHV}} \cdot \eta_c$, the total amount of heat released from the combustion process is expressed as:

$$Q_{in} = K_t \cdot H_u \frac{p_0 V_0}{R T_0 \text{AFR}} \tag{5.30}$$

Substitution for $Q_{in}$from Equation (5.24), obtains

$$\Delta U = K_t \cdot H_u \frac{p_0 V_0}{R T_0 \text{AFR}} \tag{5.31}$$

For ideal gas, the increase of internal energy leads to the temperature of the gas mixture:

$$\Delta U = C_{\text{v}}(m_{\text{air}} + m_{\text{fuel}})\Delta T \tag{5.32}$$

Where C_v is the heat capacity at constant volume (J/m^3·K); ΔT is the temperature increase of the mixture (K).

Applying the ideal gas law to the in-cylinder gas mixture yields

$$\Delta p_{cm} V_c = (m_{\text{air}} + m_{\text{fuel}}) R \Delta T \tag{5.33}$$

By using Equations (5.31) – (5.33), the pressure increase Δp_{cm} can be expressed as:

$$\Delta p_{cm} = K_t \cdot H_u \frac{p_0 V_0}{C_v T_0 \text{AFR} V_c} \tag{5.34}$$

The expected geometric compression ratio of the free-piston engine CR is:

$$\text{CR} = \frac{V_0}{V_c} = \frac{L_s}{L_c} \tag{5.35}$$

Thus

$$\Delta p_{cm} = K_t \cdot H_u \frac{p_0 \mathrm{CR}}{C_v T_0 \mathrm{AFR}} \tag{5.36}$$

5.1.4 Linear approximation of cylinder pressure

To compare the properties with a forced vibration with viscous damping, the nonlinear expressions on the right side of gas force Equations (5.21) and (5.22) are expanded in Taylor series around the equilibrium point:

$$x = 0 \tag{5.37}$$

Let

$$f_l(x) = \left(p_0 \left(\frac{L_s}{L_s+x}\right)^{\gamma} + \Delta p_{cm} \left(\frac{L_c}{L_s+x}\right)^{\gamma} \cdot \sigma_l\right) \tag{5.38}$$

$$f_r(x) = \left(p_0 \left(\frac{L_s}{L_s-x}\right)^{\gamma} + \Delta p_{cm} \left(\frac{L_c}{L_s-x}\right)^{\gamma} \cdot \sigma_r\right) \tag{5.39}$$

Then the Taylor series for f_l and f_r are expressed as:

$$f_l(x) = f_l(0) + \frac{f_l'(0)}{1!}x + \frac{f_l''(0)}{2!}x^2 + \frac{f_l^3(0)}{3!}x^3 + \cdots \tag{5.40}$$

$$f_r(x) = f_r(0) + \frac{f_r'(0)}{1!}x + \frac{f_r''(0)}{2!}x^2 + \frac{f_r^3(0)}{3!}x^3 + \cdots \tag{5.41}$$

As a linear approximation is desired, all the high order terms in the above equations are neglected. The linear approximations are listed below

$$f_l(x) = a_l + b_l x \tag{5.42}$$

$$f_r(x) = a_r + b_r x \tag{5.43}$$

Where

$$a_l = p_0 + \Delta p_{cm} \left(\frac{L_c}{L_s}\right)^{\gamma} \cdot \sigma_l \tag{5.44}$$

$$b_l = -\left(\frac{\gamma p_0}{L_s} + \Delta p_{cm} \frac{\gamma {L_c}^{\gamma}}{{L_s}^{\gamma+1}} \cdot \sigma_l\right) \tag{5.45}$$

$$a_r = p_0 + \Delta p_{cm} \left(\frac{L_c}{L_s}\right)^{\gamma} \cdot \sigma_r \tag{5.46}$$

$$b_r = \frac{\gamma p_0}{L_s} + \Delta p_{cm} \frac{\gamma {L_c}^{\gamma}}{{L_s}^{\gamma+1}} \cdot \sigma_r \tag{5.47}$$

Then the linear approximations of the cylinder gas force Equation (5.21) and (5.22) are

$$F_l(x) = \left(p_0 + \Delta p_{cm} \left(\frac{L_c}{L_s}\right)^{\gamma} \cdot \sigma_l\right) A - \left(\frac{\gamma p_0}{L_s} + \Delta p_{cm} \frac{\gamma {L_c}^{\gamma}}{{L_s}^{\gamma+1}} \cdot \sigma_l\right) A \cdot x \tag{5.48}$$

$$F_r(x) = \left(p_0 + \Delta p_{cm} \left(\frac{L_c}{L_s}\right)^{\gamma} \cdot \sigma_r\right) A + \left(\frac{\gamma p_0}{L_s} + \Delta p_{cm} \frac{\gamma {L_c}^{\gamma}}{{L_s}^{\gamma+1}} \cdot \sigma_r\right) A \cdot x \tag{5.49}$$

5.1.5 Forced vibration equation

From Equation (5.5) - (5.49), the final dynamic equation is given by

$$m\ddot{x} + k_v\dot{x} + \left(\frac{2\gamma p_0 A}{L_s} + \frac{\Delta p_{cm} A \gamma {L_c}^{\gamma}}{{L_s}^{\gamma+1}} (\sigma_l + \sigma_r)\right) x = \Delta p_{cm} A \left(\frac{1}{\mathrm{CR}}\right)^{\gamma} (\sigma_l - \sigma_r) \tag{5.50}$$

Since the combustion takes place in each cylinder on an alternate basis, according to Equation (5.11) and (5.12), yields:

$$\sigma_l + \sigma_r = 1 \tag{5.51}$$

and

$$\sigma_l - \sigma_r = \begin{cases} 1, \dot{x} \geq 0 \\ -1, \dot{x} < 0. \end{cases} \tag{5.52}$$

The rectangular wave of the excitation can be described by a Fourier series. If the initial position of the piston is assumed to be at its left dead centre, and the combustion takes place at the left cylinder, then the comparison of $(\sigma_l - \sigma_r)$ with the first mode of its Fourier series is demonstrated in Figure 5.4. The first mode of $(\sigma_l - \sigma_r)$ is defined as:

$$\sigma_l - \sigma_r \approx \frac{4}{\pi} \sin \omega t \tag{5.53}$$

Where ω is the angular frequency of combustion for each cylinder.

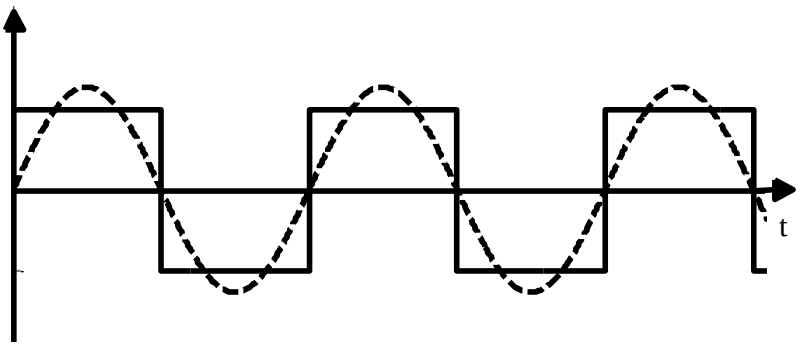

Figure 5.4 Rectangular wave and first mode of its Fourier series

Finally, substituting for $(\sigma_l + \sigma_r)$ and $(\sigma_l - \sigma_r)$ from Equation (51) and (53) respectively, Equation (5.50) can be written as:

$$m\ddot{x} + c\dot{x} + kx = F_0 \sin \omega t \tag{5.54}$$

Where

$$c = k_v \tag{5.55}$$

$$k = \frac{2\gamma p_0 A}{L_s} + \frac{\Delta p_{cm} A \gamma {L_c}^{\gamma}}{{L_s}^{\gamma+1}} \tag{5.56}$$

$$F_0 = \frac{4}{\pi} \Delta p_{cm} A \left(\frac{1}{\mathrm{CR}}\right)^{\gamma} \tag{5.57}$$

Then the dynamic model of FPEG is linearized to the same form with the single degree-of-freedom forced vibration system with viscous damping. Where k is the stiffness of the air-spring system; c is the damping coefficient; the excitation $F_0 \sin \omega t$ is a continuing force whose magnitude F_0 varies sinusoidally with time.

A mass spring system usually reciprocates with a natural frequency, and the system is ideally operated near to this frequency as this requires the least additional energy [130]. According to Equation (5.8) the angular natural frequency ω_n of a FPEG is:

$$\omega_n = \sqrt{k/m} = \sqrt{\left(\frac{2\gamma p_0 A}{L_s} + \frac{\Delta p_{cm} A \gamma {L_c}^{\gamma}}{{L_s}^{\gamma+1}}\right)/m} \tag{5.58}$$

Since combustion is assumed to take place when the piston reaches its top dead centre (TDC), the frequency of the ignition is required to be the same as an air-spring system of FPEG in order to maintain stable operation. Thus yielding:

$$\omega_n = \omega \tag{5.59}$$

Then the solution of Equation (5.54) can be obtained according to vibration theory [130] , and the displacement of the viscous damped, single degree-of-freedom system shown in Figure 5.4 undergoes vibration as defined by:

$$x = -\frac{F_0 \cos \omega_n t}{c\omega_n} \tag{5.60}$$

Where F_0, ω_n, and c can be obtained from Equation (5.57), (5.58) and (5.55) respectively.

More characteristics of the viscous damping vibration system can be defined from the vibration theory. If the mechanical system shown in Figure 5.2 is assumed to be a linear system, the external force $F(t)$ is the input to the system, and the piston displacement $x(t)$ is the output, which means this system is a single-input, single-output system. From the diagram and Equation (5.60), the system is of second order. If state variables $x_1(t)$ and $x_2(t)$ are defined as:

$$x_1(t) = x(t) \tag{5.61}$$

$$x_2(t) = \dot{x}(t) \tag{5.62}$$

$$u(t) = F(t) \tag{5.63}$$

Then we can get

$$\dot{x}_1 = x_2 \tag{5.64}$$

$$\dot{x}_2 = -\frac{k}{m}x_1 - \frac{c}{m}x_2 + \frac{1}{m}u \tag{5.65}$$

The output equation is:

$$y = x_1 \tag{5.66}$$

Then Equations (5.64) and (5.65) can be written in a vector-matrix state equation form as:

$$\begin{bmatrix} \dot{x}_1 \\ \dot{x}_2 \end{bmatrix} = \begin{bmatrix} 0 & 1 \\ -\frac{k}{m} & -\frac{c}{m} \end{bmatrix} \begin{bmatrix} x_1 \\ x_2 \end{bmatrix} + \begin{bmatrix} 0 \\ \frac{1}{m} \end{bmatrix} u \tag{5.67}$$

The output Equation (5.66) for the system is:

$$y = [1 \quad 0] \begin{bmatrix} x_1 \\ x_2 \end{bmatrix} \tag{5.68}$$

The state-space Equations (5.67) and (5.68) can be rewritten in the standard form:

$$\dot{\mathbf{x}} = \mathbf{A}\mathbf{x} + \mathbf{B}u \tag{5.69}$$

$$y = \mathbf{C}\mathbf{x} + Du \tag{5.70}$$

Where

$$\mathbf{A} = \begin{bmatrix} 0 & 1 \\ -\frac{k}{m} & -\frac{c}{m} \end{bmatrix}, \quad \mathbf{B} = \begin{bmatrix} 0 \\ \frac{1}{m} \end{bmatrix}, \quad \mathbf{C} = [1 \quad 0], \quad D = 0 \tag{5.71}$$

The transfer function of the system given by $G(s) = \frac{Y(s)}{U(s)}$ can be obtained from the state-space equations:

$$G(s) = \mathbf{C}(s\mathbf{I} - \mathbf{A})^{-1}\mathbf{B} + D \tag{5.72}$$

By substituting $\mathbf{C}, \mathbf{A}, \mathbf{B}$ and D into Equation (5.72), the transfer function is then expressed by:

$$G(s) = \frac{1}{ms^2 + cs + k} \tag{5.73}$$

The system has no zero point, and the poles can be obtained by the two roots of:

$$ms^2 + cs + k = 0 \tag{5.74}$$

The roots of equation are:

$$s = \frac{-c \pm \sqrt{c^2 - 4mk}}{2m} \tag{5.75}$$

As the poles must be in the left half plane for the system to be stable [131], which means:

$$c^2 - 4mk > 0 \tag{5.76}$$

Substituting Equation (5.55) and (5.56) yields,

$$k_v{}^2 - 4mp_0A\left(\frac{2\gamma}{L_s} + \frac{K_t H_u \gamma}{C_v T_0 L_s \mathrm{AFR} CR^{\gamma-1}}\right) > 0 \tag{5.77}$$

5.2 Fast response model validation

The linear dynamic model was developed in Matlab/Simulink, calibrated using parameters and test data obtained from an operating FPEG prototype. This prototype configuration is identical to the input parameters used in this model. The fast response model was validated with test data from a running prototype with a maximum stroke of 70 mm, the parameters for the prototype is listed in Table 5.2. During the steady operation, the fuel delivery and ignition systems are activated and the electrical discharge between the spark plug electrodes starts the combustion process close to the end of the compression stroke. Further information on the prototype for the fast-response model validation is presented in Appendix II.

Parameters	Value
Bore [mm]	52.5
Maximum total stroke [mm]	70.0
Compression stroke [mm]	35.0
Moving mass [kg]	5.0

Table 5.2 Prototype specifications [118]

The data presented in Figure 5.5 shows the simulated piston displacement as a function of time during the combustion process, compared with the test data at the same

operating condition. The simulation results of the piston dynamics show similar trends with the test results, and the tested amplitudes are almost identical with the model prediction. There is difference in the frequency value (nearly 20 Hz according to the test data and approximately 18 Hz from the simulation model). Therefore a time scale factor of 1.15 is applied on the simulation results (as shown in Figure 5.5) to compensate for the frequency difference. The value of the scale factor is considered acceptable due to the simplification made when linearizing the model, and the model is of considered sufficient robustness to predict the actual engine dynamic performance.

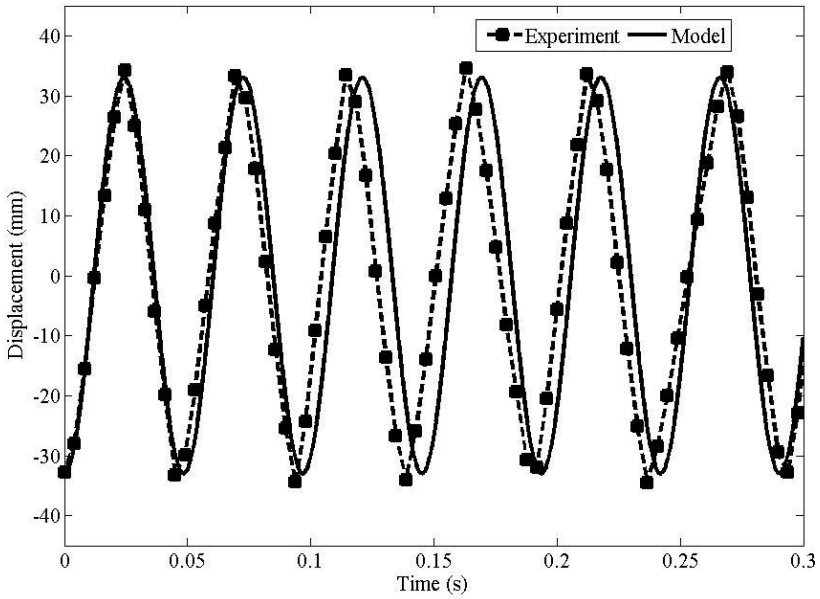

Figure 5.5 Model validation results for the fast response model [118]

Basic assumptions and simplifications for the model are summarised as:

- the frictional forces are neglected;
- the ideal running cycle of the FPEG is described by two adiabatic processes connected by a constant volume heat release process;
- the cylinder pressure is linearized using Taylor expansion around the zero-point, and all high order terms are neglected.

Due to the simplifications mentioned above, the proposed model shows limitations in predicting of the cylinder pressure and the thermodynamic properties of the in-cylinder

charge. However, compared to the previous numerical model with differential equations introduced in Chapter 3, the model presented in this section provides the following advantages:

- Simple and flexible. Implementation into several computing software, *i.e.* Matlab, AMESim, Labview, Dymola, *et al*. All the input parameters for the simplified model are constant values, and a trigonometric function is the only function changing with time. It is easy to solve for the piston dynamic profile for implementation to several software and various programming languages.
- Significantly reduced solving time, and the model can easily be coupled with real-time HIL simulation model for the future control system development. The required solving time of the differential equations in the previous numerical model are avoided in obtaining the dynamic and thermodynamic solutions. With the proposed simplified model, fast predictions of the piston dynamics with the feedback from the actual working condition are possible, which potentially makes it technically feasible to implement the model into real-time hardware for a stable operating control system.

5.3 Analysis of system disturbance using the fast response model

5.3.1 Potential system disturbance analysis

As illustrated in Figure 5.6, any disturbance originating either internally from the engine or externally from the electric load may induce variations in piston motion profile between consecutive cycles. The disturbances could be immediate change of electric load, engine cycle-to-cycle variations, or misfire.

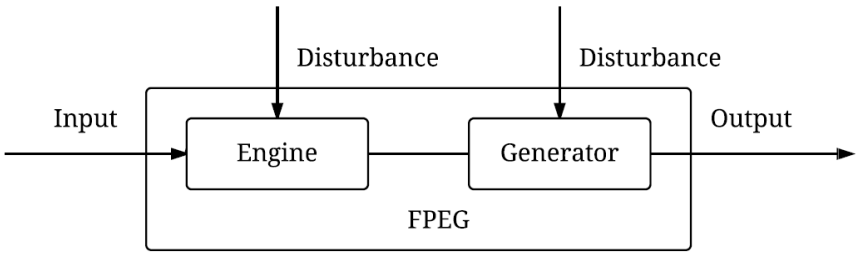

Figure 5.6 Illustration of system disturbance

A series of the two engine cycles mainly consist of four working processes: heat release, expansion, gas exchange and compression. As demonstrated in Figure 5.7, the cycle-to-cycle variations and engine misfire can only take place during the heat release process. However, the electric load change can occur anytime throughout out the operation. During the engine operation, there could be one disturbance that occurs or several disturbances take place at the same time. Five disturbance sources are listed below and their differences on the engine performance will be discussed in the following section.

- Electric load change during the expansion/gas exchange/compression/ heat release process.
- Cycle-to-cycle variations during the heat release process.
- Unsuccessful ignition during the heat release process.
- Electric load change and cycle-to-cycle variations during the heat release process.
- Electric load change and unsuccessful ignition during the heat release process.

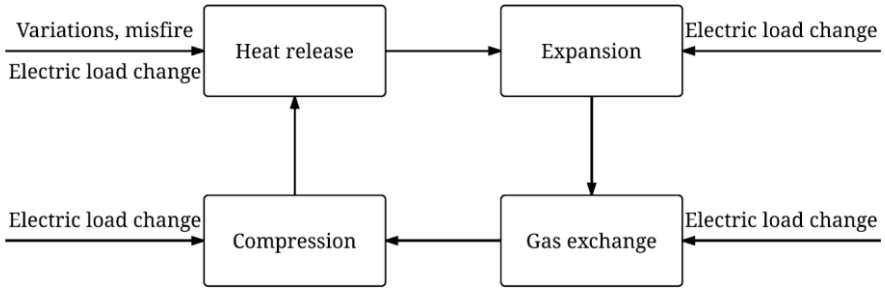

Figure 5.7 Working processes with possible disturbances

5.3.2 Influence on system performance

<u>Electric load change</u>

As an immediate electric load change can occur anytime during the engine operation, a simulation of immediate change at different working processes was undertaken to investigate the influence of the changing time on the piston dynamics. The engine is simulated to be operated at high load, and an immediate step change of the electric load occurs at expansion, gas exchange, compression and heat release process respectively.

Simulation results demonstrate that the corresponding changes of piston TDC is similar to a step, and with different changing time, the TDC achieved during stable operation is the same. Figure 5.8 demonstrates an example piston profile with a step decrease of the electric load by 15%. Figure 5.9 shows an example of engine response to step increase of electric load by 5%.

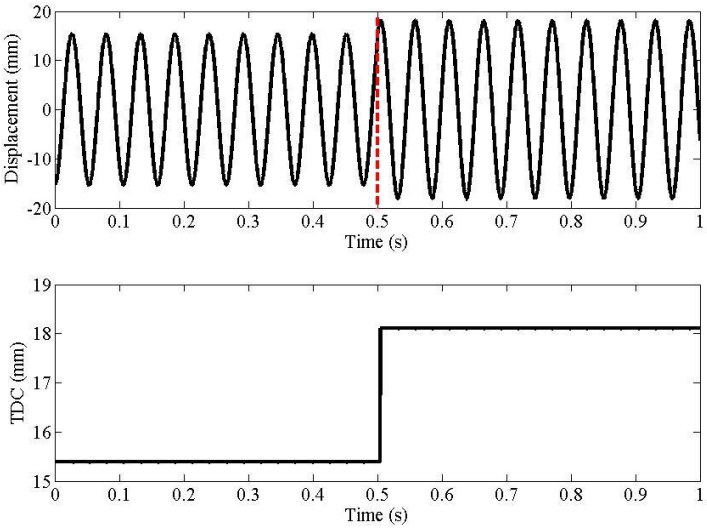

Figure 5.8 Piston profile with step electric load decrease by 15%

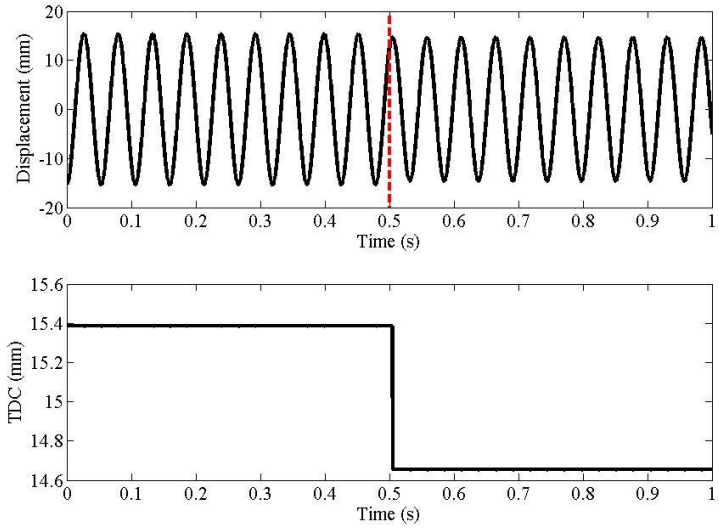

Figure 5.9 Piston profile with step electric load increase by 5%

Cycle-to-cycle variations

Severe cycle-to-cycle variations have been described by experimental research articles in the operation of dual-piston FPEG [41]. The possible reasons of these variations could be a combination of a number of factors, *i.e.* intake/exhaust pressure variations in the manifold, combustion variations, air/fuel mixture formation variations. As a result, the corresponding effective combustion efficiency, η_c varies. Then a random value of η_c from the range of $[0.95 - 1]$ is used to investigate the influence of the variations on the engine performance [123]. As shown in Figure 5.10, variations on the achieved piston TDC are observed. However, unlike conventional reciprocating engines, the unstable combustion in FPEs could affect the combustion process in the next cycle without the limitation of the crankshaft mechanism.

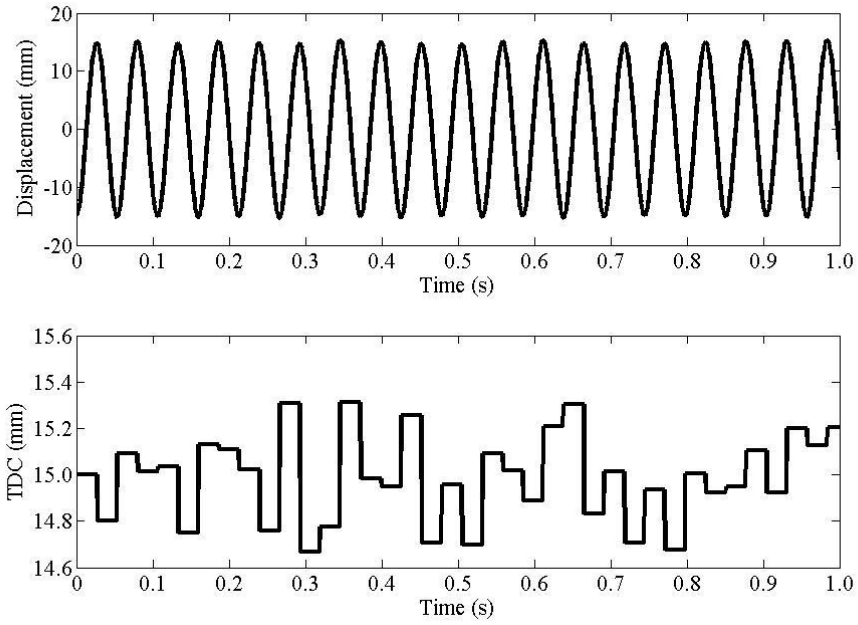

Figure 5.10 Piston dynamics with cycle-to-cycle variations

Unsuccessful ignition

During the operation of the FPEG, unsuccessful ignition could take place at any time. This problem could be caused by the unexpected failure of the spark plug/injector, or the power supply to the electronics. When unsuccessful ignition happens, the excitation

force changes to zero. Then the FPEG system can be represented by a free vibration system with viscous damping, which is described by:

$$m\ddot{x} + c\dot{x} + kx = 0 \tag{5.78}$$

$$c = k_v \tag{5.79}$$

$$k = \frac{2\gamma p_0 A}{L_s} \tag{5.80}$$

As the damping coefficient is less than the critical damping coefficient c_c:

$$c_c = 2\sqrt{km} \tag{5.81}$$

The solution of Equation (5.78) is underdamped according to the vibration theory [130], which can be expressed by:

$$x = e^{-ct/2m}(C_1 \sin \omega_d t + C_2 \cos \omega_d t) \tag{5.82}$$

Where the value of C_1 equals to $\dot{x}/\omega$ at the time when unsuccessful ignition occurs, and C_2 is the value of x when unsuccessful ignition takes place. The damped natural frequency after misfire is then given by [130]:

$$\omega_d = \omega(1 - \zeta^2)^{1/2} \tag{5.83}$$

$$\zeta = c/c_c \tag{5.84}$$

After substituting the constant parameter to Equation (5.82), the piston profile after unsuccessful ignition is demonstrated in Figure 5.11. It was observed that when an unsuccessful ignition occurs in one operation cycle, the piston will be driven to the other side by the compressed air in the cylinder. Without the power force from the heat released by the gas mixture, the TDC achieved in the following cycle is significantly reduced, and cannot reach the required position for successful ignition. As a result when unsuccessful ignition happens, the engine stops after one oscillation cycle, and the piston stays in the middle of the stroke.

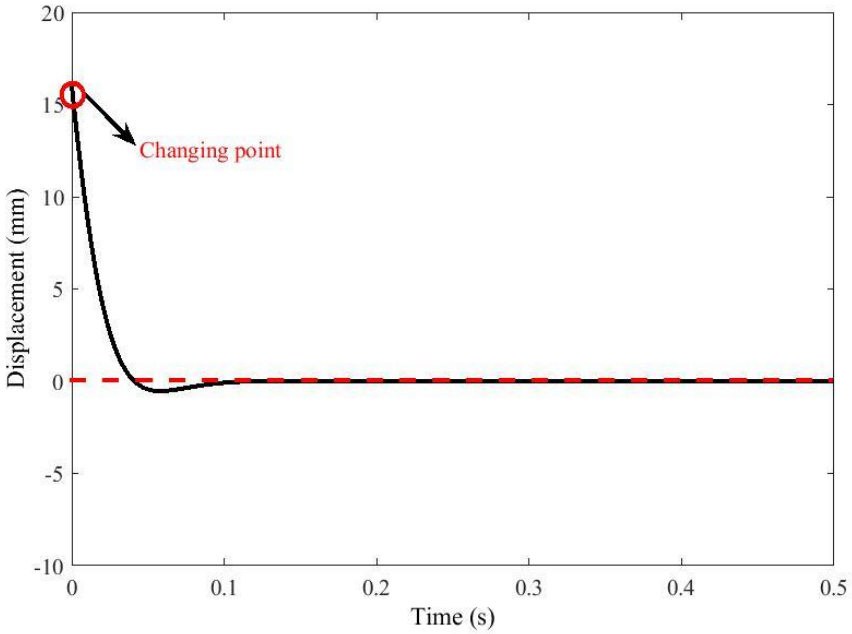

Figure 5.11 Piston profile after misfire

Electric load change with cycle-to-cycle variations

The data in Figure 5.12 shows the influence of step electric load change along with cycle-to-cycle variations. At the time of 0.3s, the electric load is controlled to decrease immediately by 15%. The model uses a random number generator $[0.95 - 1]$ to vary the cycle-to-cycle variations [123]. The piston TDC is observed to experience a step increase with small variations. Compared with the electric load change, the influence of the cycle-to-cycle variations to the piston TDC is minimal but could affect the future controller performance. As a result, both the electric load change and cycle-to-cycle variations are suggested to taken into account in the design process of the controller.

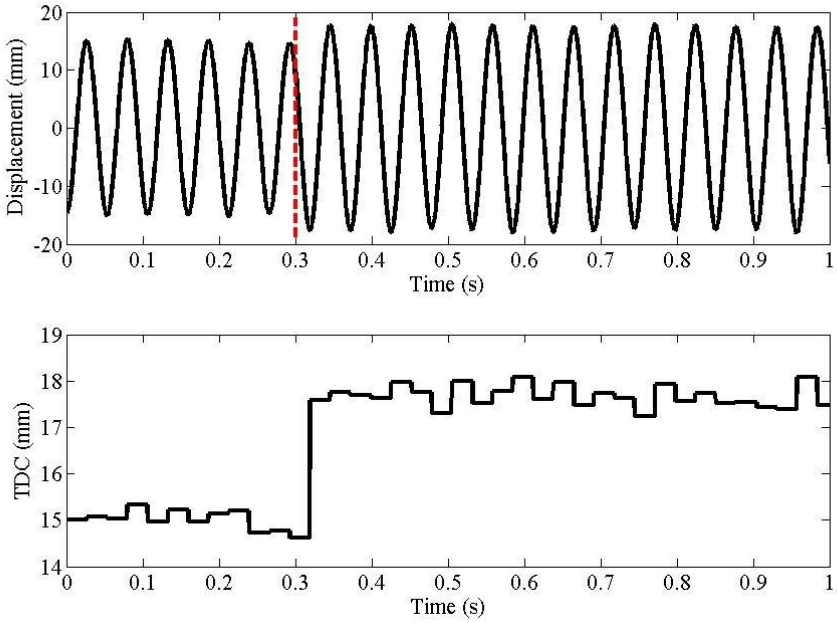

Figure 5.12 Piston dynamics after electric load change along with variations

Unsuccessful ignition with electric load change

When an unsuccessful ignition occurs, the excitation source for the FPEG system is then reduced, and the system becomes a free vibration system with viscous damping. As the damping coefficient equals to the coefficient of the load force, when misfire happens, the piston profile is supposed to vary with the electric load. When the electric load is reduced to 0, the damping is eliminated, and the FPEG system can be described by:

$$m\ddot{x} + kx = 0 \tag{5.85}$$

The solution to Equation (5.85) is then:

$$x = C_1 \sin \omega t + C_2 \cos \omega t \tag{5.86}$$

The data in Figure 5.13 illustrates the piston trace after unsuccessful ignition along with immediate electric load change in percentage of the initial set value. The engine stops at the middle stroke after several oscillation cycles when disturbance occurs. With lower electric load, more oscillation cycles are observed for the engine to stop. It means that

when unsuccessful ignition occurs, the engine will stop if the electric generator is still in operation, even with part load. If the electric load is reduced to zero, the sinusoidal oscillation of the mass will repeats continuously, and the TDC position remains unaffected. As a result, the recommended action is that the generator should be switched off (or to a motor) immediately after unsuccessful ignition occurs to restart the engine.

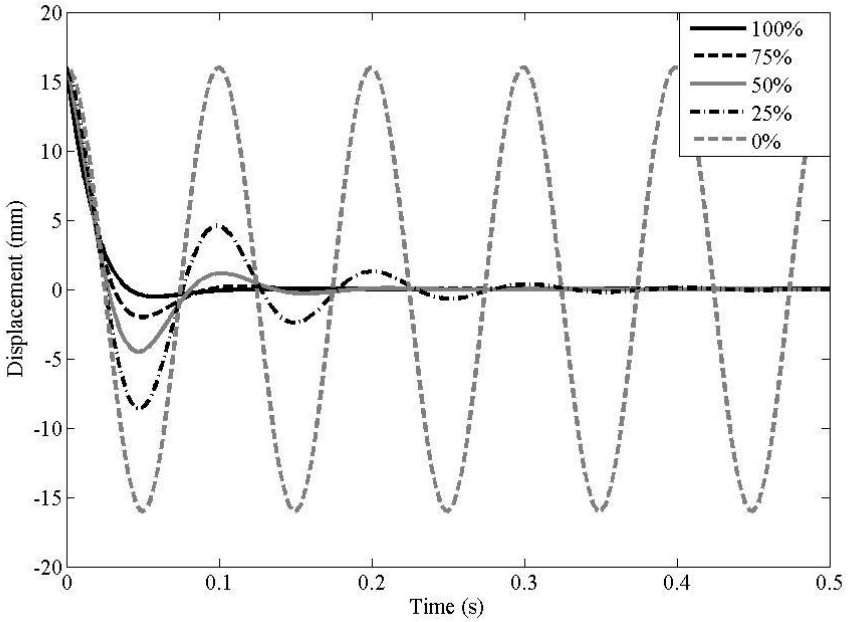

Figure 5.13 Piston dynamics after misfire along with electric load change

5.4 Summary

The response of a dual piston FPEG was simplified to be represented as a one degree forced vibration mass spring damper system, and the solution for reciprocating engines was identified, *i.e.* $x = -\frac{F_0 \cos \omega_n t}{c\omega_n}$. The model was successfully validated with respect to experimental data obtained from a FPE prototype. The simulated piston displacement during steady operation showed similar trends with the test results and the error both of the displacement amplitude and the engine running frequency were acceptable. Basic assumptions and simplifications for the model are summarised as:

(1) the frictional forces are neglected;

(2) the ideal running cycle of the FPEG is described by two adiabatic processes connected by a constant volume heat release process;
(3) the cylinder pressure is linearized using Taylor expansion around the zero-point, and all high order terms are neglected.

The model is designed specifically for use in control applications. Similarly with the adoption of virtual engineering tools in reciprocating engine technologies, other more appropriate numerical solutions should be employed for thermodynamic or component level analysis *etc*. However, the simplicity and flexibility of the proposed model make it feasible for implementation and coupling with a real-time HIL simulation model for the future piston dynamic control system development. In addition, since it reveals how an FPEG operates based on a resonant principle, the model is also useful for parameter selection in the FPEG design process.

The possible disturbances to the FPEG prototype were analyzed using the proposed fast-response numerical model. Immediate electric load change, engine cycle-to-cycle variations, and unsuccessful ignition are identified as three potential disturbances. For various disturbances, the engine responds in three different ways, *i.e.* TDC step change, TDC small variations and stop. For FPEs, without the aid of the crankshaft mechanism, the TDC must be controlled within tight limits to ensure sufficient compression and to avoid mechanical contact between the piston and cylinder head [40].

Chapter 6. Stable operation control of the free-piston engine generator

As the piston motion of the FPEG is not restricted by a crankshaft-connection rod mechanism, the piston is free to move between its instantaneous TDC and BDC positions, and the movement is only controlled by the gas and load forces acting upon it. This induces problems such as challenges in the starting process, risk of misfire, and unstable operation [31, 66]. In this chapter, control challenges for the FPEG will be analysed and the global control structure will be presented. As the control of piston dead centres are crucial for the FPEG compared with conventional reciprocating engines, the piston motion control is selected as the main objective in this research. Cascade control is proposed to be implemented, and the controller performance will be simulated and discussed.

6.1 Fundamental analysis

6.1.1 Control challenge

For the conventional engine, an engine control unit (ECU) is now used widely to control a series of actuators to ensure optimal engine performance. The ECU reads data from sensors, and interprets the values using a multidimensional lookup tables, and then adjusts the corresponding actuators. The ECU is used widely to control the air/fuel ratio, ignition timing, engine idle speed and valve timing [132]. The crankshaft mechanism determines the piston profile and provides piston motion control. Due to the high inertia of the flywheel, the piston movement cannot be easily affected by potential disturbance in one cycle. A starting motor is widely used on gasoline engines to initiate engine

rotary motion and operation. When current from the starting battery is applied to the solenoid of the motor, the solenoid engages a lever that pushes out the drive pinion on the starter driveshaft and meshes the pinion with the starter ring gear on the flywheel of the engine [133].

Compared with conventional reciprocating engines, the crankshaft mechanism is eliminated in a FPEG. Its piston motion is not limited by the mechanical system, and the compression ratio is a controlled parameter or variable. The piston profile is therefore not fixed, and it is more prone to be influenced by disturbances. Another crucial technical challenge in the FPEG operation is the starting process, which is the initial process of overcoming the compression force to achieve a certain piston speed and compression ratio for stable and continuous operation [134-140]. Despite these challenges, only a few detailed investigations on the control strategy of the FPEs have been reported, as most of the research work concentrate on the design, simulation or performance prediction of FPEs in stable operation [10, 12, 32, 141-143].

6.1.2 Control objectives

A sophisticated engine system normally contains a large number of control loops [144-149]. For the design of these feedforward and feedback control systems [149], the main design objectives are:

> Objective (1) - The system's demands for energy supply, and low fuel consumption must be met.
> Objective (2) - The piston is controlled to move stably between its target BDC and TDC, or to reach and maintain the target dead centers.
> Objective (3) - The engine must be kept in a safe operation region to avoid damage or fatigue of the material. Engine knocking, overheating, or poor lubrication must be prevented.
> Objective (4) - The emission limits must be met. For spark ignited engines, precise stationary air/fuel ratio control is required.

It is observed that, the (1) , (3) and (4) are identical with the main objectives listed for the control of conventional spark ignited engines, while objective (2) is unique for the

control of FPEG. Since these objectives are partially in contradiction, they must be fulfilled according to the set priorities. The hardware implementation of all control problems arising in the FPEG system is beyond the current research stage. Thus objective (2), the piston motion control is selected as the main objective in this research to investigate the stable operation of the FPEG.

6.1.3 Control structure

The proposed control structure for the FPEG is illustrated in Figure 6.1, which is a multi-layer control system. The general working principles for each control level are discussed below, and further explanation is presented in the following section.

(1) The top level is the engine start/restart control level, which identifies the engine start and misfire signals, which are the input signals to this level, to decide the working mode of the linear electric machine. When the FPEG system starts from the cold condition, the linear electric machine is operated as a motor to drive the piston assembly move back and forth to reach the required compression ratio for ignition, and will be switched to generator mode to output electricity during the stable generating process. During the operation of the FPEG, if engine misfire is detected, the controller will output the working model signal for the linear electric machine, and the linear electric machine will be switched from generator to motoring mode to restart the engine.

(2) The supervisory control level decides and outputs the TDC set point, the throttle opening as well as the external load according to the engine performance and the target output power. It takes the power output data of the system as the input.

(3) The piston control level reads the input piston TDC data, updates and outputs the control variables to the system. Feasible controllers and algorithms will be applied in this level. The TDC setpoint received from the upper level will be taken as the input to the controller, and updated values for the control variables will be generated and provided to the lower level.

(4) The timing control level receives the input updated values of the control variables, and output the suitable values for the ignition timing, injection timing, and valve timing. This level can be considered as a software implementation level for the actuators, and it is programmed in LabVIEW software in the real

prototype. It further calculates the piston TDC value from the piston displacement data, and feeds this back to the piston control level.

(5) The actuator control level receives the input updated timing setting, and outputs transistor-transistor logic (TTL) command signals to the actuators of the FPEG prototype. It acts as a hardware level for the actuators, and it is implemented using the National Instruments CompactRIO hardware in the real prototype. It also reads and decodes the electric signals from the sensors, and outputs the engine performance data to the upper level.

(6) The basic level on the structure is the FPEG prototype with control actuators and sensors. The linear electric machine, the injector, the ignition plug, the throttle and the intake/exhaust valves are controlled by the input command signals from the upper level. Signals output from the sensors are collected and fed back to the upper level for further analysis.

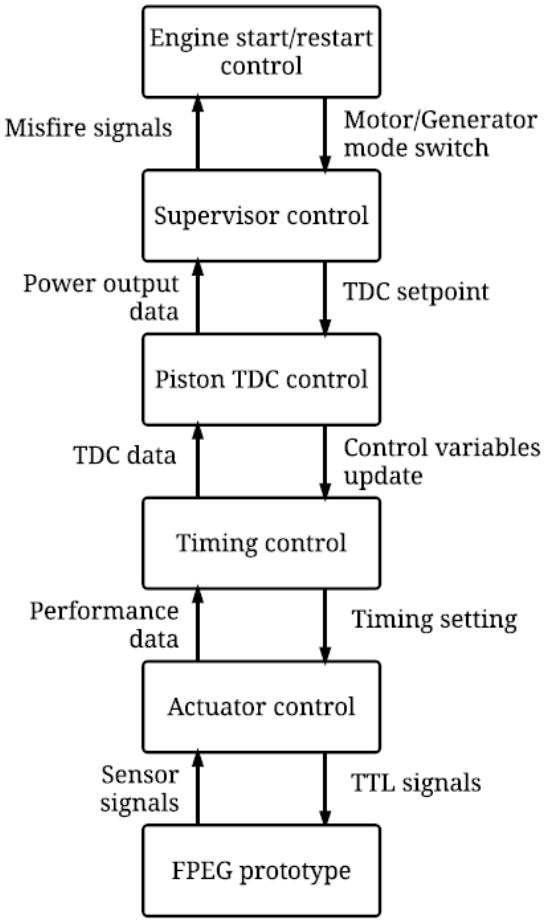

Figure 6.1 FPEG control structure

6.2 Piston stable motion control

6.2.1 System input and output analysis

As the control system is aimed for piston stable running control, the piston is controlled to reach and maintain the target TDC, x_{TDC}. As a result, the TDC is selected as the system output. x_{TDC} can be calculated from Equation (5.55) to Equation (5.60), which can be described by:

$$x_{TDC} = \frac{F_0}{c\omega} = \frac{\frac{4m_f H_u R}{\pi CR^{\gamma-1} L_s C_v}}{k_v \sqrt{\frac{2\gamma p_0 A}{mL_s} + \frac{m_f H_u R\gamma}{mC_v {L_s}^2 CR^{\gamma-1}}}} \tag{6.1}$$

Where F_0 is the magnitude of the excitation force (N); the constant c is the damping coefficient; ω_n is the angular natural frequency; m_f is the injected fuel amount to the combustion chamber (kg); H_u is the low heating value of the fuel with the combustion efficiency (J/kg); R is the ideal gas constant; CR is the set geometric compression ratio, which is affected by the ignition timing due to the ideal constant volume heat release process; L_s is the length of half stroke (m); C_v is the heat capacity at constant volume (J/m^3·K); k_v is the coefficient of the load force; γ is the heat capacity ratio; p_0 is the ambient pressure (Pa); A is the piston surface area (m^2); m is the moving mass of the mover with the pistons (kg).

The engine speed, H_n (Hz) is a useful output sign for the observation of the engine operation, which is obtained from Equation (5.58):

$$H_n = \frac{\omega_n}{2\pi} = \sqrt{\frac{2\gamma p_0 A}{mL_s} + \frac{m_f H_u R\gamma}{mC_v {L_s}^2 CR^{\gamma-1}}}/2\pi \tag{6.2}$$

From Equation (6.1) and (6.2), it is apparent that both the TDC and engine speed are influenced by various input parameters, which can be further selected as control variables. The potential control parameters are summarised in three categories, which are demonstrated in Table 6.1. The engine capacity is decided during the hardware design process, thus the piston area, stroke length and moving mass are not considered as feasible real-time control inputs. The injected fuel amount is found to be effective to

both piston TDC and engine speed, while the electric load is only effective to the piston TDC according to Equation (6.1) and (6.2), and it is often considered as a disturbance to the system [40, 113]. As a result, the injected fuel amount is selected as the main control variable in this research.

	Input parameters		
	Engine size	Working conditions	Electric load
TDC	○ Piston area, A ○ Half stroke length, L_s ○ Moving mass, m	○ Injected fuel amount, m_f	○ Coefficient of the load force, k_v
Engine speed	○ Piston area, A ○ Half stroke length, L_s ○ Moving mass, m	○ Injected fuel amount, m_f	-

Table 6.1 Potential parameters influential to TDC

Varying the injected fuel mass will affect the amount of energy released in the combustion process. The data in Figure 6.12 shows the effect of the injected fuel mass per cycle on engine operation performance using Equation (6.1) and (6.2). When the fuel mass changes from a wide range from -90% to 90% in the model, i.e. without considering its physical feasibility, the TDC increases from 2 mm to 24 mm (engine stroke length from -20 mm to 20 mm). The engine TDC is directly sensitive to the injected fuel mass amount, and small variations in the current engine can lead to large changes in TDC and compression ratio. For an engine with a stroke length of 40 mm, as considered here, a TDC variation of ±1% of the stroke length would be equivalent to 0.4mm and would produce a compression ratio variation of approximately ±1.0. However, the influence of the injected fuel mass on the engine speed is not that obvious compared with that on the piston TDC, the equivalent engine speed is limited within the range from 700 to 1500 rpm with the fuel mass changes from a wide range from -90% to 90%.

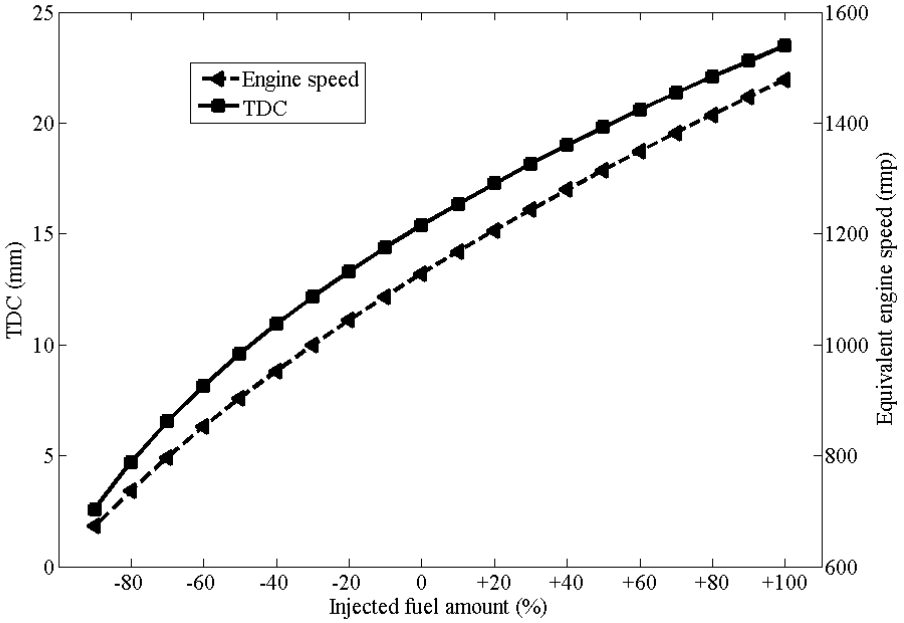

Figure 6.2 Effects of injected fuel amount to TDC and engine speed

6.2.2 Cascade control introduction

The special configuration and characteristics of the FPEG make it different from the control system for conventional engines. From the above simulation results, for any disturbance there will be corresponding effect on the piston TDC, and the disturbance will influence the TDC for every following cycle. From the reported literature, most of the controllers for the FPEs are designed to be single loop controller with single control input and single output (SISO) [38, 98, 113, 150-153]. If the piston TDC is used a feedback signal, and the injection amount is the control variable of the control system, the information flow diagram for a single feedback controller is illustrated in Figure 6.3.

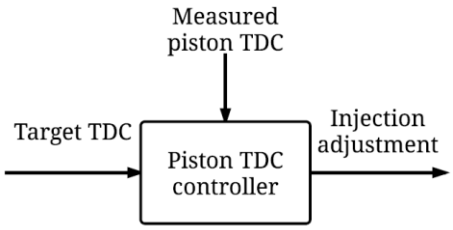

Figure 6.3 Information flow with single feedback control

A series events of a two-stroke FPEG cycles with SISO controller actions are summarised in Table 6.2. It is observed that the control variable can be updated once per stroke. When a disturbance occurs during event (1) or (2), the piston TDC of the right cylinder will be affected and further detected by the controller at (3). The controller action will be set during (4) and the injection will be updated at (5), then the error will be corrected gradually from (6). A significant delay is found in this SISO control system. When a disturbance happens in stroke 1# of cycle 1#, correction will not take place until the stroke 1# of cycle 2#, one full cycle after the disturbance occurs.

Cycle	Stroke	Event	FPEG		Controller action
			Left cylinder	Right cylinder	
Cycle 1#	Stroke 1#	(1)	TDC	BDC	Read TDC position
		(2)	Power	Compression	Set controller action
	Stroke 2#	(3)	BDC	TDC	Read TDC position
		(4)	Compression	Power	Set controller action
Cycle 2#	Stroke 1#	(5)	TDC	BDC	Read TDC position
		(6)	Power	Compression	Set controller action
	Stroke 2#	(7)	BDC	TDC	Read TDC position
		(8)	Compression	Power	Set controller action

Table 6.2 A series events of a two-stroke FPEG cycles with SISO controller actions

If the error of the SISO controller is significant, and cannot be corrected at the current cycle due to the controller delay, this may induce misfire or mechanical contact between piston and cylinder head. In order to improve the controller performance and to reduce the controller delay, cascade control strategy is proposed to be implemented in the FPEG piston stable motion control system. The cascade control, in contrast with SISO control, makes use of multiple control loops that involve multiple feedback signals for one control variable [154-158]. The information flow with cascade control is shown in Figure 6.4. It uses the measured piston TDC and velocity signals to control the fuel injection rate.

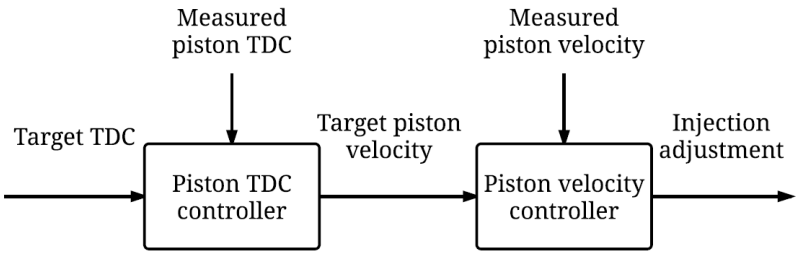

Figure 6.4 Information flow with cascade control

The block diagram of the FPEG coupled with cascade control is illustrated in Figure 6.5. In such a control system, the output of the outer loop will determine the set point for the inner loop, and the output of the inner loop is used to update the control variable. The implementation of cascade control make it possible to take both of the measured TDC of the previous stroke and the measured piston velocity at the current stroke as feedback, the injected fuel mass being the control variable, thus potentially providing better performance than a single loop controller. It will detect the fluctuations from the secondary controller, and reduce the influence to the primary controller. If disturbance occurs during (1) or (2) in Table 6.2, the secondary controller can detect the piston velocity at the middle stroke of the current operation stroke, and then correct the error at (3). Thus the control delay will be reduced significantly compared with the single feedback controller.

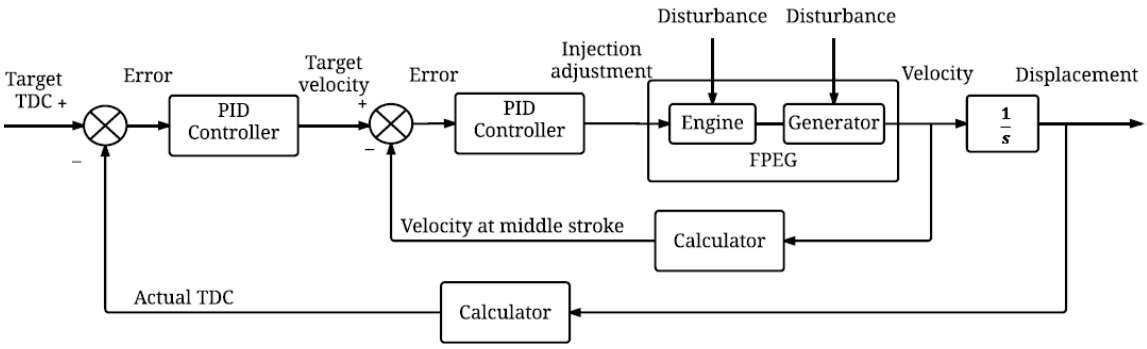

Figure 6.5 Block diagram FPEG coupled with cascade control

The Proportional-Integral-Derivative (PID) controllers are used in both of the outer loop and inner loop. PID controller is a three-term controller that has a long history in the

automatic control field [159, 160]. Due to its intuitiveness and its relative simplicity, in addition to satisfactory performance, it has become in practice the standard controller in industrial settings [161-165]. Applying a PID control law consists of applying properly the sum of three types of control actions: a proportional action, an integral action and a derivative one. In the Laplace domain, the three actions can be described by the following equation [166]:

$$U(s) = \left(K_p + \frac{K_i}{s} + K_d s\right) E(s) \tag{6.3}$$

The controller transfer function $C(s)$ can be written as:

$$C(s) = K_p + \frac{K_i}{s} + K_d s \tag{6.4}$$

Where $U(s)$ is the control variable; $E(s)$ is the control error; K_p, K_i and K_d are the proportional gain, integral gain and derivative gain respectively.

6.2.3 Controller performance simulation

The FPEG system coupled with cascade control illustrated in Figure 6.5 is simulated in Matlab/Simulink. Shown in Figure 6.6, a subsystem "Disturbance Subsystem" is developed to simulate the occurrence of potential disturbance, and immediate change on the electric load is used to represent the effects of all kinds of possible disturbance to the system. The set target of the piston TDC is 15.5 mm, or 4.5 mm from the cylinder head. Two PID controllers are used in both of the outer loop and inner loop. The output of the inner loop will update the control variable (injected fuel amount). An "Injector" sub model is developed to simulation the injection with the updated injection amount at proper injection timing. A subsystem "FPEG system" is developed to simulate the piston displacement using Equation (5.54). The "Velocity monitor" and "TDC calculator" subsystems are used to calculated the piston velocity at the middle stroke of the current cycles and the piston TDC of the previous cycle respectively. As the piston motion is decided by the net forces acting on the piston, any type of disturbance will lead to an immediate change of the net forces, which acts as an extra force on the piston. Thus the results of electric load change may be taken to represent the effects of other

disturbances. The parameters of the PI controller are manually tuned, and the controller performance could be further improved with optimised control parameters.

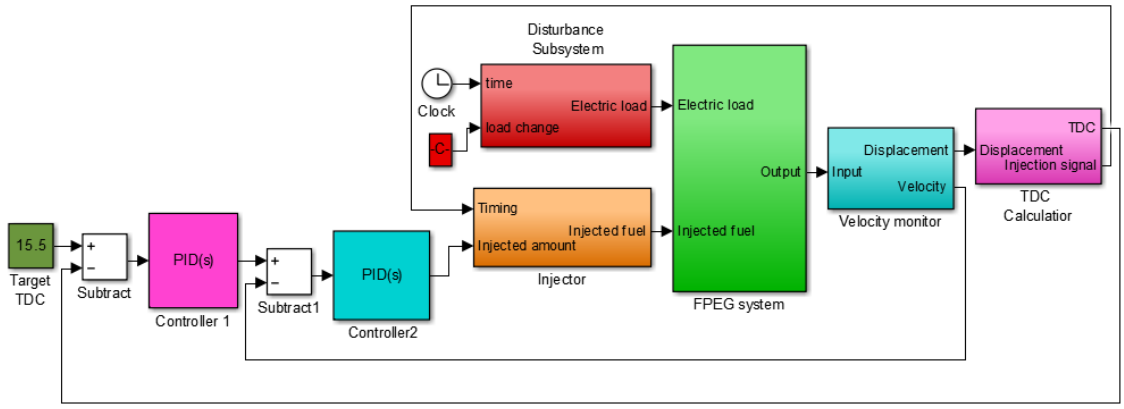

Figure 6.6 Cascade control simulation in Matlab/Simulink

The electric load, injected fuel mass, as well as the other initial parameters are taken as inputs to the FPEG fast response numerical model, and the piston displacement and velocity are thus obtained. The piston TDC and the piston velocity at middle stroke are then further evaluated and fed back to the controllers. When an error on either the piston TDC or the piston velocity at middle stroke is detected, the cascade control algorithm will take action, and adjust the injected fuel mass. The updated injection information will be output to the injection system, and the corrected fuel mass will be delivered when the piston reaches its TDC.

According to the previous literatures on the FPE control using PID controller, the effect of the derivative gain term was reported to be limited in the TDC control loop[113], thus the controller performance was investigated using a PI controller only. By setting the values of the proportional gain and integral gain in the feedback control system, two PI controllers were successfully implemented to the simulation programme. An example of the engine response to a 15% step decrease of electric load is shown in Figure 6.7. The disturbance occurs immediately at 1.1 s, and the controller performance is proved robust. The cascade control takes action during the current cycle when disturbance occurs, and the piston TDC is gradually reduced from the current cycle. The piston TDC is controlled to be back to its set point in 0.5 s.

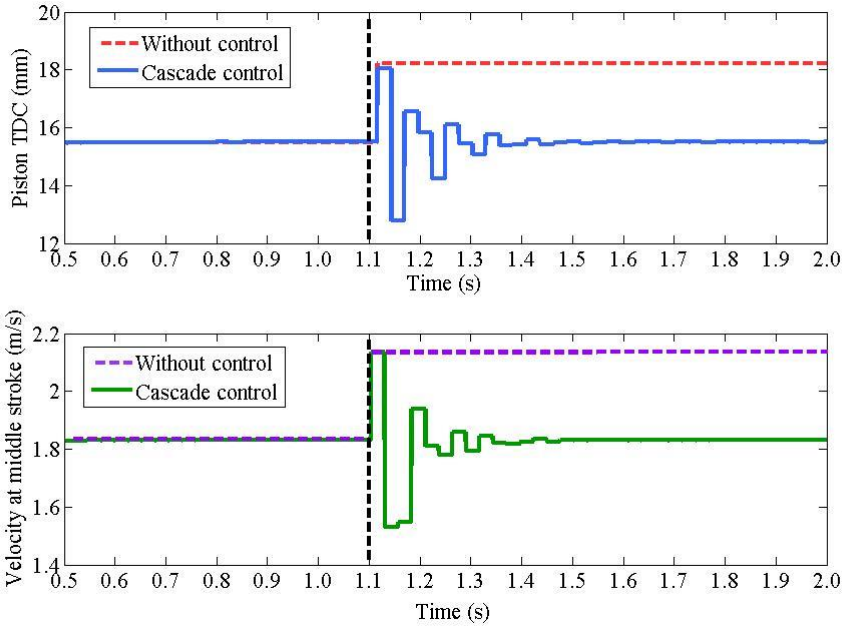

Figure 6.7 Cascade control performance with load step decrease

The injected fuel mass for each cycle after the occurrence of the disturbance is illustrated in Figure 6.8. It is observed that when an error on the piston velocity at the middle is detected by the controller, the injector is controlled to take action from the current cycle to reduce the error. However, the variations on the injected fuel mass seen in Figure 6.8 are not that significant, which change from 2.0 mg to 3.0 mg. The port injection system sprays the fuel behind the intake valve, and the fuel will be draw into the cylinder when the intake valve opens. This may induce to some fuel drop out of the air, and may affect the control accuracy.

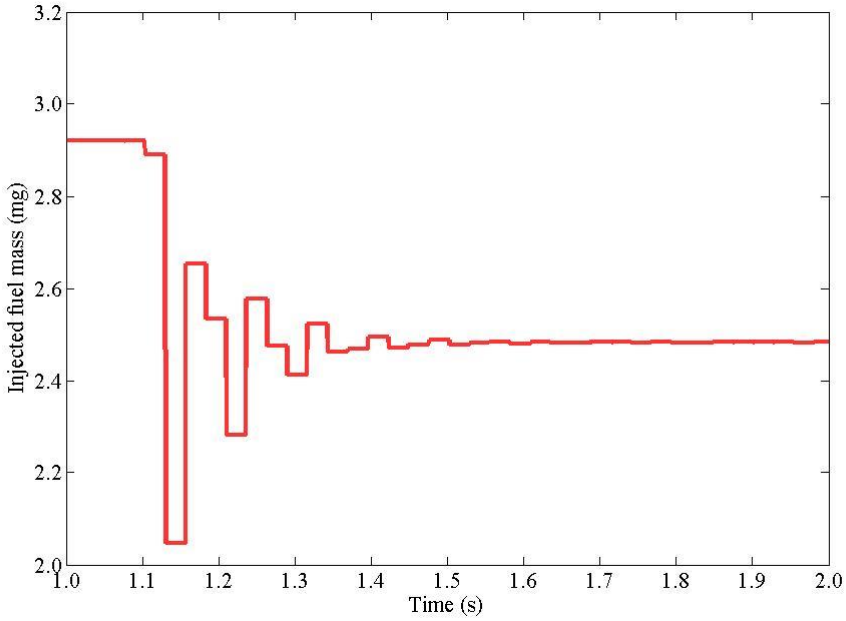

Figure 6.8 Injected fuel mass information after cascade control action

The data in Figure 6.9 demonstrates the engine response to a 15% step increase of electric load. The disturbance takes place at 1.1 s, and the controller takes action when the error is detected. The piston TDC increases from the current cycle when disturbance occurs, both of the piston TDC and the piston velocity are controlled to the target value in less than 0.5 s, indicating that the controller's performance is robust. From Figure 6.8 and 6.9, it is observed that the proposed cascade control implemented in the FPEG is feasible for both immediate load decrease and increase. The system will be back to the stable state in an acceptable period. The parameters of the PI controller are manually tuned, and the controller performance could be further improved with optimised control parameters.

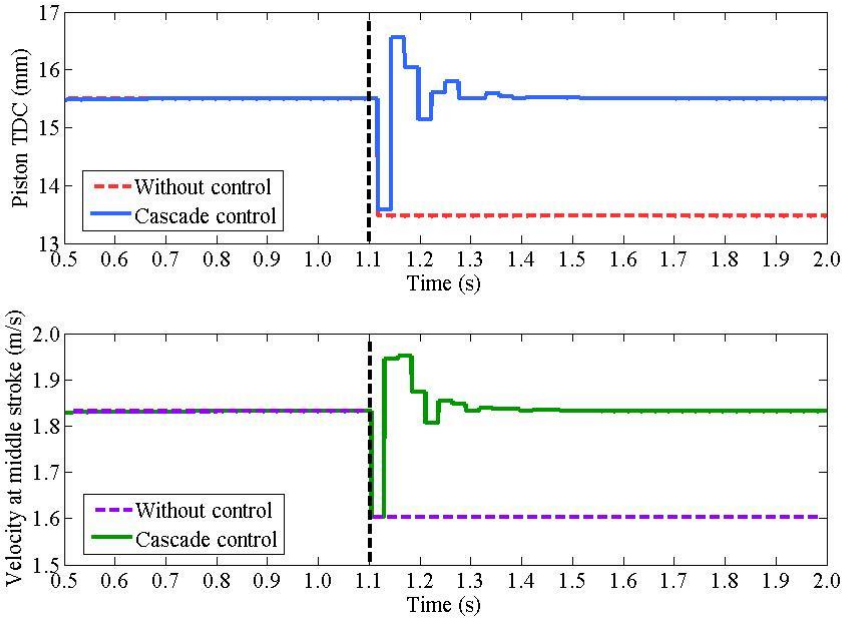

Figure 6.9 Cascade control performance with load step increase

The error of cascade control is demonstrated in Figure 6.10, with the error of the single loop control as well as the error without active control compared in the same figure. The maximum error happens at the first cycle after the disturbance occurs. With the designed cascade control, the error for piston TDC begins to decrease from the first cycle. While with the single loop PID control, the error decreases from the second cycle as the controller is unable to update the injected fuel mass only when an error for the first cycle is detected. The purple lines in Figure 6.10 are ±0.1 mm from the TDC, and the orange lines are the settling time, *i.e.* the time it takes for the controller to bring the response within these bounds. It is obvious that, by implementing the cascade control, the outcome is better in terms of both peak error and the settling time.

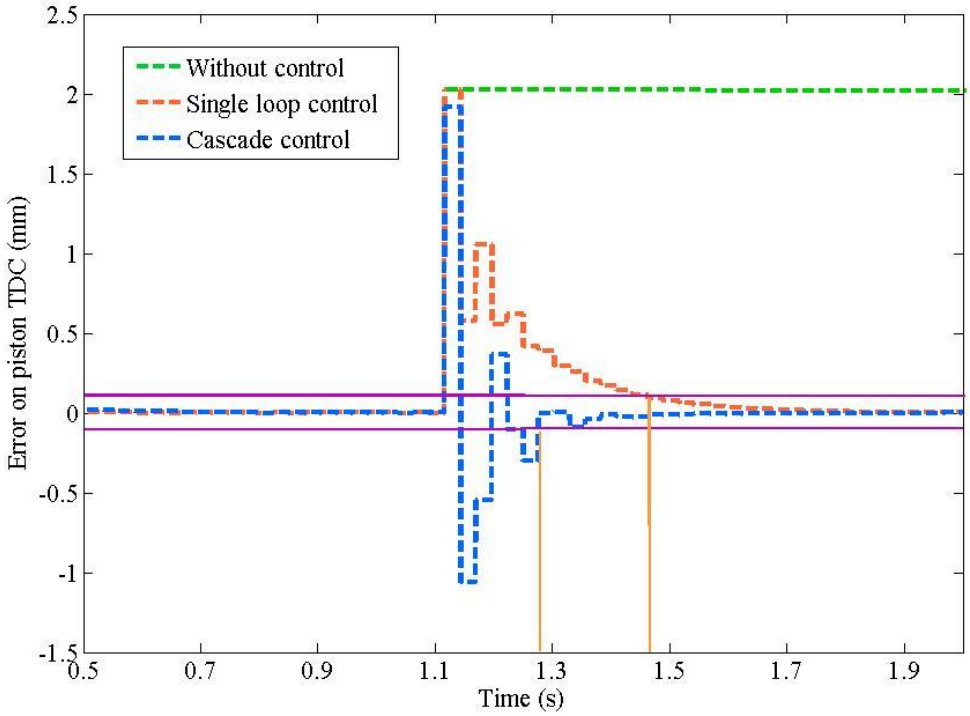

Figure 6.10 Cascade control error analysis

As the disturbance may occur anywhere during the operation of the FPEG, the performance of the proposed cascade control is simulated with different disturbance occurrence time. Four typical points for the disturbance occurrence are highlighted in Figure 6.11, which are:

- point a between the BDC and the middle stroke during stroke 1# (marked as Stroke 1# a);
- point b between the middle stroke and the TDC during stroke 1# (marked as Stroke 1# b);
- point c between the TDC and the middle stroke during stroke 2# (marked as Stroke 2# c);
- point d between the middle stroke and the BDC during stroke 2# (marked as Stroke 2# d).

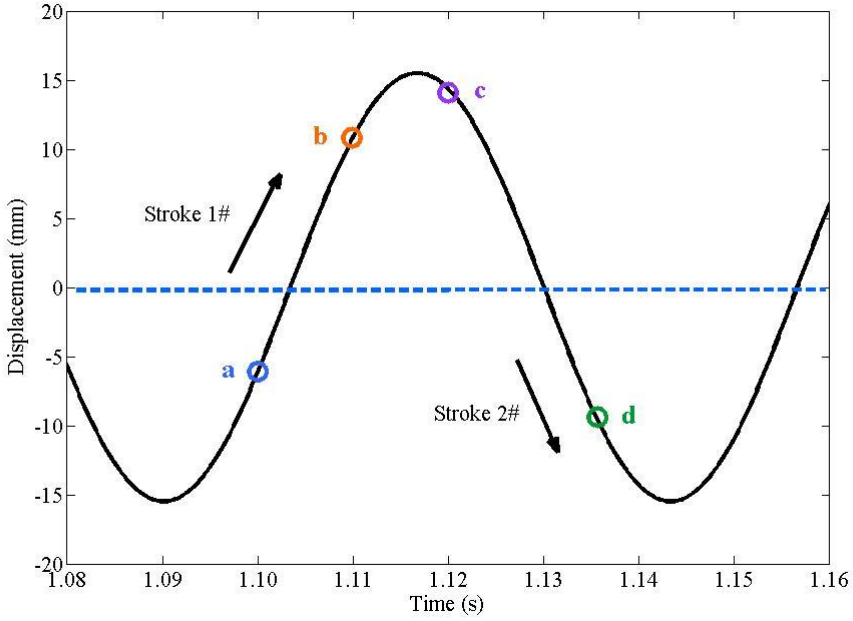

Figure 6.11 Illustration of disturbance occurrence time

As demonstrated in Figure 6.12, the error of the cascade control on the piston TDC varies with different disturbance occurrence time. Nevertheless, independent of whenever the disturbance takes place, the controller performance is proved to be robust, and the system will be back to stable state in 0.5 s. It is observed that if the disturbance occurs earlier before the piston arrives the middle stroke, the peak error will be reduced compared with which that takes place after the piston reaches the middle stroke position. This is because once a disturbance occurs shortly after TDC/BDC (Stroke 1# a and Stroke 2# c), an error on the piston velocity will be detected by the controller at the middle of the stroke, and the control variable will be updated in the current stroke. However, if the disturbance takes place after the piston arrives the middle of the stroke (Stroke 1# b and Stroke 2# d), the controller will not take action until the following stroke. As a result, the proposed cascade control implemented in the FPEG system is slightly more effective when the disturbance occurs before the piston arrives the middle position. However the difference is very small. It is also not critical for the engine when the disturbance occurs, and there is no particularly bad time for a load change.

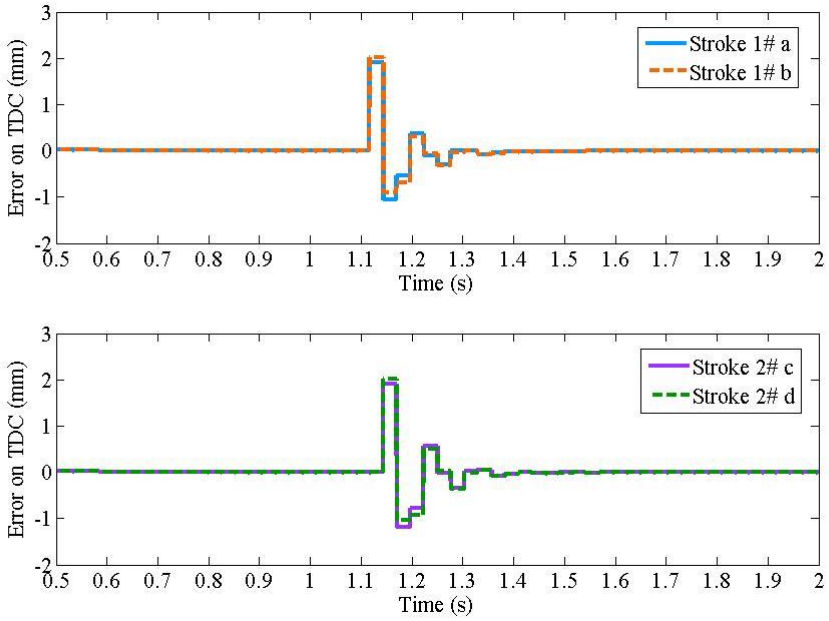

Figure 6.12 Cascade control performance with different time of disturbance occurrence

For the single loop controller, shown in Figure 6.13, the peak errors are the same whenever the disturbance occurs. The piston TDC for the previous cycle is the only feedback, thus it does not take action until the next cycle. As a result, for the disturbance occurs in the current cycle, the error will not be detected immediately during the same cycle, and the timing of the disturbance is of little importance to the controller performance.

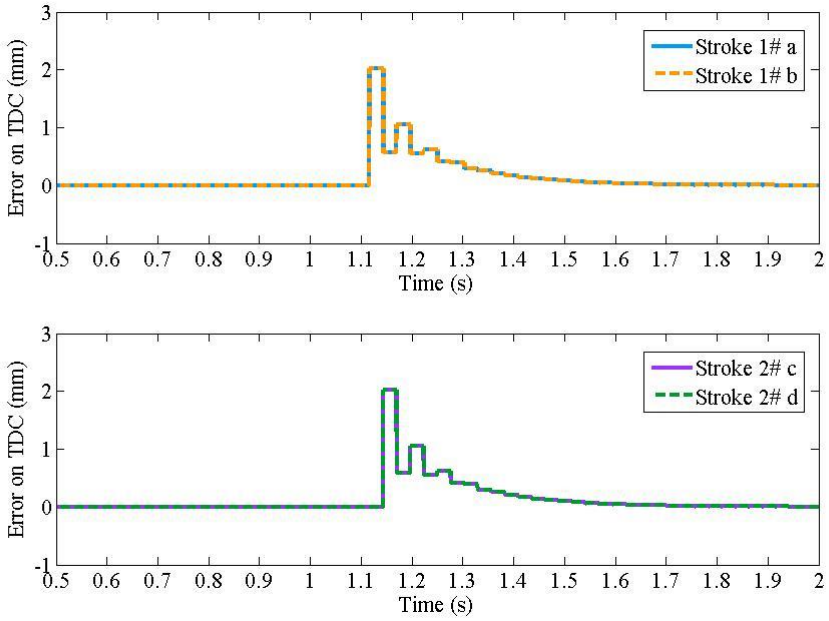

Figure 6.13 Single-loop control error with different time of disturbance occurrence

6.3 Summary

In this chapter, the global control structure for the FPEG prototype is presented, which is a multi-layer control system including the engine start/restart control level, supervisory control level, piston control level, timing control level, actuator control level, and the prototype level with actuators and sensors. Cascade control strategy is proposed for the piston stable operation level and PI controllers are used in both of the outer loop and inner loop. Both the measured TDC of the previous stroke and the piston velocity at the current stroke are taken as feedbacks, and the fuel injection amount is used as the control variable.

According to the simulation results, the proposed cascade control implemented in the FPEG shows good performance, and it is feasible for correcting both immediate load decrease and increase disturbances. The system will be back to the stable state in 0.5 s, which is acceptable. Compared with single loop control, the performance is improved by implementing the cascade control in terms of the control delay, peak error and settling time, and it is slightly more effective when the disturbance occurs before the piston arrives the middle position in each stroke.

Chapter 7. Conclusions

This thesis has presented the detailed numerical modelling, simulation and control strategy of a spark ignition free-piston engine generator, and the details of the findings have been provided at the end of each chapter. In this chapter, they will be summarised and evaluated in relation to the performance of the FPEG, and recommendations for future research will be discussed.

7.1 Summary of the results

Chapter 2 presented the recent research finding on the FPEG development, including numerical modelling, prototype design, and control strategy. It is found that the FPEG was commonly modelled using simplified zero-dimensional models for conventional engines. Most of the reported models are valid for an adiabatic and isentropic processes, in which no heat or mass is gained or lost. However, the actual system cannot be taken as isentropic system because of the low operating speed. Moreover, there has not been any model validation reported due to the limited amount of experimental test data from the running prototype. Various FPEG prototypes have been reported, however, very few of them have operated successfully. The lack of crankshaft mechanism makes it difficult to start, and prone to unstable operation, therefore a robust control strategy is necessary. In summary, a validated numerical model and an effective control strategy are still required to bring the FPEG technology forward.

Chapter 3 provided the design and simulation of a FPEG which can be operated using either a two-stroke or four-stroke cycle gas exchange process. The working principles for both gas exchange processes were described and compared. For the two-stroke cycle, the linear electric machine was operated as a generator throughout, and the

system was balanced without an external force. While for the four-stroke cycle, the system was not balanced and the generator had to be switched to motor mode to drive the piston during the gas exchange process. A detailed system dynamic sub-model, friction model, engine in-cylinder thermodynamic model, and linear electric machine model were derived and presented. The compression and expansion processes were not regarded as ideal gas isentropic processes; both heat transfer and air leakage were considered. The model was implemented in Matlab/Simulink. Specifications for both cycles on valve timings were described, and sequence events for four-stroke were presented.

In Chapter 4, the model validation and the simulation results were described. The prototype developed at Newcastle University was introduced. During the starting process, the piston was controlled to move with constant speed, and change its direction when the piston reaches the expected dead centres. The test data showed good agreement with the simulation results, indicating that the numerical model was validated. The simulation results of the piston dynamics, engine performance, and indicated power distribution during the stable generating process were presented for both two-stroke and four-stroke thermodynamic cycle, along with a detailed parametric sensitivity analysis. Simulation results indicated that the two-stroke FPEG showed advantages of high power output, high engine speed, low vibration, balanced without external force, wide range of power output. The four-stroke FPEG showed advantages of better scavenging performance, high engine efficiency, low fuel consumption, high compression ratio. Due to the higher power output and simpler control system, the two-stroke cycle was applied to the FPEG prototype in Newcastle University.

In Chapter 5, the response of a dual piston FPEG was simplified to be a one degree forced vibration mass spring damper system. The solution for reciprocating engines was $x = -\frac{F_0 \cos \omega_n t}{c\omega_n}$. The model was successfully validated with respect to experimental data obtained from a prototype. The simplicity and flexibility of the proposed model made it feasible to be implemented to several computing software, *i.e.* Matlab, AMESim, Labview, Dymola *et al.* The potential disturbances to the FPEG prototype were analyzed using the proposed fast-response numerical model. Immediate electric load change, engine cycle-to-cycle variations, and unsuccessful ignition were identified as

three potential disturbances. For various disturbances, the engine responses in three different ways, *i.e.* TDC step change, TDC small variations and stop. For FPEs, without the limitation of the crankshaft mechanism, the TDC must be controlled within tight limits to ensure sufficient compression and to avoid mechanical contact between piston and cylinder head.

Chapter 6 presented the global control structure for the FPEG prototype, which was a multi-layer control system including the engine start/restart control level, supervisory control level, piston control level, timing control level, actuator control level, and the prototype level with actuators and sensors. Cascade control strategy was proposed for the piston stable operation level, and PID controller were used in both the outer and inner loop. Both of the measured TDC of the previous stroke and the piston velocity at the current stroke were taken for controller feedback, and the injected fuel mass was used as the control variable. According to the simulation results, the proposed cascade control implemented in the FPEG showed good performance, and it was feasible for both immediate load decrease and increase. The system returned to the stable state in 0.5 s, which was acceptable. Compared with single loop control, the performance was improved by implementing the cascade control in terms of the control delay time, peak error and settling time, and it is more effective when the disturbance occurred before the piston arrived at the middle position in each stroke. However, as the variations on the injection were not that significant, the injector was suggested to be controlled with high accuracy.

7.2 Significant contributions

The design and simulation of a dual-piston spark-ignited FPEG suitable for operation using either a two-stroke or four-stroke thermodynamic cycle were presented. Model validation and the general engine performance of the system were discussed. For the first time, this research demonstrates the potential advantages and disadvantages of the FPEG on using different thermodynamic gas-exchange cycles.

A fast response real time model of the FPEG was designed and validated. Since the model is the first of a kind, all results of the model are novel and of high value to those engaged in relevant research. The simplicity and flexibility of the proposed model make

it feasible to be implemented and coupled with real-time HIL control system development. In addition, since it reveals how an FPEG operates in a resonant principle, the model is useful for parameter selection in the FPEG design process.

For the first time, cascade control is proposed for the piston stable operation control, using both of the measured TDC of the previous stroke and the measured piston velocity at the current stroke as feedback, the injected fuel mass as the control variable. The system performance is improved by implementing the cascade control compared with single loop control in terms of the control delay, peak error and settling time.

There has been a fundamental bottleneck in the development of the FPE technology, and very few of the reported FPE prototypes are successful. The lack of crankshaft mechanism makes it difficult to start, and prone to unstable operation. The methods presented in this thesis could be used the basis for all FPE design, modelling and control strategies.

7.3 Recommendations to future work

Although the FPEG shows promising advantages over the conventional reciprocating engines, significant development efforts are still required for it to advance forward a commercial application. It is considered that there are several areas that need to be further investigated.

7.3.1 Multi-dimensional simulation

Free-piston engines are commonly modelled by most researchers using zero-dimensional, single zone models developed for conventional engines. Such models can be useful for investigating basic engine performance and piston dynamics. There is a strong coupling relationship between the piston motion of the FPEG and scavenging and combustion processes. While using the current numerical simulation methods, researcher are unable to identify details of the engine operation such as in-cylinder gas motion and emissions formation. As a result, in response to the simulation of the combustion process, it is essential to set up a multi-dimensional simulation model based on accurate free-piston motion profile to predict the detailed characteristics of the in-cylinder gas during the combustion and scavenging processes.

7.3.2 Prototype improvement

With the designed prototype introduced in Chapter 4.1.1, it was found that current pneumatic actuators is difficult to meet the requirement during the combustion process due to the delay in the response time. It is suggested that the current actuators should be replaced with electronic solenoid valve actuator with better response performance. Meanwhile, the operation optimisation of the FPEG prototype should be investigated and implemented in detail. The operation parameters like the ignition timing, valve timing, *etc*. have been optimised, and any change on these parameters would lead to variations on the engine compression ratio and also power output. As a result, much work can be done to improve the performance of the prototype.

7.3.3 Control system implementation

Further work in the control of the FPEG may include the implementation of the proposed control strategy. The application of the cascade control should be studied as such controller is proved to perform better than the simple single loop controller. The integration of the control strategy with the designed prototype should be investigated, which will include the control of the linear electric machine, the external load, the injector, the ignition system, as well as the valve timing. This will require knowledge of the sensor testing system, data signal processing, software programming, *etc*. This will finally meet the main objectives of the control system, and ensure the stable operation of the FPEG prototype.

References

[1]. R. Mikalsen, A. P. Roskilly, The design and simulation of a two-stroke free-piston compression ignition engine for electrical power generation. Applied Thermal Engineering, 2008. 28(5): p. 589-600.

[2]. Rikard Mikalsen, A. P. Roskilly, A review of free-piston engine history and applications. Applied Thermal Engineering, 2007. 27(14): p. 2339-2352.

[3]. Erland Max. Fpec, free piston energy converter. in Proceedings of the 21st Electric Vehicle Symposium & Exhibition, EVS. 2005.

[4]. Peter A. J. Achten, A review of free piston engine concepts. 1994, SAE Technical Paper, No. 941776.

[5]. Peter A. J. Achten, Johan P. J. Van Den Oever, Jeroen Potma, Georges E. M. Vael, Horsepower with brains: The design of the chiron free piston engine. 2000, SAE Technical Paper, No. 2000-01-2545.

[6]. Norman H. Beachley, Frank J. Fronczak, Design of a free-piston engine-pump. 1992, SAE Technical Paper, No. 921740.

[7]. Martin Goertz, Lixin Peng, Free piston engine its application and optimization. 2000, SAE Technical Paper, No. 2000-01-0996.

[8]. Jeffrey G. Schreiber, Steven M. Geng, Gary V. Lorenz, Re-1000 free-piston stirling engine sensitivity test results. National Aeronautics and Space Administration Report, 1986. 1.

[9]. Peter Van Blarigan, Nicholas Paradiso, Scott Goldsborough, Homogeneous charge compression ignition with a free piston: A new approach to ideal otto cycle performance. 1998, SAE Technical Paper, No. 982484.

[10]. Christopher M. Atkinson, Sorin Petreanu, Nigel Clark, Richard J. Atkinson, Thomas I. McDaniel, Subhash Nandkumar, Parviz Famouri, Numerical

simulation of a two-stroke linear engine-alternator combination. 1999, SAE Technical Paper, No. 1999-01-0921.

[11]. S. Scott Goldsborough, Peter Van Blarigan, Optimizing the scavenging system for a two-stroke cycle, free piston engine for high efficiency and low emissions: A computational approach. 2003, SAE Technical Paper, No. 2003-01-0001.

[12]. Qingfeng Li, Jin Xiao, Zhen Huang, Simulation of a two-stroke free-piston engine for electrical power generation. Energy & fuels, 2008. 22(5): p. 3443-3449.

[13]. Researcher Seppo Tikkanen, Professor Matti Vilenius. Hydraulic free piston engine-the power unit of the future? in Proceedings of the JFPS International Symposium on Fluid Power. 1999. The Japan Fluid Power System Society.

[14]. Seppo Tikkanen, Matti Vilenius. On the dynamic characteristics of the hydraulic free piston engine. In ICMA'98: International conference on machine automation. 1998.

[15]. Jin Xiao, Qingfeng Li, Zhen Huang, Motion characteristic of a free piston linear engine. Applied energy, 2010. 87(4): p. 1288-1294.

[16]. Shuaiqing Xu, Yang Wang, Tao Zhu, Tao Xu, Chengjun Tao, Numerical analysis of two-stroke free piston engine operating on hcci combustion. Applied Energy, 2011. 88(11): p. 3712-3725.

[17]. Seppo Tikkanen, Mika Lammila, Mika Herranen, Matti Vilenius, First cycles of the dual hydraulic free piston engine. 2000, SAE Technical Paper, No. 2000-01-2546.

[18]. Zhenfeng Zhao, Fujun Zhang, Ying Huang, Changlu Zhao, Feng Guo, An experimental study of the hydraulic free piston engine. Applied Energy, 2012. 99: p. 226-233.

[19]. A. Hibi, T. Ito, Fundamental test results of a hydraulic free piston internal combustion engine. Proceedings of the Institution of Mechanical Engineers, Part D: Journal of Automobile Engineering, 2004. 218(10): p. 1149-1157.

[20]. X. I. A. Bizhong Wang Jinsong F. U. Xin, Yang Huayong, Development of a dual piston hydraulic free piston engine prototype and its compression ratio [j]. Chinese Journal of Mechanical Engineering, 2006. 3: p. 021.

[21]. Matthew Brusstar, Charles Gray, Kasser Jaffri, Patrick McCarthy, Marc Pomerleau, Design, development and testing of multi-cylinder hydraulic free-piston engines. 2005, SAE Technical Paper, No. 2005-01-1167.

[22]. Justin W. Raade, Timothy G. McGee, H. Kazerooni. Design, construction, and experimental evaluation of a monopropellant powered free piston hydraulic pump. in ASME 2003 International Mechanical Engineering Congress and Exposition. 2003. American Society of Mechanical Engineers.

[23]. Zhenfeng Zhao, Fujun Zhang, Ying Huang, Changlu Zhao, An experimental study of the cycle stability of hydraulic free-piston engines. Applied Thermal Engineering, 2013. 54(2): p. 365-371.

[24]. Boru Jia, Andrew Smallbone, Zhengxing Zuo, Huihua Feng, Anthony Paul Roskilly, Design and simulation of a two-or four-stroke free-piston engine generator for range extender applications. Energy Conversion and Management, 2016. 111: p. 289-298.

[25]. Boru Jia, Zhengxing Zuo, Huihua Feng, Guohong Tian, Andrew Smallbone, A. P. Roskilly, Effect of closed-loop controlled resonance based mechanism to start free piston engine generator: Simulation and test results. Applied Energy, 2016. 164: p. 532-539.

[26]. Chia-Jui Chiang, Jing-Long Yang, Shao-Ya Lan, Tsung-Wei Shei, Wen-Shu Chiang, Bo-Liang Chen, Dynamic modeling of a si/hcci free-piston engine generator with electric mechanical valves. Applied Energy, 2013. 102: p. 336-346.

[27]. M. Razali Hanipah, R. Mikalsen, A. P. Roskilly, Recent commercial free-piston engine developments for automotive applications. Applied Thermal Engineering, 2015. 75: p. 493-503.

[28]. Boru Jia, Zhengxing Zuo, Huihua Feng, Guohong Tian, A. P. Roskilly, Investigation of the starting process of free-piston engine generator by mechanical resonance. Energy Procedia, 2014. 61: p. 572-577.

[29]. Huihua Feng, Yu Song, Zhengxing Zuo, Jiao Shang, Yaodong Wang, Anthony Paul Roskilly, Stable operation and electricity generating characteristics of a single-cylinder free piston engine linear generator: Simulation and experiments. Energies, 2015. 8(2): p. 765-785.

[30]. Hans Thomas Aichlmayr, Design considerations, modeling, and analysis of micro-homogeneous charge compression ignition combustion free-piston engines. 2002, Dissertation, University of Minnesota.

[31]. R. Mikalsen, A. P. Roskilly, Performance simulation of a spark ignited free-piston engine generator. Applied Thermal Engineering, 2008. 28(14): p. 1726-1733.

[32]. Wei Wu, Jibin Hu, Shihua Yuan, Semi-analytical modelling of a hydraulic free-piston engine. Applied Energy, 2014. 120: p. 75-84.

[33]. Zhenfeng Zhao, Fujun Zhang, Ying Huang, Changlu Zhao, Determination of tdc in a hydraulic free-piston engine by a novel approach. Applied Thermal Engineering, 2014. 70(1): p. 524-530.

[34]. Shuanlu Zhang, Changlu Zhao, Zhenfeng Zhao, Stability analysis of hydraulic free piston engine. Applied Energy, 2015. 157:805-13.

[35]. A. F. Underwood, The gmr 4-4 “hyprex” engine a concept of the free-piston engine for automotive use. 1957, SAE Technical Paper. No. 570032.

[36]. Chang-ping Lee, Turbine-compound free-piston linear alternator engine. 2014, Dissertation, University of Michigan.

[37]. Zhou Sheng Xu Bing Yang Huayong, Zhao Yang, Simulation on dual hydraulic free piston engine. Chinese Journal of Mechanical Engineering, 2005. 4: p. 018.

[38]. Seppo Tikkanen, Matti Vilenius, Control of dual hydraulic free piston engine. International journal of vehicle autonomous systems, 2006. 4(1): p. 3-23.

[39]. Jakob Fredriksson, Miriam Bergman, Valeri I. Golovitchev, Ingemar Denbratt, Modeling the effect of injection schedule change on free piston engine operation. 2006, SAE Technical Paper, No. 2006-01-0449.

[40]. R. Mikalsen, A. P. Roskilly, The control of a free-piston engine generator. Part 1: Fundamental analyses. Applied Energy, 2010. 87(4): p. 1273-1280.

[41]. Boru Jia, Guohong Tian, Huihua Feng, Zhengxing Zuo, A. P. Roskilly, An experimental investigation into the starting process of free-piston engine generator. Applied Energy, 2015, 157:798-804..

[42]. Waqas Arshad, A low-leakage linear transverse-flux machine for a free-piston generator. 2003, Dissertation, Royal Institute of Technology.

[43]. Alija Cosic, Jens Lindbäck, Waqas Mahmood Arshad, Mats Leksell, Peter Thelin, Erik Nordlund, Application of a free-piston generator in a series hybrid vehicle. 2003, 541-544.

[44]. Jiabin Wang, David Howe. A linear permanent magnet generator for a free-piston energy converter. in Electric Machines and Drives, 2005 IEEE International Conference on. 2005. IEEE.

[45]. Flavio Caresana, Gabriele Comodi, L. Pelagalli, Design approach for a two-stroke free piston engine for electric power generation. 2004, SAE Technical Paper, No. 2004-32-0037.

[46]. Florian Kock, Johannes Haag, Horst E. Friedrich, The free piston linear generator-development of an innovative, compact, highly efficient range-extender module. 2013, SAE Technical Paper, No. 2013-01-1727.

[47]. Johannes Haag, Cornelius Ferrari, Jan Hendrik Starcke, Michael Stöhr, Uwe Riedel, Numerical and experimental investigation of in-cylinder flow in a loop-scavenged two-stroke free piston engine. 2012, SAE Technical Paper, No. 2012-32-0114.

[48]. Johannes Haag, et al., Development approach for the investigation of homogeneous charge compression ignition in a free-piston engine. 2013, SAE Technical Paper, No. 2013-24-0047.

[49]. Hidemasa Kosaka, Tomoyuki Akita, Kazunari Moriya, Shigeaki Goto, Yoshihiro Hotta, Takaji Umeno, Kiyomi Nakakita, Development of free piston engine linear generator system part 1-investigation of fundamental characteristics. 2014, SAE Technical Paper, No. 2014-01-1203.

[50]. Shigeaki Goto, Kaznunari Moriya, Hidemasa Kosaka, Tomoyuki Akita, Yoshihiro Hotta, Takaji Umeno, Kiyomi Nakakita, Development of free piston engine linear generator system part 2-investigation of control system for generator. 2014, SAE Technical Paper, No. 2014-01-1193.

[51]. Jinlong Mao, Zhengxing Zuo, Huihua Feng, Parameters coupling designation of diesel free-piston linear alternator. Applied Energy, 2011. 88(12): p. 4577-4589.

[52]. Jaeheun Kim, Choongsik Bae, Gangchul Kim, The effects of spark timing and equivalence ratio on spark-ignition linear engine operation with liquefied petroleum gas. 2012, SAE Technical Paper, No. 2012-01-0424.

[53]. Qing-feng Li, Jin Xiao, Zhen Huang, Flat-type permanent magnet linear alternator: A suitable device for a free piston linear alternator. Journal of Zhejiang University Science A, 2009. 10(3): p. 345-352.

[54]. Boru Jia, Zhengxing Zuo, Huihua Feng, Guohong Tian, A. P. Roskilly, Development approach of a spark-ignited free-piston engine generator. 2014, SAE Technical Paper, No. 2014-01-2894.

[55]. Yan-xiao Li, Zheng-xing Zuo, Hui-hua Feng, Bo-ru Jia, Parameters matching requirements for diesel free piston linear alternator start-up. Advances in Mechanical Engineering, 2015. 7(3): p. 1687814015574408.

[56]. Ling Huang, An opposed-piston free-piston linear generator development for HEV. 2012, SAE Technical Paper, No. 2012-01-1021.

[57]. Terry A. Johnson, Michael T. Leick. Experimental evaluation of the free piston engine – linear alternator (FPLA). 2015, Sandia National Laboratories.

[58]. Zhaoping Xu, Siqin Chang, Prototype testing and analysis of a novel internal combustion linear generator integrated power system. Applied Energy, 2010. 87(4): p. 1342-1348.

[59]. Ehab Shoukry, Samuel Taylor, Nigel Clark, Parviz Famouri, Numerical simulation for parametric study of a two-stroke direct injection linear engine. 2002, SAE Technical Paper, No. 2002-01-1739.

[60]. N. Clark, et al. Modeling and development of a linear engine. in Spring Technical Conference of the ASME Internal Combustion Engine Division, Fort Lauderdale, FL, Apr. 1998.

[61]. Nigel Clark, Subhash Nandkumar, Parviz Famouri, Fundamental analysis of a linear two-cylinder internal combustion engine. 1998, SAE Technical Paper, No. 982692.

[62]. Ehab F. Shoukry, Numerical simulation for parametric study of a two-stroke compression ignition direct injection linear engine. 2003, Dissertation, West Virginia University.

[63]. Subhash Nandkumar, Two-stroke linear engine. 1998, Dissertation, West Virginia University.

[64]. Rikard Mikalsen, Anthony P. Roskilly. The free-piston reciprocating joule cycle engine: A new approach to efficient domestic chp generation. in In: Proceeding of ICAE2012 Conference. 2012.

[65]. R. Mikalsen, A. P. Roskilly, Coupled dynamic–multidimensional modelling of free-piston engine combustion. Applied Energy, 2009. 86(1): p. 89-95.

[66]. S. Scott Goldsborough, Peter Van Blarigan, A numerical study of a free piston ic engine operating on homogeneous charge compression ignition combustion. 1999, SAE Technical Paper, No. 1999-01-0619.

[67]. S. Scott Goldsborough, A numerical investigation of a two-stroke cycle, hydrogen-fueled, free piston internal combustion engine. 1998, Dissertation, Sandia National Laboratories.

[68]. J. Hannson, Mats Leksell, Fredrik Carlsson. Minimizing power pulsations in a free piston energy converter. in Power electronics and applications, 2005 European Conference on. 2005. IEEE.

[69]. Jakob Fredriksson, Ingemar Denbratt, Simulation of a two-stroke free piston engine. 2004, SAE Technical Paper, No. 2004-01-1871.

[70]. Jorgen Hansson, Mats Leksell. Performance of a series hybrid electric vehicle with a free-piston energy converter. in Vehicle Power and Propulsion Conference, 2006. VPPC'06. IEEE. 2006. IEEE.

[71]. Jörgen Hansson, Mats Leksell, Fredrik Carlsson, Chandur Sadarangani. Operational strategies for a free piston energy converter. in Proceedings of the fifth international symposium on linear drives for industry applications, Kobe-Awaji, Japan. 2005. Citeseer.

[72]. Miriam Bergman, Valeri I. Golovitchev, CFD modeling of a two-stroke free piston energy converter using detailed chemistry. 2005, SAE Technical Paper, No. 2005-24-074.

[73]. Boru Jia, Zhengxing Zuo, Guohong Tian, Huihua Feng, A. P. Roskilly, Development and validation of a free-piston engine generator numerical model. Energy Conversion and Management, 2015. 91: p. 333-341.

[74]. Wang Dongjie Yuan Chenheng Xu Datao, Zuo Zhengxing, Design and characteristics analysis of free-piston linear alternator with piston-mounted passive inlet valve. Transactions of the Chinese Society for Agricultural Machinery, 2013. 1: p. 004.

[75]. Jinlong Mao, Zhengxing Zuo, Wen Li, Huihua Feng, Multi-dimensional scavenging analysis of a free-piston linear alternator based on numerical simulation. Applied Energy, 2011. 88(4): p. 1140-1152.

[76]. Chun Lai Tian, Hui Hua Feng, Zheng Xing Zuo. Oscillation characteristic of single free piston engine generator. In Advanced Materials Research, 2012. Vol. 383, pp. 1873-1878.

[77]. Chun Lai Tian, Hui Hua Feng, Zheng Xing Zuo. Load following controller for single free-piston generator. In Applied Mechanics and Materials, 2012. Vol. 157, pp. 617-621.

[78]. Jinlong Mao, Huihua Feng, Zhengxing Zuo, Dimensionless parametric analysis of spark ignited free-piston linear alternator. 2011: INTECH Open Access Publisher.

[79]. Tian Chunlai, Feng Huihua, Shang Jiao, Zuo Zhengxing, Energy conversion and transfer process of free-piston engine generator. Transactions of the Chinese Society for Agricultural Machinery, 2012. 11: p. 004.

[80]. Chen-heng Yuan, Hui-hua Feng, Meng-qiu Wang, Zheng-xing Zuo, Combustion characteristics of free-piston gasoline engine for linear alternator. Journal of Jilin University (Engineering and Technology Edition), 2015. 1: p. 019.

[81]. Chen-heng Yuan, Hui-hua Feng, Meng-qiu Wang, Zheng-xing Zuo, Study on starting characteristics of free-piston gasoline engine for linear alternator. Chinese Internal Combustion Engine Engineering, 2015. 1: p. 017.

[82]. Xin Zhenfang, Mao Jinlong, Zuo Zhengxing, Feng Huihua. The affection of spray time to the performance of the free piston engine. in Digital Manufacturing and Automation (ICDMA), 2010 International Conference on. 2010. IEEE.

[83]. Pavel Deutsch, Ondřej Vysoký. In-cycle thermodynamic model of linear combustion engine. in Computer Aided Control System Design, 2006 IEEE International Conference on Control Applications, 2006 IEEE International Symposium on Intelligent Control, 2006 IEEE. 2006. IEEE.

[84]. Ondřej Vysoký, Linear combustion engine as main energy unit for hybrid vehicles. Proceedings of Transtec Prague. Prague: Czech Technical University, 2007: p. 236-244.

[85]. Pavel Novotný, Václav Píštěk, Lubomír Drápal, Modeling of piston ring pack dynamics. Journal of Middle European Construction and Design of Cars, 2011. 9(2): p. 8-13.

[86]. Pavel Novotný, Peter Raffai, Jozef Dlugoš, Ondřej Maršálek, Jiří Knotek, Role of computational simulations in the design of piston rings. Journal of Middle European Construction and Design of Cars, 2015. 13(1): p. 1-6.

[87]. R. W. Redlich, D. M. Berchowitz, Linear dynamics of free-piston stirling engines. Proceedings of the Institution of Mechanical Engineers, Part A: Journal of Power and Energy, 1985. 199(3): p. 203-213.

[88]. G. Nakhaie Jazar, M. Farid Golnaraghi, Nonlinear modeling, experimental verification, and theoretical analysis of a hydraulic engine mount. Journal of Vibration and Control, 2002. 8(1): p. 87-116.

[89]. Q. F. Li, Jin Xiao, Zhen Huang, Parametric study of a free piston linear alternator. International Journal of Automotive Technology, 2010. 11(1): p. 111-117.

[90]. Jörgen Hansson, Analysis and control of a hybrid vehicle powered by free-piston energy converter. 2006, Dissertation, Royal Institute of Technology.

[91]. Sven-Erik Pohl, Markus Gräf. Dynamic simulation of a free-piston linear alternator in modelica. Proceedings of the 4th International Modelica Conference, Hamburg, March 7-8, 2005.

[92]. Cornelius Ferrari, Horst E. Friedrich. Development of a free-piston linear generator for use in an extended-range electric vehicle. in Proc. Symposium EVS26, Los Angeles, USA. 2012.

[93]. Dr Markus Gräf, Dr Peter Treffinger, Sven-Erik Pohl, Frank Rinderknecht, Investigation of a high efficient free piston linear generator with variable stroke and variable compression ratio. World Electr Veh Assoc J, 2007. 1: p. 116-120.

[94]. Dipl-Ing Florian Kock, Dipl-Ing Alex Heron, Ing Horst E. Friedrich, The free-piston linear generator potentials and challenges. MTZ worldwide, 2013. 74(10): p. 38-43.

[95]. David Houdyschell, A diesel two-stroke linear engine. 2000, Dissertation, West Virginia University.

[96]. Gregory Paul Gibbes, Numerical modelling of the gas dynamics of a prototype free-piston engine. 2011, Dissertation, University of Technology Sydney.

[97]. Douglas Carter, Edward Wechner, The free piston power pack: Sustainable power for hybrid electric vehicles. 2003, SAE Technical Paper, No. 2003-01-3277.

[98]. Pavel Němeček, Michal Šindelka, Ondřej Vysoký, Ensuring steady operation of free-piston generator. SYSTEMICS, CYBERNETICS AND INFORMATICS, 2006: p. 19-23.

[99]. Ocktaeck Lim, Nguyen Ba Hung, Seokyoung Oh, Gangchul Kim, Hanho Song, Norimasa Iida, A study of operating parameters on the linear spark ignition engine. Applied Energy, 2015. 160: p. 746-760.

[100]. Ocktaeck Lim, Yongil Oh, Jaewan Lee, Kanchul Kim. An investigation about generating electric power on operated parameters of powerpack utilizing linear engine. in Electric Vehicle Symposium and Exhibition (EVS27), 2013 World. 2013. IEEE.

[101]. Nam-Yuer Kim, Gang-Chul Kim, Ock-Taeck Lim, A study for development of compact powerpack used hydrogen. Transactions of the Korean hydrogen and new energy society, 2010. 21(4): p. 321-327.

[102]. Yong-Il Oh, Gang-Chul Kim, Ock-Taeck Lim, A study for generating power on operating parameters of powerpack utilizng linear engine. Transactions of the Korean hydrogen and new energy society, 2012. 23(2): p. 183-190.

[103]. Nguyen Ba Hung, Ock Taeck Lim, A study of a two-stroke free piston linear engine using numerical analysis. Journal of Mechanical Science and Technology, 2014. 28(4): p. 1545-1557.

[104]. Y. Woo, Y. J. Lee, Free piston engine generator: Technology review and an experimental evaluation with hydrogen fuel. International Journal of Automotive Technology, 2014. 15(2): p. 229-235.

[105]. Peter Van Blarigan, Free-piston engine. United States patent US 6,199,519. 2001 Mar 13.

[106]. Zhaoping Xu, Siqin Chang, Improved moving coil electric machine for internal combustion linear generator. Energy Conversion, IEEE Transactions on, 2010. 25(2): p. 281-286.

[107]. Si-qin Chang, Zhao-ping Xu, Conceptual design of internal combustion-linear generator integrated power system. Journal of Nanjing University of Science and Technology (Natural Science), 2008. 4: p. 015.

[108]. Zhaoping Xu, Siqin Chang. Hierarchical hybrid control of a four-stroke free-piston engine for electrical power generation. in Mechatronics and Automation, 2009. ICMA 2009. International Conference on. 2009. IEEE.

[109]. Jiming Lin, Siqin Chang, Zhaoping Xu, Optimal motion trajectory for the four-stroke free-piston engine with irreversible miller cycle via a gauss pseudospectral method. Journal of Non-Equilibrium Thermodynamics, 2014. 39(3): p. 159-172.

[110]. Jiming Lin, Zhaoping Xu, Siqin Chang, Ningxia Yin, Hao Yan, Thermodynamic simulation and prototype testing of a four-stroke free-piston engine. Journal of Engineering for Gas Turbines and Power, 2014. 136(5): p. 051505.

[111]. Sorin Petreanu, Conceptual analysis of a four-stroke linear engine. 2001, Dissertation, West Virginia University.

[112]. Willard W. Pulkrabek, Engineering fundamentals of the internal combustion engine. 2004: Prentice Hall.

[113]. R. Mikalsen, A. P. Roskilly, The control of a free-piston engine generator. Part 2: Engine dynamics and piston motion control. Applied Energy, 2010. 87(4): p. 1281-1287.

[114]. R. Mikalsen, E. Jones, A. P. Roskilly, Predictive piston motion control in a free-piston internal combustion engine. Applied Energy, 2010. 87(5): p. 1722-1728.

[115]. Tor Arne Johansen, Olav Egeland, Erling Aa Johannessen, Rolf Kvamsdal, Free-piston diesel engine timing and control-toward electronic cam-and crankshaft. Control Systems Technology, IEEE Transactions on, 2002. 10(2): p. 177-190.

[116]. Tor A. Johansen, Olav Egeland, Erling Aa Johannessen, Rolf Kvamsdal, Dynamics and control of a free-piston diesel engine. Journal of dynamic systems, measurement, and control, 2003. 125(3): p. 468-474.

[117]. Tor Johansen, Olav Egeland, Erling Aa Johannessen, Rolf Kvamsdal. Free-piston diesel engine dynamics and control. in American Control Conference, 2001. Proceedings of the 2001. 2001. IEEE.

[118]. Boru Jia, Andrew Smallbone, Huihua Feng, Guohong Tian, Zhengxing Zuo, A. P. Roskilly, A fast response free-piston engine generator numerical model for control applications. Applied Energy, 2016. 162: p. 321-329.

[119]. Jörgen Hansson, Analysis and control of a hybrid vehicle powered by free-piston energy converter. Phd Dissertation, 2006.

[120]. Rikard Mikalsen, Anthony Paul Roskilly, Free-piston internal combustion engine. 2015, United States patent US 9,032,918. 2015 May 19.

[121]. Rowland S. Benson, Norman Dan Whitehouse, Internal combustion engines: A detailed introduction to the thermodynamics of spark and compression ignition engines, their design and development. Vol. 1. 2013: Elsevier.

[122]. Richard Stone, Introduction to internal combustion engines. 2012: Palgrave Macmillan.

[123]. John B. Heywood, Internal combustion engine fundamentals. Vol. 930. 1988: Mcgraw-Hill New York.

[124]. Günter F. Hohenberg, Advanced approaches for heat transfer calculations. 1979, SAE Technical paper, No. 790825.

[125]. Ion Boldea, Syed A. Nasar. Linear electric actuators and generators. in Electric Machines and Drives Conference Record, 1997. IEEE International.

[126]. L. Boldea, Syed A. Nasar, Linear electric actuators and generators. Energy Conversion, IEEE Transactions on, 1999. 14(3): p. 712-717.

[127]. Ion Boldea, S. A. Naser, Linear motion electromagnetic systems. 1985: A John Wiley & Sons, New York.

[128]. Ion Boldea, Linear electric machines, drives, and maglevs handbook. 2013: CRC Press.

[129]. Mohd Razali Hanipah, Development of a spark ignition free-piston engine generator. 2015, Dissertation, Newcastle University.

[130]. Cyril M. Harris, Allan G. Piersol, Thomas L. Paez, Harris' shock and vibration handbook. Vol. 5. 2002: McGraw-Hill New York.

[131]. Katsuhiko Ogata, Modern control engineering. Fifth Edition, 2010, Prentice Hall.

[132]. Uwe Kiencke, Lars Nielsen, Automotive control systems: For engine, driveline, and vehicle. Measurement Science and Technology, 2000. 11(12): p. 1828.

[133]. Charles Fayette Taylor, The internal-combustion engine in theory and practice: Combustion, fuels, materials, design. Vol. 2. 1985: MIT press.

[134]. Saiful Zulkifli, Mohd N. Karsiti. Starting of a free-piston linear engine-generator by mechanical resonance and rectangular current commutation. in Vehicle Power and Propulsion Conference, 2008. VPPC'08. IEEE.

[135]. Ezrann Zharif Zainal Abidin, Abdulwehab A. Ibrahim, A. Rashid A. Aziz, Saiful A. Zulkifli, Investigation of starting behaviour of a free-piston linear generator. Journal of Applied Sciences, 2012. 12(24): p. 2592.

[136]. Saiful Zulkifli, Mohd N. Karsiti. Investigation of linear generator starting modes by mechanical resonance and rectangular current commutation. in Electric Machines and Drives Conference, 2009. IEMDC'09. IEEE International.

[137]. Saiful Zulkifli, Mohd N. Karsiti, Abd Rashid Abd Aziz. Rectangular current commutation and open-loop control for starting of a free-piston linear engine-generator. in Power and Energy Conference, 2008. PECon 2008. IEEE 2nd International.

[138]. S. A. Zulkifli, Modeling, simulation and implementation of rectangular commutation for starting of free-piston linear generator. 2007, Dissertation, Universiti Teknologi Petronas.

[139]. Abdulwehab A. Ibrahim, A. Rashid A. Aziz, Zainal Abidin, Z. Ezrann, Saiful A. Zulkifli, Operation of free-piston linear-generator engine using mosfet and igbt drivers. Journal of Applied Sciences, 2011: p. 1-6.

[140]. Chenheng Yuan, Huihua Feng, Yituan He, Jing Xu, Motion characteristics and mechanisms of a resonance starting process in a free-piston diesel engine generator. Proceedings of the Institution of Mechanical Engineers, Part A: Journal of Power and Energy, 2015: p. 0957650915622343.

[141]. Chong Xiao, Zheng-xing Zuo, Nonlinear model and first order approximate solution of a free piston generator. Transactions of Beijing Institute of Technology, 2008. 11: p. 006.

[142]. Zhenfeng Zhao, Dan Wu, Zhenyu Zhang, Fujun Zhang, Changlu Zhao, Experimental investigation of the cycle-to-cycle variations in combustion process of a hydraulic free-piston engine. Energy, 2014. 78: p. 257-265.

[143]. Jaeheun Kim, Choongsik Bae, Gangchul Kim, Simulation on the effect of the combustion parameters on the piston dynamics and engine performance using the wiebe function in a free piston engine. Applied Energy, 2013. 107: p. 446-455.

[144]. Devor Hrovat, Jing Sun, Models and control methodologies for ic engine idle speed control design. Control Engineering Practice, 1997. 5(8): p. 1093-1100.

[145]. Andrea Balluchi, Luca Benvenuti, Maria Domenica Di Benedetto, Claudio Pinello, Alberto Luigi Sangiovanni-Vincentelli, Automotive engine control and hybrid systems: Challenges and opportunities. Proceedings of the IEEE, 2000. 88(7): p. 888-912.

[146]. John Joseph Moskwa, Automotive engine modeling for real time control. 1988, Disssertation, Massachusetts Institute of Technology.

[147]. Heinz Heisler, Advanced engine technology. 1995, Society of Automotive Engineers, Warrendale, PA (United States).

[148]. R. Isermann, J. Schaffnit, S. Sinsel, Hardware-in-the-loop simulation for the design and testing of engine-control systems. Control Engineering Practice, 1999. 7(5): p. 643-653.

[149]. Lino Guzzella, Christopher Onder, Introduction to modeling and control of internal combustion engine systems. 2009: Springer Science & Business Media.

[150]. Ke Li, Ali Sadighi, Zongxuan Sun, Active motion control of a hydraulic free piston engine. Mechatronics, IEEE/ASME Transactions on, 2014. 19(4): p. 1148-1159.

[151]. Yongsheng Zhu, et al., The control of an opposed hydraulic free piston engine. Applied Energy, 2014. 126: p. 213-220.

[152]. Ke Li, Chen Zhang, Zongxuan Sun, Precise piston trajectory control for a free piston engine. Control Engineering Practice, 2015. 34: p. 30-38.

[153]. Rongbin Yang, Xun Gong, Yunfeng Hu, Hong Chen. Motion control of free piston engine generator based on LQR. In Control Conference (CCC), 2015 34th Chinese. 2015. IEEE.

[154]. Adilson E. Motter, Cascade control and defense in complex networks. Physical Review Letters, 2004. 93(9): p. 098701.

[155]. Carlos A. Smith, Armando B. Corripio, Principles and practice of automatic process control. Vol. 2. 1985: Wiley New York.

[156]. Werner Leonhard, Control of a separately excited dc machine. Control of Electrical Drives, 2001: p. 77-96.

[157]. Thomas E. Marlin, Process control. 1995: McGraw-Hill New York.

[158]. Hsiao-Ping Huang, I. Lung Chien, Yueh-Chung Lee, Gow-Bin Wang, A simple method for tuning cascade control systems. Chemical Engineering Communications, 1998. 165(1): p. 89-121.

[159]. Karl Johan Åström, Tore Hägglund, Advanced PID control. 2006: ISA-The Instrumentation, Systems, and Automation Society; Research Triangle Park, NC 27709.

[160]. Kiam Heong Ang, Gregory Chong, Yun Li, PID control system analysis, design, and technology. Control Systems Technology, IEEE Transactions on, 2005. 13(4): p. 559-576.

[161]. Karl Johan Åström, Chang C. Hang, Per Persson, Weng Kuen Ho, Towards intelligent PID control. Automatica, 1992. 28(1): p. 1-9.

[162]. Karl Johan Åström, Tore Hägglund, The future of PID control. Control engineering practice, 2001. 9(11): p. 1163-1175.

[163]. Gene F. Franklin, J. David Powell, Michael L. Workman, Digital control of dynamic systems. Vol. 3. 1998: Addison-wesley Menlo Park.

[164]. Michael A. Johnson, Mohammad H. Moradi, PID control. 2005: Springer.

[165]. Kok K. Tan, Qing-Guo Wang, Chang C. Hang, Advances in PID control. 2012: Springer Science & Business Media.

[166]. Tony Roskilly, Rikard Mikalsen, Marine systems identification, modeling and control. 2015: Butterworth-Heinemann.

Appendix I

Energy Conversion and Management 91 (2015) 333–341

Contents lists available at ScienceDirect

Energy Conversion and Management

journal homepage: www.elsevier.com/locate/enconman

Development and validation of a free-piston engine generator numerical model

Boru Jia [a,b], Zhengxing Zuo [b], Guohong Tian [a,*], Huihua Feng [b], A.P. Roskilly [a]

[a] Sir Joseph Swan Centre for Energy Research, Newcastle University, Newcastle upon Tyne NE1 7RU, UK
[b] School of Mechanical Engineering, Beijing Institute of Technology, Beijing 100081, China

ARTICLE INFO

Article history:
Received 4 September 2014
Accepted 28 November 2014
Available online 26 December 2014

Keywords:
Free-piston generator
Linear electric machine
Numerical model

ABSTRACT

This paper focuses on the numerical modelling of a spark ignited free-piston engine generator and the model validation with test results. Detailed sub-models for both starting process and steady operation were derived. The compression and expansion processes were not regarded as ideal gas isentropic processes; both heat transfer and air leakage were taken into consideration. The simulation results show good agreement with the prototype test data for both the starting process and steady operation. During the starting process, the difference of the in-cylinder gas pressure can be controlled within 1 bar for every running cycle. For the steady operation process, the difference was less than 5% and the areas enclosed on the pressure–volume diagram were similar, indicating that the power produced by the engine and the engine efficiency could be predicted by this model. Based on this model, the starting process with different starting motor forces and the combustion process with various throttle openings were simulated. The engine performance during stable operation at 100% engine load was predicted, and the efficiency of the prototype was estimated to be 31.5% at power output of 4 kW.

1. Introduction

As an alternative to conventional engines, free-piston engine generator (FPEG) is a promising power generation system due to its simplicity and high thermal efficiency therefore has attracted considerable research interests recently [1–6]. It integrates a linear combustion engine and a linear electrical machine into a single unit. Combustion in the engine chambers drives the translator to reciprocate in an almost resonant way and the linear electric machine converts part of the mover's kinetic energy to electricity. The thermal efficiency was estimated to be up to 46% (including friction and compressor losses) at a power level of 23 kW and the research showed promising results with respect to engine performance and emissions [7].

However, as the piston motion of the FPE is not restricted by the crankshaft mechanism, the piston is free to move between its top dead centre (TDC) and bottom dead centre (BDC), therefore the piston is only influenced by the gas and load forces acting upon it. This induces to problems such as difficulties in engine start, misfire, unstable operation and overall complex control strategies [8]. As a result, there has not been any stably operating prototype reported by now. Despite the research specifically addressing the modelling of FPEG, most researchers tended to adapt simplified ideal models widely used in conventional engines to simulate FPEG. Moreover, since free-piston engines have specific operating characteristics compared to conventional engines, the validation of the free-piston engine model still needs to be acknowledged.

Christopher M. Atkinson along with the co-researchers in West Virginia University developed an engine computational model with the combination of dynamic and thermodynamic analysis. The dynamic model consisted of an evaluation of the frictional forces and the load of the engine. The thermodynamic analysis consisted of an evaluation of each process that characterise the engine cycle based on the First Law of Thermodynamics. A time-based Wiebe function was used to calculate the heat release during the combustion process. The parameters used were based on test data collected from a running prototype, including in-cylinder pressure, displacement and velocity. A parametric investigation was also performed to predict the behaviour of the engine over a wide operating range [9–11].

Mikalsen and Roskilly presented a modelling investigation of a free-piston engine generator and they discussed the feasibility of the implemented models. The sub-models to simulate the in-cylinder combustion were based on existing single-zone models commonly used in conventional diesel engines. The output parameters of the model were validated against test data from a Volvo

* Corresponding author. Tel.: +44 (0) 191 208 3902.
E-mail address: guohong.tian@ncl.ac.uk (G. Tian).

http://dx.doi.org/10.1016/j.enconman.2014.11.054
0196-8904/

Nomenclature

A	piston area (m^2)
A_{cyl}	the in-cylinder surface area in contact with the gas (m^2)
$A_{leakage}$	leakage area (m^3)
A_f	friction parameter (−)
D_f	friction parameter (−)
C	capacitance of the circuit
C_d	combustion duration (s)
C_D	discharge coefficient
C_v	specific heat capacity at constant volume (J/kg K)
C_p	heat capacity at constant pressure
d	cylinder diameter (mm)
d_0	reference cylinder diameter
E	average temperature of lubrication oil at liner (°C)
f	overall scaling factor (−)
F_e	load force from the linear generator (N)
F_f	friction force (N)
F_l	gas force from the left cylinder (N)
F_m	force output from the linear electric machine (N)
F_r	gas force from the right cylinder (N)
F_{sl}	gas force from the left scavenging pump (N)
F_{sr}	gas force from the right scavenging pump (N)
H_e	enthalpy of the exhaust air (J)
H_i	enthalpy of the intake air (J)
H_l	enthalpy of the air leaked from the piston rings (J)
h	heat transfer coefficient (W/m^2 K)
i	current of the circuit (A)
K_A	proportionality constant for the thrust force of the motor
K_v	friction parameter (−)
L	inductance of the circuit
m	moving mass of the piston assembly
m_{air}	mass of the in-cylinder gas (kg)
$\dot{m}_{air}$	mass flow rate of the in-cylinder gas (kg/s)
p	in-cylinder pressure (Pa)
p_0	reference pressure or ambient pressure (Pa)
p_s	pressure in scavenge case (Pa)
Q_c	heat released from the combustion process (J)
Q_{in}	overall heat input for each cylinder in one running cycle
Q_{ht}	heat transferred to the cylinder wall (J)
$\dot{Q}_{ht}$	transferred heat flow rate (J/s)
R	resistance of the circuit
T_0	air temperature in the scavenging pump (K)
T_w	average temperature of the cylinder wall surfaces (K)
t_s	time at which the combustion process starts
x	mover's displacement
U	internal energy of the in-cylinder gas (J)
V	instantaneous cylinder volume (m^3)
V_s	volume of scavenge case (m^3)
v	axial velocity of piston (m/s)
v_p	mean piston speed (m/s)
λ	fuel mass fraction burned
γ	ratio of heat capacities
ϕ	magnetic flux
θ_0	reference temperature (°C)

TAD1240 six-cylinder, turbocharged diesel engine. The results showed that it was able to predict real trends of the free-piston engine for varying engine operating conditions [8].

Goldsborough et al. at Sandia National Laboratories analysed the steady-state operating characteristics of a free-piston engine using a zero-dimensional, thermodynamic model with detailed chemical kinetics, and heat transfer, scavenging, and friction sub-models. Hydrogen was used as fuel. The simulation identified the critical parameters affecting the engine performance, and suggested the limits of possible improvement compared to conventional internal combustion engines. However, validation of the free-piston engine model was difficult due to the limited experimental data available from their prototype [12].

Zuo et al. at Beijing Institute of Technology provided numerical simulation on piston motion. A time-based numerical model was developed in Matlab to define the piston motion profiles. Multi-dimensional gas flow in the scavenging process of the free-piston engine was studied based on the numerical simulation results. A wide range of design and operating options including stroke length, valve overlapping distance, operation frequency and charging pressure were investigated to evaluate their effects on the scavenging performance. The measured in-cylinder pressure and scavenging pressure were used as the boundary conditions for their model development [13,14].

Nemecek Pavel at Czech Technical University described modelling and control of a free-piston generator. The model was based on simplified thermodynamic processes. Assumptions of ideal gas and ideal reversible processes were adapted. Despite the simplifications of the model, simulations results showed good agreement with the real system. However, the development of more precise thermodynamic identification was suggested for further work [15].

Free-piston engine is commonly modelled using simplified zero-dimensional models. Most of the reported models used idealised close system processes, in which no heat or mass transfer was considered [16–18]. However, the actual system cannot be assumed as isentropic close system because when the engine usually operates at relatively low speed, the effects of heat transfer and gas leakage become significant and cannot be simply neglected. Meanwhile, when the charge temperature rises above the wall temperature, heat is transferring from the air to the wall, which affects the piston's dynamics as well [19]. Thus, the ideal gas relationship is not sufficiently accurate for the present modelling of the FPEG. Moreover, friction force in previous models was considered to be a constant value, which is not accurate either. Furthermore, there has not been any model validation reported due to the limited test data available from operating prototypes.

This paper focuses on a spark ignited free-piston engine generator. Detailed sub-models for both starting process and steady operation were derived and developed in Matlab/Simulink. The compression and expansion processes were not regarded as ideal gas isentropic process; both heat transfer and air leakage were taken into consideration. Model validation was undertaken with the test data from a running prototype, which showed good agreement. Using this model, the starting process and steady operation performance were analysed.

2. Model description

2.1. Holistic model structure

The numerical model primarily aims to precisely describe the piston motion which is governed by the Newton's second law. Therefore an engine dynamic model was developed on the top level. The specific forces acting upon the pistons are determined by the in-cylinder gas thermodynamic processes, mechanical friction force and linear electric machine force. Thus three sub-models

that describe the abovementioned three groups of forces were developed on a lower level and the calculated forces are fed into the top level dynamic model to determine the piston motion.

The in-cylinder thermodynamic processes include compression or expansion process of the piston, heat transfer from the in-cylinder gas to the wall, gas leakage through the piston rings, and heat release of the combustion process. The scavenging process was also included since a two stroke engine was considered in this paper. The friction sub-model describes the friction force acting on the piston rings which is determined by a number of operating factors and is always a resistance force. The linear electric machine force however, can be either driving force or resisting force depending on its working mode. A schematic diagram of the model architecture is illustrated in Fig. 1.

The model was developed in Matlab/Simulink. It was calibrated by the parameters from a prototype. The input variables and output engine performance parameters are also demonstrated in Fig. 1. Each sub-model is enabled or disabled based on the piston displacement using State flow Chart function in Simulink. The equations were solved using Runge–Kutta solver with a fixed step size of 10^{-6}.

This model was used for both starting process and steady operation investigation. In starting mode, the combustion sub-model was disabled and the linear electric machine was requested to work as a motor, i.e. providing driving force. In steady operation mode, the combustion sub-model was enabled and the linear electric machine works as a generator which provided a resistance force. It was assumed that at the end of starting process, the engine can be switched smoothly into steady operation mode. Therefore the calculated in-cylinder pressure, piston displacement and velocity at the end of the starting process were taken as the initial values for the steady operation simulation. The other constant input parameters for the simulation model are summarised in Table 1.

2.2. Engine dynamic model

This top level model considers the dynamics of the mover (piston assembly). The forces acting on the pistons include in-cylinder gas forces, linear motor force, mechanical friction force and the inertial force of the mover [8–14]. A dynamic equation of the mover can be derived from Newton's Second Law and illustrated in Fig. 2.

Table 1
Simulation parameters.

Parameters	Value
Bore	52.5 mm
Stroke	70.0 mm
Effective stroke length	35.0 mm
Moving mass	5.0 kg
Constant of back electromagnetic voltage	85.0 V/(m s^{-1})
Thrust force constant	74.4 N/A
Coil resistance	14.0 Ω

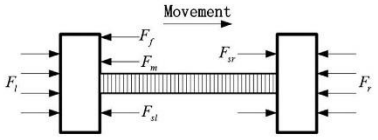

Fig. 2. Dynamics of the piston.

$$\overrightarrow{F_l} + \overrightarrow{F_r} + \overrightarrow{F_{sr}} + \overrightarrow{F_{sl}} + \overrightarrow{F_m} + \overrightarrow{F_f} = m\frac{d^2x}{dt^2} \quad (1)$$

where x is the mover's displacement; m is the moving mass of the piston assembly; F_l is the gas force from the left cylinder; F_r is the gas force from the right cylinder, which is on the opposite direction of F_l; F_{sr} is the gas force from the right scavenging pump; F_{sl} is the gas force from the left scavenging pump. The gas forces are calculated from the gas pressure and piston area according to Eqs. (2) and (3). F_m is the force output from the linear electric machine, and it varies from motoring (starting) and generation (steady operation) modes; F_f is the friction force which is always on the opposite direction to the piston's velocity. More detailed description of the above forces will be introduced in the following sections.

$$F_r = p_r \cdot A; \quad F_l = p_l \cdot A \quad (2)$$

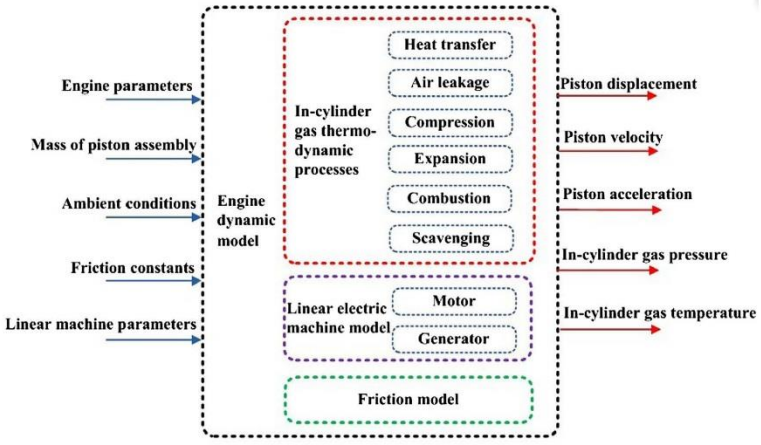

Fig. 1. Diagram of the simulation model.

$$F_{sr} = p_{sr} \cdot A; \quad F_{sl} = p_{sl} \cdot A \tag{3}$$

where p is the pressure, A is the piston area, and the subscripts r and l represent the values of the right and left cylinder.

2.3. In-cylinder thermodynamic sub-model

The in-cylinder gas was considered as ideal gas in closed system with corrections such as gas leakage and heat transfer. The analysis of the in-cylinder gas property during the compression and expansion phases of the cycle is based on a zero-dimensional, thermodynamic approach. When the intake or exhaust port is open during the gas exchange process, the in-cylinder pressure is assumed to be ambient pressure. Other important assumptions are: the in-cylinder gas exists as a homogeneous medium, uniform in temperature and composition; the in-cylinder gas kinetic and potential energy are neglected. The thermodynamic model is derived based on the energy conservation equations and the ideal gas equations.

2.3.1. Thermodynamic equations in compression and expansion processes

During compression and expansion processes, the models for both side cylinders are identical. A graphical demonstration of this thermodynamic system for one cylinder is shown in Fig. 3. The in-cylinder gas pressure is calculated by applying the First Law of Thermodynamics on the cylinder charge:

$$\frac{dU}{dt} = -p\frac{dV}{dt} - \left(\frac{dQ_c}{dt} - \frac{dQ_{ht}}{dt}\right) + \sum_i \dot{H}_i - \sum_e \dot{H}_e - \sum_l \dot{H}_l \tag{4}$$

where U is the internal energy of the in-cylinder gas (J); V is the volume of the cylinder (m^3); Q_c is the heat released from the combustion process (J); Q_{ht} is the heat transferred to the cylinder wall (J); H_i is the enthalpy of the intake air (J); H_e is the enthalpy of the exhaust air (J); H_l is the enthalpy of the air leaked from the piston rings (J).

When the intake and exhaust ports are both closed, the energy conservation equation can be written as:

$$\frac{dU}{dt} = -p\frac{dV}{dt} - \left(\frac{dQ_c}{dt} - \frac{dQ_{ht}}{dt}\right) - \sum_l \dot{H}_l \tag{5}$$

As the in-cylinder charge is assumed to be ideal gas, its internal energy is a function of temperature only, giving

$$U = m_{air} C_v T \tag{6}$$

The differential form of the equation above is derived as

$$dU = m_{air} C_v dT + C_v T dm_{air} \tag{7}$$

where m_{air} is the mass of the in-cylinder gas (kg); C_v is the specific heat capacity at constant volume (J/kg K) that is considered constant through the temperature range; T is the temperature of the in-cylinder gas (K).

As the in-cylinder gas follows the ideal gas equation,

$$pV = m_{air} RT \tag{8}$$

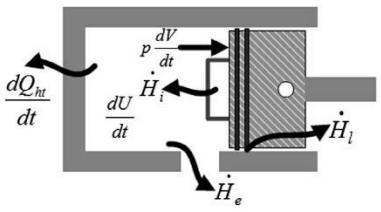

Fig. 3. Schematic diagram of in-cylinder thermodynamic process.

The ideal gas state equation is formulated in its differential form for further deriving the model,

$$pdV + Vdp = m_{air} RT + RT dm_{air} \tag{9}$$

Using the Mayer's relation for the ideal gas,

$$C_p = C_v + R \tag{10}$$

where C_p is the heat capacity at constant pressure, which is again considered constant through the temperature range.

The ratio of heat capacities is expressed as

$$\gamma = \frac{C_p}{C_v} \tag{11}$$

where γ is the ratio of heat capacities.

The following correlation can be derived from Eqs. ((4)–(11)), which can be used to calculate the in-cylinder gas pressure during the compression, combustion and expansion processes.

$$\frac{dp}{dt} = \frac{\gamma - 1}{V}\left(\frac{dQ_c}{dt} - \frac{dQ_{ht}}{dt}\right) - \frac{p\gamma}{m_{air}}\frac{dm_{air}}{dt} - \frac{p\gamma}{V}\frac{dV}{dt} \tag{12}$$

2.3.2. Heat transfer

The in-cylinder charge temperature and the flow pattern vary enormously through the cycle. Both of these variables have a major influence on heat transfer. During the intake process, the intake charge is usually cooler than the walls and the flow velocity is high. During compression the charge temperature rises above the wall temperature, and gas velocity decreases, therefore heat is then transferred from the cylinder gas to the chamber walls [19]. The heat transfer between the cylinder walls and the in-cylinder gas is modelled according to Hohenber [20]:

$$\dot{Q}_{ht} = hA_{cyl}(T - T_w) \tag{13}$$

where $\dot{Q}_{ht}$ is heat flow rate (J/s); h is the coefficient of heat transfer (W/m^2 K); A_{cyl} is area of the in-cylinder surface in contact with the gas (m^2); T_w is the average surfaces temperature of the cylinder wall (K).

The heat transfer coefficient is given by [20]

$$h = 130V^{-0.06}\left(\frac{p(t)}{10^5}\right)^{0.8} T^{-0.4}(v_p + 1.4)^{0.8} \tag{14}$$

where V is the instantaneous cylinder volume (m^3); v_p is the average piston speed (m/s).

2.3.3. Gas leakage

The mass flow rate through piston rings is described by the equation for compressible flow through a flow restriction. It is determined by temperature, composition, the in-cylinder gas pressure, gas pressure in the scavenging pump and a reference air leakage area. The mass flow rate equation is given as [19]:

$$\dot{m}_{air} = \frac{C_D \cdot A_{leakage}}{(RT_0)^{1/2}} p(t)\left[\frac{p_s}{p(t)}\right]^{1/\gamma}\left\{\frac{2\gamma}{\gamma - 1}\left[1 - \left(\frac{p_s}{p(t)}\right)^{(\gamma-1)/\gamma}\right]\right\}^{1/2} \tag{15}$$

where $\dot{m}_{air}$ is the mass flow rate (kg/s); C_D is the discharge coefficient; $A_{leakage}$ is the leakage area (m^3); T_0 is the air temperature in the scavenging pump (K) and is assumed to be equal to the ambient temperature; p_s represents the air pressure in the scavenging pump (Pa).

When the flow is choked,

$$p_s/p(t) \leqslant [2/(\gamma + 1)]^{\gamma/(\gamma-1)} \tag{16}$$

The appropriate equation for mass flow rate becomes:

$$\dot{m}_{air} = \frac{C_D \cdot A_{leakage}}{(RT_0)^{1/2}} p(t) \gamma^{1/2} \left(\frac{2}{\gamma+1}\right)^{(\gamma+1)/2(\gamma-1)} \quad (17)$$

2.3.4. Combustion process

The simulation of the free-piston engine heat release in combustion process is one of the factors with the highest degree of uncertainty in this model. The piston motion of the FPEs differs significantly from that of conventional engines, and very little research result has been reported on how this influences the combustion process [8]. According to previous research, the energy released in the combustion is modelled using a modified Wiebe function [9]. Generally, the Wiebe function is related to the crankshaft angle, however this is not suitable for a linear engine. Therefore, a time based Wiebe function is used to express the mass fraction burned in the combustion process as:

$$\lambda = 1 - \exp\left(-a\left(\frac{t - t_s}{C_d}\right)^{b-1}\right) \quad (18)$$

$$\frac{dQ_c}{dt} = Q_{in}\frac{d\lambda(t)}{dt} \quad (19)$$

where λ is the fuel mass fraction burned; a and b are shape factors, with the fitting value of 5 and 2 respectively [19]; C_d is the combustion duration with a constant value of 5 ms; t_s is the time at which the combustion process starts. Q_{in} is the overall heat input for each cylinder in one running cycle. Combining Eqs. (18) and (19), we have:

$$\frac{dQ_c}{dt} = a\frac{b+1}{C_d}\left(\frac{t - t_s^b}{C_d}\right)\exp\left(-a\left(\frac{t - t_s}{C_d}\right)^{b-1}\right)Q_{in} \quad (20)$$

Eq. (20) is used to predict the thermal energy delivered to the gas and the resulting pressure in the cylinder.

2.3.5. Scavenging process

Scavenging is considered part of the thermodynamic model for simplification. In fact, it is very difficult to represent the scavenging pressure using accurate numerical model, as it depends on the design details of the scavenging pump. However, estimating the scavenging performance is important to investigate its influence on engine performance, particular due to the variable stroke [14]. As a result, a simplified model is used to estimate the gas pressure in the scavenging pump. When both of the scavenging ports and intake port are covered, the gas mixture in the scavenging pump is assumed to go through an adiabatic process, and the equation for this is illustrated as

$$\frac{dp_s}{dt} = -\gamma\frac{p_s}{V_s}\frac{dV_s}{dt} \quad (21)$$

where p_s is the pressure in the scavenge case (Pa), V_s is the volume of the scavenge case (m^3).

2.4. Linear electric machine model

Linear electric machines are electromagnetic devices capable of producing directly progressive unidirectional or oscillatory short-stroke motion. Linear electric generators are also linear motion electromagnetic devices which transform short-stroke oscillatory motion mechanical energy into single-phase AC electrical energy. Just as a rotary electric machine may operate either as a motor or as a generator, a linear electric machine may be switched to a generator to produce electricity in stable operation. As a result, two models are developed for the linear electric machine, namely the linear electric motor model and the linear electric generator model.

2.4.1. Linear electric motor for starting process

During the starting process, the linear electric machine operates as a linear motor. The static power to the linear motor is supplied by a three-phase AC source, which is specified in term of voltage and frequency: rated values and usual deviations. We use dq-model for the three phase linear synchronous motor. The dq-transformation for currents from the three phase abc variables is presented as [22]:

$$\begin{bmatrix} I_d \\ I_q \end{bmatrix} = \frac{2}{3}\begin{bmatrix} \cos\theta & \cos(\theta - \frac{2\pi}{3}) & \cos(\theta + \frac{2\pi}{3}) \\ -\sin\theta & -\sin(\theta - \frac{2\pi}{3}) & -\sin(\theta + \frac{2\pi}{3}) \end{bmatrix}\begin{bmatrix} i_a \\ i_b \\ i_c \end{bmatrix} \quad (22)$$

The thrust force F_m can be obtained from the derivative of the magnetic stored energy, and is expressed as [23]

$$F_m = K_A I_q \quad (23)$$

where K_A is the proportionality constant. It is determined by the characteristics of the permanent magnet of the mover. From Eq. (5), only I_q contributes to the thrust, which, when controlled, yields the desired mechanical characteristics [21].

In the linear motor control system, the motor is coupled with compensators to reduce the influence from back electromagnetic voltage. Using actual current as feedback signal, the injected current to the coil varies with the mover's motion in order to maintain the output motor force as a constant value. The starting process is thoroughly investigated in another publication [24], and in the scale of this paper, the thrust force during starting process is a constant force determined by:

$$F_m = sign(v) \cdot |F_m| \quad (24)$$

2.4.2. Linear electric generator for steady operation

During steady operation, the linear electric machine operates as a generator. The translator of the generator forms part of the moving piston assembly. Through the continuous back and forth movement of the mover, the electrical current is generated from the alternator coils. According to linear generator fundamentals, the equivalent circuit of the generator and electrical load can be shown in Fig. 4.

The voltage across the generator ε can be written as

$$\varepsilon = Ri + L\frac{di}{dt} + C\int idt \quad (25)$$

where R is the resistance of the circuit; i is the current; L is the inductance of the circuit and C is the capacitance.

Assuming the load circuit is purely resistive ($C = 0$, $L = 0$), Faraday's electromagnetic induction laws give the back electromotive voltage ε as:

$$\varepsilon = N\frac{d\phi}{dt} = k_v\frac{dx}{dt} \quad (26)$$

where ϕ is the magnetic flux and k_v is a generator property. It is assumed that the total mechanical energy of the piston movement

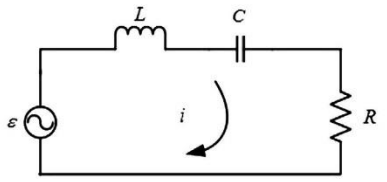

Fig. 4. Equivalent circuit of the linear generator.

is converted to electricity, and there is no efficiency loss in the generator.

As the load force of the electric machine is assumed to be proportional to the current of the circuit, from Eqs. (25) and (26) the load force F_e can be written as [12],

$$F_e = -cv \tag{27}$$

where c is the load constant of the generator, which can be found from the physical parameters of the generator design specifications.

2.5. Friction sub-model

An analysis of engine friction mechanisms in four stroke spark ignition and diesel engines is presented by Heywood [19]. An approximate breakdown of rubbing and accessory friction is piston assembly 50%; valve train 25%; crankshaft bearings 10%; accessories 15% [19]. Friction work in the FPEG is expected to be lower than conventional internal combustion engines due to the elimination of the crank mechanism. Thus the friction in the wrist pin, big end, crankshaft, camshaft bearings, the valve mechanism, gears, or pulleys and belts which drive the camshaft and engine accessories is removed. Frictional losses of FPEG are mainly from the piston assembly, along with the linear electrical machine.

As there is no side forces act on the piston of FPEG and the movement of the piston is linear, piston assembly friction is dominated by the ring friction, and the friction from piston skirt is negligible. Thus the friction force of the FPEG is divided to three components, i.e. friction force from the linear electrical machine (F_{fm}) and friction forces between the piston rings and cylinder wall from both left (F_{fl}) and right (F_{fr}) cylinders of the engine. The total friction force is written as follows

$$F_f = F_{fm} - F_{fl} + F_{fr} \tag{28}$$

The friction of linear electrical machine comes from the contact of the mover and the stator. It is assumed to be constant as the velocity of the piston is low.

In the model (and prototype) each piston contains two compression rings and no oil ring. The initial tensions in both piston rings hold them out against the cylinder wall and hence generate friction. The in-cylinder gas pressure normally acts on the top and back of the rings and the pressure acting on the back of the rings increases this radial force and consequently the friction force. Correlations for piston ring friction have been developed by Bishop in the following categories: boundary condition friction (primarily between the rings and the cylinder wall due to ring tension, and gas pressure behind the compression rings) and viscous ring and piston friction. The component due to ring tension is essentially constant, and the component due to in-cylinder gas pressure behind the rings will vary depending on operation conditions.

Based on the discussion above, an empirical relationship is used to calculate the parameterized friction for the contact between the rings and the cylinder wall [25].

$$F_{fring/liner} = f\left[-sign(v)\cdot A_f\cdot\sqrt{|v|}\right]\left[1-B_f\cdot\frac{E-\theta_0}{\theta_0}\right]\left[1+K_v\cdot\frac{p(t)}{p_0}\right]\left(\frac{d}{d_0}\right) \tag{29}$$

where f is the overall scaling factor (–); v is axial velocity of piston (m/s) and $sign\,(v)$ means the direction of piston velocity; A_f, B_f and K_v are all friction parameter (–); E is the average temperature of lubrication oil at liner (°C); d is cylinder diameter (mm); p is simultaneous in-cylinder pressure (bar); θ_0 is reference temperature (°C); p_0 is reference pressure (1 bar); d_0 is reference cylinder diameter (165 mm).

3. Model validation

The model was validated for both starting process and stable operation against test data obtained from a prototype. The in-cylinder gas pressure, piston displacement and compression ratio were collected and calculated for analysis and the results of the comparison between simulation results and test data were demonstrated.

3.1. Prototype test bench

The schematic FPEG prototype is shown in Fig. 5. This prototype configuration is identical with the input parameters used in the simulation. Further information of this prototype can be found in our previous publication [24]. When the engine is started by the linear electric machine by mechanical resonance method, the linear electric machine operates as a linear motor. It generates a constant motor force in the direction of the piston velocity, controlled by the aforementioned closed-loop strategy. The displacement amplitude as well as the peak in-cylinder gas pressure is expected to gradually grow and finally reach the required values for ignition. During the steady operation, the fuel delivery and ignition systems are activated and the electrical discharge between the spark plug electrodes starts the combustion process close to the end of the compression stroke. In this paper, the ignition timing is not optimised to the best performance.

3.2. Validation results for the starting process

Fig. 6 shows the simulated in-cylinder gas pressure for the right cylinder during the starting process (noted as advanced model), compared with the test data at the same motoring force. As a comparison, an ideal model without considering gas leakage and heat transfer is demonstrated in the same figure (noted as ideal model). The fixed motor force acted on the mover is 110 N, which is in the direction of the mover's velocity. In general, the maximum in-cylinder pressure grows and tends to reach a stable state after a few cycles. But the difference between the test results and ideal model simulation results is significant. For the ideal model, the compression and expansion processes are regarded as isentropic; the in-cylinder gas pressure is much higher and the maximum

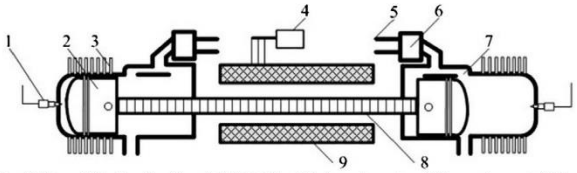

1 Spark plug; 2 Piston; 3 Cooling fin; 4 Load; 5 Air intake; 6 Fuel supply system; 7 Scavenging port; 8 Mover; 9 Stator

Fig. 5. Schematic diagram of the FPEG prototype.

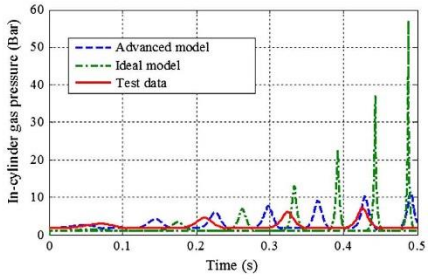

Fig. 6. Comparison of test data and model results.

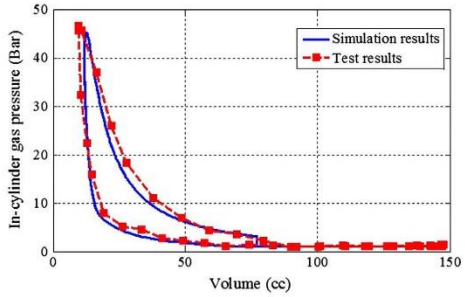

Fig. 9. Pressure volume diagram.

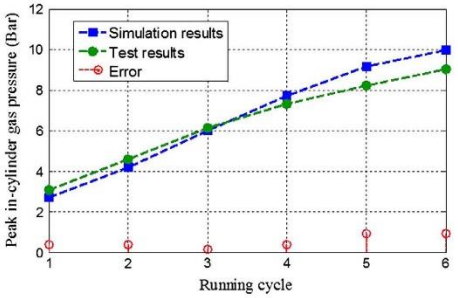

Fig. 7. Comparison of peak in-cylinder pressure.

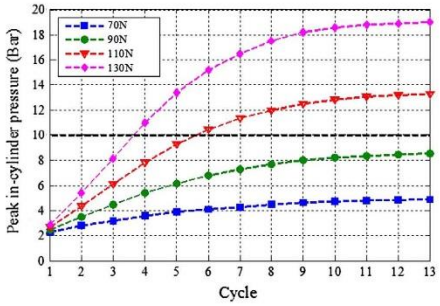

Fig. 10. Peak in-cylinder gas force with different motor force.

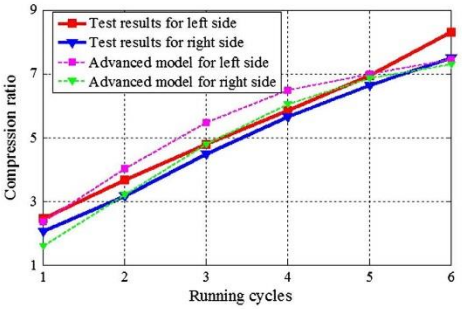

Fig. 8. Comparison of compression ratio.

value can reach 55 bars in 0.5 s. However, from the test data, the actual peak in-cylinder pressure grows to 12 bars during that period, which is almost the same value as the improved model predicted.

The advanced model shows a substantial improvement compared with the ideal model, and the prediction is much more accurate to the test results. The peak in-cylinder pressure for the first 6 cycles from the advanced model results and the test data are compared and plotted in Fig. 7 that shows a good agreement. Even though there is some difference in the frequency and the pressure value, the error can be controlled within a reasonable range (e.g. 1 bar for pressure). This can provide great confidence for the advanced model to be used for further investigation.

The compression ratios of the advanced model simulation and test results for both cylinders were calculated and presented in Fig. 8. For the first six cycles during the starting process, the compression ratio grows from 2:1 to nearly 8:1, which indicates the readiness for ignition. The simulation results for both left and right cylinders show similar trend with the test results, and the error of the advanced model can be controlled within 10%, indicating that the advanced model is valid and can predict the basic performance of the engine during the starting process.

3.3. Validation results for the steady operation

During the steady operation, the engine was operated at stoichiometric air–fuel ratio ($\lambda = 1.0$), and medium open throttle was applied. Fig. 9 shows the simulated pressure volume diagram for one running cycle, compared with the test results.

From the results, the simulate model is of high accuracy to predict the actual engine performance. Both of the compression and expansion processes from the simulation are in good correspondence with the test results. The pressure difference is less than 5%, which is acceptable. Moreover, the areas enclosed by these two cycles are similar, which means that the work produced by the engine and the engine efficiency can be confidently predicted using this simulation model.

However it is necessary to point out, as the piston motion of FPEG is not restricted by a crankshaft-connection rod mechanism, the piston is free to move between its TDC and BDC, and the

movement is only controlled by the gas and load forces acting upon it. As a result, the peak in-cylinder gas pressure will differ from each cycle due to the cyclic variation introduced by many uncontrollable factors such as gas flow, mixture quality, spark quality and initial flame propagation. In order to validate the model, the in-cylinder gas pressure is an average of ten running cycles. Besides, in simulation, the in-cylinder gas pressure is regarded as ambient pressure once the exhaust port is opened, but it actually changes smoothly in the real prototype.

4. Simulation results and discussion

4.1. Starting force

The starting process was simulated with different motoring forces from 70 N to 130 N in 20 N interval. The peak in-cylinder gas pressure of the right cylinder for the first few running cycles is illustrated in Fig. 10. For a fixed motoring force with the proposed mechanical resonance starting strategy (see [24] for details of the mechanical resonance starting strategy), the peak in-cylinder gas pressure grows rapidly and reaches a stable value after about 10 cycles.

With an increased motoring force, the final stabilised peak pressure is higher and the peak pressure increase rate is greater. When 10 bar peak pressure is considered as the target, which is equivalent to a compression ratio of over 7:1, it takes 4 cycles to achieve with a motor force of 130 N, and 6 cycles with 110 N. However, with a motoring force of 90 N or less, the peak in-cylinder pressure cannot achieve the target. When the motoring force is 130 N, the peak pressure can even achieve 19 bar reasonably rapidly in less than half second, which is equivalent to a compression ratio of nearly 12:1 and considered sufficient for compression ignition engine start, since a low speed diesel engine usually has a compression ratio of approximately 14. This discussion can provide an indication for the linear electric machine selection to avoid oversizing but at the same time, ensure adequate motoring force can be generated to smoothly start the engine.

4.2. Engine load

The engine's power output can be adjusted by varying the throttle opening. The effect of varied engine load on the engine performance was simulated to determine the optimal working conditions and corresponding control strategies. The engine was assumed in normal operation after warm up and a stoichiometric air/fuel mixture was supplied. The combustion process was assumed to be perfect and no loss was considered.

Fig. 11 shows the simulated piston dynamics of the FPEG at varying engine load from 65% to 95% in 10% interval, and the engine performance with varied loads is summarised in Table 2.

The ignition timing was fixed at 28 mm from the central position regardless of the operation condition. It can be observed that the engine load has significant influence on the piston velocity and the engine stroke. Both the maximum piston velocity and the compression ratio vary in positive correlation with the load, with higher engine load corresponding to higher velocity and greater compression ratio.

Meanwhile, the velocity profile is relatively constant at the middle of the stroke, while changes greatly at BDC and TDC. The piston acceleration is much lower when piston approaching TDC/BDC than that when piston moving after TDC/BDC, mainly due to the combustion process. This also results in a high piston speed during the expansion process after TDC, which could be desirable in terms of heat transfer since the time is shorter when the gas temperature is high, therefore less heat losses is expected [12]. In addition, this particular feature of FPEG may lead to a reduction in the formation of temperature dependent emissions such as NOx.

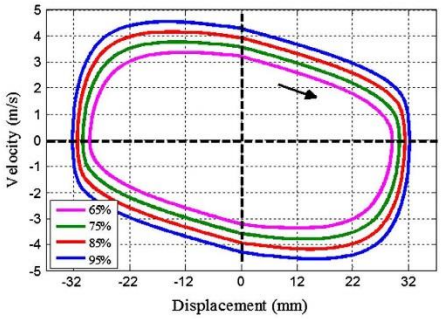

Fig. 11. Velocity vs displacement with different engine loads.

Table 2
Engine performance with varied loads.

Engine load (%)	Peak speed (m/s)	Average speed (m/s)	Equivalent speed (rpm)	Compression ratio
65	3.3	2.2	1200	5.6
75	3.8	2.6	1400	6.4
85	4.2	3.0	1560	7.9
95	4.6	3.2	1680	8.8

Table 3
Engine performance.

Parameters	Value
Engine speed	30 Hz
Engine power	4 kW
Mean piston velocity	3.5 m/s
Maximum piston velocity	4.9 m/s
Compression ratio	10:1
Engine overall efficiency	35%

4.3. Engine performance

The output engine performance parameters when the throttle is open at 100% are summarised in Table 3. The engine is running at 30 Hz (equivalent to 1800 rpm) which is low compared to the normal operation speed of a conventional spark-ignited engine. As a result, the maximum power output will be lower than a conventional engine at the same size. However, the estimated engine overall efficiency (including the friction loss, heat transfer loss, gas leakage loss, compression loss etc.) can reach 35% without turbocharger. As the efficiency of the linear electric generator is estimated to be more than 90%, the efficiency of FPEG can achieve 31.5% at a power level of approximately 4 kW. Please note the model was calibrated towards the bespoke prototype machine which has a relatively high gas leakage. For mass production engines with better quality control, the efficiency could be further improved.

Fig. 12 shows the simulated pressure–volume diagram under full load condition. It is suggested that the combustion is close to a constant volume heat release process, and the peak in-cylinder gas pressure can reach 80 bars. This can result in high efficiency. However unlike traditional engines, cyclic variations and imperfect

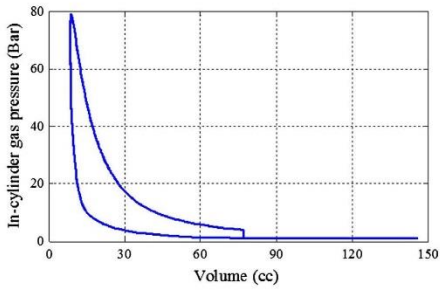

Fig. 12. Pressure volume diagram.

combustion in a free-piston engine may lead to significant variations in piston trajectory as the piston motion is not restricted by a crankshaft-connection rod mechanism. This induces to challenges to develop robust control strategies to ensure stable and smooth engine operation. As a result, the TDC must be controlled within a small range, as insufficient compression ratio may result in misfire, and overshoot may lead to mechanical contact between the piston and the cylinder head [26,27].

5. Conclusion

This paper introduced a complex model of a spark ignited free-piston engine generator. Detailed sub models for both starting process and steady operation process were derived. The simulation results showed a good agreement with the prototype test data for both the starting process and steady operation. During the starting process, the tested peak in-cylinder pressure grew to 12 bars in 0.5 s, which was almost the same as the numerical model predicted. The difference of the in-cylinder gas pressure history can be controlled within 1 bar. For the steady operation, the peak pressure difference was less than 5%, and the engine performances such as power and efficiency can be predicted at a high accuracy using this numerical model.

Using this model, the starting process at different motoring forces and the combustion process with varied throttle opening were investigated. The simulation results suggested that the peak in-cylinder gas pressure increased with higher motoring force, and a proper electric machine needs to be selected to match the engine to be able to provide sufficient motoring force and avoid oversizing at the same time. Both of the maximum piston velocity and the compression ratio varied in positive correlation with the throttle during steady operation. Higher throttle opening results in higher velocity and greater compression ratio. The velocity profile was relatively constant at the middle portion of the stroke, while changed greatly at BDC and TDC.

When the engine operated at 30 Hz (equivalent to1800 rpm) during stable combustion process at full open throttle, the simulated combustion process was considered to be close to a constant volume heat release process, and the peak in-cylinder gas pressure reached 80 bars. The maximum power output of free-piston engine would be lower than a conventional engine of the same size. The estimated engine overall efficiency was 35% without a turbocharger at a power level of approximately **4** kW.

Acknowledgements

This project is supported by the Programme of Introducing Talents of Discipline to Universities of China (B12022) and National Nature Science Foundation of China (51006010). We would like to thank the sponsors.

References

[1] Mikalsen R, Roskilly AP. A review of free-piston engine history and applications. Appl Therm Eng 2007;27(14):2339–52. http://dx.doi.org/10.1016/j.applthermaleng.2007.03.015.
[2] Goertz M, Peng LX. Free piston engine its application and optimization. SAE paper 2000-01-0996; 2000. http://dx.doi.org/10.4271/2000-01-0996.
[3] Petreanu Sorin. Conceptual analysis of a four-stroke linear engine. Dissertation, West Virginia University; 2000.
[4] Hansson Jorgen. Analysis and control of a hybrid vehicle powered by a free-piston energy converter, Dissertation, Royal Institute of Technology; 2006.
[5] Kock F, Haag J, Friedrich H. The free piston linear generator – development of an innovative, compact, highly efficient range-extender module. SAE technical paper 2013-01-1727; 2013. http://dx.doi.org/10.4271/2013-01-1727.
[6] Kosaka H, Akita T, Moriya K, Goto S, et al., Development of free piston engine linear generator system part 1 – investigation of fundamental characteristics. SAE technical paper 2014-01-1203; 2014. http://dx.doi.org/10.4271/2014-01-1203.
[7] Max, Erland. FPEC, Free piston energy converter. In: Proceedings of the 21st Electric Vehicle Symposium & Exhibition, EVS, vol. 21; 2005.
[8] Mikalsen R, Roskilly AP. The design and simulation of a two-stroke free-piston compression ignition engine for electrical power generation. Appl Therm Eng 2008;28(5):589–600. http://dx.doi.org/10.1016/j.applthermaleng.2007.04.009.
[9] Atkinson C, Petreanu S, Clark N, Atkinson R. Numerical simulation of a two-stroke linear engine-alternator combination. SAE technical paper 1999-01-0921; 1999. http://dx.doi.org/10.4271/1999-01-0921.
[10] Nandkumar Subhash. Two-stroke linear engine. Dissertation, West Virginia University; 1998.
[11] Houdyschell David. A diesel two-stroke linear engine. Dissertation, West Virginia University; 2000.
[12] Goldsborough S. Scott, Peter Van Blarigan. A numerical study of a free piston IC engine operating on homogeneous charge compression ignition combustion. SAE technical paper, 1999-01-0619; 1999. http://dx.doi.org/10.4271/1999-01-0619.
[13] Mao Jinlong, Zuo Zhengxing, Feng Huihua. Parameters coupling designation of diesel free-piston linear alternator. Appl Energy 2011;88:4577–89. http://dx.doi.org/10.1016/j.apenergy.2011.05.051.
[14] Mao JL, Zuo ZX, Lin W, Feng H. Multi-dimensional scavenging analysis of a free-piston linear alternator based on numerical simulation. Appl Energy 2011;88(4):1140–52. http://dx.doi.org/10.1016/j.apenergy.2010.10.003.
[15] Němeček P, Šindelka M, Vysoký O. Modeling and control of linear combustion engine. In: IFAC symposium on advances in automotive control, Oxford: Elsevier Science; 2004. p. 320–5.
[16] Duan Chen, Wang Xinggang, Shu Shuiming, Jing Changwei, Chang Huawei. Thermodynamic design of Stirling engine using multi-objective particle swarm optimization algorithm. Energy Convers Manage 2014;84:88–96. http://dx.doi.org/10.1016/j.enconman.2014.04.003.
[17] Toghyani Somayeh, Kasaeian Alibakhsh, Ahmadi Mohammad H. Multi-objective optimization of Stirling engine using non-ideal adiabatic method. Energy Convers Manage 2014;80:54–62. http://dx.doi.org/10.1016/j.enconman.2014.01.022.
[18] Kim Jacheun, Bae Choongsik, Kim Gangchul. Simulation on the effect of the combustion parameters on the piston dynamics and engine performance using the Wiebe function in a free piston engine. Appl Energy 2013;107:446–55. http://dx.doi.org/10.1016/j.apenergy.2013.02.056.
[19] Heywood John B. Internal combustion engine fundamentals. McGraw-Hill press; 1988.
[20] Hohenberg Günter F. Advanced approaches for heat transfer calculations. SAE technical paper, No. 790825; 1979. http://dx.doi.org/10.4271/790825.
[21] Boldea I, Nasar Syed A. Linear electric actuators and generators. Cambridge University Press; 1997.
[22] Boldea I, Nasar SA. Permanent magnet linear alternator: Part 1. Fundamental equations. IEEE Trans 1987;AES-23:73–8. http://dx.doi.org/10.1109/TAES.1987.313337.
[23] Chiang, Chia-Jui, et al. Dynamic modeling of a SI/HCCI free-piston engine generator with electric mechanical valves. Appl Energy 2013;102:336–46. http://dx.doi.org/10.1016/j.apenergy.2012.07.033.
[24] Jia B, Zuo Z, Feng H, Tian G, Roskilly AP. Development approach of a spark-ignited free-piston engine generator. SAE technical paper, 2014-01-2894; 2014. http://dx.doi.org/10.4271/2014-01-2894.
[25] AVL EXCITE Piston & Rings Version 2010 Users Guide. Edition 11/2010.
[26] Mikalsen R, Roskilly AP. The control of a free-piston engine generator. Part 1: Fundamental analyses. Appl Energy 2010;87(4):1273–80. http://dx.doi.org/10.1016/j.apenergy.2009.06.036.
[27] Mikalsen R, Roskilly AP. The control of a free-piston engine generator. Part 2: Engine dynamics and piston motion control. Appl Energy 2010;87.4:1281–7. http://dx.doi.org/10.1016/j.apenergy.2009.06.035.

Appendix II

Applied Energy 162 (2016) 321–329

Contents lists available at ScienceDirect

Applied Energy

journal homepage: www.elsevier.com/locate/apenergy

A fast response free-piston engine generator numerical model for control applications

Boru Jia [a,b], Andrew Smallbone [b], Huihua Feng [a,*], Guohong Tian [b], Zhengxing Zuo [a], A.P. Roskilly [b]

[a] School of Mechanical Engineering, Beijing Institute of Technology, Beijing 100081, China
[b] Sir Joseph Swan Centre for Energy Research, Newcastle University, Newcastle upon Tyne NE1 7RU, UK

HIGHLIGHTS

- The numerical model of FPEG is simplified to a one-degree forced vibration system.
- Simplified model was successfully validated with respect to experimental data.
- The state-space equations and the transfer function of the system can be obtained.
- Feasible to be implemented to HIL simulation due to simplicity and flexibility.

ARTICLE INFO

Article history:
Received 4 May 2015
Received in revised form 16 October 2015
Accepted 17 October 2015

Keywords:
Free-piston engine generator
Fast response model
Forced vibration system
Control application

ABSTRACT

This paper presents a linearization of the dynamic equation for a free-piston engine generator (FPEG), and simplifies it to a one-degree forced vibration system with viscous damping. The analogy between a mass-spring damper and a FPEG system is expressed, and the solution to the vibration system is solved. The model was successfully validated with respect to experimental data obtained from a prototype. The simulated piston displacement during steady operation showed similar trends with the test results and the error of the displacement amplitude was controlled within 3%. The state-space equations and the transfer function of the system are obtain using the fast response numerical model. An example of model application in the real FEPG control system was provided. Compared to the previous numerical model with differential approaches, the solving time of the proposed fast response model can be significantly reduced. The simplicity and flexibility of the proposed model make it feasible to be implemented to several computing software, *i.e.* Matlab, AMESim, Labview, Dymola et al. It can be easily implemented to real-time Hardware-in-the-Loop (HIL) simulation model for the future piston dynamic control system development. In addition, since it reveals how an FPEG operates in a resonant principle, the model is useful for parameter selection in the FPEG design process.

1. Introduction

1.1. Background

The free-piston engine (FPE) is a promising power generation device which offers the benefits of simplicity and high thermal efficiency [1–5]. Unlike conventional reciprocating engines, the piston is not restricted by a crankshaft mechanism, and therefore its application has a number of reported advantages such as: mechanical simplicity, high efficiency, reduced NO_x formation and multi-fuel/combustion mode flexibility [6].

Known FPE applications include electric generators, hydraulic pumps and air compressors [1]. The dual piston free-piston engine generator (FPEG) considered here consists of a dual piston type FPE coupled with a linear electric generator. Combustion occurs alternately in each chamber to drive the mechanically unconstrained mover back and forth, a linear generator converts parts of the kinetic energy of the mover to electricity. Much work has been undertaken by a number of research groups worldwide including the authors' group to explore the operation characteristics of FPEG [7–12].

Different FPEG prototype designs have been reported by now. The FPEG prototype developed by the German Aerospace Centre consisted of an engine, a linear generator and a gas spring [13,14]. A power output of approximately 10 kW at 21 Hz was reported [13]. Researcher at Nanjing Institute of Technology

* Corresponding author. Tel.: +86 10 68911062.
E-mail address: fenghh@bit.edu.cn (H. Feng).

http://dx.doi.org/10.1016/j.apenergy.2015.10.108
0306-2619/

Nomenclature

A	piston area (m^2)	p	cylinder gas pressure (Pa)
AFR	air–fuel ratio	p_0	ambient pressure (Pa)
B	cylinder bore (m)	p_{cm}	pressure due to heat release (Pa)
c	damping coefficient	p_{cp}	cylinder pressure due to volume change (Pa)
C_v	heat capacity at constant volume (J/m^3 K)	Q_{in}	heat released from the combustion process (J)
CR	set compression ratio	Q_{LHV}	low heating value (J/kg)
F	excitation force (N)	V	cylinder volume (m^3)
F_0	magnitude of excitation force (N)	V_o	cylinder volume at the middle stroke (m^3)
F_e	resistant force from generator (N)	V_c	clearance volume (m^3)
F_l	gas force from the left cylinder (N)	V_l	volume for the left chamber (m^3)
F_r	gas force from the right cylinder (N)	V_r	right chamber's volume (m^3)
k	spring constant or stiffness	W	output work (J)
k_v	coefficient of the load force	x	mover displacement (m)
K_t	throttle opening coefficient	Δp_{cm}	pressure increase heat release process (Pa)
L_s	half stroke length (m)	ΔU	the difference of the internal energy (J)
m	moving mass (kg)	ΔT	temperature increase of the mixture (K)
m_{air0}	air mass at full throttle (kg)	ω_n	angular natural frequency
m_{fuel}	fuel mass in the mixture (kg)	σ	unit step function
L_c	clearance length (m)	η_c	combustion efficiency

proposed a novel new FPEG design, which was consisted of a single cylinder operating on four-stroke cycle, a linear electric generator, and a mechanical spring kickback system [15]. A 2.2 kW average power output was obtained with an efficiency of 32% [15]. The dual piston FPEG prototype developed by Beijing Institute of Technology was reported to misfire every one to two cycles, with severe cycle-to-cycle variations [16]. The possible reasons of the variations and unstable operation were analyzed.

Modeling and simulation are key elements of machine design, and the FPE is commonly modeled using zero-dimensional models to obtain the piston dynamics and predict engine performance. There have been detailed numerical models validated and reported, in which the effects of the heat transfer, gas leakage were considered [17–25]. Many of the numerical models were developed in Matlab/Simulink, and multiple sub-systems were required to represent each equation. In our previous paper, a detailed numerical modeling of a spark-ignited FPEG and the model validation with test results have been presented [26]. However, the differential equations were solved iteratively and required a considerable computational cost, which makes it challenging to be implemented to real-time Hardware-in-the-Loop control systems. Therefore, when more complicated control strategy needs to be developed and implemented, a simplified model is necessary for the further real-time control system development.

As there is gas in both cylinders, which is compressible. Therefore, the gas in the cylinder acts like nonlinear springs, and the FPEG system is analogous to a mass-spring system. For a dual piston FPE, the engine is operated in a two-stroke cycle, and combustion occurs alternately in each chamber during stable operation. This means that the system is running under an external excitation, which is determined by the heat released during the combustion process. As a result, the dual piston FPE will show similar characteristics with a vibration system under external excitations after proper simplification.

1.2. Previous work on FPE oscillation characteristics analysis

A free-piston Stirling engine was considered as a heat driven mechanical oscillator by Redlich et al. from which power can be extracted. Linear dynamics was applied to obtain a stability criterion, means for calculating the frequency, characteristics of the oscillation system, and effects of friction force on starting process and the locus of the roots of the system determinant. Three common configurations of these engines were investigated [27].

Nakhaie Jazar and Farid Golnaraghi presented a nonlinear model for a hydraulic engine mount. They introduced a simple nonlinear mathematical model, which showed agreement with the test results available in the literature [28]. Applying the multiple scale perturbation method, they examined the behavior of the mount at resonance. The significant difference between the performance of the nonlinear model and the linear model at resonance was the existence of a jump phenomenon [28].

Xiao et al. established a numerical model of the FPEG [29–31]. The natural frequency of the oscillation system was obtained from their model. A simulation program was developed in Matlab/Simulink to solve these mathematical equations, and the simulation results showed that the motion of FPEG was a forced vibration system with variable damping coefficient and stiffness [29].

Hansson et al. investigated the resonant behavior of a FPEG. They linearized the system after expanding the equation around an equilibrium point [32]. Finally, the approximations of the free-piston oscillation characteristics were achieved. However, only compression pressure forces were calculated in their model, and the pressure increased by the heat release of the gas fuel mixture was not considered.

1.3. Research aims and methodologies

This paper aims to describe the dynamic operation of a dual piston FPEG, with the objective of obtaining an understanding of the piston oscillation characteristics. Both of the compression pressure force and the pressure increased by the heat release were considered. By linearizing the system, a forced vibration equation with viscous damping can be achieved, and the approximations of the mass spring constant and the natural frequency can be obtained. Based on that, the vibration equation and the solution for the displacement can be derived.

2. Linear dynamics model

2.1. Dynamic equation

The main parts of the FPEG consist of two opposing combustion chambers and a linear electric machine. A linear magnet mover

with pistons at each end is located between the two combustion chambers, which is the only significant moving part of the FPEG. As the piston is not restricted by the crankshaft, its movement is influenced by in-cylinder gas forces, linear motor force, and mechanical friction force. Due to the elimination of the crank mechanism, the frictions in the wrist pin, big end, crankshaft, camshaft bearings, the valve mechanism, gears, or pulleys and belts which drive the camshaft and engine accessories are removed. As the movement of the piston is linear, the side forces acting on the piston is minimal compared with the conventional engines, thus the friction between the piston rings, piston skirt, and cylinder wall will be significantly reduced. As a result, frictional loss in the FPEG prototype is expected to be much lower than a reciprocating engine, and is insignificant compared with the in-cylinder gas forces. Because of this, the friction force is neglected in this investigation.

If friction force is neglected, a dynamic equation of the mover can be derived from Newton's second law and illustrated in Fig. 1.

$$m\ddot{x} = \vec{F}_l + \vec{F}_r + \vec{F}_e \tag{1}$$

where m is the moving mass of the mover with the pistons (unit: kg); x is the mover displacement (m); F_l is the gas force from the left cylinder (N); F_r is the gas force from the right cylinder (N); F_e is the resistant force from the linear electric generator (N). The gas force can be calculated using the gas pressure, p (Pa) and piston surface area, A (m^2) which can be approximated from the cylinder bore, B (m), as:

$$A = \frac{\pi B^2}{4} \tag{2}$$

The in-cylinder pressure and the gas force are functions of the mover displacement, x.

$$F_l = p_l \cdot A \tag{3}$$

$$F_r = p_r \cdot A \tag{4}$$

The load force of the electric generator is known to have a high influence on the performance of the FPEG. According to a paper by Mikalsen and Roskilly, the load force is a function of the design parameters of the machine, the mover's velocity as well as the load resistance [3]. It is assumed to be proportional to the mover's speed [3,26], and is expressed in Eq. (5). The direction of the load force is always opposite to the direction of piston velocity,

$$F_e = -k_v\dot{x} \tag{5}$$

where k_v is the coefficient of the load force, and it varies with the load resistance [26].

By rewriting Eq. (1),

$$m\ddot{x} = \vec{F}_l(x) + \vec{F}_r(x) + \vec{F}_e(\dot{x}) \tag{6}$$

it can be seen that if the nonlinear in-cylinder pressure force is simplified properly, the dynamic equation of FPEG can be linearized to a forced vibration system with viscous damping, which is illustrated in Fig. 2. The analogy between a mass-spring damper and a FPEG

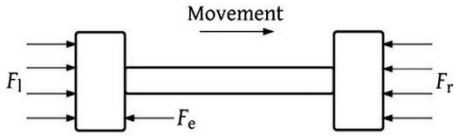

Fig. 1. Schematic figure of the dynamic equation.

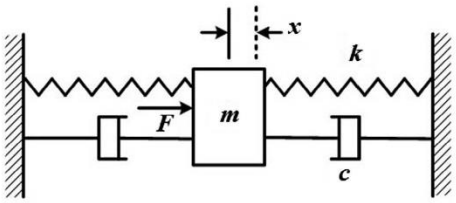

Fig. 2. Illustration of the analogous forced vibration system.

Table 1
Analogy between a mass-spring damper and a FPEG system.

Mass-spring damper	FPEG system
Moving mass, m	Mass of the piston assembly and mover
Damping coefficient, c	Linear generator load force
Spring constant, k	In-cylinder pressure
Excitation force, F	Heat release force

system is expressed in Table 1. The objective form of the dynamic equation after the linearization is expressed as:

$$m\ddot{x} - c\dot{x} + kx = F(t) \tag{7}$$

where the constant c is the damping coefficient; the constant of proportionality k is the spring constant; and $F(t)$ is the continuing excitation force.

Then the angular natural frequency, ω_n of FPEG can be defined as:

$$\omega_n = \sqrt{\frac{k}{m}} \tag{8}$$

2.2. Thermodynamic cycle

The typical thermodynamic cycle of FPEG can be described by a compression process, a heat release process (combustion) followed by an expansion process. As a result, the in-cylinder pressure is influenced by two factors, *i.e.* the cylinder volume change caused by the piston motion and the heat release from the chemical energy of the burnt fuel. The in-cylinder pressure can be written as:

$$p_l = p_{lcp} + p_{lcm} \cdot \sigma_l \tag{9}$$

$$p_r = p_{rcp} + p_{rcm} \cdot \sigma_r \tag{10}$$

where p is the in-cylinder pressure (Pa); p_{cp} is the pressure due to the cylinder volume change (Pa); p_{cm} is the pressure due to heat release during the combustion process (Pa); the subscripts r and l represent the values of the right and left cylinder respectively.

Usually a spark is the start of combustion, initially the pressure rise is very small and compression will still continue until it is large enough to reverse the piston direction into an expansion stroke. A unit step function σ is induced to enable/disable the influence from the heat release for both cylinders, which is shown in Eqs. (11) and (12) respectively.

$$\sigma_l = \begin{cases} 1, & \dot{x} \geqslant 0 \\ 0, & \dot{x} < 0 \end{cases} \tag{11}$$

$$\sigma_r = \begin{cases} 0, & \dot{x} \geqslant 0 \\ 1, & \dot{x} < 0 \end{cases} \tag{12}$$

According to the reported simulation and experimental results, the combustion process of FPEG can be simplified to be represented by a constant volume heating process [3,26]. If no heat transfer to the cylinder walls and no gas leakage through the piston rings are considered in the thermodynamic model, the ideal running cycle of FPEG can be described by two adiabatic processes connected by a constant volume heat release process, illustrated in Fig. 3.

The cylinder pressures due to the adiabatic volume change for both sides are expressed by the following equations:

$$p_{lcp} = p_0\left(\frac{V_0}{V_l}\right)^{\gamma} \tag{13}$$

$$p_{rcp} = p_0\left(\frac{V_0}{V_r}\right)^{\gamma} \tag{14}$$

$$V_0 = L_s \cdot A \tag{15}$$

where the in-cylinder pressure is assumed to be equal to the ambient pressure, p_0 (Pa) at the middle stroke; V_o is the cylinder volume at the middle stroke (m^3); V is the cylinder volume (m^3), and L_s is the length of half stroke (m).

The volume for the left chamber, V_l is:

$$V_l = (L_s + x) \cdot A \tag{16}$$

The right chamber's volume, V_r can be calculated by:

$$V_r = (L_s - x) \cdot A \tag{17}$$

The in-cylinder pressures due to heat release can be expressed as:

$$p_{lcm} = \Delta p_{cm}\left(\frac{V_c}{V_l}\right) \tag{18}$$

$$p_{rcm} = \Delta p_{cm}\left(\frac{V_c}{V_r}\right) \tag{19}$$

$$V_c = L_c \cdot A \tag{20}$$

where Δp_{cm} is the pressure increase during the constant volume heat release process (Pa) and the value is the same for both sides; L_c is the length of the clearance (m); and V_c is the clearance volume (m^3).

From Eqs. (9)–(20), the cylinder force can be written as:

$$F_l = A \cdot \left(p_0\left(\frac{L_s}{L_s + x}\right)^{\gamma} + \Delta p_{cm}\left(\frac{L_c}{L_s + x}\right)^{\gamma} \cdot \sigma_l\right) \tag{21}$$

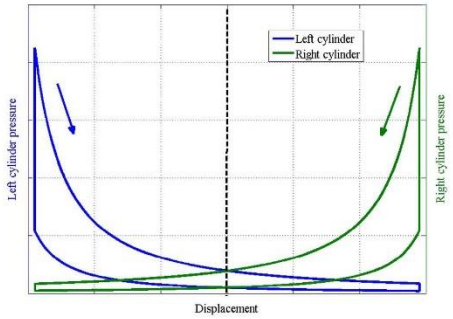

Fig. 3. Ideal operating cycle of the FPEG.

$$F_r = A \cdot \left(p_0\left(\frac{L_s}{L_s - x}\right)^{\gamma} + \Delta p_{cm}\left(\frac{L_c}{L_s - x}\right)^{\gamma} \cdot \sigma_r\right) \tag{22}$$

2.3. Constant volume heat release process

A constant-volume combustion assumption is used to obtain the pressure difference, Δp_{cm} after heat release process. Applying the first law of thermodynamics on the cylinder charge, it can be obtained that:

$$\Delta U - Q_{in} - W \tag{23}$$

where ΔU is the difference of the internal energy of the in-cylinder charge (J); Q_{in} is the total amount of heat released from the combustion process (J); and W is the output work done by the cylinder charge (J).

Since the heat release process is assumed to be constant-volume process, the output work done by the cylinder charge is zero. Then all of the heat released from the combustion process is transferred to increase the internal energy of the in-cylinder gas, that is:

$$\Delta U = Q_{in} \tag{24}$$

If m_{air0} (kg) is trapped mass of air at wide open throttle, thus at maximum load. Applying the ideal gas equation, m_{air0} can be calculated from

$$p_0 V_0 = m_{air0} R T_0 \tag{25}$$

When the engine is operated at part load, the amount of trapped intake air is:

$$m_{air} = K_t \cdot m_{air0} \tag{26}$$

where K_t is a proportional factor [0 – 1] which would be considered to be function of the throttle opening, volumetric efficiency, etc.

The engine is assumed to be operated at stoichiometric air–fuel ratio (AFR). The mass of fuel in the mixture m_{fuel} is:

$$m_{fuel} = m_{air}/\mathrm{AFR} \tag{27}$$

Substitution for m_{air} from Eqs. (25)–(27), gives

$$m_{fuel} = K_t \cdot \frac{p_0 V_0}{R T_0 \mathrm{AFR}} \tag{28}$$

Then Q_{in} is calculated from m_{fuel} and the low heating value of the fuel Q_{LHV} (J/kg) with the combustion efficiency of η_c

$$Q_{in} = m_{fuel} \cdot Q_{LHV} \cdot \eta_c \tag{29}$$

By using Eq. (28), and assume $H_u = Q_{LHV} \cdot \eta_c$, the total amount of heat released from the combustion process is expressed as:

$$Q_{in} = K_t \cdot H_u \frac{p_0 V_0}{R T_0\ \mathrm{AFR}} \tag{30}$$

Substitution for Q_{in} from Eq. (24), obtains

$$\Delta U = K_t \cdot H_u \frac{p_0 V_0}{R T_0\ \mathrm{AFR}} \tag{31}$$

For ideal gas, the increase of internal energy leads to the temperature of the gas mixture:

$$\Delta U = C_v (m_{air} + m_{fuel}) \Delta T \tag{32}$$

where C_v is the heat capacity at constant volume (J/m^3 K); ΔT is the temperature increase of the mixture (K).

Applying the ideal gas law to the in-cylinder gas mixture, yields

$$\Delta p_{cm} V_c = (m_{air} + m_{fuel}) R \Delta T \tag{33}$$

By using Eqs. (31)–(33), the pressure increase Δp_{cm} can be expressed as:

$$\Delta p_{cm} = K_t \cdot H_u \frac{p_0 V_0}{C_v T_0 \mathrm{AFR} V_c} \tag{34}$$

The expected geometric compression ratio of the free-piston engine CR is:

$$\mathrm{CR} = \frac{V_0}{V_c} = \frac{L_s}{L_c} \tag{35}$$

Thus

$$\Delta p_{cm} = K_t \cdot H_u \frac{p_0 \mathrm{CR}}{C_v T_0 \mathrm{AFR}} \tag{36}$$

2.4. Linear approximation of cylinder pressure

To compare the properties with a forced vibration with viscous damping, the nonlinear expressions on the right side of gas force Eqs. (21) and (22) are required to be linearized.

Taylor series is selected in this research, and they are expanded around the equilibrium point:

$$x - 0 \tag{37}$$

Let

$$f_l(x) = \left(p_0\left(\frac{L_s}{L_s + x}\right)^{\gamma} + \Delta p_{cm}\left(\frac{L_c}{L_s + x}\right)^{\gamma} \cdot \sigma_l\right) \tag{38}$$

$$f_r(x) = \left(p_0\left(\frac{L_s}{L_s - x}\right)^{\gamma} + \Delta p_{cm}\left(\frac{L_c}{L_s - x}\right)^{\gamma} \cdot \sigma_r\right) \tag{39}$$

Then the Taylor series for f_l and f_r are expressed as:

$$f_l(x) = f_l(0) + \frac{f_l'(0)}{1!}x + \frac{f_l''(0)}{2!}x^2 + \frac{f_l^3(0)}{3!}x^3 + \cdots \tag{40}$$

$$f_r(x) = f_r(0) + \frac{f_r'(0)}{1!}x + \frac{f_r''(0)}{2!}x^2 + \frac{f_r^3(0)}{3!}x^3 + \cdots \tag{41}$$

As a linear approximation is desired, all high order terms in the above equations are neglected. Taylor expansion with the first order term provides a reasonable performance on such problems. Despite the error in average value introduced by method, the global trend and period are similar. The simplification results will be further validated by test data.

The linear approximations are listed below

$$f_l(x) = a_l + b_l x \tag{42}$$

$$f_r(x) = a_r + b_r x \tag{43}$$

where

$$a_l = p_0 + \Delta p_{cm}\left(\frac{L_c}{L_s}\right)^{\gamma} \cdot \sigma_l \tag{44}$$

$$b_l = -\left(\frac{\gamma p_0}{L_s} + \Delta p_{cm}\frac{\gamma L_c^{\gamma}}{L_s^{\gamma+1}} \cdot \sigma_l\right) \tag{45}$$

$$a_r = p_0 + \Delta p_{cm}\left(\frac{L_c}{L_s}\right)^{\gamma} \cdot \sigma_r \tag{46}$$

$$b_r = \frac{\gamma p_0}{L_s} + \Delta p_{cm}\frac{\gamma L_c^{\gamma}}{L_s^{\gamma+1}} \cdot \sigma_r \tag{47}$$

Then the linear approximations of the cylinder gas force Eqs. (21) and (22) are

$$F_l(x) = \left(p_0 + \Delta p_{cm}\left(\frac{L_c}{L_s}\right)^{\gamma} \cdot \sigma_l\right)A - \left(\frac{\gamma p_0}{L_s} + \Delta p_{cm}\frac{\gamma L_c^{\gamma}}{L_s^{\gamma+1}} \cdot \sigma_l\right)A \cdot x \tag{48}$$

$$F_r(x) = \left(p_0 + \Delta p_{cm}\left(\frac{L_c}{L_s}\right)^{\gamma} \cdot \sigma_r\right)A - \left(\frac{\gamma p_0}{L_s} + \Delta p_{cm}\frac{\gamma L_c^{\gamma}}{L_s^{\gamma+1}} \cdot \sigma_r\right)A \cdot x \tag{49}$$

2.5. Forced vibration equation

From Eqs. (5)–(49), the final dynamic equation is given by

$$m\ddot{x} - k_v\dot{x} + \left(\frac{2\gamma p_0 A}{L_s} + \frac{\Delta p_{cm} A \gamma L_c^{\gamma}}{L_s^{\gamma+1}}(\sigma_l + \sigma_r)\right)x = \Delta p_{cm} A\left(\frac{1}{\mathrm{CR}}\right)^{\gamma}(\sigma_l - \sigma_r) \tag{50}$$

Since the combustion takes place in each cylinder on an alternate basis, according to Eqs. (11) and (12), we obtain

$$\sigma_l + \sigma_r = 1 \tag{51}$$

and

$$\sigma_l - \sigma_r = \begin{cases} 1, & \dot{x} \geqslant 0 \\ -1, & \dot{x} < 0 \end{cases} \tag{52}$$

The rectangular wave of the excitation can be described by a Fourier series. If the initial position of the piston is assumed to be at its left dead centre, and the combustion takes place at the left cylinder, then the comparison of $(\sigma_l - \sigma_r)$ with the first mode of its Fourier series is demonstrated in Fig. 4. The first mode of $(\sigma_l - \sigma_r)$ is defined as:

$$\sigma_l - \sigma_r \approx \frac{4}{\pi}\sin\omega t \tag{53}$$

where ω is the angular frequency of combustion happens for each cylinder.

Finally, substituting for $(\sigma_l - \sigma_r)$ and $(\sigma_l - \sigma_r)$ from Eqs. (51) and (53) respectively, Eq. (50) can be written as:

$$m\ddot{x} - c\dot{x} + kx = F_0 \sin\omega t \tag{54}$$

where

$$c = k_v \tag{55}$$

$$k = \frac{2\gamma p_0 A}{L_s} + \frac{\Delta p_{cm} A \gamma L_c^{\gamma}}{L_s^{\gamma+1}} \tag{56}$$

$$F_0 = \frac{4}{\pi}\Delta p_{cm} A\left(\frac{1}{\mathrm{CR}}\right)^{\gamma} \tag{57}$$

Then the dynamic model of FPEG is linearized to the same form with the single degree-of-freedom forced vibration system with viscous damping. Where k is the stiffness of the air-spring system; c is the damping coefficient; the excitation $F_0 \sin\omega t$ is a continuing force whose magnitude F_0 varies sinusoidally with time.

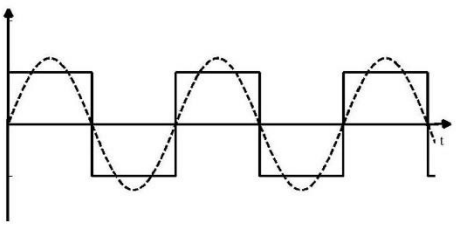

Fig. 4. Rectangular wave and first mode of its Fourier series.

A mass spring system usually reciprocates with a natural frequency, and the system is ideally operated near to this frequency as this requires the least additional energy [32]. According to Eq. (8) the angular natural frequency ω_n of a FPEG is:

$$\omega_n = \sqrt{k/m} = \sqrt{\left(\frac{2\gamma p_0 A}{L_s} + \frac{\Delta p_{cm} A \gamma L_c^{\gamma}}{L_s^{\gamma+1}}\right)\Big/ m} \tag{58}$$

Since combustion is assumed to take place when the piston reaches its top dead centre (TDC), the frequency of the ignition is required to be the same as an air-spring system of FPEG in order to maintain stable operation. Thus yielding:

$$\omega_n = \omega \tag{59}$$

Then the solution of Eq. (54) can be obtained according to vibration theory [33], and the displacement of the viscous damped, single degree-of-freedom system shown in Fig. 4 undergoes vibration as defined by:

$$x = -\frac{F_0 \cos \omega_n t}{c\omega_n} \tag{60}$$

where F_0, ω_n, and c can be obtained from Eqs. (57), (58) and (55) respectively.

More characteristics of the viscous damping vibration system are able to be obtained by applying the vibration theory.

3. Model validation

The linear dynamic model was developed in Matlab/Simulink, calibrated using parameters and test data obtained from an operating FPEG prototype presented in Fig. 5. More details about this prototype can be found in our previous paper [34]. This prototype configuration is identical to the input parameters used in this model as summarized in Table 2. During the steady state operation, the fuel delivery and ignition systems are activated and the electrical discharge between the spark plug electrodes starts the combustion process close to the end of the compression stroke. Widely throttle opening was applied, and engine was assumed to operate at stoichiometric air–fuel ratio.

Fig. 6 shows the simulated piston displacement as a function of time during the combustion process compared with the test data at the same operating condition. The simulation results of the piston dynamics show similar trends with the test results, and the tested amplitudes are almost identical with the model prediction. The error can be controlled within 3%. There is however difference in the frequency value (nearly 20 Hz according to the test data and approximately 18 Hz from the simulation model) which is believed

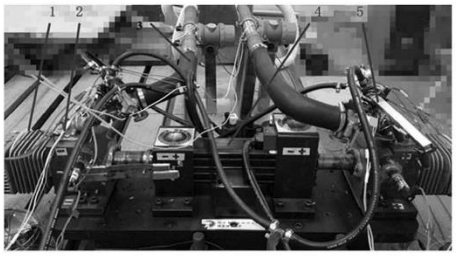

1 cylinder; 2 scavenging pump; 3 air intake manifold;
4 linear electric machine; 5 fuel injection system

Fig. 5. FPEG prototype.

Table 2
Prototype specifications.

Parameters	Value
Bore (mm)	52.5
Maximum total stroke (mm)	70.0
Compression stroke (mm)	35.0
Moving mass (kg)	5.0
Coefficient of the load force (N/(m s^{-1}))	395.0
Ambient temperature (°C)	25.0
Ignition position from middle stroke (mm)	30.0

to be introduced by the simplifications. Therefore a time scale factor of 1.15 is applied on the simulation results (as shown in Fig. 6) to compensate for the frequency difference.

This difference is supposed to be caused by the linearization of the cylinder gas force and elimination of friction force during the simplification process. From Eq. (58), the error in predicting Δp_{cm} will also cause the corresponding error in the simulated results. The error is considered acceptable due to the simplification made when linearizing the model, and the model is considered sufficiently robust to predict the actual engine dynamic performance.

4. Model analysis

If the mechanical system shown in Fig. 2 is assumed to be a linear system. The external force $F(t)$ is the input to the system, and the piston displacement $x(t)$ is the output, which means this system is a single-input, single-output system. From the diagram and Eq. (60), the system is of second order. If state variables $x_1(t)$ and $x_2(t)$ are defined as:

$$x_1(t) = x(t) \tag{61}$$

$$x_2(t) = \dot{x}(t) \tag{62}$$

$$u(t) = F(t) \tag{63}$$

Then we can get

$$\dot{x}_1 = x_2 \tag{64}$$

$$\dot{x}_2 = -\frac{k}{m}x_1 - \frac{c}{m}x_2 + \frac{1}{m}u \tag{65}$$

The output equation is:

$$y = x_1 \tag{66}$$

Then Eqs. (64) and (65) can be written in a vector–matrix state equation form as:

$$\begin{bmatrix}\dot{x}_1 \\ \dot{x}_2\end{bmatrix} = \begin{bmatrix}0 & 1 \\ -\frac{k}{m} & -\frac{c}{m}\end{bmatrix}\begin{bmatrix}x_1 \\ x_2\end{bmatrix} + \begin{bmatrix}0 \\ \frac{1}{m}\end{bmatrix}u \tag{67}$$

The output Eq. (66) for the system is:

$$y = [1 \quad 0]\begin{bmatrix}x_1 \\ x_2\end{bmatrix} \tag{68}$$

The state-space Eqs. (67) and (68) can be rewritten in the standard form:

$$\dot{\mathbf{x}} = \mathbf{A}\mathbf{x} - \mathbf{B}u \tag{69}$$

$$y = \mathbf{C}\mathbf{x} - Du \tag{70}$$

where

$$\mathbf{A} = \begin{bmatrix}0 & 1 \\ -\frac{k}{m} & -\frac{c}{m}\end{bmatrix}, \quad \mathbf{B} = \begin{bmatrix}0 \\ \frac{1}{m}\end{bmatrix}, \quad \mathbf{C} = [1 \quad 0], \quad D = 0 \tag{71}$$

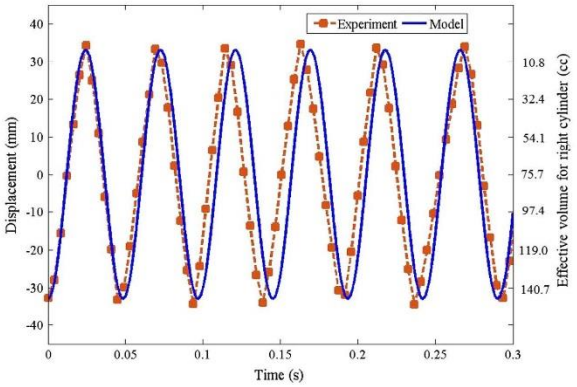

Fig. 6. Model validation results of piston displacement.

The transfer function of the system given by $G(s) = \frac{Y(s)}{U(s)}$ can be obtained from the state-space equations:

$$G(s) = \mathbf{C}(s\mathbf{I} - \mathbf{A})^{-1}\mathbf{B} + D \tag{72}$$

By substituting $\mathbf{C}$, $\mathbf{A}$, $\mathbf{B}$ and D into Eq. (72), the transfer function is then expressed by:

$$G(s) = \frac{1}{ms^2 + cs + k} \tag{73}$$

The system has no zero point, and the poles can be obtained by the two roots of:

$$ms^2 + cs + k = 0 \tag{74}$$

The roots of equation are

$$s = \frac{-c \pm \sqrt{c^2 - 4mk}}{2m} \tag{75}$$

As the poles must be in the left half plane for the system to be stable, which means:

$$c^2 - 4mk > 0 \tag{76}$$

Substituting Eqs. (55) and (56) yields,

$$k_v^2 - 4mp_0A\left(\frac{2\gamma}{L_s} + \frac{K_iH_u\gamma}{C_vT_0L_s\mathrm{AFR}CR^{\gamma-1}}\right) > 0 \tag{77}$$

5. Model application

From Eq. (60), it is apparent that the profile of the piston is influenced by the engine design parameters, throttle opening, air fuel ratio, as well the set compression ratio which is decided by the ignition timing. As a result, the TDC of the engine can be estimated with the actual working conditions of the engine. An example implementation to the real-time control system model is illustrated in Fig. 7.

The control system for the FPEG prototype illustrated in Fig. 7 consists of four main parts: the TDC estimator, the controllers providing control signals to the ignition system and the fuel supply system, a running prototype, as well as the test data measurement and storage system. The TDC estimator predicts the expected TDC position, x_{TDC} based on the input of fuel supply ($Fuel$), ignition timing (t_{ign}), and the design parameters of the prototype. The initial value of the fuel supply ($Fuel_0$) and ignition timing (t_{ign0}) will be replaced by the actual working conditions of the engine. The actual TDC position is calculated from the test data of the piston displacement, and fed back to estimate the error. Two controllers are used, which has the input of the estimated TDC error, and the output is fuel supply control signal and ignition signal respectively. Please refer reference [16,34] for more details about the definition and calculation of ignition timing.

Compared to the previous numerical model with differential approaches [26], the model presented in this paper provides the following advantages:

(1) Simple and flexible. Implementation into several computing software, *i.e.* Matlab, AMESim, Labview, Dymola et al. All the input parameters for the simplified model are constant value, and a trigonometric function is the only function changing with time. It is easy to solve for the piston dynamic profile for implementation to several software and various programming languages.
(2) Significantly reduced solving time, and can be easily coupled with real-time HIL simulation model for the future control system development. The required solving time of the differential equations in the previous numerical model are

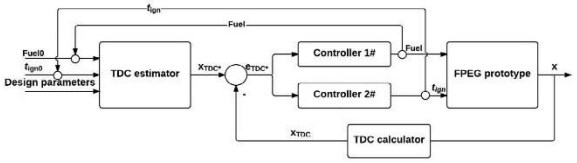

Fig. 7. Model implementation to control system.

avoided in obtaining the dynamic and thermodynamic solutions. With the proposed simplified model, it is fast to predict the piston dynamics with the feedback from the actual working condition, which makes it technically feasible to be implemented to real-time hardware for a stable operating control system.

6. Conclusion

The development of advanced algorithms for FPE control is the key enabling technology for accessing the high thermal efficiency, lower fuel consumption of FPE technologies. Whilst work to model the thermodynamic performance of FPE technologies have been completed by the authors (and others), the novelty and main impact of this work is the development and validation of the first new real time model for a FPE applications. Since the model is the first of a kind, all results of the model are novel and of high value to those engaged in relevant research.

The response of a dual piston FPEG was simplified to be a one degree forced vibration mass spring damper system, and the solution for reciprocating engines was clear, *i.e.* $x = -\frac{F_0 \cos \omega_n t}{c\omega_n}$. The model was successfully validated with respect to experimental data obtained from a prototype. The simulated piston displacement during steady operation showed similar trends with the test results and the error both of the displacement amplitude and the engine running frequency were acceptable. The state-space equations and the transfer function of the system are obtain using the fast response numerical model.

Basic assumptions and simplifications for the model are summarized as:

(1) the frictional forces are neglected;
(2) the ideal running cycle of the FPEG is described by two adiabatic processes connected by a constant volume heat release process; and
(3) the cylinder pressure is linearized using Taylor expansion around the zero-point, and all high order terms are neglected.

The model is designed specifically for use in control applications. Similarly with the adoption of virtual engineering tools in reciprocating engine technologies, other more appropriate numerical solutions should be employed for thermodynamic or component level analysis, etc. However, the simplicity and flexibility of the proposed model make it feasible to be implemented and coupled with real-time HIL simulation model for the future piston dynamic control system development. In addition, since it reveals how an FPEG operates in a resonant principle, the model is useful for parameter selection in the FPEG design process.

Acknowledgement

This project is supported by the Programme of Introducing Talents of Discipline to Universities of China (B12022) and National Nature Science Foundation of China (51006010). We would like to thank the sponsors.

References

[1] Mikalsen R, Roskilly AP. A review of free-piston engine history and applications. Appl Therm Eng 2007;27(14):2339–52. http://dx.doi.org/10.1016/j.applthermaleng.2007.03.015.
[2] Goertz M, Peng LX. Free piston engine its application and optimization. SAE paper 2000-01-0996, 2000. http://dx.doi.org/10.4271/2000-01-0996.
[3] Mikalsen R, Roskilly AP. Performance simulation of a spark ignited free-piston engine generator. Appl Therm Eng 2008;28(14):1726–33. http://dx.doi.org/10.1016/j.applthermaleng.2007.11.015.
[4] Tikkanen S, Lammila M, Herranen M, Vilenius M. First cycles of the dual hydraulic free piston engine. SAE technical paper 2000-01-2546, 2000. http://dx.doi.org/10.4271/2000-01-2546.
[5] Boucher J, Lanzetta F, Nika P. Optimization of a dual free piston Stirling engine. Appl Therm Eng 2007;27(4):802–11. http://dx.doi.org/10.1016/j.applthermaleng.2006.10.021.
[6] Mao Jinlong, Zuo Zhengxing, Li Wen, Feng Huihua. Multi-dimensional scavenging analysis of a free-piston linear alternator based on numerical simulation. Appl Energy 2011;88(4):1140–52. http://dx.doi.org/10.1016/j.apenergy.2010.10.003.
[7] Mikalsen R, Roskilly AP. The control of a free-piston engine generator. Part 1: Fundamental analyses. Appl Energy 2010;87(4):1273–80. http://dx.doi.org/10.1016/j.apenergy.2009.06.036.
[8] Mikalsen R, Roskilly AP. The control of a free-piston engine generator. Part 2: Engine dynamics and piston motion control. Appl Energy 2010;87(4):1281–7. http://dx.doi.org/10.1016/j.apenergy.2009.06.035.
[9] Kosaka H, Akita T, Moriya K, Goto S, et al. Development of free piston engine linear generator system: Part 1 – Investigation of fundamental characteristics. SAE technical paper 2014-01-1203, 2014. http://dx.doi.org/10.4271/2014-01-1203.
[10] Goto S, Moriya K, Kosaka H, Akita T, et al. Development of free piston engine linear generator system: Part 2 – Investigation of control system for generator. SAE technical paper 2014-01-1193, 2014. http://dx.doi.org/10.4271/2014-01-1193.
[11] Zhang Chen, Li Ke, Sun Zongxuan. Modeling of piston trajectory-based HCCI combustion enabled by a free piston engine. Appl Energy 2015;139:313–26. http://dx.doi.org/10.1016/j.apenergy.2014.11.007.
[12] Jia Boru, Zuo Zhengxing, Feng Huihua, Tian Guohong, Roskilly AP. Investigation of the starting process of free-piston engine generator by mechanical resonance. Energy Proc 2014;61:572–7. http://dx.doi.org/10.1016/j.egypro.2014.11.1173.
[13] Haag J, Ferrari C, Starcke J, Stöhr M, et al. Numerical and experimental investigation of in-cylinder flow in a loop-scavenged two-stroke free piston engine. In: Small engine technology conference & exhibition, SAE technical paper 2012-32-0114, 2012.
[14] Kock F, Haag J, Friedrich H. The free piston linear generator – development of an innovative, compact, highly efficient range-extender module. SAE technical paper 2013-01-1727, 2013.
[15] Xu Zhaoping, Chang Siqin. Prototype testing and analysis of a novel internal combustion linear generator integrated power system. Appl Energy 2010;87.4:1342–8. http://dx.doi.org/10.1016/j.apenergy.2009.08.027.
[16] Jia Boru, Tian Guohong, Feng Huihua, Zuo Zhengxing, Roskilly AP. An experimental investigation into the starting process of free-piston engine generator. Appl Energy 2015. http://dx.doi.org/10.1016/j.apenergy.2015.02.065.
[17] Atkinson C, Petreanu S, Clark N, Atkinson R. Numerical simulation of a two-stroke linear engine-alternator combination. SAE technical paper 1999-01-0921, 1999. http://dx.doi.org/10.4271/1999-01-0921.
[18] Goldsborough S Scott, Van Blarigan Peter. A numerical study of a free piston IC engine operating on homogeneous charge compression ignition combustion. SAE technical paper, 1999-01-0619, 1999. http://dx.doi.org/10.4271/1999-01-0619.
[19] Wu W, Hu J, Yuan S. Semi-analytical modelling of a hydraulic free-piston engine. Appl Energy 2014;120:75–84. http://dx.doi.org/10.1016/j.apenergy.2014.01.059.
[20] Yang Q, Luo E, Dai W, Yu G. Thermoacoustic model of a modified free piston Stirling engine with a thermal buffer tube. Appl Energy 2012;90(1):266–70. http://dx.doi.org/10.1016/j.apenergy.2011.03.028.
[21] Chiang Chia-Jui et al. Dynamic modelling of a SI/HCCI free-piston engine generator with electric mechanical valves. Appl Energy 2013;102:336–46. http://dx.doi.org/10.1016/j.apenergy.2012.07.033.
[22] Zhao Z, Zhang F, Zhao C, Chen Y. Modelling and simulation of a hydraulic free piston diesel engine. SAE technical paper 2008-01-1528, 2008. http://dx.doi.org/10.4271/2008-01-1528.
[23] Toghyani Somayeh, Kasaeian Alibakhsh, Ahmadi Mohammad H. Multi-objective optimization of Stirling engine using non-ideal adiabatic method. Energy Convers Manage 2014;80:54–62. http://dx.doi.org/10.1016/j.enconman.2014.01.022.
[24] Kim Jaeheun, Bae Choongsik, Kim Gangchul. Simulation on the effect of the combustion parameters on the piston dynamics and engine performance using the Wiebe function in a free piston engine. Appl Energy 2013;107:446–55. http://dx.doi.org/10.1016/j.apenergy.2013.02.056.
[25] Hunga Nguyen Ba, Limb Ocktaeck, Iida Norimasa. The effects of key parameters on the transition from SI combustion to HCCI combustion in a two-stroke free piston linear engine. Appl Energy 2015;137:385–401. http://dx.doi.org/10.1016/j.apenergy.2014.10.001.
[26] Jia B, Zuo Z, Tian G, Feng H, Roskilly AP. Development and validation of a free-piston engine generator numerical model. Energy Convers Manage 2015;91:333–41. http://dx.doi.org/10.1016/j.enconman.2014.11.054.
[27] Redlich RW, Berchowitz DM. Linear dynamics of free-piston Stirling engines. Proc Inst Mech Eng, Part A: J Power Energy 1985;199(3):203–13. http://dx.doi.org/10.1243/PIME_PROC_1985_199_025_02.
[28] Nakhaie Jazar G, Farid Golnaraghi M. Nonlinear modelling, experimental verification, and theoretical analysis of a hydraulic engine mount. J Vib Control 2002;8(1):87–116. http://dx.doi.org/10.1177/1077546302008001519.

[29] Xiao J, Li Q, Huang Z. Motion characteristic of a free piston linear engine. Appl Energy 2010;87(4):1288–94. http://dx.doi.org/10.1016/j.apenergy.2009.07.005.
[30] Li Q, Xiao J, Huang Z. Simulation of a two-stroke free-piston engine for electrical power generation. Energy Fuels 2008;22(5):3443–9.
[31] Li QF, Xiao J, Huang Z. Parametric study of a free piston linear alternator. Int J Autom Technol 2010;11(1):111–7. http://dx.doi.org/10.1007/s12239-010-0015-3.
[32] Hansson Jörgen. Analysis and control of a hybrid vehicle powered by a free-piston energy converter. Dissertation, Royal Institute of Technology; 2006.
[33] Harris Cyril M, Piersol Allan G. Harris' shock and vibration handbook, 5th ed.; 2012.
[34] Jia B, Zuo Z, Feng H, Tian G, Roskilly AP. Development approach of a spark-ignited free-piston engine generator. SAE technical paper, 2014-01-2894, 2014. http://dx.doi.org/10.4271/2014-01-2894.